Solid Mechanics and Its Applications

Peter Davies
Yapa D. S. Rajapakse *Editors*

Durability of Composites in a Marine Environment

Springer

Solid Mechanics and Its Applications

Volume 208

Series Editor

G. M. L. Gladwell
Department of Civil Engineering, University of Waterloo, Waterloo, Canada

For further volumes:
http://www.springer.com/series/6557

Aims and Scope of the Series

The fundamental questions arising in mechanics are: *Why*? *How*? and *How much*? The aim of this series is to provide lucid accounts written by authoritative researchers giving vision and insight in answering these questions on the subject of mechanics as it relates to solids.

The scope of the series covers the entire spectrum of solid mechanics. Thus it includes the foundation of mechanics; variational formulations; computational mechanics; statics, kinematics and dynamics of rigid and elastic bodies: vibrations of solids and structures; dynamical systems and chaos; the theories of elasticity, plasticity and viscoelasticity; composite materials; rods, beams, shells and membranes; structural control and stability; soils, rocks and geomechanics; fracture; tribology; experimental mechanics; biomechanics and machine design.

The median level of presentation is the first year graduate student. Some texts are monographs defining the current state of the field; others are accessible to final year undergraduates; but essentially the emphasis is on readability and clarity.

Peter Davies · Yapa D. S. Rajapakse
Editors

Durability of Composites in a Marine Environment

Springer

Editors
Peter Davies
Marine Structures Laboratory
IFREMER, Centre de Bretagne
Plouzane
France

Yapa D. S. Rajapakse
Solid Mechanics Division
Office of Naval Research
Arlington, VA
USA

ISSN 0925-0042 ISSN 2214-7764 (electronic)
ISBN 978-94-007-7416-2 ISBN 978-94-007-7417-9 (eBook)
DOI 10.1007/978-94-007-7417-9
Springer Dordrecht Heidelberg New York London

Library of Congress Control Number: 2013953198

Printed on acid-free paper

Springer is part of Springer Science+Business Media (www.springer.com)

Contents

Durability of Composites in the Marine Environment 1
John Summerscales

Water Sorption Thermodynamics in Polymer Matrices 15
Pellegrino Musto, Michele Galizia, Giuseppe Scherillo
and Giuseppe Mensitieri

Humid Ageing of Organic Matrix Composites 47
X. Colin and J. Verdu

Water–Mechanical Property Coupling 115
F. Jacquemin and S. Fréour

Effect of Sea Water on Polymeric Marine Composites 129
Akawut Siriruk and Dayakar Penumadu

Seawater Aging of Vinylester and Carbon Reinforced Vinylester 143
A. M. Figliolini and L. A. Carlsson

Effect of Water Absorption on Time–Temperature Dependent Strength of Unidirectional CFRP 155
Masayuki Nakada and Yasushi Miyano

Accelerated Aging Tests for Marine Energy Applications 165
Peter Davies

Integrating Durability in Marine Composite Certification 179
Andreas T. Echtermeyer

Durability of Composite Materials for Underwater Applications 195
D. Choqueuse and P. Davies

Design of Racing Yachts for Durability 209
H. Devaux, A. Miller, R. Balze, S. Guého and J. Maguet

Service Experience and Life Time Prediction of Naval Composites . . . 239
J. Dalzel-Job, G. Kotsikos and J. Mawella

Conclusion 253

Introduction

This book brings together 13 chapters by international experts based on the presentations made at the IFREMER/ONR workshop, "Durability of Composites in a Marine Environment", held at the IFREMER Centre in Nantes, in August 2012. The main objective, of both the workshop and this book, is to give a state-of-the-art overview of current research in Europe and the USA, on the behaviour of composite materials in a marine environment. This was achieved by bringing together leading researchers in this field, providing invited lectures and discussions over two days. A round table discussion then focussed on further research required to improve the long-term reliability of composite marine structures, and finally all presenters were invited to prepare a chapter for this book.

While fibre reinforced polymer composites have been used in marine applications for over 50 years (pleasure boats, military vessels and submarines), design with respect to long-term durability has been largely based on experience, and safety factors are often high. In recent years, there have been concerted efforts to rationalize design of small boats culminating in the appearance of the ISO 12215 in 2006. This provides a common basis for the determination of scantlings, but long-term behaviour is hardly considered.

Some aspects of durability have been studied in military R&D programmes, notably the EUCLID projects (RTP3.8 and RTP 3.21) and the ONR Solid Mechanics Core program. However, it is only recently that we have the capability to establish physically based models for the coupling between water ingress and mechanical behaviour. This is a relatively new field of research. Discussion between those with experience of materials in a marine environment, and those developing predictive tools, is essential if these tools are to provide designers of naval structures with realistic descriptions of long-term behaviour.

In addition to the traditional marine boat and ship structures, there are two other areas in which composite materials are starting to provide key contributions. The first is the offshore industry which, despite several attempts over the past 30 years to integrate these materials, notably for drilling risers, is only now starting to realise the weight gain potential of high performance composites. A second emerging area is renewable marine energy, which covers structures both above water such as

floating wind turbines, and immersed systems such as tidal turbines. Guaranteeing the long-term reliability of such devices is critical to limit maintenance and ensure economic viability. Understanding the long-term behaviour of components such as composite turbine blades in a marine environment is one of the major challenges facing this industry. Several prototype blades have failed during trials and designing for long-term durability is becoming a major issue.

Given both the traditional use of composites at sea and the exciting new applications on the horizon, it was therefore very timely today to propose (and conduct) a meeting to address durability issues for those involved in the area of marine composite structures. The workshop was designed to provide a background to previous work, a forum for discussion of current projects in Europe and the USA, and a framework to prioritise future research and encourage the development of new collaborations. It was supported by the Office of Naval Research, IFREMER and the Institut Carnot EDROME. The chairmen would like to thank Marie-Michèle Pedel, Yvon Le Guen and Colette Davies-Courty for their enthusiasm and assistance with the organization. The workshop was attended by 65 participants, from academia, research and industry. The structure of this book parallels the agenda for the workshop. An overview by Summerscales introduced the event (Durability of Composites in the Marine Environment). This is followed by two very detailed chapters describing the influence of water on matrix resins and composites, from Mensitieri et al. and Colin & Verdu (Water Sorption Thermodynamics in Polymer Matrices and Humid Ageing of Organic Matrix Composites). Coupling between water absorption and mechanical behaviour is then presented by Jacquemin & Fréour (Water–Mechanical Property Coupling).

Examples of how sea water affects the properties of marine composites are described by Siriuk and Penumadu (Effect of Sea Water on Polymeric Marine Composites) and Figliolini and Carlsson (Seawater Aging of Vinylester and Carbon Reinforced Vinylester).

Two chapters discussing accelerated aging follow, from Nakada and Miyano (Effect of Water Absorption on Time–Temperature Dependent Strength of Unidirectional CFRP) and Davies (Accelerated Aging Tests for Marine Energy Applications), the latter specifically aimed at marine energy applications.

The second day of the workshop focussed more on applications. Echtermeyer described how durability issues could be included in certification (Integrating Durability in Marine Composite Certification). Choqueuse then described some underwater applications (Durability of Composite Materials for Underwater Applications). A chapter by Devaux et al. presents three case studies on durability of racing yachts (Design of Racing Yachts for Durability). This is followed by in-service experience of the UK Navy described by Dalzel-Job et al. (Service Experience and Life Time Prediction of Naval Composites).

The book is completed by a short concluding chapter by Rajapakse and Davies (Conclusion), based on the discussions at the workshop to identify future R&D requirements, and including an overview of ONR programmes and how they are addressing future requirements.

Peter Davies
IFREMER

Yapa D. S. Rajapakse
ONR

Durability of Composites in the Marine Environment

John Summerscales

Abstract This chapter presents an overview of key considerations for the successful application of fibre reinforced composites in the marine environment. It is intended to complement and update an earlier text Searle and Summerscales (Effect of Water Absorption on Time–Temperature Dependent Strength of Unidirectional CFRP). After consideration of factors affecting the environmental resistance of conventional composites, the potential for natural fibre reinforced polymer composites is briefly discussed. Finally it is argued that Quantitative Life Cycle Assessment is essential to establish the "sustainability" of any system.

1 Environmental Resistance

Fibre-reinforced polymer (FRP) matrix composites have a long history of use in the marine environment. Over the course of the 1950s, glass fibre reinforced polyester (GRP) displaced wood as the material of choice for recreational craft and some workboats. The current interest in marine renewable energy (MRE) should create a significant new market for composites in MRE device components.

Wood degrades when moist and is attacked by marine boring organisms. Steel rusts, and aluminium corrodes, in seawater unless protected by surface coatings. Hence a major factor in the adoption of GRP/FRP for use in seawater over extended periods of time has been their potential/proven durability in this context.

However, successful application of FRP does require the selection of appropriate materials and careful design to avoid inappropriate stresses. The long-term performance of composites is the subject of books by Pritchard [1], Harris [2], Martin [3] and of course the volume in your hands with chapters relevant to

J. Summerscales (✉)
Advanced Composites Manufacturing Centre, School of Marine Science and Engineering, Plymouth University, Reynolds Building, Plymouth, Devon PL4 8AA, England
e-mail: jsummerscales@plymouth.ac.uk

P. Davies and Y. D. S. Rajapakse (eds.), *Durability of Composites in a Marine Environment*, Solid Mechanics and Its Applications 208,
DOI: 10.1007/978-94-007-7417-9_1,

marine composites by Searle and Summerscales [4], Davies et al. [5], Davies and Choqueuse [6], Choqueuse and Davies [7] and Davies et al. [8]. This chapter will address key issues for the successful design of composite vessels and components that will see service in the earth's seas and oceans.

1.1 Temperature

Polymers have a number of key transition temperatures. The most important is the glass transition temperature, T_g, which marks the point at which cooling causes segmental motion of the polymer chains to be frozen out. Below T_g the polymer is normally elastic and brittle, while above T_g the polymer is viscoelastic and tough. For polymers which are subjected to stress, it is normal to use the material below T_g to avoid creep under sustained loads.

When exposed to direct sunlight, the colour of a surface will affect the surface temperature of the component (Fig. 1). For dark surfaces, this could move the working temperature above the T_g range and hence affect the durability of the composite.

1.2 Water Diffusion, Absorption and Swelling and Their Effects on Mechanical Properties

The Flory–Huggins theory considers a polymer as a lattice of cells each of which may be occupied by either (a) a polymer molecule (with the chain segments occupying a continuous sequence of cells) or (b) a solvent molecule. A polymer molecule can adopt many different conformations (distinguishable spatial arrangements of the segments). The proportion of cells not occupied by the polymer chain can be considered as the fractional free volume (FFV). The distribution and connectivity of the FFV will determine the porosity and permeability of the polymer and thus the ease with which molecules from the surrounding environment can penetrate the material.

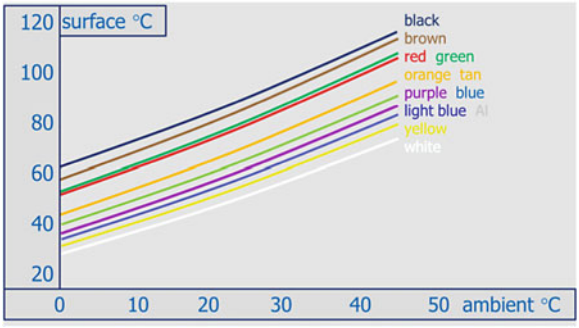

Fig. 1 The effect of direct sunlight on the surface temperature of different coloured objects (redrawn from the SP systems design allowable handbook)

At the macroscopic scale, the diffusion of gases, vapours or liquids into a material is normally modelled using Fick's law with the fluid (*e.g.* moisture) content initially increasing with exposure time then approaching a saturation level. For systems where sorption and/or reaction–diffusion produce a non-Fickian response, the diffusion coefficient can directly be derived from sorption isotherms such as Henry's or Langmuir's laws [9].

Derrien and Gilormini (DG) [10] have presented a model for the time-dependent evolution of the moisture content during unidirectional diffusion in a polymer submitted to hydrostatic load. Jacquemin and Fréour (JF) [11] presented two multi-physics models (a thermodynamic approach and a free volume theory) for the effects of plasticisation during water sorption and the internal mechanical state profile at both constituent and ply scales. Discrepancies between the DG and JF models were found to increase significantly with the coefficient of moisture expansion (CME).

Nakada and Miyano [12] have described a general and advanced accelerated testing methodology (ATM-2) for the long-term life prediction of polymer matrix composites. The time, temperature and water absorption dependencies for static strength of UD-CFRP were found to be a function of the viscoelastic compliance of the matrix resin.

Perreux [13] presented a general behavior model to account for time-dependent mechanical and environmental (water) loading of laminates and the induced damage. The first-stage micro-mesomodel describes the variation in stiffness due to microcracks. The second stage kinetic model is based on the thermodynamic definition of the forces driving damage and other dissipation potentials.

Summerscales [14] has reviewed the non-destructive evaluation techniques for the measurement of the moisture content in composites. Nuclear magnetic resonance spectroscopy and/or imaging is of especial interest as it is able to discriminate between chemically-bound water (e.g. hydrogen bonded to the polymer) and free water.

1.3 The Potential for Osmosis and Blistering

Osmosis is the process by which solution strengths are equalised by passage of the solvent (usually water) through a semi-permeable membrane. In fibre-reinforced composites, the polymer matrix can act as the membrane. As water diffuses through the polymer, any soluble solid material can dissolve and thus form a strong solution. Water will then diffuse to this solution until the concentration gradient is reduced to zero. The volume of the solution will increase with dilution and exert pressure on the surrounding material. When the stresses exceed a critical level, delamination will occur (normally at the gelcoat-laminate interface) and will be manifest as blisters on the surface of the laminate. A comprehensive list of chemical factors implicated in osmosis and blistering and other measures to reduce or eliminate the problem are given in [4].

1.4 Stress and Stress Corrosion

The long-term performance of composites may be limited by fatigue (cyclic stress loading) considerations. The fatigue data for a material is normally acquired by subjecting samples to a (sinusoidal as default or square, triangular, sawtooth or pre-recorded) waveform alternating between a maximum absolute stress, S_{max}, and a minimum absolute stress, S_{min}. The stress ratio is -1 when loading varies between the same magnitude of load in tension and compression. If loads are restricted to just tension then $0 < R < 1$, while if loads are solely compressive then $R > 1$.

ISO 13003:2003 [15] requires that five specimens are tested to establish the static/monotonic strength, before at least five specimens are tested in fatigue loading at a minimum of four levels of imposed stress/strain. The data are normally plotted with linear y-axis [peak stresses or strains (S)] against log x-axis [number of cycles (N)] and is known as a Wohler diagram. Basquin's relationship [16] states that:

$$\sigma_a = \sigma_{f'} \left(2N_f\right)^b \tag{1}$$

where σ_a is the constant stress amplitude, σ_f' is the fatigue strength coefficient, N_f is the number of cycles to failure and b is the fatigue strength exponent (the slope of the S–N plot, which is usually negative).

Stinchcomb and Reifsnider [17], Post et al. [18] and Passipoularidis and Philippidis [19] have each reviewed aspects of the fatigue performance of composites. Vassilopoulos et al. [20] have reviewed commonly used and recently developed models for the derivation of constant life diagrams (CLD) for composite materials. Six methods were described and compared for their prediction accuracy over a wide range of constant amplitude fatigue data from GFRP materials. The influence of the chosen CLD method on the fatigue life prediction of composite materials was quantified.

1.5 Marine Fouling and Biodegradation

Any vessel or device in the marine environment should be protected against fouling organisms. As a "sustainable" technology, the MRE sector must ensure that their operations minimise environmental burdens. Ideally MRE devices should require no intervention for repair and maintenance over the complete device life cycle. A number of technologies are available to deter or displace fouling by marine organisms although the commercial technologies each have potential issues:

- toxic formulations (e.g. cuprous oxide paints) increase levels of heavy metals or other biocides in the ecosystem. Tributyl tin is now banned worldwide and

copper is under increasing pressure from the environmental lobby. Qian et al. [21] have reviewed important natural anti-fouling compounds discovered in a variety of organisms.
- self-polishing (exfoliating) surfaces release polymer microdebris which concentrate toxins and are ingested by animals at the base of the food chain [22, 23, 24].
- low surface energy coatings (e.g. silicone or PTFE) require aggressive surface preparation to ensure firm attachment of the non-stick material to the component. Genzer and Efimenko [25] have reviewed superhydrophobicity (i.e. extreme non-wettability) which can involve tailoring the surface chemistry, texture, and responsiveness.
- pulsed high-strength electric fields (PEF) with low voltages [26] developed for the protection of marine sensors. This requires optimisation for energy consumption and, on a larger scale, practical application would require geometries other than the interdigitated electrode (IDE) architecture.
- biomimetic topography (*e.g.* shark-skin replica) technologies are normally too soft to work for extended periods without wearing away [27–32].

1.6 Cavitation Erosion

The phenomenon of bubble collapse in fluids was identified by [33] in considering the design and performance of a water wheel and, in the context of marine steam engines, by Reynolds [34]. The first use of the term *cavitation* is attributed to Froude [35]. In rapidly flowing fluids with local pressure below the vapour pressure and sources for nucleation, a vapour bubble can form and will continue to grow until it moves to a region of higher pressure where it collapses. Rayleigh [36] proposed that when the bubble collapsed close to a boundary it would produce high energy pressure waves (stress pulses) which could cause mechanical damage in the adjacent solid. Eisenberg [37] proposed that bubble collapse was asymmetrical with a high-velocity reentrant liquid jet forming and impinging on the surface. The magnitude of the stress pulse may be up to 1,000 MPa (i.e. comparable to the strength of many materials) and the duration is $\sim$2–3 μs [38].

Composites are now finding applications as hydrofoils and sterngear which operates in cavitating environments, *e.g.* propellers [39]. Anon. [40–48] and rudders [49–51]. Lightweight composite propellers have lower inertia which results in higher acceleration and deceleration rates with consequent increases in speed and fuel efficiency. Hydroelastic tailoring of the laminate may be a route to delaying the onset of cavitation [52, 53].

Kallas and Lichtman [54] and Karimi and Martin [38] have reviewed cavitation phenomena and the response of materials to cavitation. Bhagat [55] presented a materials perspective on cavitation erosion of metal-matrix composites based on crystal dislocation mechanics. The open literature on cavitation erosion in polymer

matrix composites is very limited [56–62]. National defence research laboratories probably hold classified data restricted by stealth considerations.

Hammond et al. [59] found that cavitation erosion resistance could be ranked aluminium (poor) < GRP < nickel aluminium bronze (NAB, good). Yamatogi et al. [62] found that cavitation erosion resistance could be ranked glassfibre (poor) < carbon fibre = unreinforced epoxy resin < aramid fibre < NAB.

Kallas and Lichtman [54] identify that some elastomeric coatings show very high erosion resistance although such systems may be compromised by coating-substrate separation leading to early failure.

A non-marine example of the excellent cavitation erosion resistance of composites was a diffuser section used to join two pipes of different cross-sectional area in a Middle East oilfield [63]. The company quality procedure was for regular replacement of the steel component after one month in service when the pipeline began to leak. On one occasion, the steel component was delayed so a temporary fibreglass replacement was installed. After nine months service in a cavitation-rich acid-gas environment, the component was removed. As shown in Fig. 2, the component had suffered damage but was still giving good service.

1.7 Galvanic Corrosion

The corrosion of metals and semiconductors involves the flow of an electric current within the material. Most of the constituent materials in fibre-reinforced laminates are insulators and, in consequence, electrochemical corrosion is not an issue. However, carbon acts as a noble metal, lying between platinum and titanium in the galvanic series. Carbon fibres should not be used where they can come into contact with structural metals (especially light alloys such as aluminium or magnesium) in the presence of a conducting fluid (*e.g.* sea-water). A thin glass fibre surface layer, or polymer liners around bolt-holes, should be sufficient to prevent the formation of such a galvanic corrosion cell and consequent loss of the alloy.

2 Bio-Based Composites in Wet Conditions

The use of natural fibres as the reinforcement for composites has recently been reviewed by several authors including [64–77]. Summerscales and Grove [76] consider conditioning the reinforcement fibres before composite manufacture to be essential.

A potential problem with natural fibre-reinforced polymer matrix composites is the hydrophilic nature of the ligno-cellulose fibres and hence the moisture sensitivity of the resulting composites. Embedding the hydrophilic fibres in a hydrophobic matrix will delay the absorption of water but diffusion and damage may

Fig. 2 Oilfield pipeline fibreglass diffuser section after cavitation erosion damage [plan view (*top*) and elevation (*bottom*), scale indicated by €1 coin]

compromise the material over extended periods of time. Moisture will induce dimensional changes (swelling), mechanical performance changes (plasticisation and hence higher strains to failure but lower moduli) and higher susceptibility to microbiological attack.

Costa and D'Almeida [78] studied the effect of water absorption on the flexural properties of jute *or* sisal fibre reinforced polyester *or* epoxy matrix composites. The diffusion behaviour in both composites could be described by the Fickian model. The jute-epoxy composites showed the best mechanical properties for all immersion times studied. This behaviour was attributed to better fibre–matrix interface integrity with epoxy resin and better moisture resistance of the jute fibres.

Acetylation of plant fibres can improve the mechanical properties of their composites [79]. Acetylation increases the hydrophobicity of the fibres. Bast fibres from jute and flax were considered along with coconut fibre (coir), oil palm empty fruit bunch (OPEFB) and oil palm frond. The two bast fibres were found to be the least reactive of the five fibres studied. Acetylation has also been reported to

enhance the stability of composites during environmental exposure [80]. Hill et al. [81] reported that acetylated fibres showed a high degree of decay resistance in a variety of microbiological decay tests over a five-month test period, while control samples failed in less than one-month.

Shah et al. [82, 83] have recently presented fatigue life evaluations for aligned plant fibre composites through S–N curves and constant-life diagrams. The normalised fatigue performance (the fatigue strength exponent, b, defined by the stress intercept at twice the number of load reversals to failure) of the natural fibre composites was found to lie between that of glass- and carbon-fibre reinforced composites.

There is increasing interest in the use of bio-based and/or biodegradable thermoplastic polymers or thermosetting resins as the matrix for composites with varying proportions of precursor materials extracted from plants (see *e.g.* [76]). Ishimaru et al. [84] reported that polycaprolactone, polyhydroxyalkanoate and polylactide thermoplastics or their copolymers (amongst others) have been applied as self-polishing/exfoliating matrices for controlled release of antifouling compositions. They conducted experiments which showed that barnacle settlement was significantly reduced by the slow release of low molecular weight poly(L-lactic acid) (PLLA without antifoulant chemical) in natural seawater.

3 End of Life Considerations

Since the Brundtland report [85], there has been increased concern for the choice of systems which meet the needs of the present without compromising the ability of future generations to meet their own needs.

However, many materials selection decisions are based on opinion without validated evidence. It is essential that full Quantitative Life Cycle Assessment (QLCA) is undertaken before committing to mass production of marine composites [86]. This should include the design, manufacture and marketing, use and disposal phases and should address all eight burdens identified by ISO/TR 14047:2003 [87]. Azapagic et al. [88, 89] proposed a route to quantification of these burdens as Environmental Impact Classification Factors (EICF—Table 1). Another major sustainability issue is Land Use as included in BS8905:2011 [90].

Singh et al. [91] have reviewed the options for the disposal of composite boats and other marine composites. In the case of thermoset composites, popular opinion suggests that these materials are inappropriate as there may be limited options for disposal at the end of the component life. This arises from political decisions intended to minimise the use of landfill for components that cannot easily be recycled. However, the use of thermoplastic matrix composites requires higher temperatures during manufacture with consequent potential for up-front global warming and climate change. QLCA should help to resolve this dilemma.

Table 1 Azapagic et al. EICF mapped to ISO/TR 14047 environmental burdens

ISO/TR 14047:2003(E)	Azapagic et al.
Acidification	Acidification potential (AP)
Ecotoxicity	Aquatic toxicity potential (ATP)
Eutrophication/nitrification	Eutrophication potential (EP)
Climate change	Global warming potential (GWP)
Human toxicity	Human toxicity potential (HTP)
Depletion of abiotic/biotic resources	Non-renewable/abiotic resource depletion (NRADP)
Stratospheric ozone depletion	Ozone depletion potential (ODP)
Photo-oxidant formation	Photochemical oxidants creation potential (POCP)

4 Conclusions

This chapter has presented an overview of key considerations for the successful application of fibre reinforced composites in the marine environment. After consideration of factors affecting the environmental resistance of conventional composites, the potential for natural fibre reinforced polymer composites was discussed. Finally it is important to defend any chosen composite system as sustainable through Quantitative Life Cycle Assessment.

Acknowledgments The author is grateful to colleagues, Jasper Graham-Jones and Stephen Grove, for their respective comments on the draft manuscript of this Chapter. Thanks are also due to Paul Harder Cohen (KMT Nord in Denmark) for additional references on cavitation erosion of composites.

References

1. Pritchard G (1999) Reinforced plastics durability. Woodhead Publishing, Cambridge. ISBN: 1 85573 320 X
2. Harris B (2003) Fatigue in composites: science and technology of the fatigue response of fibre-reinforced plastics. Woodhead Publishing, Cambridge. ISBN: 978 1 85573 608 5
3. Martin R (2008) Ageing of composites. Woodhead Publishing, Cambridge. ISBN: 1 84569 352 3
4. Searle TJ, Summerscales J (1999) Review of the durability of marine laminates, chapter 7. In Pritchard G (1999) Reinforced plastics durability. Woodhead Publishing, Cambridge. ISBN: 1 85573 320 X, pp 219–266
5. Davies P, Choqueuse D, Roy A (2003) Fatigue and durability of marine composites, chapter 27. In: Harris B (2003) Fatigue in composites: science and technology of the fatigue response of fibre-reinforced plastics. Woodhead Publishing, Cambridge. ISBN: 978 1 85573 608 5, pp 709–729
6. Davies P, Choqueuse D (2008) Ageing of composites in marine vessels, chapter 12. In Martin R (2008) Ageing of composites. Woodhead Publishing, Cambridge. ISBN: 1 84569 352 3, pp 326–353
7. Choqueuse D, Davies P (2008) Ageing of composites in underwater applications, chapter 18. In Martin R (2008) Ageing of composites. Woodhead Publishing, Cambridge. ISBN: 1 84569 352 3, pp 467–517

8. Davies P, Choqueuse D, Devaux H (2012) Failure of polymer matrix composites in marine and off-shore applications, chapter 10. In: Robinson P, Greenhalgh E, Pinho S (eds) Failure mechanisms in polymer matrix composites: criteria, testing and industrial applications. Woodhead Publishing, Cambridge. ISBN: 987 1 84569 750 1, pp 300–336
9. Verdu J, Colin X (2012) Humid aging of polymers and organic matrix composites, Ifremer-ONR Workshop on the Durability of composites in a marine environment, Nantes, pp 27–33 of the abstracts book
10. Derrien K, Gilormini P (2009) The effect of moisture-induced swelling on the absorption capacity of transversely isotropic elastic polymer-matrix composites. Int J Solids Struct 46(6):1547–1553
11. Jacquemin F, Fréour S (2012) Water-mechanical property coupling, Ifremer-ONR Workshop on the durability of composites in a marine environment. Nantes, pp 41–46 of the abstracts book
12. Nakada M, Miyano Y (2012), Accelerated testing methodology for long term durability of CFRP, Ifremer-ONR Workshop on the Durability of composites in a marine environment, Nantes, pp 47–52 of the abstracts book
13. Perreux D (2012) Life prediction of composite materials under complex loading, Ifremer-ONR workshop on the durability of composites in a marine environment, Nantes, pp 75–80 of the abstracts book
14. Summerscales J (1994) Non-destructive measurement of the moisture content in fibre-reinforced plastics. Br J Nondestr Test 36(2):64–72
15. ISO 13003:2003 International standard: fibre-reinforced plastics: determination of fatigue properties under cyclic loading conditions. BSI Group, London
16. Basquin OH (1910) The exponential law of endurance tests. Proc Am Soc Test Mater 10(2):625–630
17. Stinchcomb WW, Reifsnider KL (1979) Fatigue damage mechanisms in composite materials: a review, ASTM STP675 Fatigue Mechanisms, American Society for Testing and Materials, pp 762–787
18. Post NL, Case SW, Lesko JJ (2008) Modeling the variable amplitude fatigue of composite materials: a review and evaluation of the state of the art for spectrum loading. Int J Fatigue 30(12):2064–2086
19. Passipoularidis VA, Philippidis TP (2009) A study of factors affecting life prediction of composites under spectrum loading. Int J Fatigue 31(3):408–417
20. Vassilopoulos AP, Manshadi BD, Keller T (2010) Influence of the constant life diagram formulation on the fatigue life prediction of composite materials. Int J Fatigue 32(4):659–669
21. Qian P-Y, Xu Y, Fusetani N (2010) Natural products as antifouling compounds: recent progress and future perspectives. Biofouling: J Bioadhesion Biofilm Res 26(2):223–234
22. Hoare C, Thompson RC (1997) Microscopic plastic: a shore thing. Mar Conserv 3(11):4
23. Thompson RC, Olsen Y, Mitchell RP, Davis A, Rowland SJ, John AWG, McGonigle D, Russell AE (2004) Lost at sea: where does all the plastic go? Science 304(5672):838
24. Thompson R, Moore C, Andrady A, Gregory M, Takada H, Weisberg S (2005) Letter: new directions in plastic debris. Science 310(5751):1117
25. Genzer J, Efimenko K (2006) Recent developments in superhydrophobic surfaces and their relevance to marine fouling: a review. Biofouling: J Bioadhesion Biofilm Res 22(5):339–360
26. Pérez-Roa RE, Anderson MA, Rittschof D, Orihuela B, Wendt D, Kowalke GL, Noguera DR (2008) Inhibition of barnacle (*Amphibalanus amphitrite*) cyprid settlement by means of localized, pulsed electric fields. Biofouling: J Bioadhesion Biofilm Res 24(3):177–184
27. Liedert R, Kesel AB (2005) Biomimetic fouling control using microstructured surfaces, Bionics: innovations inspired by nature SEB annual meeting, society for experimental biology, Barcelona. Poster paper
28. Kesel A, Liedert R (2006) Antifouling nach biologischem Vorbild, Hochschule Bremen Forschungsbericht 2006, pp 107–108
29. Ralston E, Swain G (2009) Bioinspiration—the solution for biofouling control? Bioinspiration Biomimetics 4(1):015007

30. Scardino AJ, de Nys R (2011) Mini review: biomimetic models and bioinspired surfaces for fouling control. Biofouling: J Bioadhesion Biofilm Res 27(1):73–86
31. Sullivan T, Regan F (2011) The characterization, replication and testing of dermal denticles of *Scyliorhinus canicula* for physical mechanisms of biofouling prevention. Bioinspiration Biomimetics 6(4):046001
32. Schumacher JF, Aldred N, Callow ME, Finlay JA, Callow JA, Clare AS, Brennan AB (2007) Species specific engineered antifouling topologies: correlations between the settlement of algal zoospores and barnacle cyprids. Biofouling Bioadhesion Biofilm Res 23(5–6):307–317
33. Euler M (1756) Théorie plus complète des machines qui sont mises en movement par la réaction de l'eau. L'Académie Royale des Sciences et Belles Lettres, Berlin
34. Reynolds O (1873) The causes of the racing of the engines of screw steamers investigated theoretically and by experiment. Trans Inst Naval Architects 14:56–67
35. Thornycroft JI, Barnaby SW (1895) Torpedo boat destroyers, minutes of the proceedings (Institution of Civil Engineers) 122:51–69
36. Strutt JW (1917) On the pressure developed in a liquid during the collapse of a spherical cavity. Philos Mag Ser 6 34(200):94–98
37. Eisenberg P (1950) On the mechanisms and prevention of cavitation. Navy Department David W Taylor Model Basin Report 712, Washington, DC
38. Karimi A, Martin JL (1986) Cavitation erosion of materials. Int Metals Rev 31(1):1–26
39. Anon (2003) World's largest composite propeller successfully completes sea trials. Naval Architect 16
40. Anon (2012) The intelligent propeller made of carbon fiber. http://www.compositecarbonfiberprop.com/ Accessed 16:37 on 19 Aug 2013
41. Black S (2011) Composite propeller for Royal Navy minehunter: composite-for-metal replacement brings multiple benefits. High-Perform Compos 19(5):70–72
42. Hardy G (2003) New composites reduce cavitations in giant marine propeller tests. Mater World 11(7):8
43. Leenders W, van Santen M (2010) Composite main propeller for Dutch minehunter. EuroNaval, Paris
44. Motley MR, Liu Z, Young YL (2009) Utilizing fluid–structure interactions to improve energy efficiency of composite marine propellers in spatially varying wake. Compos Struct 90(3): 304–313
45. Searle TJ (1998) The manufacture of marine propellers in moulded anisotropic polymer composites, PhD thesis, University of Plymouth
46. Searle TJ (1999) Composites final frontier: a composites propeller for commercial marine applications. Design Eng 51–52
47. Searle T, Short D (1994) Are composite propellers the way forward for small boats? Mater World 2(2):69–70
48. Searle T, Chudley J, Short D (1993) Composites offer advantages for propellers. Reinf Plast 37(12):24–26
49. Anon (2012) Green marine build one of the world's largest-ever composite rudders. http://www.greenmarine.co.uk/news/green-marine-build-one-of-the-world-s-largest-ever-composite-rudders/ Accessed 16:39 on 19 Aug 2013
50. Anon (2012) Rudders and stocks. http://www.gmtcomposites.com/rudders-stocks Accessed 16:41 on 19 Aug 2013
51. Griffiths R (2006) Rudder gets new twist with composites: the U.S. Navy's specially contoured ship rudder commands composite construction. Compos Technol 12(4):60–62
52. Young YL (2007) Hydroelastic behavior of flexible composite propellers in wake inflow. Proceedings of the 16th international conference on composite materials, (ICCM 16). Kyoto/Tokyo
53. Young YL (2008) Fluid–structure interaction analysis of flexible composite marine propellers. J Fluids Struct 24(6):799–818
54. Kallas DH, Lichtman JZ (1968) Chapter 2: cavitation erosion. In: Rosato DV, Schwartz RT (eds) Environmental effects on polymeric materials, vol 1., Environments, Interscience, London-Sydney-New York, pp 223–280

55. Bhagat RB (1987) Cavitation erosion of composites: a materials perspective. J Mater Sci Lett 6(12):1473–1475
56. Djordjevic V, Kreiner J, Stojanovic Z (1988) Cavitation erosion approximation of composite materials. Preprints 33rd international symposium: materials—pathway to the future, SAMPE, Anaheim CA, pp 1561–1570
57. Rao PV (1988) Evaluation of epoxy resins in flow cavitation erosion. Wear 122(1):77–96
58. Saetre O (1991) Testing of composite pipes in high velocity seawater, 10th international OMAE conference. Stavanger, IIIB/577
59. Hammond DA, Amateau MF, Queeney RA (1993) Cavitation erosion performance of fiber reinforced composites. J Compos Mater 27(16):1522–1544
60. Lindheim T (1995) Erosion performance of glass fibre reinforced plastics (GRP), Revue de l'Institut Francais du Petrole, 50(1):83–95
61. Light KH (2005) Development of a cavitation erosion resistant advanced material system. MS dissertation, University of Maine, Aug 2005
62. Yamatogi T, Murayama H, Uzawa K, Kageyama K, Watanabe N (2009) Study of cavitation erosion of composite materials for marine propeller. Proceedings of ICCM-17. Edinburgh, 27–31 July 2009
63. Short D (2012) Private communication (e-mail of Monday 15 Oct 2012 at 17:23)
64. Hill C, Hughes M (2010) Natural fibre reinforced composites opportunities and challenges. J Biobased Mater Bioenergy 4:148–158
65. Pandey JK, Ahn SH, Lee CS, Mohanty AK, Misra M (2010) Recent advances in the application of natural fiber-reinforced composites. Macromol Mater Eng 295:975–989
66. Summerscales J, Dissanayake N, Hall W, Virk AS (2010) A review of bast fibres and their composites. Part 1: fibres as reinforcements. Compos A Appl Sci Manuf 41(10):1329–1335
67. Summerscales J, Dissanayake N, Hall W, Virk AS (2010) A review of bast fibres and their composites. Part 2: composites. Compos A Appl Sci Manuf 41(10):1336–1344
68. Ku H, Wang H, Pattarachaiyakoop N, Trada M (2011) A review on the tensile properties of natural fiber reinforced polymer composites. Compos B Eng 42(4):856–873
69. La Mantia FP, Morreale M (2011) Green composites: a brief review. Compos A Appl Sci Manuf 42(6):579–588
70. Zini E, Scandola M (2011) Green composites: an overview. Polym Compos 32(12): 1905–1915
71. Mukherjee T, Kao N (2011) PLA based biopolymer reinforced with natural fibre: a review. J Polym Environ 19(3):714–725
72. Hughes M (2012) Defects in natural fibres: their origin, characteristics and implications for natural fibre-reinforced composites. J Mater Sci 47(2):599–609
73. Shahzad A (2012) Hemp fiber and its composites—a review. J Compos Mater 46(8):973–986
74. Faruk O, Bledzki AK, Fink H-P, Sain M (2012) Biocomposites reinforced with natural fibers: 2000–2010. Prog Polym Sci 37(11):1552–1596
75. Ho M-P, Wang H, Lee J-H, Ho C-K, Lau K-T, Leng J, Hui D (2012) Critical factors on manufacturing processes of natural fibre composites. Compos B Eng 43(8):3549–3562
76. Summerscales J, Grove S (2013) Manufacturing methods for natural fibre composites, chapter 16. In: Hodzic A, Shanks R (eds) Handbook of natural fibre composites: properties, processes, failure and applications. Woodhead Publishing, Cambridge Accepted on 26 Sept 2012
77. Summerscales J, Virk AS, Hall W (2013) A review of bast fibres and their composites. Part 3: modelling. Compos Part A: Appl Sci Manuf 44(1):132–139
78. Costa FHMM, D'Almeida JRM (1999) Effect of water absorption on the mechanical properties of sisal and jute fiber composites. Polym-Plast Technol Eng 38(5):1081–1094
79. Abdul Khalil HPS, Rozman HD, Ahmad MN, Ismail H (2000) Acetylated plant-fiber reinforced polyester composites: a study of mechanical, hygrothermal, and aging characteristics. Polym-Plast Technol Eng 39(4):757–781
80. Hill CAS, Abdul Khalil HPS (2000) Effect of fiber treatments on mechanical properties of coir or oil palm fiber reinforced polyester composites. J Appl Polym Sci 78(9):1685–1697

81. Hill CAS, Abdul Khalil HPS, Hale MD (1998) A study of the potential of acetylation to improve the properties of plant fibres. Ind Crops Prod 8(1):53–63
82. Shah DU, Schubel PJ, Clifford MJ, Licence P (2012) Fatigue characterisation of plant fibre composites for rotor blade applications. JEC Compos Mag 73:51–54
83. Shah DU, Schubel PJ, Clifford MJ, Licence P (2013) Fatigue life evaluation of aligned plant fibre composites through S–N curves and constant-life diagrams. Compos Sci Technol 74:139–149
84. Ishimaru N, Tsukegi T, Wakisaka M, Shirai Y, Nishida H (2012) Effects of poly(l-lactic acid) hydrolysis on attachment of barnacle cypris larvae. Polym Degrad Stab 97(11):2170–2176
85. World Commission on Environment and Development (1987) Our common future (The Brundtland Report). Oxford Paperbacks, Oxford. ISBN: 0-19-282080-X
86. Dissanayake NPJ, Summerscales J (2013) Life cycle assessment for natural fibre composites. In: Thakur VK (ed) Green composites from natural resources. Taylor and Francis Group LLC, USA. ISBN: 978-1-4665-7069-6
87. ISO/TR 14047:2003(E) Environmental management: life cycle impact assessment—examples of application of ISO14042. International Organisation for Standards. ISBN: 0-580-43112-6
88. Azapagic A, Emsley A, Hamerton I (2003) In: Hamerton I (ed) Polymers, the environment and sustainable development. Wiley. ISBN: 0-471-87741-7
89. Azapagic A, Perdan S, Clift R (eds) (2004) Sustainable development in practice: case studies for engineers and scientists. Wiley, New York. ISBN: 0-470-85609-2
90. BS 8905:2011 Framework for the assessment of the sustainable use of materials: guidance. BSI Group, London
91. Singh M, Summerscales J, Wittamore K (2010) Disposal of composite boats and other marine composites, chapter 18 (pages 495–519). In: Goodship V (ed) Management, recycling and reuse of waste composites. Woodhead Publishing, Cambridge. ISBN: 978-1-84569-462-3 (book). ISBN: 978-1-84569-462-3 (e-book). CRC Press LLC, Boca Raton, 2010. ISBN: 978-1-4398-0104-8

Water Sorption Thermodynamics in Polymer Matrices

Pellegrino Musto, Michele Galizia, Giuseppe Scherillo and Giuseppe Mensitieri

Abstract Water sorption is a key issue in assessing the durability of polymer matrix composites. In fact absorbed water can adversely affect mechanical properties of the matrix and fibre-matrix interface integrity. In this contribution the general issue of water sorption thermodynamics in polymers is addressed from the experimental and theoretical point of view. The case of both rubbery and glassy polymers is considered modelling thermodynamics of water-polymer systems using lattice fluid theories accounting also for the occurrence of possible self- and cross-hydrogen bonding interactions. Outcomes of theoretical analyses are compared to experimental results obtained by vibrational spectroscopy and gravimetric measurements.

1 Introduction

Hygrothermal aging of polymer matrices is related to sorption of water molecules within the material [1] which promotes plasticization of the polymer depressing its glass transition temperature, T_g, [1] and, eventually, hydrolytic degradation. The amount of water absorbed at equilibrium heavily depends upon the chemical

P. Musto
Institute of Chemistry and Technology of Polymers, National Research Council of Italy, Via Campi Flegrei 34, Olivetti Buildings 80078 Pozzuoli, NA, Italy
e-mail: pellegrino.musto@ictp.cnr.it

M. Galizia · G. Scherillo · G. Mensitieri (✉)
Department of Chemical, Materials and Production Engineering, University of Naples Federico II, P.le Tecchio 80 80125 Naples, Italy
e-mail: mensitie@unina.it

M. Galizia
e-mail: michele-galizia@unina.it

G. Scherillo
e-mail: gscheril@unina.it

P. Davies and Y. D. S. Rajapakse (eds.), *Durability of Composites in a Marine Environment*, Solid Mechanics and Its Applications 208,
DOI: 10.1007/978-94-007-7417-9_2,

structure and morphology of the polymer. The understanding of this phenomenon is a crucial task for the assessment of long term durability of a polymer based composite material and for the understanding of possible effects like matrix cracking, microvoid generation, outer-ply delamination or surface blistering. In Fig. 1 is reported a schematic illustration of water transport, sorption and interaction mechanisms occurring in polymer matrix composites along with possible induced damages.

In view of these premises, understanding and modelling sorption thermodynamics of water in rubbery and glassy polymers is of great importance from both fundamental and technological standpoints. Synergic combination of theoretical and experimental approaches allows a quantitative treatment of water sorption thermodynamics accounting also for water-polymer specific interactions. In fact, the use of infrared vibrational spectroscopy combined with gravimetric measurements can lead to a quantitative experimental evaluation of the amount of different water species as well as of self and cross H-bonding interactions. Construction and validation of suitable water sorption thermodynamic models against these experimental data supply an important tool for interpretation and quantification of the behaviour of a polymer matrix exposed to a humid environment.

In this chapter, the general issue of sorption thermodynamics of water in rubbery and glassy polymers is addressed, using a modelling approach which accounts for possible hydrogen bonding (HB) interactions and, in the case of glassy polymers, for the out-of-equilibrium state of the glassy system. It is illustrated how it is possible to investigate molecular interactions, evaluate the number of interacting species (penetrant–penetrant and polymer–polymer self interactions as well as

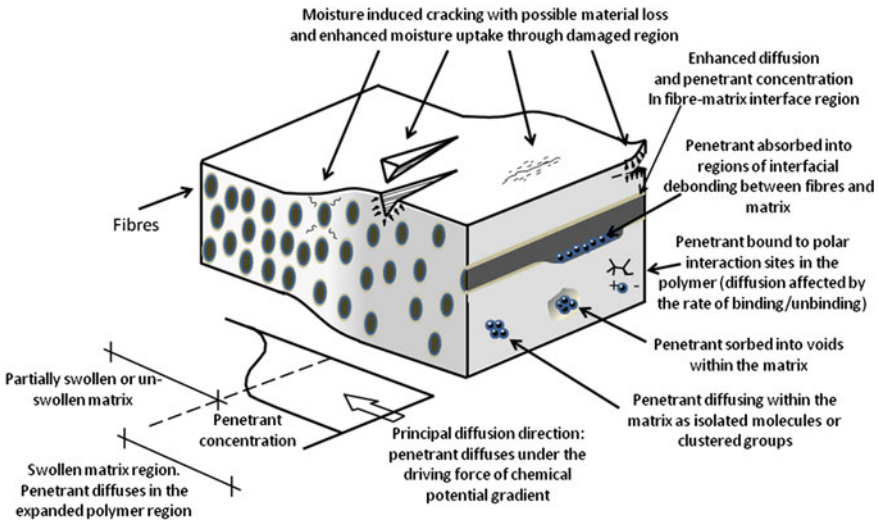

Fig. 1 Schematic illustration of possible moisture sorption locations and mechanisms (re-adapted from Ref. [2])

penetrant and polymer cross interactions) and quantify the relative amount of each interacting complex present at equilibrium state and during the transient sorption stage. Experimental and theoretical analyses are in fact combined to analyze sorption of water in rubbery (polycaprolactone, PCL) and glassy polymers (polyimides, with different degree of fluorination, epoxies and polyetheretherketone). In this manuscript, for the sake of brevity, attention is mainly focused upon thermodynamic aspects, without reporting the analysis of mass transport properties, which can also be performed using the same experimental tools.

2 Sorption Thermodynamics of Water in Polymer Matrices

2.1 Rubbery Polymers: The NRHB Model

Equation of state (EoS) approaches based on statistical thermodynamics provide a powerful framework to model thermodynamic properties and phase equilibria of mixtures of rubbery polymers and low molecular weight compounds (penetrants). A class of theoretical EoS models proposed is that grounded on compressible "mean field" lattice fluid theory (LF-EoS) [3–7]. However, these approaches are well suited only for systems where no specific interactions occur and, therefore, should not be used for polymer-water mixtures displaying Hydrogen Bondings (HB). To this aim, Panayiotou and Sanchez [8] have modified the original Sanchez-Lacombe LF-EoS theory [4–6] to account for the formation of possible self and cross HB in multicomponent systems. The mean field contribution adopted in their model (in the following PS model) is based on a simplified statistical framework, in which a random arrangement of r-mers and holes is assumed. Actually, in the case of non-athermal mean field contacts between different kind of r-mers and/or holes, such an assumption is likely to be incorrect. More recently, to overcome this intrinsic limitation of PS model, Panayiotou et al. developed the 'Non-Random lattice fluid Hydrogen Bonding' (NRHB) model [9–11] that is based on the factorization of the configurational partition function in two separate contributions: one related to mean field interactions and one accounting for the effects of specific HB interactions. The first contribution is constructed starting from the idea that the partition function related to mean field interactions can be further factorized into an ideal random contribution and a non-random contribution that is obtained treating each kind of contact as a reversible chemical reaction (i.e. the so-called *Quasichemical* approximation [12]). This latter contribution accounts for non-randomness of all the possible couple of contacts between mers of the components of the mixture as well as hole sites [13]. The second contribution, accounting for the effect of HB interactions, is formulated by using a combinatorial approach first proposed by Veytsman [14, 15], already adopted in the formulation of PS model.

We focus here on the phase equilibrium between a binary rubbery polymer-water mixture and pure water in a vapour phase, assuming that the polymer is not soluble within the gaseous phase. Therefore here we will consider only binary mixtures, with subscript '1' referring to water and subscript '2' referring to polymer. Establishment of this equilibrium implies the equality of the chemical potentials of water in the two coexisting phases. According to NRHB model, the general, non-equilibrium, expression of water chemical potential in the polymer-water mixture and in the pure water phase is expressed as sum of a LF and a HB contribution [10]:

$$\mu_1 = \mu_{1,LF} + \mu_{1,HB} \tag{1}$$

where

$$\begin{aligned}\frac{\mu_{1,LF}}{RT} = {} & \ln\frac{\phi_1}{\omega_1 r_1} - r_1\sum_{j=1}^{2}\frac{\phi_j l_j}{r_j} + \ln\tilde{\rho} + r_1(\tilde{v}-1)\ln(1-\tilde{\rho}) \\ & - \frac{z}{2}r_1\left[\tilde{v} - 1 + \frac{q_1}{r_1}\right]\ln\left[1 - \tilde{\rho} + \frac{q}{r}\tilde{\rho}\right] \\ & + \frac{zq_1}{2}\left[\ln\Gamma_{11} + \frac{r_1}{q_1}(\tilde{v}-1)\ln\Gamma_{00}\right] + r_1\frac{\tilde{P}\tilde{v}}{\tilde{T}} - \frac{q_1}{\tilde{T}_1} + \frac{\mu_{1,HB}}{RT}\end{aligned} \tag{2}$$

and

$$\frac{\mu_{1,HB}}{RT} = r_1 v_H - \sum_i^m d_i^1 \ln\left(\frac{v_d^i}{v_{i0}}\right) - \sum_j^n a_j^1 \ln\left(\frac{v_a^j}{v_{0j}}\right) \tag{3}$$

The reported expressions for LF and HB contributions to chemical potential are given in a general form which is valid for both pure penetrant in the gas phase and for penetrant in the binary polymer mixture. Refer to the fundamental literature on NRHB theory [9–11] for a detailed description of the relevant equations, of the parameters and of the variables, as well as of their corresponding symbols, which define the model as expressed by Eqs. 1–3.

In order to evaluate the equilibrium water chemical potential, the non equilibrium expressions (2) and (3) must be coupled with the proper expressions defining the equilibrium minimization conditions of Gibbs energy as a function of the internal state variables of the model [i.e. density, number of HB, number of site contacts; see points (b), (c) and (d) in the next paragraph], at fixed pressure, temperature and concentration.

In summary, the set of coupled non linear algebraic equations to be solved to determine the water solubility in a rubbery polymer according to the NRHB model is the following:

(a) equivalence of chemical potentials of water in the pure gas phase (μ_1^{GAS}) and in the polymer phase (μ_1^{POL}).

(b) Equations of State for the vapour and for the polymer mixture phases. The EoS in each phase formalizes the Gibbs energy minimization condition as a function of the internal state variable represented by the density. These equations solved simultaneously with the set of equations (a), (c) and (d) provide the density of the two phases at equilibrium.
(c) Equations formalizing the minimization condition of the Gibbs energy as a function of the set of internal state variable $\underline{N}_{ij}$ whose component *i*-*j* expresses the number of HB between proton donors of kind *i* and proton acceptors of kind *j* present in the phase investigated. These equations, solved simultaneously with the set of equations (a), (b) and (d) provide the number of the different kind of hydrogen bonds established in the two phases at equilibrium.
(d) Equations representing the Gibbs minimization condition as a function of the set of internal state variables $\underline{N}_{rs}^{NR}$ whose generic component *r*-*s* expresses the number of lattice contacts between mers of kind *r* and mers of kind *s* (including voids as tipology of mers). It is worth noting that the vector variable $\underline{N}_{rs}^{NR}$ contains only a subset of independent N_{rs}^{NR} as determined by the material balance equations (see Ref. [10]). In particular, the related internal state variables Γ_{00} and Γ_{11} appearing in the equations are, respectively, the non-random factors for the distribution of an empty site around another empty site and of molecular segments of penetrant around a molecular segment of the penetrant itself, in the two phases [10].

Relevant parameters of the model are:

1. k_{12}, (or, equivalently, $\psi_{12} = 1 - k_{12}$) that is the mean field lattice fluid interactional parameter which measures the departure of the mixing rule for the characteristic energies of the lattice fluid from the geometric mean:

$$\varepsilon_{12}^{*} = (1 - k_{12})\sqrt{\varepsilon_{11}^{*}\varepsilon_{22}^{*}} \tag{4}$$

2. E_{ij}^{0}, S_{ij}^{0} and V_{ij}^{0} representing, respectively, the molar internal energy of formation, the molar entropy of formation and the molar volume change upon formation of hydrogen bonding between the proton donor group of type *i* and the proton acceptor group of type *j* present in the system investigated.

It is important to note that the LF models, such as the NRHB theory, are in principle only suitable for totally amorphous rubbery polymer-penetrant mixtures and do not account for the presence of crystalline domains. For the sake of interpretation of experimental water sorption isotherms in semi-crystalline polymers whose amorphous phase is in a rubbery state—as is the case of water sorption in the semi-crystalline PCL in the present contribution—crystals can be modelled as being impervious to the penetrant and therefore the overall solubility is predicted by

rescaling the solubility of the pure amorphous phase to account for the presence of the crystalline fraction. The solubility in the amorphous phase is hence calculated using the approaches illustrated above, simply assuming that the presence of crystals does not alter the thermodynamic behaviour of the amorphous domains. Although this assumption could be considered questionable, it has been proven to be the most reliable choice as discussed in detail in the literature [16, 17].

In this contribution NRHB model has been adopted to investigate water sorption thermodynamics in semi-crystalline PCL.

2.2 Glassy Polymers: The NETGP-NRHB Model

Polymers in the glassy state display physical properties which significantly differ from those of the same polymer in the rubbery state. Consistently, also sorption thermodynamics differ substantially and modelling should properly account for non-equilibrium state. In particular, modelling thermodynamics of water sorption in glassy polymers displaying possible HB interactions is characterized by a twofold theoretical complexity: need to account for the out-of-equilibrium state of the glassy system and need to account for the occurrence of specific interactions.

A first successful and simple way to describe the sorption of penetrants within glassy polymers is represented by the so-called *Dual Sorption* model [18, 19]. Sorption of penetrants is assumed as being contributed by two 'populations': one is made of penetrant molecules molecularly dispersed in the bulk of polymer matrix, assumed to behave like an equilibrium rubbery system, and the other is made of penetrant molecules adsorbed onto the surfaces of the frozen micro-voids, which are intrinsically associated to the glassy state. Accordingly, the model is in the form of the sum of two contributions: the first is typically based on a mean field equilibrium approach, while the second one is in the form of a Langmuir-type adsorption contribution. In the case of interacting polymer-penetrant glassy systems (such as the case of water in hydrophilic polymers) the *Dual Sorption* model can be integrated with a second, additional, Langmuir's contribution accounting for the presence of specific adsorption sites where penetrant molecules establish interactions with chemical moieties present on polymer backbone.

Although rather successful in supplying a physically sound framework to interpret sorption in glassy polymers, *Dual Sorption* approach is suitable for correlation purposes but it is not predictive. Furthermore it does not account for the occurrence of possible penetrant clustering phenomena [20].

A more consistent approach is provided by a theoretical framework aimed at extending the equilibrium mixture theories suitable for rubbery polymers to the non-equilibrium glassy polymer-penetrant mixtures, by introducing internal state variables which act as *order parameters* quantifying the departure from the equilibrium conditions at fixed pressure and temperature. In this respect, Doghieri and Sarti [21, 22] have proposed the use, as *order parameter,* of the density of the polymer in the mixture and developed a procedure to extend equilibrium statistical

thermodynamics theories to non equilibrium glassy systems (the so-called NETGP model). Following this line of thought more recently Scherillo et al. have proposed [17, 23] the extension of NRHB theory to non equilibrium glassy systems to provide a suitable model for sorption of HB interacting penetrants in glassy polymers (the so-called NETGP-NRHB model). In the following we briefly report the development of NETGP-NRHB model referring to Ref. [17] for full details.

To extend to non-equilibrium the equilibrium statistical thermodynamics NRHB theory, it has been taken [21, 22] as non-equilibrium Gibbs energy the general expression derived for it from the developments of statistical thermodynamics, before the application of the minimization conditions that mark the equilibrium state. The constitutive class identifying the system, in the case of a spatially uniform phase, is considered to be the following set of variables: temperature (T), pressure (p), number of moles of penetrant (n_1), number of moles of polymer (n_2), density of the polymer in the mixture (ρ_2), set of number of HBs $\underline{N}_{ij}$ and set of effective number of nonrandom contacts $\underline{N}_{rs}^{NR}$. In such a case, the *internal state variables* to be selected for the description of the non-equilibrium state naturally emerge as the set of variables for which the minimization procedure is performed to obtain the equilibrium expression for G. In the case of NRHB model, ρ_2, $\underline{N}_{ij}$ and $\underline{N}_{rs}^{NR}$ can all be selected as *internal state variables* (see Ref. [17] for a more detailed discussion about the choice of possible *internal state variables* of the model). At equilibrium their value is only related to the equilibrium state variables through the minimization conditions for G mentioned in Sect. 2.1. Conversely, in non-equilibrium conditions, their values are dictated by the intrinsic evolution kinetics that, consistently with theory of *internal state variables*, must depend only on the actual state of the system.

Expressions for the evolution kinetics of the *internal state variables* hence need to be introduced. Regarding both the sets $\underline{N}_{ij}$ and $\underline{N}_{rs}^{NR}$ it is assumed, to simplify the matter, that an 'instantaneous' evolution kinetics holds for them. As a consequence, the HB contacts, $\underline{N}_{ij}$, and the non random contacts, $\underline{N}_{rs}^{NR}$, are the ones which the system would exhibit at equilibrium at the current values of pressure, temperature, number of moles of components and polymer density (this is referred as "instantaneous equilibrium" hypothesis, IE). In other words their values are obtained by using the minimization equations of points (c) and (d) of Sect. 2.1. With this assumption NETGP NRHB model formally displays the same constitutive class of the original NETGP theory of Doghieri et al. [21, 22] provided that the general non equilibrium expression of Gibbs energy is substituted by its IE form, i.e.:

$$\begin{aligned} G^{IE} &= g\left(T, p, n_1, n_2, \rho_2, \underline{N}_{rs}^{IE,NR}(T, p, n_1, n_2, \rho_2), \underline{N}_{ij}^{IE,HB}, (T, p, n_1, n_2, \rho_2)\right) \\ &= g^{IE}(T, p, n_1, n_2, \rho_2) \end{aligned} \tag{5}$$

Consistently, the rate of variation of ρ_2, which is a function of the state, becomes:

$$\begin{aligned}\frac{d\rho_2}{dt} &= f\left(T, p, \omega_1, \rho_2, \underline{N}_{rs}^{IE,NR}(T, p, \omega_1, \rho_2), \underline{N}_{ij}^{IE,HB}(T, p, \omega_1, \rho_2)\right) \\ &= f^{IE}(T, p, \omega_1, \rho_2)\end{aligned} \tag{6}$$

where ω_1 is the mass fraction of penetrant and the superscript IE in Eqs. (5) and (6) underlines that we are referring to the "instantaneous equilibrium" form for the dependence of $\underline{N}_{ij}$ and $\underline{N}_{rs}^{NR}$.

Although ρ_2 is, in the general formulation, a time dependent property characterized by a thermodynamically consistent kinetic expression [22], in the applications of the model to polymer systems well below glass transition temperature, it is frequently assumed that f takes a value close to zero due to the very slow relaxation kinetics of glassy polymers and ρ_2 is assumed to take a constant non-equilibrium value, referred to as $\rho_{2,\infty}$. This value has not to be confused with the equilibrium value, i.e. ρ_2^{EQ}, and it cannot be determined by using an equilibrium EoS. It is, hence, generally assumed that the polymer mixture is in a pseudo-equilibrium (PE) state for which:

$$\frac{d\rho_2}{dt} \cong 0 \tag{7}$$

$$\rho_2 = \rho_{2,\infty} \neq \rho_2^{EQ}(T, p, \omega_1) \tag{8}$$

For non-swelling penetrants $\rho_{2,\infty}$ can be simply considered as being equal to the value it takes for the pure polymer, ρ_2^0. Conversely, when penetrants induce a non negligible swelling, its value needs to be retrieved from dilation measurements on the mixture or, at low pressures, can be calculated using the simple expression [24]:

$$\rho_{2,\infty}(p) = \rho_2^0(1 - k_{sw}p) \tag{9}$$

where k_{sw} is the swelling coefficient, that can eventually be used as a fitting parameter for sorption isotherms. The kinetically hindered polymer-penetrant mixture, when in contact with an external phase of pure penetrant, reaches a phase pseudo-equilibrium (pseudo equilibrium attribute is used here since the mixture is itself in a pseudo-equilibrium glassy state). In the hypothesis that the polymer is insoluble in the external (*EXT*) penetrant phase, it can be demonstrated [22] that the thermodynamic condition for phase PE is still dictated by:

$$\mu_1^{POL}\left(T, p, \omega_1^{PE}, \rho_{2,\infty}\right) = \mu_1^{EXT}(T, p) \tag{10}$$

where the superscript PE has been used here to underline the fact that the value of the mass fraction of penetrant which satisfies the condition given by Eq. (10) is, actually, a PE value. The equilibrium penetrant potential in the pure external phase

μ_1^{EXT} is provided by the NRHB theory and, being an equilibrium value, it is only dependent upon T and p.

On the other hand, in view of the IE hypothesis it is possible to show (see Ref. [17] for details) that the expression for μ_1^{POL} is given by:

$$\begin{aligned}\frac{\mu_1^{POL}}{RT} &= \ln\frac{\phi_1}{\delta_1 r_1} - r_1\sum_{j=1}^{2}\frac{\phi_j l_j}{r_j} + \ln\tilde{\rho} + r_1(\tilde{v}-1)\ln(1-\tilde{\rho}) \\ &- \frac{z}{2}r_1\left[\tilde{v}-1+\frac{q_1}{r_1}\right]\ln\left[1-\tilde{\rho}+\frac{q}{r}\tilde{\rho}\right] \\ &+ \frac{zq_1}{2}\left[\ln\Gamma_{11}+\frac{r_1}{q_1}(\tilde{v}-1)\ln\Gamma_{00}\right] \\ &- \frac{q_1}{\tilde{T}_1} + \tilde{T}\left[\begin{array}{c}\ln(1-\tilde{\rho}) - \tilde{\rho}\left(\sum_i \phi_i\frac{l_i}{r_i}\right) \\ -\frac{z}{2}\ln\left(1-\tilde{\rho}+\frac{q}{r}\tilde{\rho}\right)+\frac{z}{2}\ln\Gamma_{00}\end{array}\right]\cdot\frac{rx_2\cdot\left.\frac{\partial\tilde{v}}{\partial x_1}\right|_{P,T,\rho_2,\underline{N}_{ij},\underline{N}_{rs}^{NR}}}{\tilde{T}} + \frac{\mu_{1,HB}^{POL,}}{RT}\end{aligned} \tag{11a}$$

where

$$\begin{aligned}\frac{\mu_{1,HB}^{POL}}{RT} &= r_1 v_H - \sum_i^m d_i^1\ln\left(\frac{v_d^i}{v_{i0}}\right) - \sum_j^n a_j^1\ln\left(\frac{v_a^j}{v_{0j}}\right) \\ &+ v_H\left.\frac{\partial\ln\tilde{v}}{\partial x_1}\right|_{P,T,\rho_2,\underline{N}_{ij},\underline{N}_{rs}^{NR}} x_2 r\end{aligned} \tag{11b}$$

It is worth noting that Eq. (11a) has to be calculated at $\rho_2 = \rho_{2,\infty}$.

In summary, the set of equations to be solved to predict, in PE conditions, sorption isotherms of a penetrant in a glassy polymer exhibiting HB interactions, is made of:

(a) equation expressing the equivalence of penetrant chemical potential in the gas phase (μ_1^{EXT}) and polymer phase (μ_1^{POL}).
(b) Minimization conditions for $\underline{N}_{ij}$ and $\underline{N}_{rs}^{NR}$ for the polymer phase and for the penetrant vapour phase.
(c) NRHB EoS for the vapour phase.

The model described in this section for the case of glassy polymers is suited only for amorphous polymers. As already discussed for the case of rubbery polymers, also in the case of semi-crystalline polymer-penetrant mixtures in which the amorphous phase is in a glassy state, it is assumed here that the overall PE solubility can be still predicted by simply rescaling the solubility of the pure amorphous phase to account for the presence of the crystalline fraction. It is hence hypothesized that only the crystalline and amorphous phases are present, neglecting the occurrence of

a third 'interphase'. In this respect it is worth noting that in the case of glassy systems the PE density $\rho_{2,\infty}$ to be used represents the one of the actual amorphous phase of the semi-crystalline polymer. As a first approximation, its value can be retrieved by information on the overall density of semi-crystalline polymer, once the degree of crystallinity and the density of the pure crystalline phase are available. An example of this procedure is illustrated in the section devoted to water sorption in semicrystalline PEEK.

In this contribution NETGP NRHB model has been adopted to investigate water sorption thermodynamics in amorphous glassy polyimides and in a semicrystalline PEEK. In the case of a glassy epoxy water sorption thermodynamics is only analysed experimentally in view of the unavailability of dilatometric data in the rubbery state, which are needed to determine the EoS parameters. This is due to chemical degradations occurring in these polymers at the high temperatures required to reach the equilibrium rubbery state.

2.3 Evaluation of Tg Depression

One of the most relevant physical effects of the presence of absorbed penetrants in glassy polymers is the decrease of T_g, a phenomenon that is known as *plasticization*. Although we will not discuss here any experimental data on T_g change promoted by water sorption, we think it is worth presenting theoretical developments on this issue related to the NRHB thermodynamic approach.

The first theories developed to predict the plasticization accounted only for the concentration of absorbed penetrant while more recent approaches, grounded on the EoS theories developed for the interpretation of sorption thermodynamics, account also for the effect of the mechanical action of pressure that, in some operative environments, can be quite high.

One of the first models for glass transition rooted on a thermodynamic framework is the theory of Gibbs and Di Marzio [25–27]. This LF theory assumes the occurrence of a true thermodynamic second order transition, for a fixed composition and pressure, at a temperature T_2 where the equilibrium configurational entropy of the system becomes equal to zero: at temperatures below or equal to T_2 the system is frozen in an out-of equilibrium state. The measurable T_g is higher than T_2: it is a kinetically affected, experimentally accessible, value for T_2 which represents the lower bound of the actually detectable T_g.

The criterion for the identification of the glass transition temperature for pure polymers and polymer-penetrant mixtures as the point at which the equilibrium configurational entropy becomes zero, can be extended to other thermodynamic models able to supply an expression for entropy. According to this line of thought the models of Chow [28], Gordon [29], and Ellis and Karasz [30–32] were developed. In a more recent series of papers [9, 33, 34] Panayiotou and co-workers used the NRHB lattice fluid model to calculate the entropy of pure amorphous polymers and of polymer-penetrant mixtures and, in turn, to evaluate T_g according

to the Gibbs–Di Marzio procedure. In order to perform the calculation of the T_g of the mixture, the flex energy of the pure polymer is needed. It can be typically calculated by equating the entropy of the pure polymer to zero at atmospheric pressure, if the T_g of the pure polymer is known. It is worth noting that the NRHB model accounts also for specific hydrogen bonding interactions and hence it has the distinctive feature of being able to supply an expression for T_g suited for systems displaying such specific interactions. This is a relevant result to the aim of assessing environmental resistance of composite matrices.

According to the NRHB model, the expression of the entropy of a polymer-penetrant mixtures can be expressed as the sum of three contributions:

$$S_{tot} = S_r + S_{nr} + S_{HB} \tag{12}$$

In the previous expression S_{tot} is the total configurational entropy of the system, S_r is a *randomicity* contribution, S_{nr} is a contribution related to *non-randomicity* of the site contacts in the lattice and S_{HB} is the hydrogen bonding contribution involved in the system. For a binary polymer-penetrant mixture, the NRHB non equilibrium expressions for these contributions are:

$$\begin{aligned} S_r/(RrN) = &\sum_{i=1}^{2}\left(\frac{\phi_i}{r_i}\right)\ln\delta_i + (1-\tilde{v})\ln(1-\tilde{\rho}) + (l+\ln(r\tilde{v}))/r \\ &- \sum_{i=1}^{2} x_i \ln x_i + (z/2)(\tilde{v}-1+q/r)(1-\tilde{\rho}+q/r) \end{aligned} \tag{13a}$$

$$\begin{aligned} S_{nr}/(RrN) = &(z/2)[-(\tilde{v}-1)\ln(\Gamma_{00}) - (q_1/r_1)\phi_1\ln(\Gamma_{11}) \\ &- (q_2/r_2)\phi_2\ln(\Gamma_{22}) + (\tilde{v}-1)(\Theta_1\Theta_r\ln(A_{01})\Gamma_{01} \\ &+ \Theta_2\Theta_r\ln(A_{02})\Gamma_{02}) + (q_1/r_1)\phi_1\Theta_2\Theta_r\ln(A_{12})\Gamma_{12}] \end{aligned} \tag{13b}$$

$$\begin{aligned} S_{HB}/(RrN) = &-\sum_{\alpha=1}^{m}\sum_{\beta=1}^{n}\upsilon_{\alpha\beta} - \sum_{\alpha=1}^{m}\upsilon_d^{\alpha}\ln\left(\frac{\upsilon_{\alpha o}}{\upsilon_d^{\alpha}}\right) \\ &- \sum_{\beta=1}^{m}\upsilon_a^{\beta}\ln\left(\frac{\upsilon_{0\beta}}{\upsilon_a^{\beta}}\right) + \left(\sum_{\alpha=1}^{m}\sum_{\beta=1}^{n}\upsilon_{\alpha\beta}H^0_{\alpha\beta}\right)/RT \end{aligned} \tag{13c}$$

In Eq. (13a)

$$\begin{aligned} \ln\delta_i = &\ln(Z) + f_i r_i \ln(Z-2) - f_i r_i \ln(f_i) \\ &- r_i(1-f_i)\ln(1-f_i) - f_i r_i u_i/(RT) \end{aligned} \tag{14a}$$

with

$$f_i = \frac{(Z-2)\exp(-u_i/(RT))}{(Z-2)\exp(-u_i/(RT)) + 1} \tag{14b}$$

where u_i represents the flex energy of bond i.

In order to obtain the expression for the equilibrium total configuration entropy the Eqs. (12–14b) must be coupled with the NRHB minimization equations reported in Sect. 2.1. For the complete description of the symbols in Eqs. (12–14b) the reader is referred to the relevant literature on NRHB [9–11]. Equation (13a) has been obtained by the authors of the present contribution in cooperation with prof. Tsivinzelis and it has been reported for first time in [35]. Note that Eq. (13c) is different from the corresponding expression erroneously reported, due to misprints, in the literature [35, 36].

In the case of crosslinked systems, a further term needs to be added to Eq. 13a–13c, i.e.:

$$S_{cross}/(RrN) = -\frac{3}{2}R\left(\frac{v_e}{M_2}\right)\phi_2\rho_2^*v^*\left(\alpha^2 + \frac{1}{\alpha^2} - 2 + \log\alpha\right) \tag{13d}$$

The theories illustrated so far are based on an equilibrium thermodynamics approach. Alternative models have been proposed rooted on molecular mobility arguments [37] based on the free volume theory originally developed by Turnbull and Cohen [38, 39].

A final point that is worth mentioning here concerns the effect of the presence of crystalline regions on the T_g of the amorphous phase. Actually, the crystalline regions place a constraint to the mobility of the amorphous phase and influence its conformational motions. As a consequence one cannot rule out the possibility that this constraint could affect the reliability the procedures illustrated above for the prediction of T_g change. This is a controversial point and it is expected that extension to semi-crystalline polymers of the models mentioned above is not a trivial task.

2.4 Combined Theoretical/Experimental Procedure

The theoretical approach illustrated in Sects. 2.1 and 2.2 has been used to analyze water sorption thermodynamics in several polymer systems in combination with experimental investigation based on vibrational spectroscopy and gravimetric measurements. A summary of the steps of the combined theoretical/experimental procedure is reported below:

1. The wealth of information available from FTIR in situ spectroscopy is used to identify proton donor and acceptor groups present on polymer backbone as well as the kinds of water species as distinguished by the number of hydrogen bonds they form in cross- and self-interactions.
2. Based on this information, model is tailored by specifying the number of possible types of HB interactions.
3. Once the model structure has been built up, gravimetric sorption isotherms data can be interpreted thus determining the mean field interaction parameter and the HB interaction parameters, by a fitting procedure.

4. At this stage the theoretical model is completely specified and can be used to provide a quantitative prediction of the amount of each type of HB interaction as a function of water vapour activity.
5. Self consistency of the thermodynamic theory can be hence assessed by comparing this prediction with results of the vibrational spectroscopy analysis. In fact, on the grounds of the results of 2D-COS as well as of quantitative elaboration of spectra based on determination of molar absorptivity of each water species derived from calibration against gravimetric data, an estimate of the amount of each type of HB interaction is provided.

Details of the experimental procedures are reported in the following sections.

2.4.1 In-Situ FTIR Time-Resolved Transmission Spectroscopy and 2D Correlation Spectroscopy

A custom built cell, operating at controlled relative humidity and temperature, was used to perform the time-resolved acquisition of FTIR spectra during the sorption experiments. The cell, positioned in the sample compartment of the spectrometer, was connected through service-lines, to a water reservoir, a turbo-molecular vacuum pump, and pressure transducers. Data collection on the polymer films exposed to water vapour at constant relative pressures (relative pressure, also referred to as relative humidity, is given by the ratio p/p_0, where p is the pressure of water vapour and p_0 is vapour pressure of water at the temperature of the test) was carried out in the transmission mode. A single data collection per spectrum was performed, which took 2.0 s to complete in the selected instrumental conditions. Full absorbance spectra (i.e. polymer plus absorbed water) were obtained using as background the cell without sample at the test conditions. The spectra representative of absorbed water were then obtained by using as background the single-beam spectrum of the cell containing the dry polymer film. This allows one to eliminate the interference of the polymer spectrum in the regions of interest. It is explicitly noted that this data processing approach is equivalent to the more general difference spectroscopy method provided that no changes in sample thickness take place during the measurement. Curve fitting analysis of difference spectra was performed by a Levenberg–Marquardt least-squares algorithm [40, 41]. The peak function used throughout was a mixed Gauss-Lorentz line shape.

2D-Correlation Spectroscopy (2D-COS) is a technique capable of improving the resolution by spreading the data over a second frequency axis. In particular, we have examined the asynchronous spectrum, that is characterized by the fact that a peak in this spectrum at $[\nu_1, \nu_2]$ corresponds to two IR signals changing at different rates. On the other hand, a zero intensity is obtained when two signals change at the same rate, thus providing the characteristic resolution enhancement and the specificity of the asynchronous pattern. Moreover, the sign of the asynchronous peaks supplies information about the sequence of changes of the two correlated IR

signals, according to the so-called Noda rules [42, 43]. In all the cases illustrated in this contribution, 2D-COS analysis was performed on an evenly spaced sequence of 20 spectra collected with a sampling interval of 12 s.

2.4.2 Gravimetric Analysis

Gravimetric water sorption isotherms were obtained using an electronic microbalance D200 from Cahn Instruments (Madison, WI) providing a sensitivity of 0.1 μg with an accuracy of ±0.2 μg. The weight gain of the sample exposed to a controlled humidity environment was determined as a function of time after each step increase of pressure of water vapour. Equilibrium sorption values were taken at each relative humidity as those attained by the sample after its weight remained constant for a time interval equal at least to twice the time needed to get to that value within ±0.4 μg.

3 Experimental and Theoretical Analysis of Different Systems

3.1 Glassy Polymers

3.1.1 Polyimide-Water System

Water sorption thermodynamics has been investigated in three glassy polyimides with an increasing amount of fluorine atoms in the polymer backbone, i.e. PMDA-ODA obtained by thermal imidization of its polyamic acid precursor, Pyre-ML RK692 from IST, Indian Orchard, MA (no F atoms, T_g = 383 °C). 6FDA-ODA (2 F atoms per repeating unit, T_g = 308 °C) and 6FDA-6FpDA (4 F atoms per repeating unit, T_g = 315 °C) obtained by thermal imidization of polyamic acid precursors which were synthesized from the respective dianhydride and diamine monomers [(hexahydrofluoroisopropylidene) diphthalic anhydride (6FDA), 4,4′-diaminodiphenyl ether (ODA), 4,4′-(hexafluoroisopropylidene) dianiline (6FpDA)], according to the procedures described in Ref. [44].

The suppression of the polymer matrix interference by use of difference spectroscopy, allows one to isolate the spectrum of absorbed water in the different environments. In the present context it is of particular interest the OH stretching region, ν_{OH}, of the spectrum of absorbed water (i.e. the 3,800 – 3,200 cm^{-1} region). The spectra reported in Fig. 2 evidence significant differences in terms of total absorbed water among the three investigated polyimides. As expected, the amount of absorbed water decreases considerably with increasing the fluorine content. The occurrence of distinct water species involved in H-bonding

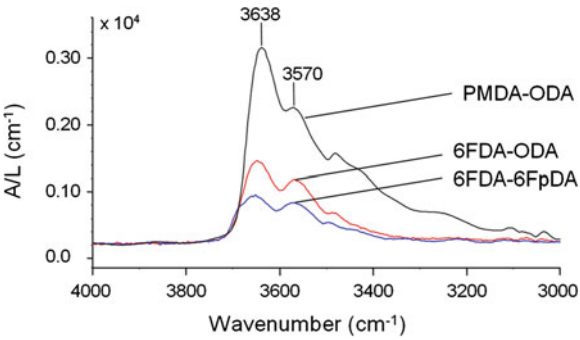

Fig. 2 Difference spectra (wet–dry) normalized for the sample thickness, representative of water absorbed in the three investigated polyimides. 4,000–3,000 cm^{-1} wavenumber range. Spectra denoted as wet were collected at equilibrium at $p/p_0 = 0.6$

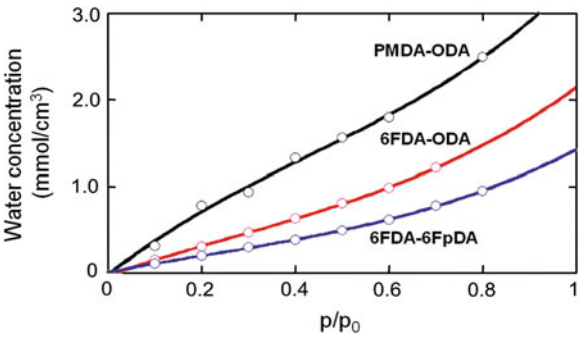

Fig. 3 Gravimetric water sorption isotherms for the three investigated polyimides. *Lines* represent only a guide for the eye

interactions is indicated by the fact that profiles display a complex, well-resolved band-shape.

Gravimetric sorption isotherms are reported in Fig. 3, confirming that the highest sorption capacity is shown by PMDA-ODA and the lowest by 6FDA-6FpDA. The upturn present in sorption isotherms at high relative pressure is likely due to the gradual onset of penetrant clustering or self-association, as will be confirmed by the analysis of spectroscopic data.

The correlations between the absorbance area of the ν(OH) band and the water concentration evaluated gravimetrically show that the three data sets can be accommodated on a single master curve, after absorbance normalization for sample thickness [45]. A significant departure from linearity (presence of an upturn) in this correlation is observed for concentration values exceeding 0.75 mmol/cm^3. The very high correlation degree between the spectroscopic and gravimetric data relative to the three polyimides for the stretching frequency range, points to the conclusion that for this vibrational mode the absorptivity values of the different water species are independent of the particular polyimide system. The mentioned upturn at higher values of water concentration qualitatively indicates an increase in the relative concentration of water species characterized by higher absorptivity values.

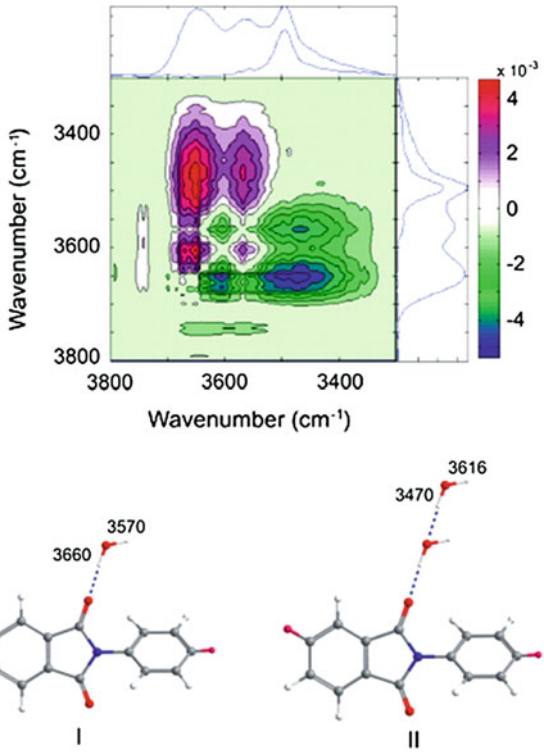

Fig. 4 *Top* 2D-FTIR correlation spectra (asynchronous) obtained from the time-resolved spectra collected during water sorption in 6FDA-ODA polyimide at a relative pressure = 0.6. *Bottom* Schematic representation of the H-bonding interactions in the investigated water/6FDA-ODA system (schemes I and II)

To elucidate the number and types of absorbed water species, 2D-COS has been performed on the three sets of data [45]. An example of correlation spectra as calculated for the case of 6FDA-ODA, is reported in Fig. 4. From the 2D results obtained from the elaboration of the spectra collected for the three investigated polyimides, it is found the presence of two couples of signals: one at 3,660 – 3,570 cm^{-1} and one at 3,616 – 3,456 cm^{-1}. The two components of each couple change at the same rate, but the two couples exhibit a different dynamics. These results can be interpreted by assuming that two different water species occur. While this pattern is common to both PMDA-ODA and 6FDA.ODA, in the case of 6FDA-6FpDA two additional correlation peaks are found indicating the presence of a further component at 3,700 cm^{-1}. The vibrational assignment of the identified signals can be performed only after the identification of interaction sites active on the macromolecule. A detailed analysis [45] of vibrational spectroscopy results indicated that the imide carbonyls are involved in HB interactions as proton acceptor groups, while the involvement of ether group (in the case of PMDA-ODA and 6FDA-ODA) as proton acceptor in H-bonding can be safely neglected.

On the basis of these findings, one can propose likely structures for the H-bonding aggregates that are formed in the investigated systems. In fact, the couple of water signals at 3,660 – 3,570 cm^{-1}, identified in all the three polyimides, can be

associated, respectively, to the out-of-phase and in-phase stretching modes of water molecules bound to imide carbonyls via a H-bonding interaction (see structure I in Fig. 4). The two peaks, present in all the three polyimides at 3,616 and 3,470 cm^{-1}, can be associated to self-associated water in the prevalent form of dimers (see structure II in Fig. 4). Concerning the signal identified only for 6FDA-6FpDA no definitive assignment can be provided. A detailed discussion on this point is available in [45].

With the aim of quantifying the concentration of the different water species, attention has been focused on ν_{OH} range. In particular two analytical peaks characteristic of the species to be quantified, i.e., at around 3,568 cm^{-1} for the monomer and at 3,495 cm^{-1} for the dimer, have been chosen.

The total integrated absorbance, A_{TOT}, in the ν_{OH} range can be expressed as:

$$\frac{A_{TOT}}{L} = \sum_{i=1}^{N} \varepsilon_i C_i \tag{14}$$

where C_i is the molar concentration of the i-th component, ε_i is the associated molar absorptivity, L is the sample thickness, and N represents the number (two, in the case at hand) of individual components in which the experimental profile has been decomposed. By interpreting the experimental data for $\frac{A_{TOT}}{L} = \frac{A_{3,568}+A_{3,495}}{L}$ as a function of total water concentration, an estimate of the values of molar absorptivities can be obtained, thus allowing the evaluation of the concentration of each species.

With the aim of comparing these results with the predictions of the NETGP–NRHB model, these data have been re-elaborated to convert the concentration of the different water species into the outcome of the model, that is the number of self- and cross-HB established within the polymer–water mixture. In particular, we have calculated the number of moles of self-HB of water normalized per mass of polymer (n_{11}^{wp}/m_2, where m_2 represents the mass of polymer) and the number of moles of cross HB occurring between the proton donor groups of water molecules and the proton acceptor groups present on the polymer backbone, normalized per mass of polymer (n_{12}^{wp}/m_2). The calculation is rather straightforward in the case of dimeric water: in fact a 1:1 ratio can be safely assumed between the number of water molecules forming the "second shell" and the number of self-HB that they establish with water molecules interacting with carbonyls. In the case of water molecules bound to carbonyls, it has been assumed a single water molecule to form two H-bonding interactions with two distinct carbonyls (i.e., a 1:2 stoichiometry), thus "bridging" two functional groups. This bridging is statistically favoured as compared to the 1:1 stoichiometry due to the large excess of carbonyl groups with respect to absorbed water. This picture is supported by a spectroscopic investigation performed by Iwamoto and Masuda [46] proving that in polymers characterized by a dense distribution of carbonyl groups, like poly vinyl acetate (PVAc) and poly methyl methacrylate (PMMA), dissolved water is generally

hydrogen bonded through each OH to two C=O. Data re-elaborated in the form of normalized amount of cross- and self-HB are reported in Fig. 5.

Gravimetric sorption isotherms have been then interpreted with NETGP-NRHB model. To this aim, scaling parameters of NRHB equation of state for pure polymers (i.e. ε_h^*, ε_s^* and $v_{sp,0}^*$) have been first determined by fitting experimental PVT data at high pressures (up to 2,000 atm) in the rubbery state (see [17]). This analysis was possible only in the case of 6FDA-ODA and 6FDA-6FpDA (results reported in Table 1) since in the case of PMDA-ODA degradation occurs in the proximity of its glass transition temperature, thus making it impossible to perform PVT characterization in the rubbery state. As a consequence, the comparison between NETGP-NRHB model and spectroscopic data(see Fig. 5) was limited to the case of fluorinated polyimides. For the case of water, the three LF scaling parameters and the two hydrogen bonding parameters have been taken from literature [47] and are reported in Table 1 as well.

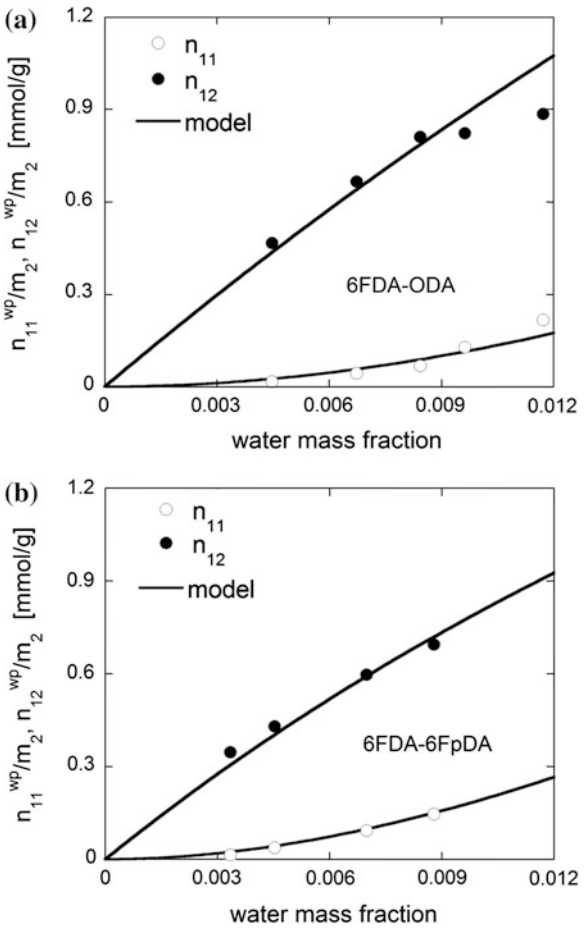

Fig. 5 Comparison of predictions of NETGP–NRHB model with experimental results for (*top*) 6FDA-ODA and (*bottom*) 6FDA-6FpDA

Table 1 NRHB parameters for pure polymides and pure water

Component	ε_s^* (J/mol)	ε_h^* (J/mol K)	$v_{sp,0}^*$ (cm^3/g)	E_{11}^{0w} (J/mol)	S_{11}^{0w} (J/mol K)	V_{11}^{0w} (cm^3/mol)	S
6FDA-ODA	5,988.5	4.3186	0.5736			–	0.7802[b]
6FDA-6FpDA	5,471.1	3.8652	0.5174			–	0.7757[b]
Water[a]	5,336.5	−6.506	0.9703	−16,100	−14.7	0	0.8610

[a] From Ref. [47]

[b] Calculated using group contribution calculation scheme UNIFAC (see Ref. [48, 49])

In the implementation of NETGP–NRHB model, in view of the small amount of absorbed water, the swelling coefficient, k_{sw}, has been taken equal to zero. Furthermore, following the assumptions made by Tsivintzelis et al. [47] $V_{11}^{0,wp}$ and $V_{12}^{0,wp}$ have been both taken as being equal to zero. Only two fitting parameters are then needed to model water sorption isotherms, i.e. the mean-field polyimide/water interaction parameter, $\psi_{12} = 1 - k_{12}$, and the molar Helmholtz energy of formation of polymer/water HB interaction, $A_{12}^{0,wp}$. In fact, since sorption data were taken only at one temperature (30 °C), it is not possible to separate the contributions of molar internal energy of formation of cross-HB interaction from the entropic one. Both these parameters are lumped in $A_{12}^{0,wp}$.

It is explicitly noted that, based on the spectroscopic findings, four proton acceptor groups (i.e., carbonyl groups) per repeating unit have been assumed to be present on the polymer backbone while two equivalent proton donor groups and two equivalent proton acceptor groups to be present on each molecule of water [10]. The NETGP–NRHB model supplies a good fitting capability of water sorption isotherms in both 6FDA-ODA and 6FDA-6FpDA. In Fig. 6 is reported

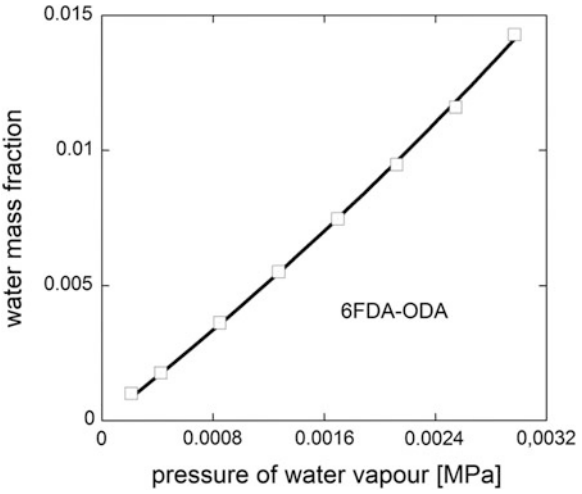

Fig. 6 Fitting of experimental water sorption isotherms for 6FDA–ODA. Continuous line represents fitting curve provided by NETGP–NRHB model

Table 2 NETGP-NRHB parameters for polyimide-water mixtures as obtained from data fitting of experimental sorption isotherms

System	ψ_{12}	A_{12}^{0wp} (J/mol)
6FDA-ODA/water	0.787	−12,400
6FDA-6FpDA/water	0.869	−12,100

the case of water sorption isotherm in 6FDA-ODA. The calculated values for best fitting parameters are reported in Table 2.

3.1.2 PEEK-Water System

Nominally amorphous PEEK films (Goodfellow Co., PA, USA) with a thickness of 12.5 μm were used in this investigation. A crystalline degree, χ_c, equal to 0.057 has been actually estimated on the basis of differential scanning calorimetry using information on enthalpy of melting available in [50]. This value has been used to scale the overall water solubility evaluated gravimetrically at different temperatures and relative humidity values, in order to obtain water solubility value referred to the sole amorphous phase. Also in this case, the NETGP-NRHB model has been used to interpret sorption thermodynamics of water in amorphous PEEK. To this aim, the "frozen" polymer density of the glassy amorphous phase of the polymer in the mixture was taken equal to that of the amorphous phase of pure polymer, $\rho_{2\,am}^0$, since no significant swelling is induced by water in view of the low concentration.

The density of the amorphous phase, ρ_{2am}^0, at 27.2 °C has been estimated to be 1.2695, using Eq. (15) that has been derived on the basis of the assumption that the volume of the semi-crystalline PEEK is the sum of those of the amorphous and crystalline phases i.e.:

$$\frac{1}{\rho_{2am}^0} = \frac{1}{(1-\chi_c)}\left(\frac{1}{\rho_2^0} - \chi_c \frac{1}{\rho_{2cr}^0}\right) \tag{15}$$

The theoretical value of density of pure crystalline phase ρ_{2cr}^0, has been taken equal to 1.400 (g/cm^3) from Ref. [51], while the overall density of the semicrystalline sample, ρ_2^0, has been evaluated to be 1.2763 g/cm^3 by Helium picnometry performed at 27.2 °C.

The values of ρ_{2am}^0 at the four temperatures at which the water sorption thermodynamics has been investigated (30, 45, 60 and 70 °C), have been then calculated, starting from its value at 27.2 °C, on the basis of the thermal expansion coefficient of the amorphous PEEK taken from Ref. [52] and are reported in Table 3.

In defining the relevant HB interactions occurring in the system to be used in the NETGP-NRHB approach, it has been assumed that self HB interaction take place only between water molecules involving the two proton donor groups and

Table 3 Densities (g/cm^3) of the amorphous phase of the investigated PEEK at the four temperatures of interest

T = 30 °C	T = 45 °C	T = 60 °C	T = 70 °C
1.2688 ± 0.001	1.2652 ± 0.001	1.2617 ± 0.001	1.2593 ± 0.001

Table 4 NRHB parameters for PEEK

Component	ε_s^* (J/mol)	ε_h^* (J/mol K)	$v_{sp,0}^*$ (cm^3/g)	s
PEEK	6,401	4.003	0.7351	0.7151[a]

[a] Calculated using group contribution calculation scheme UNIFAC (see Ref. [48, 49])

the two proton acceptor groups, present on each water molecule. Conversely, cross HB interactions are assumed to take place only between water proton donor groups and the carbonyl group located on the PEEK backbone (one for each repeating unit), even though water interaction with the ether oxygen on the polymer repeating unit cannot be presently ruled out. The LF and the self HB parameters associated to the pure components are reported in Table 4. In particular the values of ε_s^*, ε_h^* and $v_{sp,0}^*$ for PEEK have been obtained by best fitting high pressure dilatometric data (PVT data) of PEEK in the equilibrium molten state at different temperatures and pressures available in the literature [53].

Simultaneous data fitting of the four experimental sorption isotherms investigated has been performed (see Fig. 7) and the three corresponding best fitting parameters obtained are reported in Table 5. As it is evident from Fig. 7, the NETGP-NRHB model provides a good quality of fitting of equilibrium sorption isotherms of water in PEEK. In particular the self HB contribution term allows to correctly describe the upward concavity exhibited by the curves, particularly at high vapour water activity.

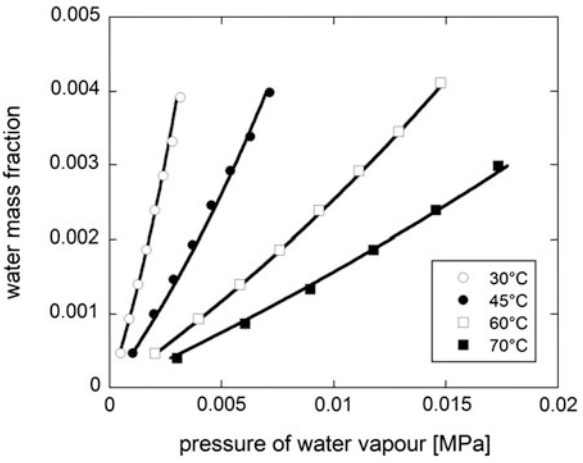

Fig. 7 Fitting of experimental water sorption isotherms for PEEK expressed as water mass fraction in the amorphous phase as a function pressure of vapour water. *Continuous lines* represent fitting curves provided by NETGP-NRHB model

Table 5 PEEK-water mixture NETGP-NRHB parameters as obtained from data fitting of experimental sorption isotherms. V_{12}^{0wp} has been assumed as being equal to 0 and does not result from fitting

ψ_{12}	E_{12}^{0wp} (J/mol)	S_{12}^{0wp} (J/mol K)	V_{12}^{0wp} (cm^3/mol)
1.023	−14,376	−13.14	0

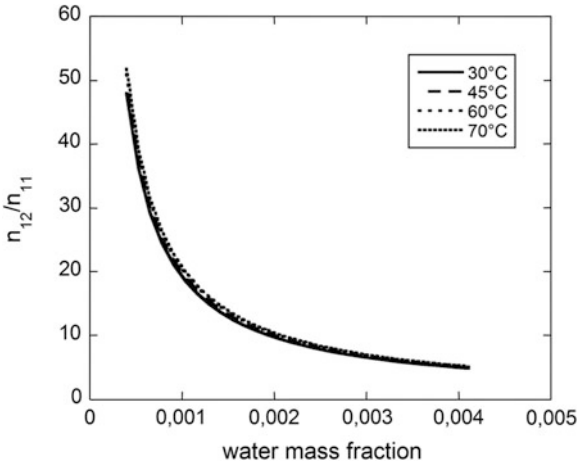

Fig. 8 Predicted values of the ratio of water self-HB and water-PEEK cross-HB, all reported as a function of water mass fraction in the PEEK amorphous phase, at 30, 45, 60 and 70 °C

As for the case of polyimides, once the optimized parameters have been determined by the fitting procedure, NETGP-NRHB model can be used to predict the amounts of self (i.e.1–1) and cross (i.e. 1–2) HB interactions occurring in the PEEK-water mixtures at the four temperatures investigated. In Fig. 8 is reported, in particular, the predicted values for the ratio n_{11}^{wp}/n_{12}^{wp} as a function of water mass fraction in the amorphous phase of PEEK. As for the case of polyimides-water systems illustrated before, at low water concentration cross-HB interactions prevail while the water self-HB interactions increase their relative importance as total water concentration increases. Vibrational spectroscopy analysis is in progress in order to provide a quantitative experimental estimate of the amount of each kind of HB interactions to be compared with model predictions.

3.1.3 Epoxy-Water System

The analysis of sorption thermodynamics of water has been performed also for epoxy resins. We present here the case of tetraglycidyl 4,4′-diaminodiphenyl methane–4,4′-diaminodiphenylsulfone (TGDDM-DDS) resin that was actually the first polymer-water system investigated by our group exploiting the wealth of information available from in situ vibrational spectroscopy. Water sorption

thermodynamics have been interpreted in the light of self- and cross-HB. The experimental results reported here are obtained at 24 °C.

Due to the higher complexity of chemical structure of this system as compared to PIs and PEEK, the theoretical interpretation of sorption thermodynamics has been based on a phenomenological model [54]. The procedures adopted for the experimental spectroscopic and gravimetric investigation and of consequent data elaboration and analysis are identical to those adopted in the case of PIs. However, 2D-COS analysis was not performed since it was not yet fully developed as a data elaboration tool at the time of the investigation.

Making use of difference spectroscopy, the spectrum of absorbed water in the ν_{OH} region has been isolated by eliminating the interference of the hydroxyl groups of the epoxy resin. The analysis has been performed during sorption of water and at sorption equilibrium at several values of relative pressure of water vapour. The collected difference spectra convey important information not only on the state of water molecules but also on the perturbation of the vibrational modes of the epoxy network. In fact peak shifts and/or intensity changes occur as a consequence of the interactions with water, thus allowing the identification of the interacting groups of the network.

An example of a sequence of subtraction spectra collected water in the ν_{OH} region during a sorption test relative to different sorption times, and hence, to different concentrations of water in the sample, is reported in Fig. 9 for the sorption test performed at $p/p_0 = 0.4$. A complex band due to the ν_{OH} modes of absorbed water is observed. In particular, a high frequency peak is identified at 3,610 cm^{-1}, partly superimposed on a much broader absorption located around 3,370 cm^{-1}. We anticipate that the 3,610 cm^{-1} component is due to non-interacting water molecules, while the 3,370 cm^{-1} band arises from H-bonded water species.

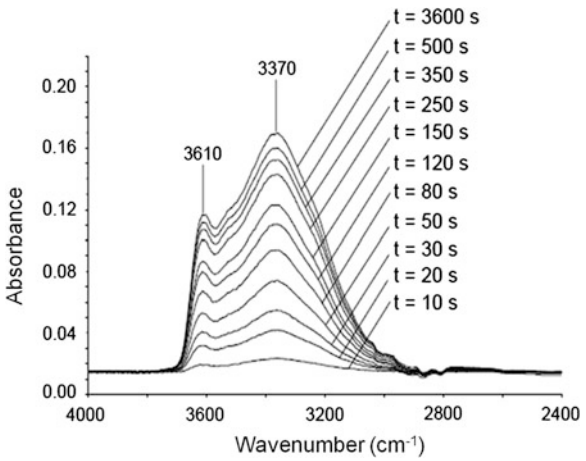

Fig. 9 Subtraction FTIR spectra collected for the system water/TGDDM-DDs at different sorption times at $p/p_0 = 0.4$. Frequency range 4,000–2,300 cm^{-1}

Concerning peaks associated to the epoxy network, we notice the displacement towards lower frequencies, upon water sorption, of the peaks located at 1,720 and 1,670 cm^{-1} in the spectrum of the dry resin. These peaks are associated to carbonyl groups (aldehydes and/or ketones at 1,720 cm^{-1} and amide groups at 1,670 cm^{-1}). This effect indicates the involvement of these carbonyls as proton acceptors in H-bonding interaction with water. However, owing to the reduced concentration of the above groups, this kind of interaction is likely to represent a relatively minor fraction of bonded species Another shift occurring upon sorption is that of the peak centred at 1,594 cm^{-1} in the dry resin. This displacement is likely to be related to the involvement of residual secondary amine groups in molecular interactions with water. The observation that the shift occurs towards lower wavenumbers is suggestive of the fact that, in this specific interactional configuration, the nitrogen is involved as a proton acceptor. Finally, displacements upon sorption are also observed for the peaks at 1,290 and 1,145 cm^{-1}, which originate from the out-of-phase and in-phase stretching modes of the sulphone groups. The downward shift of both peaks upon water absorption definitively confirms the involvement of these groups as proton acceptors in H-bonding interactions with the penetrant.

A more detailed analysis of the ν_{OH} region (4,000–2,600 cm^{-1}) by applying a least squares curve-fitting algorithm, allows to resolve the complex spectral profiles of Fig. 9 in their component peaks. This provides additional information about the different water species and their relative populations. The results of such an analysis in the 4,000–2,600 cm^{-1} range evidence the presence of four peaks. The assignments of these peaks are discussed in [54, 55]. In particular, the high frequency peak at 3,623 cm^{-1} is related to the asymmetric O–H stretching vibration (ν_{as}) of unassociated water (i.e. water which does not establish any H-bond, S_0), while the component at 3,555 cm^{-1} can be related to singly H-bonded molecules (S_1). Moreover, the two components at 3,414 and 3,272 cm^{-1} (respectively S'_2 and S''_2) arise from the S_2 species interacting with the sulphone and the amino-alcohol groups. In view of the stronger H-bonding capability of the amino-alcohol group with respect to the sulphone, the 3,272 cm^{-1} peak is assigned to the complexes (a) and (b) and the 3,414 cm^{-1} peak to the structure represented in by complex (c) in Scheme 1.

Based on $\Delta\nu$–$\Delta\varepsilon$ correlation and on the results of investigation by NIR analysis an estimation of the absolute values of absorptivity for the different water species present in the system id possible [54]. In fact, a fully spectroscopic estimate of the total concentration of absorbed water and of the concentration of each species can be obtained. In Fig. 10 are reported the concentrations of each water species as a function of total water concentration in TGDDM-DDS as determined at sorption equilibrium for several values of p/p_0 (i.e. 0.08, 0.2, 0.4 and 0.6). The linear dependence evident in all cases, implies the invariance of the molar fraction of each species with concentration, which points to a linear equilibrium between them. Furthermore, it is found that, at any concentration of absorbed water the prevailing species is S_2, which accounts for 53 % of the total.

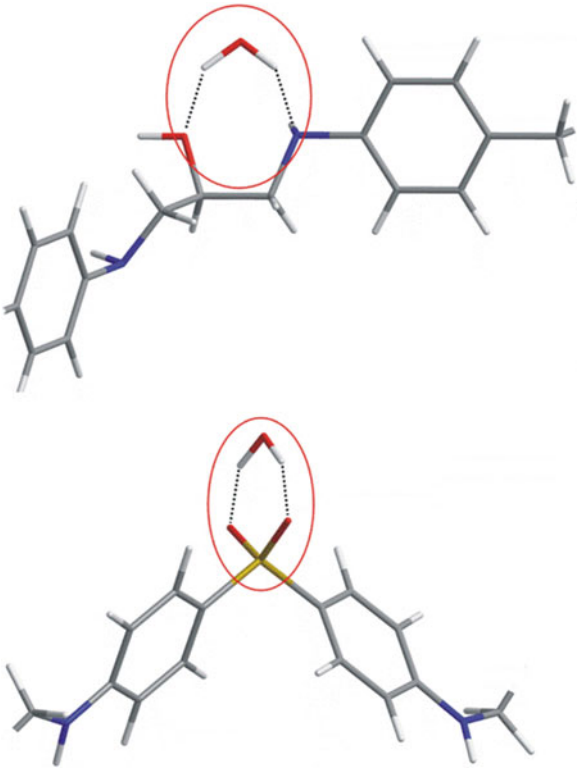

Scheme 1 Interactional complexes identified for double H-bonded water molecules (S_2 species) for the TGDDM-DDS/water system

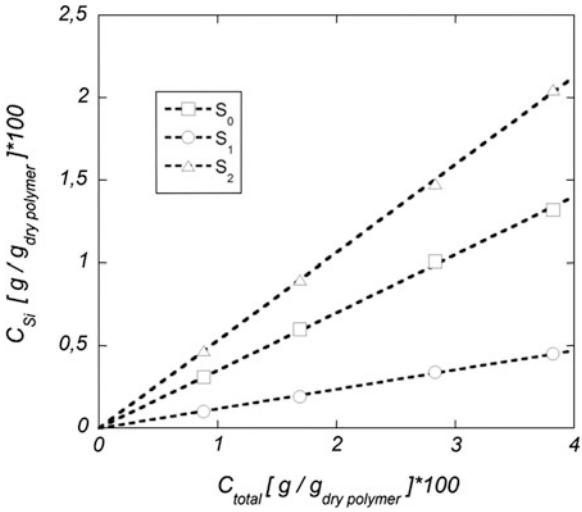

Fig. 10 Concentration of S_0, S_1, and S_2 water species reported as a function of total water concentration at sorption equilibrium n

As already pointed out, in the case of the TGDDM-DDS system no comparison was performed of the results of vibrational spectroscopy analysis with theoretical lattice fluid thermodynamic models, in view of unavailability of EoS parameters for the epoxy resin.

3.2 Rubbery Polymers

3.2.1 PCL-Water System

Experimental analysis of water sorption, by conducting gravimetric and vibrational spectroscopy experiments, has been performed also on thermoplastic polymers. In particular, we report here some recent results [23] for the system polycaprolactone-water. The results of combined gravimetric and vibrational spectroscopy analyses are compared with predictions of equilibrium NRHB model in terms of amount of water sorbed and number of self- and cross-HB. For the PCL/water system the results of 2D correlation spectroscopy are reported in Fig. 11 along with a schematic representation of self- and cross-HB interactions. In fact, only two species of water molecules have been detected: (a) water molecules HB-bonded to carbonyl groups of the polymer by cross-interactions (ether oxygen has been proven [23] not to be involved in any significant interaction with water); (b) water molecules HB-bonded by self-interaction to water molecules bonded to carbonyls.

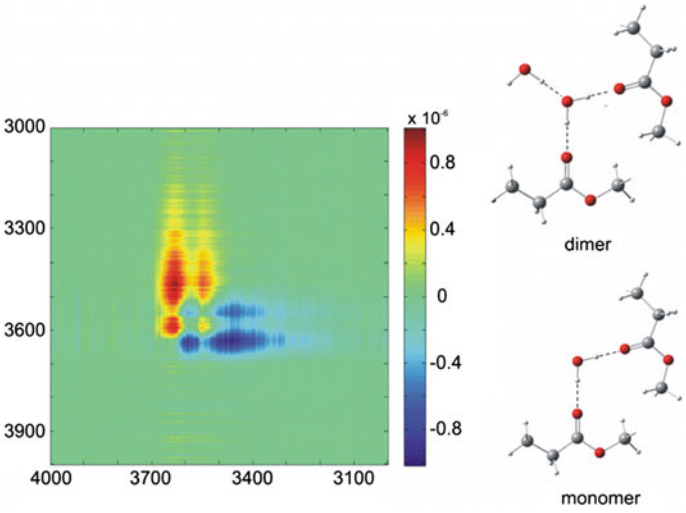

Fig. 11 *Left* 2D-FTIR correlation spectra (asynchronous) obtained from the time-resolved spectra collected during water sorption in PCL at relative pressure = 0.4. *Right* Schematic representation of the HB interactions

Adopting procedures similar to those used for polyimides, a quantitative assessment of the concentration of each water species and, in turn, of each type of HB-bond established (i.e. self- and cross-HB) has been obtained from spectroscopic data. It is worth mentioning that, in evaluating the amount of each HB interaction from each type of water species, it has been assumed, as already illustrated for the case of polyimides and based on similar arguments, that each water molecule interacting with polymer backbone actually establishes a bond with two carbonyls, thus 'brindging' two different polymer segments. Experimental gravimetric sorption isotherms at three temperatures are reported in Fig. 12. Experimental data have been normalized to the amorphous fraction of PCL, hence water mass fraction is referred to the mass of amorphous PCL. These data have been successfully interpreted using NRHB lattice theory (see continuous lines in the same figure). In Table 6 are reported the NRHB-EoS parameters, as determined from PVT measurements [23] for pure PCL. In Table 7 are reported the NRHB mean-field interaction parameter and cross-HB parameters for the PCL-water system obtained from data fitting of experimental sorption isotherms.

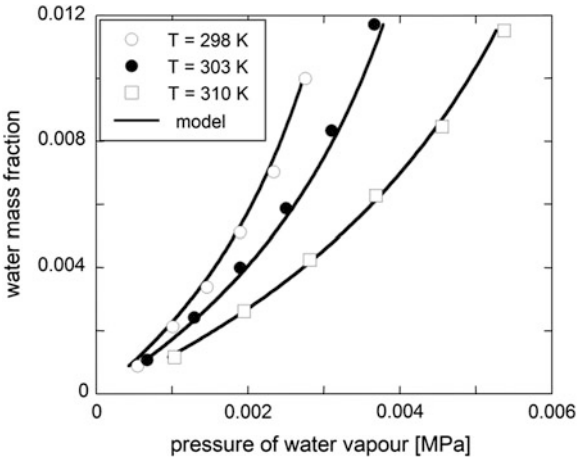

Fig. 12 Fitting of experimental water sorption isotherms for PCL expressed as water mass fraction in the amorphous phase as a function pressure of water vapour. *Continuous lines* represent fitting curves provided by NRHB model

Table 6 NRHB parameters for PCL

Component	ε_s^* (J/mol)	ε_h^* (J/mol K)	$v_{sp,0}^*$ (cm^3/g)
PCL	5876 ± 50	3.824 ± 0.01	0.8873 ± 0.005

Table 7 PCL-water mixture NRHB parameters as obtained from data fitting of experimental sorption isotherms. V_{12}^{0wp} has been assumed as being equal to 0 and does not result from fitting

ψ_{12}	E_{12}^{0wp} (J/mol)	S_{12}^{0wp} (J/mol K)	V_{12}^{0wp} (cm^3/mol)
1.115 ± 0.001	−11,130 ± 200	−6.13 ± 0.01	0

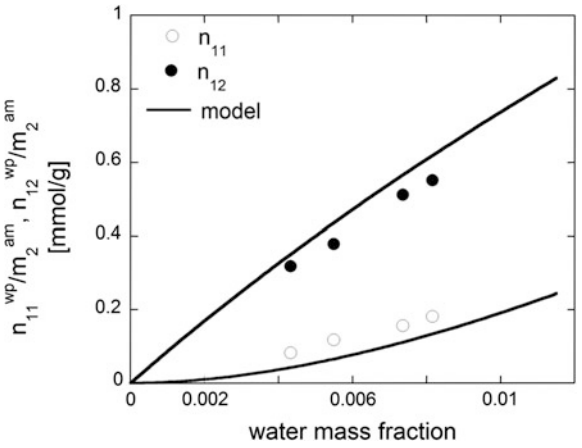

Fig. 13 Comparison of predictions of NRHB model (*continuous lines*) with experimental results for PCL-water system. Moles of water self-HB and moles of HB between absorbed water molecules and proton acceptor groups on the polymer backbone in the polymer/water mixture are per gram of dry amorphous PCL-Water mass fraction is referred to amorphous PCL

The NRHB model has been then used to predict the amount of cross- and self-HB established in the PCL-water system. As can be deduced from Fig. 13, NRHB model provides a good quantitative estimate for the number of self- and cross-HB.

4 Conclusions

Thermodynamic models for polymer-water mixtures based on non random lattice fluid EoS theories accounting for HB interactions has been proven to provide a consistent framework for the interpretation of water sorption in interacting rubbery and glassy polymers.

In fact, prediction of NRHB and of NETGP-NRHB models, respectively in the case of interacting rubbery and glassy polymers, compare well with the results of combined vibrational spectroscopy and gravimetric experimental analyses. In particular, a quantitative agreement between model predictions and experimental data has been obtained for the amount of self- and cross-HB established in poyimides and in PCL.

This approach paves the way to the interpretation of other important aspects associated with ingress of water in polymer matrices, including plasticization phenomena. In fact, an advantage of using an approach based on EoS theories for the description of sorption thermodynamics, is the availability of expressions for Gibbs energy and entropy of the polymer/water mixture that enables the easy implementation of the calculation of water effects on T_g of the system following approaches based on entropic arguments.

On the experimental side, we underline the wealth of information available on several kinds of polymer-water systems by performing on-line in situ FTIR spectroscopy coupled with analysis of 2D correlation spectra. This approach has proven to be a valuable tool to gather important information on (1) the type of

molecular interactions; (2) the interaction site(s) on the polymer backbone (3) the nature and the number of the penetrant species and, above all, (4) a method to quantitatively estimate the population of the different species present in the system.

References

1. Mensitieri G, Iannone M (2998) Modelling accelerated ageing in polymer composites. In: Martin R (ed) Ageing of composites. 1st edn. Woodhead Publishing Ltd, Cambridge (England), CRC Press, Boca Raton FL
2. Bond DA, Smith PA (2006) Modeling the transport of low-molecular-weight penetrants within polymer matrix composites. Appl Mech Rev 59:249–268
3. Flory PJ, Orwell A, Vrij RA (1964) Statistical thermodynamics of chain molecule liquids. J Am Chem Soc 86:3507–3514
4. Sanchez IC, Lacombe RH (1976) An elementary molecular theory of classical fluids. Pure fluids. J Phys Chem 80:2352–2362
5. Sanchez IC, Lacombe RH (1976) Statistical thermodynamics of fluid mixtures. J Phys Chem 80:2568–2580
6. Sanchez IC, Lacombe RH (1978) Statistical thermodynamics of polymer solution. Macromolecules 11:1145–1156
7. Simha R, Somcynsky T (1969) On the statistical thermodynamics of spherical and chain molecule fluids. Macromolecules 2:342–350
8. Panayiotou C, Sanchez IC (1991) Hydrogen bonding in fluids: an equation-of-state approach. J Phys Chem 95:10090–10097
9. Panayiotou C, Pantoula M, Stefanis E, Tsivintzelis I, Economou IG (2004) Nonrandom hydrogen-bonding model of fluids and their mixtures. 1. Pure fluids. Ind Eng Chem Res 43:6592–6606
10. Panayiotou C, Tsivintzelis I, Economou IG (2007) Nonrandom hydrogen-bonding model of fluids and their mixtures. 2. Multicomponent mixtures. Ind Eng Chem Res 46:2628–2636
11. Panayiotou CG (2009) Hydrogen bonding and nonrandomness in solution thermodynamics. In: Birdi KS (ed) Handbook of surface and colloid chemistry, 3rd edn. CRC Press, Taylor and Francis group, New York
12. Prausnitz JM, Lichrenthaler RN, Gomes de Azevedo E (1998) Molecular thermodynamics of fluid-phase equilibria, 3rd edn. Prentice Hall PTR, New Jersey
13. Taimoori M, Panayiotou C (2001) The non-random distribution of free volume in fluids: non-polar systems. Fluid Phase Equilib 192:155–169
14. Veytsman BA (1990) Are lattice models valid for fluids with hydrogen bonds? J Phys Chem 94:8499–8500
15. Veytsman BA (1998) Equation of state for hydrogen-bonded systems. J Phys Chem B 102:7515–7517
16. Bonavoglia B, Storti G, Morbidelli M (2006) Modeling of the sorption and swelling behavior of semicrystalline polymers in supercritical CO_2. Ind Eng Chem Res 45:1183–1200
17. Scherillo G, Sanguigno L, Galizia M, Lavorgna M, Musto P, Mensitieri G (2012) Non-equilibrium compressible lattice theories accounting for hydrogen bonding interactions: modelling water sorption thermodynamics in fluorinated polyimides. Fluid Phase Equilib 334:166–188
18. Barrer RM, Barrie JA, Slater J (1958) Sorption and diffusion in ethyl cellulose. Part III. Comparison between ethyl cellulose and rubber. J Polym Sci 27:177–197
19. Michaels AS, Vieth WR, Barrie JA (1963) Solution of gases in polyethylene terephthalate. J Appl Phys 34:1–12

20. Mensitieri G, Del Nobile MA, Apicella A, Nicolais L (1995) Moisture-matrix interactions in polymer based composite materials. Revue de l'Institut Français du Pétrole 50:551–571
21. Doghieri F, Sarti GC (1996) Nonequilibrium lattice fluids: a predictive model for the solubility in glassy polymers. Macromolecules 29:7885–7896
22. Sarti GC, Doghieri F (1998) Predictions of the solubility of gases in glassy polymers based on the NELF model. Chem Eng Sci 19:3435–3447
23. Scherillo G, Galizia M, Musto P, Mensitieri G (2012) Water sorption thermodynamics in glassy and rubbery polymers: modeling the interactional issues emerging from FTIR spectroscopy. Ind Eng Chem Res. doi:10.1021/ie302350w
24. Giacinti Baschetti M, Doghieri F, Sarti GC (2001) Solubility in glassy polymers: correlations through the nonequilibrium lattice fluid model. Ind Eng Chem Res 40:3027–3037
25. Gibbs JH, Di Marzio EA (1958) Nature of the glass transition and the glassy state. J Chem Phys 28:373–383
26. Gibbs JH (1956) Nature of the glass transition in polymers. J Chem Phys 25:185–186
27. Gibbs JH, Di Marzio EA (1958) Chain stiffness and the lattice theory of polymer phases. J Chem Phys 28:807–813
28. Chow TS (1980) Molecular interpretation of the glass transition temperature of polymer-diluent systems. Macromolecules 13:362–364
29. Gordon JM, Rouse GB, Gibbs JH, Risen WM (1977) The composition dependence of glass transition properties. J Chem Phys 66:4971–4976
30. Ellis TS, Karasz FE (1984) Interaction of epoxy resins with water: the depression of glass transition temperature. Polymer 25:664–669
31. Ellis TS, Karasz FE, ten Brinke G (1983) The influence of thermal properties on the glass transition temperature in styrene/divinylbenzene network-diluent systems. J Appl Polym Sci 28:23–32
32. ten Brinke G, Karasz FE, Ellis TS (1983) Depression of glass transition temperatures of polymer networks by diluents. Macromolecules 16:244–249
33. Panayiotou C, Pantoula M (2006) Sorption and swelling in glassy polymer/carbon dioxide systems: Part I. Sorption. J Supercr Fluids 37:254–262
34. Tsivintzelis I, Angelopoulou AG, Panayiotou C (2007) Foaming of polymers with supercritical CO_2: an experimental and theoretical study. Polymer 48:5928–5939
35. Mensitieri G, Scherillo G (2012) Environmental resistance of high performance polymeric matrices and composites. In: Nicolais L, Borzacchiello A (eds) Wiley encyclopedia of composites, vol. 2, 2nd edn. Wiley, Inc. Hoboken
36. Prinos J, Panayiotou C (1995) Glass transition temperature in hydrogen-bonded polymer mixtures. Polymer 36:1223–1227
37. Kelley FN, Bueche F (1961) Viscosity and glass temperature relations for polymer-diluent systems. J Polym Sci 50:549–556
38. Turnbull D, Cohen M (1959) Molecular transport in liquids and glasses. J Chem Phys 31:1164–1169
39. Turnbull D, Cohen M (1961) Free volume model of the amorphous phase: glass transition. J Chem Phys 34:120–125
40. Marquardt DW (1963) An algorithm for least squares estimation of non linear parameters. J Soc Ind Appl Math 11:431–441
41. Meier RJ (2005) On art and science in curve-fitting vibrational spectra. Vib Spectrosc 39:266–269
42. Noda I, Ozaki Y (2004) Two-dimensional correlation spectroscopy. Wiley, Chichester
43. Noda I, Dowrey AE, Marcott C, Story GM, Ozaki Y (2000) Generalized two-dimensional correlation spectroscopy. Appl Spectrosc 54:236A–248A
44. Ragosta G, Musto P, Abbate M, Scarinzi G (2011) Compatibilizing polyimide/silica hybrids by alkoxisilane-terminated oligoimides: morphology–properties relationships. J Appl Polym Sci 121:2168–2186

45. Musto P, Mensitieri G, Lavorgna M, Scarinzi G, Scherillo G (2012) Combining gravimetric and vibrational spectroscopy measurements to quantify first- and second-shell hydration layers in polyimides with different molecular architectures. J Phys Chem B 116:1209–1220
46. Iwamoto R, Matsuda T (2005) Interaction of water in polymers: poly(ethylene-*co*-vinyl acetate) and poly(vinyl acetate). J Pol Sci: Part B: Pol Phys 43:777–785
47. Tsivintzelis I, Kontogeorgis GM (2009) Modeling the vapor—liquid equilibria of polymer—solvent mixtures: systems with complex hydrogen bonding behavior. Fluid Phase Equilib 280:100–109
48. Fredenslund A, Jones RL, Prausnitz JM (1975) Group-contribution estimation of activity coefficients in nonideal liquid mixtures. AIChE J 21:1086–1099
49. Fredenslund A, Sorensen MJ (1994) Group contribution estimation methods. In: Sandler SI (ed) Models for thermodynamic and phase equilibria calculations. Marcel Dekker, New York
50. Fougnies C, Damman P, Dosière M, Koch MHJ (1997) Time-resolved SAXS, WAXS, and DSC study of melting of poly(aryl ether ether ketone) (PEEK) annealed from the amorphous state. Macromolecules 30:1392–1399
51. Polymer Data Handbook (1999). Mark JE (ed) Oxford University Press, New York
52. Lu SX, Cebe P, Calpel M (1996) Thermal stability and thermal expansion studies of PEEK and related polyimides. Polymer 37:2999–3009
53. Zoller P, Walsh DJ (1995) Standard pressure volume temperature data for polymers. Technomic Publishing AG, Basel
54. Cotugno S, Mensitieri G, Musto P, Sanguigno L (2005) Molecular interactions in and transport properties of densely cross-linked networks: a time-resolved FT-IR spectroscopy investigation of the epoxy/H_2O system. Macromolecules 38:801–811
55. Mensitieri G, Lavorgna M, Musto P, Ragosta G (2006) Water transport in densely crosslinked networks: a comparison between epoxy systems having different interactive character. Polymer 47:8326–8336

Humid Ageing of Organic Matrix Composites

X. Colin and J. Verdu

Abstract In this chapter, several aspects of the ageing phenomena induced by water in organic matrix composites are examined, essentially from the physico-chemical point of view. It is first important to recognize that there are two main categories of humid ageing. First there are physical processes, mainly linked to the stress state induced by matrix swelling and sometimes matrix plasticization. This kind of ageing can occur in matrices of relatively high hydrophilicity (affinity with water). Highly crosslinked amine cured epoxies are typical examples of this behavior. The second category of humid ageing involves a chemical reaction (hydrolysis) between the material and water. Unsaturated polyesters are typical examples of this category. They display a low to moderate hydrophilicity, swelling and plasticization have minor effects, but hydrolysis induces a deep polymer embrittlement and, eventually, osmotic cracking. Whatever the ageing mechanism, it needs the water to penetrate into the material and depends on the water concentration and its distribution in the sample thickness. This is the reason why the first and second sections are respectively dedicated to water solubility and diffusivity in matrices, interphases and composites. In each case, the elementary processes are distinguished, to examine the effects of temperature and stress state and to establish structure–property relationships. It is shown that, in most of these aspects, research remains largely open. The last section is devoted to hydrolysis, its kinetic modeling, including the case of diffusion controlled hydrolysis, and its consequences on polymer properties. Structure reactivity relationships are briefly presented. The very important case of osmotic cracking, which can be considered as a consequence of hydrolysis, is also examined.

X. Colin (✉) · J. Verdu
ARTS ET METIERS ParisTech, PIMM (UMR CNRS 8006), 151 boulevard de l'Hôpital
73013 Paris, France
e-mail: Xavier.COLIN@ensam.eu

P. Davies and Y. D. S. Rajapakse (eds.), *Durability of Composites in a Marine Environment*, Solid Mechanics and Its Applications 208,
DOI: 10.1007/978-94-007-7417-9_3,

1 Introduction

It is well known, for over half a century, that organic matrix composites (OMCs) can fail by "humid ageing", i.e. irreversible interaction with water in (atmospheric) vapor or liquid state. Two particular cases resulted in a considerable amount of research: (1) the case of high performance epoxy-carbon composites in military airplanes used in wet tropical environments, especially in Vietnam in the 1960–1975 period [1]; (2) the case of polyester-glass fiber boat hulls in the 1970s–1980s when pleasure sailing developed extensively. In principle, ageing problems in OMCs can involve one or several of the three components: the fibers, the matrix or the interface. It was immediately shown that, in both cases, fibers are impermeable to water and stable in the natural environments under consideration. Interfacial failure can occur but here, the weakest component is, no doubt, the matrix. It was also rapidly recognized that both cases correspond to two distinct modes of polymer-water interaction. Amine crosslinked epoxies do not react chemically with water, they fail by loss of mechanical processes linked to the water penetration and its swelling effect on the matrix. Polyesters react with water, the hydrolysis of ester groups cuts the network strands, that leads to polymer embrittlement, but the main consequence of hydrolysis is to generate small organic molecules eventually responsible for osmotic cracking (the blistering process, well known to boat users).

Considering now the whole family of OMCs, one can envisage three cases: For relatively highly hydrophilic matrices, e.g. high performance epoxies able to absorb up to 7 % by weight of water, failure is expected to result mainly from stresses induced by differential swelling linked to water concentration gradients in transient absorption or desorption regimes. For polymers of relatively low hydrophilicity but containing hydrolysable groups, e.g. linear or tridimensional polyesters, anhydride cured epoxies, polycarbonates, certain polyamides, etc., failure must result from hydrolysis. For non-hydrolysable polymers of low hydrophilicity, e.g. polyethers, polysulfones, hydrocarbon polymers, etc., failure can eventually result from interfacial degradation. Whatever the mechanism of OMC-water interaction, it involves water penetration, that leads to two series of questions which will constitute the subjects of two sections of this chapter. The first section deals with the polymer-water equilibrium: the experimental determination of equilibrium water concentration, its variation with water activity and temperature, the structure-hydrophilicity relationships, the effect of absorbed water on main polymer physical properties. The second and third sections deal with kinetic aspects of water sorption, the experimental approaches, the diffusion mechanisms and the corresponding kinetic laws, the effect of temperature and stress state on diffusivity, the structure-diffusivity relationships, the role of reinforcing agents, especially fibers on diffusion, and the stress state induced by diffusion. The fourth section deals with hydrolysis processes: experimental approaches, mechanisms and kinetics, diffusion control on kinetics, consequences on mechanical properties, osmotic cracking and interfacial hydrolysis.

2 Polymer-Water Equilibrium Characteristics

2.1 Measurement of Water Concentration in a Polymer

There is a wide variety of experimental approaches for the measurement of water concentration in a polymer (or composite) matrix. The simplest and most popular one is based on sample weighing in wet (w) and dry (w_0) states from which one can determine the water mass fraction: $m = (w - w_0)/w$ and the water concentration: $C = m\ \rho/18$, where ρ is the density of the wet polymer expressed in $g.l^{-1}$. This method can be routinely used to determine mass fractions higher than 0.1 %. Lower values can be accessible with high performance scales using precautions to suppress electrostatic interactions between the sample and the scale. It has been possible to reach concentrations of few dozens of ppm of water in polyethylene [2]. Low concentrations can also be determined using Karl Fisher chemical titration [3].

In the range of higher concentrations, various spectro-chemical methods are available, especially proton NMR (see e.g. Li and Chen. [4] for polyimides and Zhou and Lucas [5] for epoxies). Popineau et al. [6] also used NMR, but with deuterated water, to study water absorption by an epoxy resin. NMR allows distinguishing between free and bonded water or between two distinct populations of bonded water thanks to their distinct relaxation times. Dielectric spectroscopy is also abundantly used, it also allows distinguishing between free and bonded water, as shown e.g. by Reid et al. [7] or Grave et al. [8] in the case of epoxies, and by Lim et al. [9] in the case of polyimides. Infrared spectroscopy also allows both types of sorbed water to be distinguished since free water displays a sharp peak at about 3,650 cm^{-1}, whereas hydrogen bonded water displays a broader band at a lower frequency depending on the strength of the hydrogen bond and the number of associated molecules. Examples of IR studies can be found in the literature, e.g. Illinger and Schneider [10], Grave et al. [8] or Cotugno et al. [11] in the case of epoxies, but the use of IR for quantitative studies appears difficult and would need very careful preliminary analyses.

The coexistence of free and bonded water creates many problems because free water can exist in various forms: pockets linked to the initial presence of macroscopic pores and nano-pockets. In the case of macroscopic pores, differential calorimetry allows to distinguish free water by its melting endotherm at 0 °C. In small pores, this endotherm can be shifted towards low temperatures owing to confinement effect. Let us recall that in composites, porosity can be interfacial or induced by mechanical damage. In the case of nano-pockets, it is not easy to distinguish between those linked to initial nano-pores and those resulting from clustering in an initially homogeneous matrix. Preexisting pores can in principle be detected from density changes linked to water absorption at low to moderate activities. As a matter of fact, the density of a polymer-water mixture can vary between two limits ρ_{min} and ρ_{max} corresponding respectively to the case where water is fully soluble in the polymer (i.e. does not form a separate phase and both

volumes are additive) and the case where water is insoluble in the polymer and fills only the pores. Assuming that water density is equal to unity, one obtains:

$$\rho_{min} = \frac{\rho_p}{1 + m(\rho_p - 1)} \quad (1)$$

$$\rho_{max} = \rho_p\left(1 + \frac{m}{1 - m}\right) \quad (2)$$

where ρ_p is the polymer density in dry state. For all matrices of interest except hydrocarbon ones (polyolefins), $\rho_p > 1$.

Since clusters are formed only at high activities, one expects that, at low activities, density increases with the water mass fraction when water fills the pores, and decreases when water is dissolved in the matrix. Such methods are, indeed, very difficult to use in polyolefins where the density is lower than unity and where hydrophilicity is extremely low. The existence of preexisting nano-pores can be eventually detected using other penetrating fluids than water, e.g. nitrogen [12], BET [13], BJH or polarized xenon 129 [14]. It is necessary, here, to make the difference between surface (adsorption) and bulk properties, which could need the comparison of samples of different thicknesses.

2.2 *Effect of Water Activity on Equilibrium Water Concentration*

The curve of water mass (or molar) fraction against water activity a at a fixed temperature T is called the "sorption isotherm". Let us recall that the water activity is defined by:

$$\mu = \mu_0 + RT\,Ln(a) \quad (3)$$

where μ and μ_0 are the respective values of the chemical potential in the system under study and a reference state.

The activity of a component is linked to:

- Its molar fraction X in a liquid state: $a = \gamma X$, where γ is the activity coefficient. In an ideal solution, $\gamma = 1$.
- Its partial pressure p in gaseous phase: $a = F p$, where F is the fugacity. In an ideal gas, $F = p_S^{-1}$, where p_S is the component partial pressure at saturation.

The equilibrium corresponds to the equality of water chemical potentials in both the medium and polymer. Considering only cases of water sorption by homogeneous, non-porous samples, we can distinguish four basic processes corresponding to the isotherm shapes represented in Fig. 1.

Isotherms of type H correspond to the case where the equilibrium concentration is proportional to activity over the whole activity range (Henry's law). This

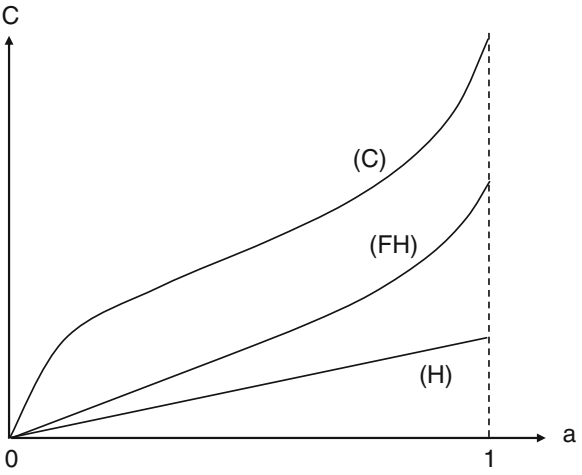

Fig. 1 Shape of main sorption isotherms for homogeneous, bulky polymer samples

behavior can be observed in many polymers of relatively low hydrophilicity. Their equation is thus:

$$W = S\ p \tag{4}$$

where S is the solubility coefficient and p the water partial pressure in the atmosphere or in equilibrium with the bath in the case of an exposure in liquid. According to the above definitions:

$$W = \frac{v}{18}\frac{1-m}{1-v} \tag{5}$$

i.e. $W \approx v/18$ for low hydrophilicities. Since $p = a\ p_S$, it comes:

$$v \approx H\ a \tag{6}$$

where $H = 18\ p_S$ for low to moderate hydrophilicities.

Isotherms of type FH (Flory–Huggins) correspond to the following law:

$$Ln(a) = Ln(v) + (1-v) + \chi(1-v)^2 \tag{7}$$

Their initial slope is:

$$\left(\frac{dv}{da}\right)_0 = \exp(-(1+\chi)) \tag{8}$$

Isotherms of C (clusters) are defined by the Zimm–Lundberg [15] function f_{ZL} for $f_{ZL} > -1$:

$$f_{ZL} = -v\left[\frac{\partial\left(a/v\right)}{\partial a}\right] - 1 \tag{9}$$

Table 1 Coefficients of the empirical power law linking the equilibrium mass uptake to relative hygrometry for the resin NARMCO 5208 and its carbon fiber laminates

Material	a_S	b	Authors
Laminate	0.0182	1.28	Shen and Springer[74]
Laminate	–	1.8	Husman[154]
Laminate	–	1.0	Mc Kague et al. [155]
Resin	0.004	1.36	Mc Kague et al. [59]

They can be represented, at least in a first approach, by a power law:

$$v = b\,a^m \tag{10}$$

In the 1970s–1980s, most authors, in the composite field, used this type of power law to represent the activity effect on mass uptake: $m_S = a_S\,(HR)^b$, where m_S and HR (relative humidity) are expressed in percents. Some literature values of the proportionality factor as and exponent b have been compiled for the highly crosslinked epoxy resin NARMCO 5208® and its carbon fiber laminates in Table 1.

However it is difficult to imagine, in homogeneous, non-porous samples, clustering without some water solubility in the polymer. In other words, isotherms of type C must always coexist with isotherms of type H. The whole isotherm, which will be called HC corresponds to the equation:

$$v = H\,a + b\,a^m \tag{11}$$

FH and HC isotherms display a positive curvature. Application of the Zimm–Lundberg criterion shows that, for the FH isotherm also, $f_{ZL} > -1$. There is thus a risk of confusion between both isotherms. The parameters of HC equation (11) can be determined from experimental data, as follows: The initial slope H is determined graphically on the isotherm. Then, one calculates the function y:

$$y = v - H\,a \tag{12}$$

As it it will be seen, y is generally close to a power law as expected from Eq. 11. The same procedure can be applied to a FH isotherm. Here:

$$H = \exp(-(1+\chi)) \tag{13}$$

So that:

$$y = v - a\,\exp(-(1+\chi)) \tag{14}$$

A numerical application was made for $\chi = 0.5$. v was calculated from Eq. 10 and y from Eq. 14. Then y was plotted against a in Fig. 2.

As can be seen, y cannot be represented in a satisfactory way by a power law. In the same way, it is clear that if experimental isotherms are well approximated by Eq. 14, they do not correspond to the Flory–Huggins law.

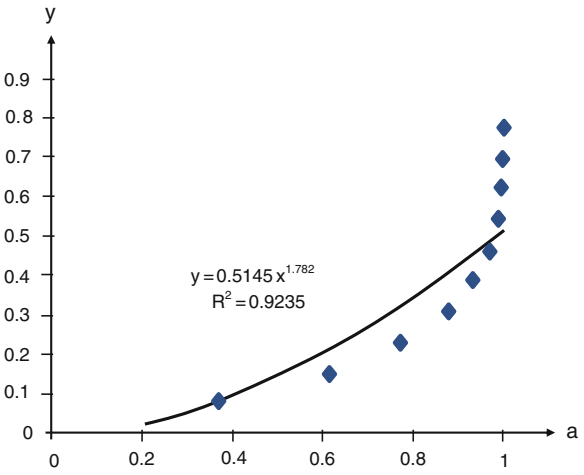

Fig. 2 y = f(a) (see text). Points: values calculated from Flory–Huggins law; Curve: best fitting by a power law

Isotherms of type L (Langmuir) have the following equation:

$$W = \frac{W_H h\, p}{1 + h\, p} \tag{15}$$

which can be written:

$$v = \frac{v_H r\, a}{1 + r\, a} \tag{16}$$

These equations come from the assumption that water is trapped in sites of maximum capacity, W_H corresponding to the isotherm asymptote. The coefficient h is named affinity constant of water vapor for Langmuir sites. In fact, as for isotherms of type C, isotherms of type L generally coexist with Henry's process so that experimental isotherms are of type LH of equation [16]:

$$v = H\, a + \frac{v_H r\, a}{1 + r\, a} \tag{17}$$

This process can be recognized by the presence of a negative curvature in the region of low activities, followed by a linear part.

Finally, H, C and L phenomena can occur in the same sorption process. This case has been named, maybe abusively, a "dual" sorption whereas, in fact, the three processes coexist. Note that all the above mechanisms operate in the whole volume of homogeneous samples.

2.3 Effect of Temperature

In the past, most of the investigations in this field started from two apparently obvious assumptions: the water equilibrium concentration in the saturated state W_S

can be used as a fundamental quantity to discuss temperature and structure effects, and ii) W_S is basically temperature independent (the case for many amine cured epoxies) or slightly temperature dependent with a small activation energy (case of polyesters for instance), so that a study of temperature effects would be of little utility. Both assumptions are in fact questionable.

Concerning the use of a single quantity to characterize hydrophilicity, it is eventually an acceptable point of departure in the case of H isotherms defined by a single parameter H or S. In contrast, in the case of HC or HL isotherms, there are at least three parameters: H, b and m for HC isotherms; H, v_H and r for LH isotherms, for which there is no reason to suppose that they are influenced in the same way by temperature or structure variations. Furthermore, in the cases of HC and LH isotherms, where the whole water concentration results from the sum of elementary components, the fact that the temperature dependence of the whole water concentration obeys Arrhenius law would result from a surprising coincidence. As a matter of fact, we know that the sum of terms obeying Arrhenius law does not obey Arrhenius law.

At this stage of our knowledge, we are only able to discuss the temperature effect on Henry's component, which is often the major component of water sorption. Let us recall that, in Henry's law (Eq. 4), the (single) parameter characterizing the polymer-water interaction is the solubility S. Let us call W_{1S} the water concentration corresponding to the Henry's component in the saturated state [17, 18]:

$$W_{1S} = S\, p_S \tag{18}$$

In the simplest approach, S is expected to obey an Arrhenius law with an activation energy E_S also called heat of dissolution:

$$S = S_0 \exp\left(-\frac{E_S}{RT}\right) \tag{19}$$

We see that the number of quantities to take into account in a study of structure–property relationships is at least 6 since, for each parameter of the isotherm, we have the pre-exponential factor and the activation energy to consider separately. There are many equations to represent the temperature dependence of the water saturated pressure p_S but, in a first approximation, we can use the Arrhenius equation:

$$p_S = p_{S0} \exp\left(-\frac{E_P}{RT}\right) \tag{20}$$

where $E_P \approx 43$ kJ.mol^{-1} can be called the heat of water vaporization.

From the combination of Eqs. 18–20, one obtains:

$$W = W_0 \exp\left(-\frac{E_W}{RT}\right) \tag{21}$$

where $W_0 = S_0\ p_{S0}$ and $E_W = E_S + E_P$.

One can now understand why E_W is always low and can be either positive (e.g. in polyesters and, more generally, in all polymers of low to moderate polarity) or negative (e.g. in highly polar (and hydrophilic) epoxies or polyimides). This can be achieved if the heat of dissolution E_S is negative, i.e. the water-polymer interaction is exothermic, and if the absolute value of E_S is not very far from 43 $kJ.mol^{-1}$, i.e., in other words, if water establishes strong hydrogen bonds (H bonds) with the polymer. When these bonds are stronger than water–water H bonds, $E_S < -E_P$ and the water concentration is a decreasing function of temperature (e.g. in highly hydrophilic epoxies). The reverse is true when $E_S > -E_P$ (e.g. in polyesters).

As will be shown below, the "Arrhenius model" is probably an oversimplification, but it is convenient to understand the trends of temperature effects on equilibrium concentration. Concerning the parameters specific to clustering or Langmuir absorption, the research domain is almost virgin.

2.4 Effect of Stresses

The water equilibrium concentration is linked to the equality of water chemical potentials in the environment and in the material. The chemical potential depends on thermodynamic parameters, among which are stresses. Stress effects on water solubility can therefore be derived from a thermodynamic approach (e.g. [19–21]). From an expression of the chemical potential of water, for the case of small, isotropic deformations with negligible changes of material elastic properties, these latter authors obtained a simple relationship for the equilibrium mass uptake m (see Sect. 2.9).

2.5 Effect of Structure on Henry's Sorption Process

First, it is important to note that structure–solubility relationships make sense only if we consider a unique sorption mechanism. This precaution was never taken in the literature, thus making the synthesis of published data difficult. In the following, the reasoning is applicable to Henry's sorption process where water concentration and its elementary components are proportional to activity.

The idea that water must fill the free volume and that hydrophilicity is linked totally or partially to the free volume fraction f is intuitive and has seduced many authors in the 1980s [22–25]. This theory calls however for three main criticisms:

1. In glassy polymers, there is no undisputable definition of the free volume fraction f. According to the theory of viscoelasticity, $f = f_g + \alpha\ (T - T_g)$, where f_g is the free volume fraction at T_g and α is the expansion coefficient of free volume. Typically, $f_g \sim 0.025$ and $\alpha \sim 5 \times 10^{-4}\ K^{-1}$, which means that

$f = 0$ at $T < T_g - 50$ K. For various authors, the "free volume" is an arbitrary fraction of the penetrable volume (the volume in excess relatively to the Van der Waals volume V_W). The fractional free volume FFV is often defined by: $FFV = (V - 1.3V_W)/V$. There are, however, structural series, e.g. amine cured epoxies, for which the hydrophilicity is a decreasing function of FFV.

2. There are free volume rich substances of very low hydrophilicity, e.g. liquid hydrocarbons, silicone rubbers, etc.
3. Water displays a relatively high plasticizing power on polymers, furthermore its absorption is highly exothermic.

These features are incompatible with the hypothesis of a sorption mechanism mainly linked to free volume occupancy by water.

Since water is able to establish strong H bonds with polar sites in the polymer, its equilibrium concentration must be first linked to these interactions. From simple hydrophilicity comparisons, it is easy to observe that there are three kinds of chemical groups:

- The non-hydrophilic groups: C–H, C–C, C = C, C–F, Si-CH_3, phenylenes etc. Polymers containing only these groups, e.g. polyethylene, polypropylene, polybutadiene, polytetrafluorethylene, polydimethylsiloxane, etc., absorb generally less than 0.1 wt% water.
- The moderately hydrophilic groups: ethers, ketones, esters, etc. Polymers containing only these groups and those of the preceding category, e.g. polyoxyphenylene, polyetheretherketone, polycarbonate, linear and tridimensional polyesters, etc., absorb generally less than 3 wt% water.
- The strongly hydrophilic groups: alcohols, acids, amides, etc. Polymers containing these groups can be water soluble if they are in high concentrations, e.g. polyvinyl alcohol, polyacrylic acid, polyacrylamide, etc. All these polymers have industrial applications but, indeed, not in the composite field. In this latter, water absorptions in the saturated state are generally limited to values lower than 10 wt%. Polyamides such as polyamide 6, 6-6 or 4-6, in which the hydrophilicity is limited by crystallinity (the crystalline phase is impermeable to water), are among the most hydrophilic linear polymers used as composite matrices. In the domain of thermosets, amine cured epoxies based on trifunctional (triglycidyl p-amino phenol, TGAP) or tetrafunctional (tetraglycidyl derivative of diamino diphenyl methane, TGDDM or TGMDA) epoxides can absorb up to 7 wt% water. In these matrices, the most hydrophilic group is the alcohol resulting from the amine-epoxide condensation, it is thus not surprising to find that hydrophilicity tends to be an increasing function of the crosslink density.

Starting from the above observations, it is tempting to suppose the existence of simple quantitative relationships between water absorption and the nature and concentration of polymer groups. The simplest relationship is a molar additive law [26–29] for epoxies, [30] for polyesters and [31] for vinyl esters).

The principle can be summarized as follows: One defines a constitutive repeat unit CRU representative of the polymer structure. This unit, of molar mass M, contains a groups A for which the molar contribution to water absorption is H_A, b groups B having a contribution H_B, etc. The group molar contributions are assumed independent of the neighboring structural groups. If the water uptake at saturation is m (expressed in weight percent), the number of water molecules absorbed by the CRU is H:

$$H = \frac{m\,M}{1{,}800} \tag{22}$$

The molar additive law stipulates:

$$H = a\,H_A + b\,H_B + \text{etc.} \tag{23}$$

This approach works relatively well in limited structural series if the chosen CRUs are large enough to take into account eventual group intramolecular interactions (intramolecular H bonds, inductive effects, etc.). The drawback is that the diversity of CRU structures imposes a large variety of elementary contributions, that reduces the practical interest of the approach. Anyhow, in wide polymer families, it appears that the contribution of a given group is an increasing function of its concentration, as seen for the alcohol group in epoxies [18] or for the sulfone group in polysulfones [32] (Fig. 3).

Starting from a suggestion of Tcharkhtchi et al. [18] and from analytical observations by NMR (e.g. [5]), IR [10] or dielectric spectroscopy (e.g. [7, 33]), Gaudichet et al. [32] proposed a theory according to which, since water molecules are doubly H bonded, this imposes restrictions on the distance between polar groups in the polymer. As a matter of fact, the length x of OH hydrogen bonds cannot be lower than the distance of a Van der Waals contact, about 0.15 nm, and

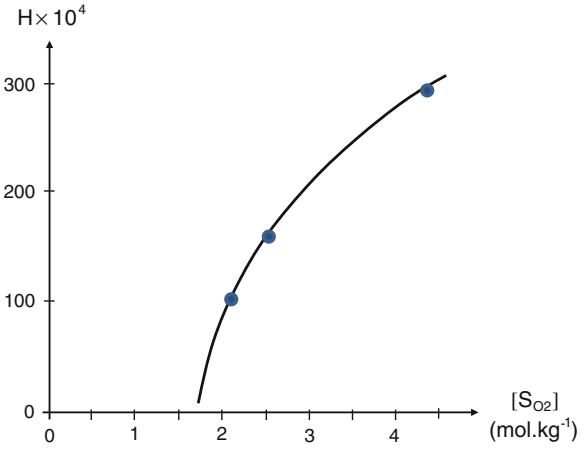

Fig. 3 Henry's solubility of aromatic polysulfones against sulfone concentration

higher than about 0.24 nm [34]. Two polar groups can constitute a hydrophilic site if their distance r is given by:

$$r = 2(x + l)\sin(\theta/2) \tag{24}$$

where l (0.096 nm) is the length of the O–H bond in water and θ (104°) is the HOH valence angle in water.

Thus, $0.39 < r < 0.53$ nm. Indeed these limits are approximations. The potential of the water-polymer bond versus interatomic separation of polar groups is expected to have the shape of Fig. 4.

Let us now consider all the pairs of polar groups in the polymer. Only a fraction of these pairs will fulfill the distance requirements to be a hydrophilic group and this fraction will generally be an increasing function of the polar groups concentration. Let us consider, for instance aliphatic polyamides. The average distance between amide groups is 0.66 nm in PA 11, and 0.55 nm in PA6. Since the highest limit for a hydrophilic site is about 0.53 nm, we see that the proportion of active amide groups in water absorption will be lower in PA 11 (equilibrium water mass uptake $m_S \sim 1.4$ % at 50 °C) than in PA6 ($m_S \sim 8$ % at 50 °C). This theory provides thus an explanation that all the polar groups are not active, that was formerly interpreted in terms of group accessibility (see, for instance, [35]), but without any possibility to give a quantitative counterpart to this concept.

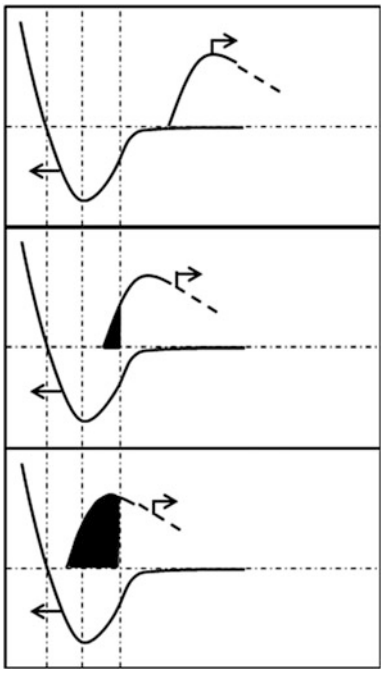

Fig. 4 Hydrogen bond potential for three cases of distribution of distances between polar groups. The dashed zone corresponds to the fraction of polar groups able to establish double H bonds with water. **Top**: Non-hydrophilic polymer. **Middle**: Moderately hydrophilic polymer. **Bottom**: Highly hydrophilic polymer

In the classical theories in which the hydrophilic site was a single polar group, the fact that, in a given structural series where hydrophilicity depends mainly on the concentration of a given group (e.g. sulfone in polysulfones or amide in polyamides), the absolute value of the heat of dissolution E_S is an increasing function of the group concentration cannot be explained. E_S is linked to the strength of the H bond. It must depend only on the nature of the group while the pre-exponential factor must be proportional to the group concentration. According to the new theory, there is a variety of H bonds differing by their length and thus, by their strength. Except in scarce cases, useless in the domain of composites, the average pair distance is higher than the distance corresponding to the minimal H bond potential, i.e. to the maximum activation energy. This carries two main consequences:

1. The temperature dependence of solubility results from the sum of an infinity of arrhenian elements, each one corresponding to a H bond distance.
2. The proportion of strongest H bonds and thus, the whole apparent activation energy, is expected to increase with the concentration of polar groups as observed.

It is noteworthy that many authors suggested the existence of a dual sorption process able to explain also the non-arrhenian character of the solubility [2, 5, 36].

It must be recognized, however, that, although theoretically possible, a quantitative prediction of water concentration by the above theory remains especially difficult because both basic elements of the reasoning: the distribution of distances between pairs of polar groups and the real shape of the hydrogen bond potential are not easily accessible. At this stage of our knowledge, only the main trends of the solubility–structure relationships can be predicted. Molecular dynamics simulations will probably bring some light in the near future (see, for instance [37]), but water solubility determinations in this way remain difficult and studies of the spatial distribution of water molecules in the polymer give results difficult to reconcile with classical physical approaches (see below).

2.6 Clustering

Van Krevelen and Te Nijenhuis [28] developed the molar additive approach and reported H_i values for several groups frequently found in polymers. It appeared that molar contributions vary nonlinearly with water activity, in other words that water sorption does not obey Henry's law. Some important molar contributions reported by Van Krevelen and Te Nijenhuis [28] are plotted against water activity in Fig. 5. All the curves display the shape expected for a HC isotherm. In other words, one can suspect the presence of clusters at high activities, in polymers used for determining molar increment values. This non-linear character of isotherms invalidates, in our opinion, the molar additivity approach since the best test for molar additivity would be precisely the proportionality between molar contributions H_i and activity a.

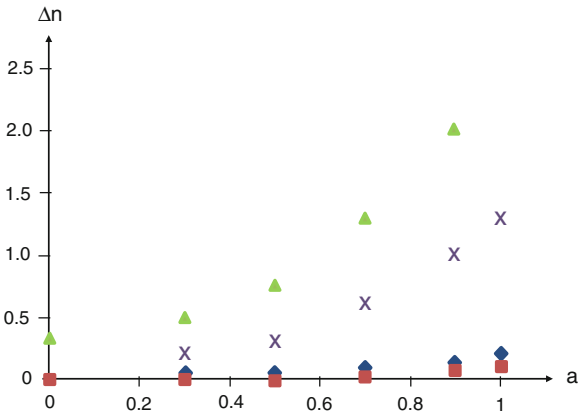

Fig. 5 Molar increments of water absorption against water activity for four chemical groups: alcohols (*triangles*), acids (*crosses*), esters (*lozenges*) and ethers (*squares*) according to Van Krevelen and Te Nijenhuis [28]

Zimm–Lundberg's theory

The curves of Fig. 5 can be well approximated by Eq. 11. Let us apply Zimm–Lundberg's theory [15, 38] to this equation:

$$f_{ZL} = -v\frac{\partial\left({}^{a}/_{v}\right)}{\partial a} - 1 = \frac{-(m-1)(v - H\,a)}{v^2} - 1 \tag{25}$$

One can arbitrarily define a critical activity a_c above which the cluster contribution begins to be significant, for instance when:

$$b\,da_c^m = dH\,a_c \tag{26}$$

i.e.

$$a_c = (dH/b)^{1/m-1} \tag{27}$$

where d is the relative error on v measurement.

We see in Eq. 30 that, as long as $a < a_c$, f_{ZL} remains close to -1 and the probability of clustering is low. When $a > a_c$, f_{ZL} becomes significantly lower than -1 and clustering must occur. The average cluster size (number of water molecules in the cluster) s is given by:

$$s = v\,f_{ZL} + 1 \tag{28}$$

The Zimm–Lundberg's theory can be applied to FH isotherms [39]. Generally, the quantitative analysis of sorption isotherms of composite matrices reveals the presence of small clusters, with few water molecules.

ENSIC theory

Zimm and Lundberg considered the problem from the point of view of statistical mechanics. The ENSIC theory (Engaged Species Induced Clustering), proposed by Pitkethly et al. [40], considers the problem from a physico-chemical point of view. A water molecule penetrating in the polymer can establish bonds with the polymer

or with previously sorbed water molecules. The probability of each mode of binding depends on the number of available sites and the strength of both bonds represented by an "affinity parameter" k_p for water-polymer bonds and k_w for water–water bonds. For a small increase of water vapor pressure dp, the number dn_w of water molecules entering the polymer is given by:

$$d\,n_w = \left(k_p n_p + k_w n_w\right) dp \tag{29}$$

where n_p and n_w are the respective numbers of polymer sites and sorbed water molecules.

The integration of this equation leads to:

$$v = \frac{k_p}{\left(k_w - k_p\right)}\left[\exp\left(k_w - k_p\right) a - 1\right] \tag{30}$$

Indeed, clustering can occur only if water has more affinity for itself than for the polymer ($k_w > k_p$). Elberaïchi et al. [41] compiled some values of k_p and k_w for polymers of high, medium and low hydrophilicity. k_w ranges between 3.1 and 5.8, whereas k_p ranges between 6×10^{-4} and 8.1×10^{-2}. In other words, water has always more affinity for itself than for polymers. The difference would be considerably smaller in the framework of the theory of doubly bonded water.

Effect of structure

Very little is known about structure-clustering relationships. Some interesting trends appear in the series studied by Gaudichet-Maurin [32] in Table 2. These results seem to indicate the existence of three domains of hydrophilicity separated by two boundaries at $57 \times 10^{-4} < H_1 < 102 \times 10^{-4}$ and $297 \times 10^{-4} < H_2 < 567 \times 10^{-4}$. Clusters seem to be formed only for very low hydrophilicity samples ($H < H_1$) where they are composed of about two water molecules, or very high hydrophilicity samples ($H > H_2$) where they are composed of about three water molecules. In the intermediary domain, there is no clustering: Water absorption obeys Henry's law over the entire activity range.

The presence of clusters in polymers of very low hydrophilicity is not surprising because water is considerably more "attractive" for itself than for polymer segments. They can also exist in polymers of high hydrophilicity as predicted by the ENSIC theory. In highly hydrophilic polymers, plasticization by water induces a rearrangement of the polymer structure favorable to a hydrophilicity increase. In the case of PA 6 for instance, the amorphous phase, initially in glassy state at $T < 60$ °C, becomes rubbery that modifies its response to water penetration. Clustering and plasticization can in principle be distinguished from diffusion coefficients (see below). These latter are a decreasing function of activity in the case of clustering and an increasing function of activity in the case of plasticization.

A generalization of the results of Gaudichet-Maurin et al. [32] seems to us premature at this stage of our knowledge. The fact that clustering begins at relatively low activities is not easy to explain. A demixing of the polymer-water mixture is unlikely because it would then be difficult to explain the existence of

Table 2 Henry's solubility coefficient and clustering characteristics for some polymers at 50 °C according to Gaudichet-Maurin et al. [32]

Polymer	$H \times 10^4$	$b \times 10^4$	m	s	References
PVC	18	4	5.16	1.7	GM
PC	42	12	3.95	1.6	GM
PA 12	51	23	4.66	2.1	L
PLA	57	19	6.41	2.2	GM
PSU	102	0	0	1	GM
BPA-IA	134	0	0	1	L
PA 11	137	0	0	1	GM
PET	148	2	0	1	GM
PPSU	156	0	0	1	GM
PEI	186	2	0	1	GM
PES	297	2	0	1	GM
PA 6	567	239	7.13	3	GM
PHEMA	2,010	1,190	7.04	3.2	L

Remark s value determined at saturation. "GM": results obtained by Gaudichet-Maurin using a Dynamic Vapor Sorption apparatus. "L": literature, references quoted by "GM"

sorption equilibrium. The hypothesis that water fills nanopores can be set out, at least for polymers of low polarity. As a matter of fact, for these polymers, the absolute value of the heat of dissolution is noticeably lower than the heat of water vaporization. In the case where the water vapor would penetrate in the polymer and recondense in pores, the thermodynamic balance of the process would be null and the water equilibrium concentration would be temperature independent.

A possible mechanism can be based on the theory of Gaudichet-Maurin et al. [32]. It is schematized by Fig. 6 where one sees a pair of polar groups able to establish a H bond with one water molecule. There is in its immediate vicinity another group, too isolated to be associated to another group to form a hydrophilic site. However, it can form a site with the water molecule when this latter takes place on the former site.

Molecular dynamics

Clustering is probably the point of major discrepancy between conventional physics [15] and molecular dynamics (MD) simulation. As a matter of fact, simulations of hydrated polymers reveal the presence of clusters even at low water concentrations, even in polymers such as polysulfones which obey Henry's law over the entire activity range. These clusters can be large and appear often as chains of water molecules rather than more or less isotropic "globules" [42]. This point is discussed in detail in the above paper. The discussion remains open in our opinion.

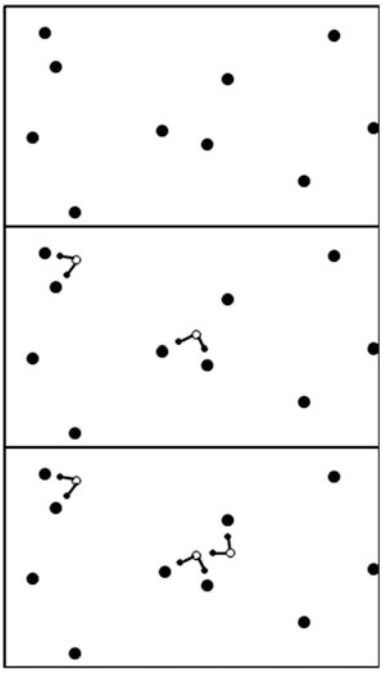

Fig. 6 Schematization of the sorption mechanism proposed by Gaudichet-Maurin et al. [32]. *Top*: dry state; *Middle*: Henry's sorption; *Bottom*: cluster formation, a new water molecule establishes a link between an isolated polar group and the oxygen of a Henry's sorbed molecule; *black circle*: polar sites

2.7 Langmuir Sorption

Examples of Langmuir sorption are common in samples of complex morphology, for instance in the domain of food engineering [43–45]. In the domain of engineering polymers, they are relatively scarce, except in samples of very peculiar morphology as, for instance, polyimide membranes with ionic domains [46]. Certain epoxy resins and their composites constitute a noticeable exception. The Langmuir process was first observed on sorption kinetic curves for composites [47]. It is noteworthy that, generally, sorption isotherms were not reported, the authors observed the consequences of the Langmuir sorption process on the water diffusion kinetics. This is why this problem will be analyzed in the next section. Sorption "anomalies" attributable to Langmuir process were soon observed in certain unreinforced epoxy samples, but they were attributed to other hypothetical mechanisms, for instance resin oxidation [48]. It seems now well established that a Langmuir process occurs only when unreacted epoxy groups are present, i.e. in insufficiently cured stoichiometric samples [48] or non-stoichiometric samples having an excess of epoxide groups [18]. More details on this phenomenon will be given in the section devoted to Langmuir's diffusion process.

Now, we are tempted to suppose that, when a sorption anomaly having the equilibrium and kinetic characteristics of a Langmuir process is observed in a polar polymer, it can be interpreted in terms of reversible chemical reaction of

water with certain reactive groups present in the polymer. As a matter of fact, it is difficult to imagine physical bonds stronger than water (double) bonds with highly polar groups. If this generalization was valid, and that remains to be demonstrated, it would open the way for a (quantitative or semi-quantitative) prediction of the Langmuir process for a given polymer.

2.8 Interfacial Water Absorption

It must be first recalled that the interface is a bi-dimensional entity which cannot, in principle, be a locus of water absorption or chemical reaction. If there is a lack of adhesion between fiber and matrix, dewetting, mechanical or thermal stresses can induce the formation of interfacial voids and these latter can be filled by liquid water at high activities. Then, the interfacial water pockets can act as initiation sites for further interfacial crack propagation by osmotic processes [49], thermal spikes in supersonic flights [50] or water freezing as in the well-known mechanism of rock erosion. The non-empirical kinetic modeling of these processes would first need a precise description of the initially present interfacial defects, which is not obvious owing to the discrepancies between the available experimental methods [40, 51].

Coupling agents are generally used to facilitate processing but also to improve the composite resistance to humid ageing. Trifunctional alkoxy silanes $(Alk\text{-}O\text{-})_3Si\text{-}(CH_2)_i\text{-}R$ (Fig. 7) are often used.

These differ mainly by the fourth group (-R) which is expected to establish a bond with the matrix. For instance, vinyl silanes can be used in unsaturated polyesters where they are expected to copolymerize with styrene or fumarate double bonds. In the same way, amino-silanes or epoxy-silanes are expected to react with amine cured epoxy matrices. The coupling agents are generally associated with other additives such as lubricants, antistatic agents or adhesive agents

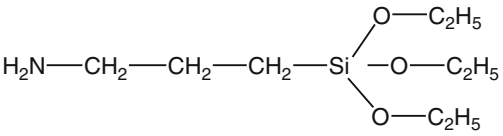

Aminopropyl triethoxy silane

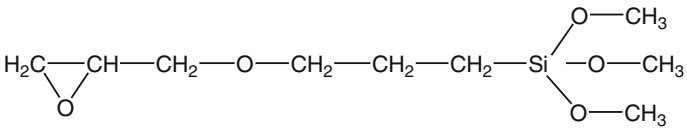

3 Glycidyloxy propyl trimethoxy silane

Fig. 7 Developed formulae of two common coupling agents

aimed at facilitating processing. All these additives contribute to the formation of an intermediary layer between the fiber and matrix. This layer is called an "interphase". Its interaction with water can, indeed, play an important role in composite durability. It is well recognized that the interphase displays a more or less diffuse multi-layer structure [52–56]. In glass-polymer composites with silanes as coupling agents for instance, one expects the presence of three concentric layers:

1. An almost monomolecular layer containing mainly the Si-O-Si bonds formed by condensation of Si-OH groups present at glass surface and Alk-O-Si- groups of the coupling agent.
2. A layer resulting of the hydrolytic condensation of alkoxysilane groups belonging to the coupling agent. This condensation forms a network.
3. A layer resulting of reactions between the coupling agent and reactive polymer groups in which the relative proportions of both components varies progressively with the distance to the fiber surface.

The thickness of layers (2) and (3) depends on the quantity of coupling agent deposited on fiber surface and processing conditions among other factors.

Let us consider, for instance, a glass fiber/polymer composite based on 24.4 w% matrix and 75 w% glass fibers of diameter d = 10 μm of density $\rho_g \sim 2.5$ coated with 0.6 w% of an organic mixture of density $\rho_c \sim 1.3$ forming a concentric layer of thickness h. The mass ratio:organic coating/glass, can be written:

$$\frac{M(\text{coating})}{M(\text{glass})} = \frac{\pi(d+h)^2}{\pi d^2}\frac{\rho_c}{\rho_g} = \frac{0.6}{75} = 8 \times 10^{-3} \tag{31}$$

The solution of this second degree equation is:

$$h \approx 4 \times 10^{-3} d \tag{32}$$

Thus, for d ~ 10 μm, h ~ 40 nm.

This value is not very far from the one (70 nm) found by Wolff by atomic force microscopy on a glass-phenolic resin model system close to industrial materials [57]. In such materials, the coating agent corresponds to about 2–3 % of the resin mass. It should not influence the overall water mass uptake in the composite, except in very rare cases. It is therefore necessary to use other methods than the gravimetric study of water absorption by the composite to appreciate the interphase hydrophilicity. Salmon et al. [58] chosen to prepare networks resulting of the condensation of pure triethoxysilanes (Fig. 5). The equilibrium water mass uptakes of these networks are given in Table 3.

In the case of amino-silane APS, however, hydrolysis is suspected to contribute to water absorption. Although very rare, these results indicate that the structure-hydrophilicity relationships found for polymers seem to be also valid for the structures participating to the interphase in composites. One can note that water concentrations of several dozens of percents, as for APS, are expected to induce a

Table 3 Water absorption at 20 °C and 75 % HR by networks resulting of the hydrolytic condensation of triethoxysilanes. Influence of the organic group R. After Salmon et al. [58]

Code	Nature of group -R	Mass uptake (%)
APS	Amine	35
GPS	Epoxide	3
PS	Propyl	0.1

noticeable swelling of the interphase but, since this latter is confined, water absorption must generate hydrostatic pressure. This latter can have contradictory effects on composite durability: on one hand, by disfavoring hydrolysis and, on the other, by inducing interfacial damage.

2.9 Main Consequences of Water Absorption on Polymer Physical Properties

We will focus here on the properties which are important from a mechanical point of view, i.e. volumetric properties (essentially swelling) and glass transition temperature (plasticization).

Swelling

To study volumetric changes induced by solvent penetration in a polymer, it is first important to distinguish the case where the swollen polymer is in a rubbery state from the case, more frequent in the domain of composites, where the swollen polymer remains in glassy state.

In the first case, the sorption equilibrium results from the equality of two opposite forces: the expansion linked to the osmotic force induced by the presence of solvent in the polymer, and the retraction linked to the entropic elasticity of the network chains which are drawn by the swelling. The thermodynamic approach based on the Flory–Huggins theory, leaded Flory and Rehner [59] to establish the equation linking the swelling ratio to the concentration of elastically active chains (n) for an unfilled polymer:

$$n = \frac{-\left\{\ln(1-v) + v + \chi v^2\right\}}{\rho V_S\left(v^{1/3} - \frac{2}{f}v\right)} \tag{33}$$

where v is the polymer volume fraction in the swollen state, χ is the polymer-water interaction coefficient, V_S is the molar volume of water, ρ is the specific mass of the polymer and f is the crosslink functionality.

In the (more frequent) case where the polymer remains in a glassy state, there is, to our knowledge, no theory to predict the swelling ratio. What is sure is that the swelling ratio (swell) must always lie between the boundaries expressed by Eqs 1 and 2, according to which:

Table 4 Equilibrium mass uptake, volume increase ($y = 100\ (v - v_0)/v_0$) and "swelling yield" (y/m) for four styrene crosslinked unsaturated polyesters [60]

Property	A	B	C	D
m (%)	1.55	1.52	5.00	2.80
y (%)	0.20	0.27	0.68	0.65
y/m	0.13	0.18	0.14	0.23

$$1 < \text{swell} < 1 + m\ (\rho_p - 1) \tag{34}$$

where swell = swollen volume/dry volume.

There is a large number of experimental data in the literature, for instance on polyesters ([60], Table 4).

The results can be summarized as follows: The swelling ratio is generally closer to the low boundary than to the higher one. In other words, water displays a relatively low swelling power. It appears that, for these networks, the volume increase is a small and almost constant fraction (0.18 ± 0.05) of the mass uptake. For highly crosslinked (and highly hydrophilic) epoxies at low activity, McKague et al. [61] found: $y/m \sim 0.51$. These authors expressed the volume change as a power law of mass change over the whole activity domain: $y = 0.527\ m^{1.17}$.

Marque et al. [62] studied the swelling ratio of three distinct polysulfones for various activity values and tried to compare its values with various theoretical values. In certain cases, it seems that the system adopts a swelling ratio in order to maintain the packing density constant, i.e. the fractional free volume (see Sect. 2.5) of the swollen polymer. This observation cannot, however, be generalized. The swelling mechanisms of glassy polymers are not well understood in our opinion and would merit supplementary research efforts.

In the case of unidirectional composites, swelling strains can develop only in the transverse direction to the fibres. In the case of absorption, compressive swelling stresses induce a certain self-limitation of deformations. In the case of desorption, in contrast, tensile forces resulting from swelling gradients (see below) have a dilatant effect. This is the reason why a significant hysteresis appears in swelling–deswelling curves, as shown for instance by Hahn [63]. Many authors have observed that the "swelling yield" y/m defined above is low at low water activities and begins to increase at mass uptakes of the order of 0.5 ± 0.2 % where $y/m \sim 0.4$–0.6 for various epoxy-carbon composites ([64, 65] reviewed in [63, 66]).

Swelling stresses

Since swelling acts as a negative pressure p on the material, one can define a *hygroelasticity coefficient* μ expressing the swelling strain per mass [67–69]. These latter authors showed that:

$$\mu = \frac{p(1 - 2v)}{E\ \Delta\ V^+/V_0} \tag{35}$$

where v is the Poisson's ratio, E is the Young's modulus and ΔV^+ is the volume of diffused liquid (higher than the volume increase due to swelling).

The upper bound of μ would be 1/3. Cracking would then occur for a critical volume of absorbed water:

$$\frac{\Delta V^+}{V_0} \approx \frac{1-2\nu}{10\,\mu} \tag{36}$$

More sophisticated approaches are derived from thermodynamic considerations. Derrien and Gilormini [19] have derived an equation expressing the influence of a hydrostatic pressure p on the water equilibrium mass uptake m in a composite of specific mass ρ_p, from an expression of the chemical potential:

$$m = Sp\,(1 - A\,\eta\,p) \tag{37}$$

where S is the solubility coefficient expressed in Pa^{-1}, and η is a lineic swelling coefficient ranging generally between 0.1 and 0.5 [21]. Coefficient A is given by:

$$A = \frac{3\,M}{RT\,\rho_p} \tag{38}$$

where M is the water molar mass.

$A \sim (1.8 \pm 0.4) \times 10^{-8}\ Pa^{-1}$ for most industrial polymers used as composite matrices. In composites, the polymer swelling is constrained by the (almost undeformable) reinforcing agent. Water absorption induces then a pressure increase into the matrix. The maximum radial stress σ_{rr} at the interface is then given by:

$$\sigma_{rr} = 3\left(\frac{1-f}{f}\right) K\,\eta\,m \tag{39}$$

where:

$$K = \frac{f}{\frac{f}{K_p} + \frac{(1-f)}{K_r} + \frac{3}{4\,G_p}} \tag{40}$$

where K_p and K_r are the respective bulk moduli of polymer and reinforcing agent, G_p is the shear modulus of polymer and f is the weight fraction of reinforcing agent.

Indeed, the pressure induced by this constrained swelling will affect the water solubility according to Eq. 35. In other words, in the absence of such interaction, a composite is expected to absorb water. At equilibrium:

$$m_c = (1-f)\,m_p \tag{41}$$

where m_p is the mass uptake, in the same conditions, in the matrix.

Equation 37 shows that the real mass uptake will be in fact lower than m_c. Derrien and Gilormini [19] showed that, in this case, the system displays Langmuir's rather than Fick's behavior.

The radial stress can cause interfacial decohesion at high swelling ratios.

Plasticization

The term "plasticization" is attributed to all the processes leading to a decrease in the glass transition temperature T_g. It can be justified by the existence of a relationship between the yield stress σ_y and T_g, according to which a T_g decrease leads to a yield stress decrease and thus makes plastic deformation easier.

$$\sigma_y = C\left(T_g - T\right) \tag{42}$$

where C is a parameter generally of the order of 1 MPa.K^{-1}.

In other words, a T_g decrease of 1 K induces about 1 MPa decrease of the yield stress. The water present in clusters cannot exert a plasticizing effect.

Solvent plasticization has stimulated an abundant literature. It can be approached by both the free volume and the entropy theories with certain simplifying assumptions more or less difficult to justify. For instance, the free volume theory starts from two hypotheses: (1) The free volumes of the polymer and the solvent are additive; (2) The free volume at T_g is an universal constant.

It is then easy to show that [70]:

$$T_g = \frac{(1-v)\,\alpha_p T_{gp} + v\,\alpha_w T_{gw}}{(1-v)\,\alpha_p + v\,\alpha_w} \tag{43}$$

where α_p and α_w are the expansion coefficients of free volume (the difference between the expansion coefficient in the liquid/rubbery state and the expansion coefficient in the glassy state), v is the volume fraction of water and T_{gw} is the glass transition temperature of water: $T_{gw} \sim 120$ K.

Equation 43 simplifies assuming that the Simha-Boyer rule is valid: $\alpha \times T_g = \text{constant} = 0.113$. Then:

$$\frac{1}{T_g} = \frac{1}{T_{gp}} + A_p v \tag{44}$$

where $A_p = T_{gw}^{-1} - T_{gp}^{-1}$.

A_p ranges between 4.8×10^{-3} K^{-1} and 6.0×10^{-3} K^{-1} for most of the glassy polymers so that:

$$588\,\text{K} < \frac{dT_g}{dv} < 2,160\,\text{K} \tag{45}$$

In other words T_g would decrease by about 6 K per percent water absorbed for polymers having a relatively low T_g (350 K). This decrease would be about 20 K per percent for polymers having the highest available T_g values (600 K). The fact that T_g depression increases with the quantity of absorbed water, its order of magnitude and the fact that, for equal concentrations of absorbed water, the T_g depression is an increasing function of the polymer glass transition temperature are experimentally verified. Indeed, the above relationships suppose that water and polymer form a single phase. Zhou and Lucas [71] found, as previously reported,

two kinds of bonded water in amine cured epoxies, and showed that both types of water molecules had distinct contributions to plasticization. Carfagna et al. [72] studied epoxy samples differing by the amine/epoxide functional ratio and compared the T_g values of wet samples, using free volume and entropy theories. The former gave better results, but the chosen value for T_{gw} (277 K) was far from the value now accepted ($\sim$120 K).

3 Water Diffusion

3.1 Introduction. Experimental Approaches. Main Types of Sorption Curves

In a bulk, non-porous polymer sample, water moves by molecular diffusion. Except in the case of interconnected pores or cracks, which will not be studied here, what penetrates the polymer is water vapor, i.e. each molecule is isolated from the others and moves by activated jumps in the direction of the concentration (chemical potential) gradient. There are basically four main diffusion processes: Fick's diffusion, Langmuir's diffusion, case II diffusion and coupled reaction–diffusion. This latter will be studied in the section devoted to hydrolysis. In all cases, diffusion kinetics can be studied from mass uptake or water concentration increase curves using the methods described previously, gravimetry being, by far, the most common. Diffusion kinetics can also be studied by measurement of water concentration thickness profiles during the sorption transient (before equilibrium), however, this latter approach is generally more difficult than the former one and is rarely used. The classical approach consists in making gravimetric measurements on microtome sections [73]. NMR imaging is a more promising solution, as illustrated by Ghi et al. [74] in the case of crosslinked PMMA, or by Braun et al. [75] in the case of polyurethane foams, where spatial resolutions of the order of 0.1×0.1 mm were reached. This resolution is too low to permit precise quantitative studies, but there are fast developments in this field and NMR imaging could become an interesting tool for the study of water diffusion in the future.

In Fick's diffusion, the water transport mechanism can be characterized by a single quantity, the coefficient of diffusion or diffusivity D. Then, one can define a characteristic time of diffusion for a sample of thickness L: $t_D = L^2/D$. Its meaning is the following: to determine D from experimental mass uptake curves, one must study the phenomenon for times of the order of t_D. If $t \ll t_D$, the mass uptake is too low to permit identification of D. If $t \gg t_D$, the sample is close to equilibrium and there is no way to determine D. The dependence of t_D with the square of the sample thickness is to be noted: a sample which would take 10 years to reach equilibrium when its thickness is 2 cm, would only take one day for a thickness of 0.1 mm. One can deduce that decreasing the sample thickness (when it is possible) is the best way to accelerate Fickian diffusion.

Table 5 The three main diffusion cases other than Fick's diffusion

Type	Second process
Langmuir	Trapping/untrapping of water by strongly interactive polymer sites
(II)	Polymer relaxation/devitrification
Diffusion–reaction	Chemical water-polymer reaction

In all diffusion processes other than Fick's, Fickian diffusion is combined with another process for which the characteristic time is t_R (Table 5). We see that if $t_D \ll t_R$, the sample is first filled by water according to Fick's law, an equilibrium can be observed for a limited time, but at long term, the second process becomes significant and a new mass change is observed. One can then say that Fick's diffusion and the second mechanism are decoupled. If on the contrary $t_D \geq t_R$, this means that both mechanisms cannot be decoupled, since Fickian diffusion occurs simultaneously with the second process.

3.2 Fickian Diffusion

Kinetic equations

In the simplest case of unidirectional diffusion (no edge effects), the equilibrium mass uptake m_s is independent of the sample thickness L and, for an initially dry material in given exposure conditions, the water diffusion obeys Fick's second law:

$$\frac{\partial C}{\partial t} = D\frac{\partial^2 C}{\partial z^2} \tag{46}$$

where C is the local water concentration and z the depth of the layer in the sample thickness.

For a parallelepipedic sample of dimensions L (in the diffusion direction), H_L and H_T, a correction must be made [76]:

$$D = D_0\left(1 + \frac{L}{H_L} + \frac{L}{H_T}\right)^2 \tag{47}$$

The resolution of this differential equation gives:

$$\frac{C(z,t)}{C_s} = 1 - \frac{4}{\pi}\sum_{n=1}^{\infty}\frac{1}{2n-1}\sin\left[(2n-1)\pi\frac{z}{L}\right]\exp\left\{-(2n-1)\,\pi^2\frac{D\,t}{L^2}\right\} \tag{48}$$

where C_s is the equilibrium concentration.

The whole mass uptake at time t is given by:

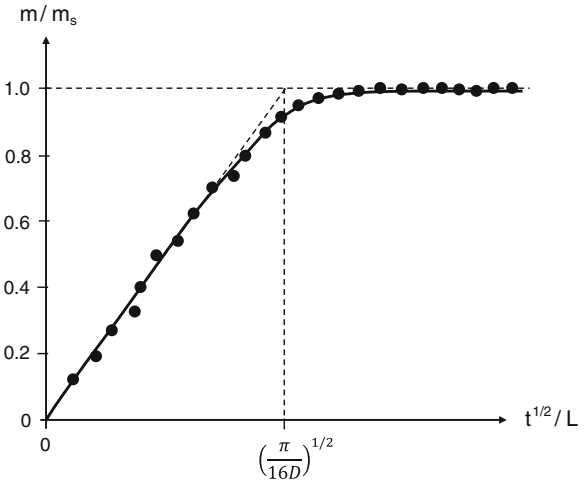

Fig. 8 Shape of a Fick's diffusion curve in reduced coordinates

$$\frac{m_t}{m_s} = 1 - \frac{8}{\pi}\sum_{n=1}^{\infty}\frac{1}{(2n-1)^2}\exp\left[-(2n-1)\,\pi^2\frac{Dt}{L^2}\right] \tag{49}$$

For a semi-infinite plate, the solution is:

$$\frac{C(z,t)}{C_s} = \text{erfc}\left[\frac{z}{2\sqrt{Dt}}\right] \tag{50}$$

As long as the water concentration on the back surface remains low, i.e. the whole mass uptake remains lower than about 60 % of the equilibrium mass uptake, the above equations can be well approximated by the following equation:

$$\frac{m_t}{m_s} = y = \frac{4}{\sqrt{\pi}}\sqrt{\frac{Dt}{L^2}} \tag{51}$$

D can thus be determined from the slope of the relative mass uptake against square root of time (Fig. 8):

$$D = \frac{\pi L^2}{16}\left(\frac{dy}{d\sqrt{t}}\right)^2 \tag{52}$$

The fact that the mass uptake increases proportionally with the square root of time is usually considered as a proof that diffusion obeys Fick's law. In fact there are cases where sorption begins as a Fickian process but deviates from this law at high relative mass uptakes. In this latter case, for Fickian diffusion, the relative mass uptake must be approximated by an exponential function:

$$\frac{m_t}{m_s} = 1 - \frac{8}{\pi^2}\exp\left(-\pi^2\frac{Dt}{L^2}\right) \tag{53}$$

Table 6 Apparent activation energy of water diffusion in some polymers

Polymer	E_D (kJ/mol)	Source
Polycarbonate (bisphenol A)	26	Ghorbel et al. [137]
Unsaturated polyester (45 % styrene)	9–13	Jacquemet and Lagrange [77]
Vinyl ester (40–45 % styrene)	22–50	Bellenger et al. [31]
Amine cured epoxy (DGEBA-DDM-PGE)	40–70	Damian et al. [156]
Polyimide (kapton)	42–46	Sacher and Susko [157]

Fick's law is obeyed by a large number of polymers and composites, at least in a limited temperature range.

Influence of water activity and temperature on diffusivity

In the simplest case, water diffusivity is independent of water activity and depends on temperature according to an Arrhenius law:

$$D = D_0 \exp\left(-\frac{E_D}{RT}\right) \tag{54}$$

Values of activation energy E_D range generally between 10 and 100 kJ.mol^{-1} (Table 6). It appears difficult to make a coherent synthesis of published data because they reveal great discrepancies. For instance, for polyesters of the orthophthalate-maleate type, Jacquemet and Lagrange [77] find $E_D \sim 11 \pm 2$ kJ.mol^{-1} for various resins and composites, whereas Belan [78] find values of the order of 38 kJ.mol^{-1} for networks of close structure. A possible explanation of this difference comes from the fact that the investigated temperature range was 5–40 °C in the first case and 30–70 °C in the second case, owing to the non-arrhenian character of the temperature dependence of water diffusivity, as already observed by Bellenger et al. [30]. A possible explanation of this behavior was given, in the case of water diffusion in polyethylene, by Mc Call et al. [2].

Influence of the stress state

In the transient regime of sorption, there are water concentration and thus, swelling ratio gradients in the sample thickness. This differential swelling induces a stress state and this latter can, in turn, influence diffusion. This problem was soon recognized by Crank [79]. Thermodynamic and mechanical aspects have been widely studied, both in resins and composites [20, 21, 80–84]. The domain profited from the contemporaneous advances in mechanics of heterogeneous solids, homogenization methods, etc.

Certain composites remain stable, i.e. undergo reversible changes during exposure to wet environments at ambient temperature, but undergo irreversible damage at high temperature where diffusion is faster, while the swelling ratio is almost unchanged. Irreversible damage modifies moisture uptake and induces sorption–desorption hysteresis.

Concerning molecular aspects of diffusion, it was for a long time supposed that it can be described by the free volume theory. In its simplest version, this theory considers that the diffusivity is linked to the molecular mobility and can receive

the same treatment as viscosity in the glass transition region. According to Doolittle, one would have:

$$D = D_0 \exp\left(-\frac{b}{v}\right) \tag{55}$$

where v is the free volume fraction and b a constant generally considered equal to unity. D_0 is a parameter characteristic of the polymer-water couple.

The free volume fraction v is the sum of the "thermal free volume" v_T linked to expansion and the "mechanical free volume" v_M linked to the stress state. According to the classical free volume theory:

$$v_T = v_g + \alpha(T - T_g) \tag{56}$$

where $\alpha = \alpha_l - \alpha_g$ is the difference between the expansion coefficients in the liquid/rubbery state and in the glassy state. α is called the expansion coefficient of free volume. v_g is the free volume fraction at the glass transition temperature T_g. Pseudo universal values of these parameters are $\alpha = 5.10^{-4}\ K^{-1}$ and $v_g = 0.025$.

According to this model, the free volume vanishes at $T_g - v_g/\alpha \sim T_g - 50$ K. Indeed, according to this equation, there would not be diffusion below $T_g - 50$ K, which is contradicted by experimental data. In this theory, an elementary free volume could be defined as the lowest hole volume allowing a cooperative segmental motion. But, the water molecule is considerably smaller than the polymer segment undergoing a cooperative motion. The study of its diffusion would thus need a new definition of free volume. Many authors consider, however, that v_g corresponds to the free volume fraction "frozen" in glassy state, i.e. is temperature independent below T_g. This latter assumption lacks justification. The classical vision of small molecule diffusion is the following: water moves by activated jumps in temporary holes formed by segmental motions. Since cooperative motions seem to fail to explain the temperature dependence of water diffusivity, it is tempting to assume that this latter is linked with the residual mobility linked to local (β, γ, etc.) motions. The "mechanical free volume" fraction V_M is an algebraic quantity. It is positive under tensile conditions:

$$v_M = \frac{\sigma}{E}(1 - 2\nu) \tag{57}$$

where σ is the tensile stress, E is the Young's modulus and ν is the Poisson's ratio.

v_M is a negative quantity under compressive conditions:

$$v_M = -\frac{\sigma}{K} \tag{58}$$

where K is the bulk modulus.

The diffusion coefficient is thus expected to increase under tensile stresses and to decrease under compressive stresses. There is no reason to refute the global trends predicted by this approach. Some published data seem to confirm its validity [85, 86], but the experimental method chosen by the former authors involves a

great quantity of simplifying assumptions and their choice of certain parameter values, for instance b, is questionable. The latter authors did not report diffusivity values, but mentioned that they disagree with the theory. Derrien and Gilormini [19] find almost undetectable stress effects on water diffusion in an amine cross-linked epoxy. As previously mentioned, results obtained on samples undergoing strong tensile stresses are difficult to interpret owing to the occurrence of creep and damage. Results obtained on samples exposed under high hydrostatic pressures would be more significant but also more difficult to obtain.

Influence of clustering and plasticization

When sorption occurs only by Henry's mechanism, the diffusivity is independent of activity. If a dependence of D on activity is observed, it indicates the presence of a complex sorption mechanism.

In the case of clustering, the water diffusivity tends to decrease at high activities [87]. There are many explanations of this behavior in the literature. For certain authors, clusters are considered as stable entities of which the diffusivity is a decreasing function of their size. For other authors, their low diffusivity is attributed to steric hindrance [46] without defining the meaning of this term. A simpler explanation could be that, since water–water interactions are stronger than water-polymer ones, the residence time of a water molecule in a cluster must be longer than in a polymer-water complex (see below). It seems that modeling of the clustering effect on diffusion is purely empirical as shown, for instance, by Detallante et al. [46] in the case of sulfonated polyimides.

In the case of plasticization, the water diffusivity is an increasing function of water activity, i.e. of water concentration. This is attributed to the plasticization effect of water on hydrophilic polymer glasses. Plasticization increases free volume and segmental mobility, at least in the temperature domain just below T_g, that favors diffusion. There is an abundant literature on this aspect [79, 88, 89]. The kinetic problem is often resolved using Fick's law with a concentration dependent diffusivity:

$$\frac{\partial C}{\partial t} = \frac{\partial}{\partial z}\left(D(C)\frac{\partial C}{\partial z}\right) \tag{59}$$

It is usual to take [90]:

$$D(C) = D_0 \exp(\gamma C) \tag{60}$$

where D_0 is the diffusion coefficient extrapolated at zero concentration and γ a "plasticization parameter".

For Van Krevelen and Te Nijenhuis [28], $\gamma = -0.08$ in the case of clustering and $\gamma = +0.08$ in the case of plasticization, C being expressed in percent of mass uptake. When plasticization and clustering coexist, D can increase with activity at low activities and decrease at high activities, as found in the case of polyimide Kapton where the water concentration value at the maximum diffusivity decreases when the temperature increases [91]. The problem becomes more complicated when polymer plasticization induces its phase change from glassy to rubbery state

where molecular mobility is considerably higher. This case, named "case II" will be examined below.

Mechanism(s) of Fickian diffusion

As seen above, the basic free volume theory fails to explain experimental observations. More sophisticated theories consider not the average free volume but rather a distribution of hole sizes. The proportion of them allowing the transport of a given molecule would be a decreasing function of the molecule size. Indeed, water molecules, which are very small, would "profit" from a greater proportion of available holes [92].

Another possible explanation is that sub-glass motions (β motions) are sufficient to permit water diffusion. This is not easy to reconcile with the fact that water diffusivity is considerably higher in polyesters (very low activity of β transition) than in amine cured epoxies (very active β transition). Finally, it appears very difficult to correlate water diffusivity with molecular mobility or with any classical volumetric criterion (as well as free volume) as fractional free volume or packing density.

It seems obvious that considerations of molecular mobility and free volume are not sufficient to explain the structure-water diffusivity relationships. A new idea was proposed by McCall et al. [2] in their work on water transport properties in polyethylenes differing by the concentration of oxygen containing structural irregularities. They found that the temperature dependence of water solubility S and diffusivity D did not obey an Arrhenius law, contrary to their product D × S. They concluded that the solubility has two components, one corresponding to the apolar PE matrix with low activation energy, another corresponding to polar sites with a higher activation energy. Diffusion would be slowed down by the interactions between these polar sites and water molecules. This theory is not easy to confirm from literature raw data, where cluster contribution is generally not separated from Henry's contribution, and where sorption isotherms are not recorded. The trends seem however be confirmed by the results obtained by Bellenger et al. [29] on a series of aromatic amine cured epoxies (Table 7).

The results obtained on series C clearly show that water solubility is independent of crosslink density. In series A and B, where crosslink density and packing density vary in the same way, diffusivity appears as a decreasing function of packing density, but with a slope four times higher for series A than for series B, (Fig. 9). It seems thus that diffusivity is not governed by packing density alone. Furthermore, if D was only dependent on free volume, its temperature dependence would display a discontinuity at T_g, as for permanent gases. Experiments showed that this discontinuity does not exist in the case of an amine cured epoxy [18].

Plotting D against m_s (Fig. 10) reveals the same type of dependence as in Fig. 9, but with better correlation coefficients. This similarity can be explained by the fact that packing density depends mainly on cohesion, i.e. on polar groups concentration [93]. It is thus tempting to assume that water diffusivity is a decreasing function of water equilibrium concentration in the saturated state, i.e. a decreasing function of water solubility. The differences between epoxies and polyesters or vinylesters confirm, at least semi-quantitatively, this difference [31],

Table 7 Glass transition temperature (T_g), concentration of crosslink nodes (X), packing density (Van der Waals volume/molar volume, P*), equilibrium water mass uptake (m_s) and diffusion coefficient (D) determined at 100 °C under 100 % RH.

Code	T_g (K)	X (mol.kg^{-1})	P*	m_s (%)	D (m^2.s^{-1}) × 10^{13}
A0	443	2.28	0.668	2.54	64
A25	466	3.30	0.670	3.40	55
A50	472	4.23	0.680	4.36	47
A80	486	5.25	0.687	5.50	35
A100	499	5.88	0.695	6.09	30
C25	470	4.98	0.690	5.47	27
C50	440	4.10	0.695	4.98	28
C75	408	3.24	0.694	4.92	33
C100	391	2.40	0.691	5.29	47
B0	417	2.02	0.667	1.81	149
B25	439	2.86	0.665	2.26	126
B50	456	3.63	0.670	2.68	121
B75	465	4.30	0.677	3.08	95
B100	471	4.90	0.678	3.52	82

Epoxides are diglycidyl ether of bisphenol A (DGEBA) and triglycidyl derivative of p-amino phenol (TGAP). Amines are diaminodiphenylmethane (DDM), or DDM with hydrogens in 2-6 position substituted by ethyl groups (DDMe) and aniline (AN). Series A is based on DGEBA-TGAP mixtures, the number corresponds to molar fraction (%) of TGAP, crosslinked by DDM. Series B is identical except that DDM is replaced by DDMe. Series C is based on TGAP crosslinked by a DDM-aniline mixture. The number corresponds to the molar fraction of aniline. After [Bellenger et al. [29]]

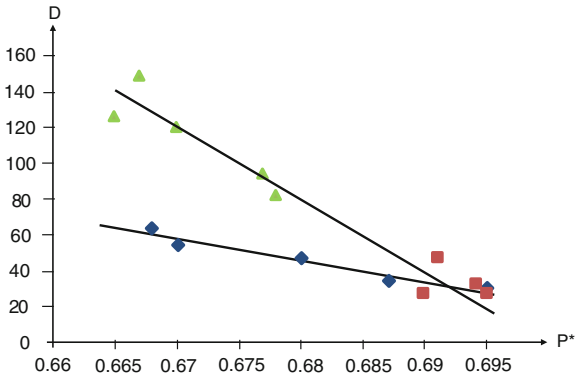

Fig. 9 Diffusivity against packing density for series A (*triangles*), B (*lozenges*) and C (*squares*)

which is also confirmed in a series of aromatic polysulfones [94]. In all these structural series, including polyethylene, D is roughly inversely proportional to m_s.

$$D \sim Q/m_s \tag{61}$$

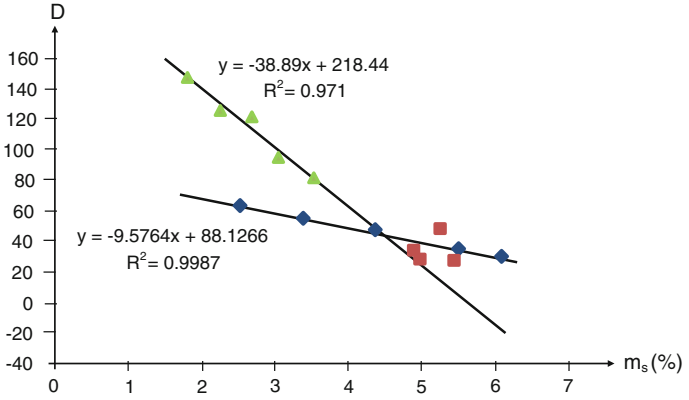

Fig. 10 Diffusivity against equilibrium water concentration for series A (*triangles*), series B (*lozenges*) and series C (*squares*)

where Q is of the order of 2×10^{-12} $m^2.s^{-1}$ for polymers of low polarity, such as polyethylene or polyesters at 50 °C, $(18 \pm 4) \times 10^{-12}$ $m^2.s^{-1}$ for aromatic polysulfones at 50 °C and $(25 \pm 6) \times 10^{-12}$ $m^2.s^{-1}$ for amine cured epoxies [94].

Thus, the specificity of water diffusion would be due to the existence of strong H bonds between water molecules and polar groups of the polymer. These interactions would slow down diffusion which could be described as a succession of jumps from a polar site to another, the whole kinetics depending on two elementary times: the lifetime of the water-polar site complexes and the time to cross the distance l between polar sites, this latter being a decreasing function of their concentration. It can be assumed that this second elementary time is proportional to l^2, but depends also on free volume. In the current state of our knowledge, we see no possibility to envisage a water diffusion mechanism ignoring the role of water-polymer interactions, but its modeling remains to be established.

3.3 Langmuir's Diffusion

It was soon recognized that, in many cases, water absorption by composites seems to display a Fickian behavior (i.e. $m \propto t^{1/2}$) at low mass uptakes, but displays an inflection or a slow but continuous mass increase, instead of an equilibrium. This behavior has been clearly identified as a Langmuir process in certain cases, but it is probably abusively considered as a Langmuir process in other cases where the slow change is not reversible at all. As shown in the section devoted to water solubility, the Langmuir process involves the existence of sites able to establish relatively strong, but reversible, bonds with water, so that two populations of water molecules coexist in the material: the "free" molecules of which the transport in

the matrix obeys Fick's law with a diffusivity D, and the "trapped" molecules temporarily retained at Langmuir sites by reversible bonds. The mathematics of Langmuir diffusion have been exposed in many articles, for instance in the widely cited paper of [Carter and Kibler [95]]. The "trapping–detrapping" process is the following:

$$\begin{aligned} F + P &\rightarrow F - P \ (k_t) \\ F - P &\rightarrow F + P \ (k_d) \end{aligned}$$

where F is a free (mobile) water molecule, P is a polar site of the polymer and F–P is the water-polymer complex. k_t and k_d are the corresponding rate constants.

The kinetic law for free molecules in a elementary layer can be written:

$$\frac{\partial F}{\partial t} = k_d[F - P] - k_t[F][P] \tag{62}$$

Assuming that the number of occupied polymer sites is small compared to the whole number of sites, one can consider that [P] = constant, and thus that:

$$\frac{dn}{dt} = \alpha N - \beta n + D\frac{\partial^2 n}{\partial z^2} \tag{63}$$

where n and N are the respective numbers of mobile and immobilized water molecules, α and β are the respective probabilities of detrapping (proportional to k_d) and trapping (proportional to k_t [P]). D is the coefficient of diffusion of free molecules.

At equilibrium:

$$\alpha N_s = \beta n_s \tag{64}$$

The total number w_s of sorbed water molecules is thus:

$$w_s = n_s\left(1 + \frac{\beta}{\alpha}\right) \tag{65}$$

When the characteristic times of complex formation and dissociation (β^{-1} and α^{-1}) are significantly longer than the characteristic time of diffusion (L^2 /D), both phenomena are distinguishable in sorption curves. These display two plateaus: the first one linked to the equilibrium concentration n_s of free water molecules, the second one to the formation of water-polymer complexes Fig. 11.

It is noteworthy that if $\beta/\alpha \gg 1$ or $\beta/\alpha \ll 1$, or if $L^2/D \geq \alpha^{-1}$ and β^{-1}, the identification of Langmuir's mechanism and the determination of its parameters can appear difficult. Sorption anomalies (non-Fickian behavior) in composites have often been attributed to the Langmuir process without a rigorous proof of its existence. A first proof would be the characteristic shape (negative curvature) of the Langmuir sorption isotherm. In many cases, a positive curvature was observed, the equilibrium mass uptake was expressed as a power function of activity:

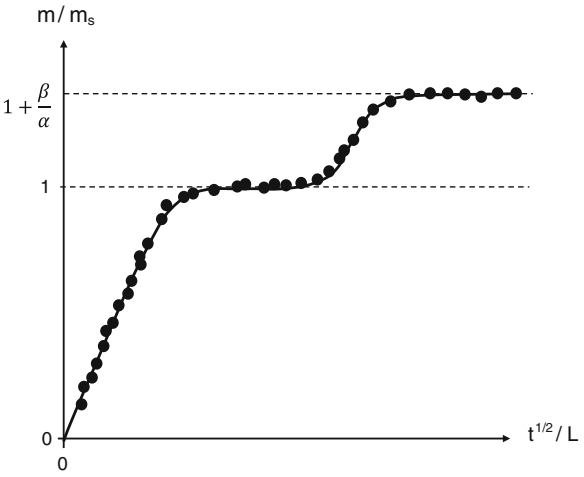

Fig. 11 Shape of a Langmuir's sorption curve

$m_s \propto a^m$ with $m > 1$, despite that sorption curves were fitted by the above set of equation. The number of adjustable parameters allows, indeed, good fittings.

The nature of Langmuir sites would merit a detailed discussion. In the literature, the main hypotheses for Langmuir loci are pores at interfaces or in the matrix, preexisting, linked to a lack of matrix/fiber adhesion or to matrix outgassing during processing, or inherent to the resin morphology [96], or induced by swelling stresses during exposure to wet environments. Various assumptions have been proposed to explain the role of pores: water adsorption on their surface, or simply high strength of water–water bonds in clusters. These assumptions lack justification in our opinion. As a matter of fact, there is a great diversity of clustering cases without Langmuir behavior.

In the 1980s, various authors, for instance Wong and Broutman [48], observed that sorption anomalies attributable to Langmuir's process appear in epoxide-amine networks having unreacted epoxide groups. Tcharkhtchi et al. [18] studied the phenomenon on samples thin enough to separate the two plateaus, and observed that the increase of mass uptake corresponding to the second process was almost proportional to the concentration of unreacted epoxide groups. They concluded that the second process is the reversible hydrolysis of epoxide groups into 1–2 diols (Fig. 12).

As quoted in Sect. 2.7, we are now tempted to assume that, in matrices, Langmuir behavior is linked to the existence of a reversible polymer-water reaction. Let us consider the hydrolysis equilibrium:

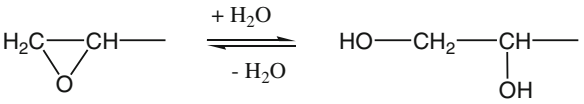

Fig. 12 Hydrolysis of epoxide groups

$$E + W \rightarrow D\ (k_H)$$
$$D \rightarrow E\ +\ W\ (k_R)$$

where W is water, E is an unreacted epoxide and D is the corresponding diol.

The equilibrium corresponds to:

$$k_H[W]\,[E]\ =\ k_R[D] \tag{66}$$

If $[E]_0$ is the epoxide concentration in dry state:

$$[D] + [E] = [E]_0 \tag{67}$$

Then:

$$[D] = \frac{[E]_0}{1 + \frac{k_H[W]}{k_R}} \tag{68}$$

Concerning water concentration [W], a simple hypothesis can be made: diols do not modify hydrophilicity, i.e. [W] = constant. In this case, the relative mass uptake Δm corresponding to the second plateau is given by:

$$\Delta m\ = 18\rho\,[D] \tag{69}$$

where ρ is the material density in $g.L^{-1}$ if [D] is in $mol.L^{-1}$.

Two extreme cases can be distinguished:

- If $k_H\,[W] \ll k_R$, then:

$$[D]\ \sim\ [E]_0 \text{ almost all epoxides have reacted} \tag{70}$$

- If $k_H\,[W] \gg k_R$, then:

$$[D] \approx \frac{k_R[E]_0}{k_H[W]} << [E]_0 \tag{71}$$

Experimental results seem to be in favor of the first case [18].

Let us now return to the mechanism of water diffusion slowed down by polymer-water interactions proposed in the previous section. It is, no doubt, a Langmuir mechanism since it involves a certain period of water molecules retention at polymer polar sites. In this case, it remains to be explained why sorption curves display, in many cases, a purely Fickian behavior. Inequality 71 gives a possible answer: the sorption curves have the shape of Fickian curves because the number of occupied Langmuir's sites is small compared to the number

of potential Langmuir's sites, as a consequence of the fact that dissociation of water-polymer complexes is considerably slower than their formation.

3.4 Case II Diffusion

This case will be only briefly evoked here, because it should be avoided in practice by a proper matrix choice. As previously seen, water plasticizes the polymer, i.e. induces a decrease of its glass transition temperature T_g. Case II occurs when, for a critical mass uptake $m_c \leq m_s$, T_g becomes equal to the test temperature, in other words when, in the sample layers where $m \geq m_c$, the polymer becomes rubbery. Since there is a strong difference in water diffusivity values between glassy and rubbery states, there will be a quasi-discontinuity in the layer where $m = m_c$. This diffusion front will move from the surface to sample core at an almost constant rate, so that the mass uptake will vary proportionally with t rather than $t^{1/2}$. After the pioneering work of Alfrey et al. [97], the theory of case II diffusion was established by Thomas and Windle [98]. For mechanical aspects of case II, one can cite the work of Argon et al. [99] and the references cited therein. Indeed, for an engineering composite having a mechanical function, the occurrence of case II would be catastrophic.

3.5 Diffusion in Composites

Diffusion laws were inspired by heat diffusion equations for homogeneous materials. The investigations on diffusion in heterogeneous media were inspired by the work of prestigious authors such as, for instance, Maxwell on electrical properties of heterogeneous materials. Barrer [100] summarized the first research on this topic at the beginning of the composite area. The discipline was then boosted by the advances in mechanics of heterogeneous materials and homogenization methods, but also by the emergence of powerful computation tools. Here, we will focus on long fiber composites.

Let us first consider the case of a unidirectional laminate with a fiber volume fraction f. Water diffusivity is expected to depend on the direction of diffusion relative to the fiber direction. In the longitudinal direction, there is a simple situation: water diffuses only into the matrix with the same coefficient D_m as into samples of pure resin (if this latter is in the same structural state). The water flux is thus expected to be proportional to the matrix cross section, i.e. to the matrix volume fraction $(1-f)$. The overall diffusivity in the longitudinal direction D_l is:

$$D_l = D_m(1 - f) \tag{72}$$

In the transverse direction, impermeable fibers impose a certain tortuosity to diffusion pathways. There are many expressions for the corresponding overall diffusivity D_t, the simplest one being derived from the Maxwell–Garnett approximation:

$$\frac{D_t}{D_m} = \frac{1 - f}{1 + f} \tag{73}$$

The equation of Kondo and Taki [101], assuming a cubic stacking of fibers, is widely used:

$$\frac{D_t}{D_l} = \frac{1 - f}{1 - 2\sqrt{\frac{f}{\pi}}} \tag{74}$$

In composites, there are many sources of complication linked to eventual interfacial diffusion and damage (pre-existing or swelling-induced). Their effects were progressively incorporated into diffusion models (see the references cited in Sect. 2.2.3, [102, 103]).

A peculiarity of diffusion in composites was shown by Derrien and Gilormini [80]. Since the matrix is swollen by water and this swelling is restrained by non-deformable fibers, a stress state appears in the matrix which modifies its water solubility and diffusivity. As a result, the diffusion behavior can take the appearance of Langmuir's diffusion while no specific sites for water-polymer interaction exist. This behavior appears however difficult to observe experimentally owing to the small contribution of the "mecano-sorptive" effects under consideration.

4 Hydrolysis

4.1 General Aspects

Hydrolysis is a chemical reaction between water and a reactive substrate leading to a bond rupture in the latter. The most general mode of writing of a hydrolysis reaction is:

$$A - B + H_2O \rightarrow A - H + B - OH$$

In industrial polymers, the most frequent reactive functions are esters in linear polyesters and copolyesters, polycarbonate, tridimensional polyesters based on unsaturated polyesters, or in anhydride cured epoxies. Amides (in linear polyamides), imides and some other groups, for instance epoxides as previously shown, are also more or less likely to react with water.

Hydrolytic chain scission

In polymers, two important cases can be distinguished:

1. Ester groups belong to polymer backbone. In this case, each hydrolysis event is a chain scission that carries important consequences for polymer mechanical properties.
2. Ester groups belong to polymer lateral groups, for instance in linear polyacrylates, polymethacrylates, or in esters of polyvinylalcohol. In such cases, hydrolysis does not modify the chain length and will not influence, at reasonably low conversions, the polymer mechanical properties.

Attention will be focused here on the first category, in which hydrolysis modifies the molar mass or the crosslink density of the polymer.

Hydrolysis is a reversible but not a symmetric process, for instance in a linear polymer (-P is a macromolecular fragment):

$$\mathrm{P-A-B-P\ +\ H_2O \rightarrow P-A-H\ +\ HO-B-P\ (k_H)}$$
$$\mathrm{P-A-H\ +\ HO-B-P \rightarrow P-A-B-P\ +\ H_2O\ (k_R)}$$

In the hydrolysis process, water is a small molecule able to diffuse rapidly in the polymer matrix (at least, for low sample thicknesses) and to accede easily to reactive sites. In contrast, in the reverse reaction, both reactants are macromolecular species with a diffusivity several orders of magnitude lower than that of water. Their condensation can thus be diffusion controlled in the time and temperature domains, where hydrolysis is not diffusion limited. From this point of view, linear and tridimensional polymers are not equivalent. In linear polymers, both groups resulting from hydrolysis can migrate far one from the other, thanks to cooperative and reptation chain motions (in rubbery state). In tridimensional polymers of relatively high crosslink density, especially in the glassy state, there is no possibility of long range migration for the (dangling) chain ends resulting from a chain scission, the reverse reaction is thus in principle favored.

Equilibrium characteristics. Reversible hydrolysis

Let us consider the above reactions with the following symbols and boundary conditions (Table 8).

The kinetic equation for substrate consumption can be written:

$$\frac{ds}{dt} = \frac{dX}{dt} = k_H[W]\,[E] - k_R[X]\,[Y] \tag{75}$$

i.e. with the chosen set of hypotheses:

Table 8 Symbols and boundary conditions for the study of hydrolysis equilibrium

Species	Concentration at time t	Initial concentration
Water	[W]	[W]
Hydrolysable groups A-B	[E]	$[E]_0$
A-H groups	[X]	0
B-OH groups	[Y] = [X]	0

$$\frac{dX}{dt} = k_H[W]\left([E]_0 - [X]\right) - k_R[X]^2 \tag{76}$$

At equilibrium:

$$k_H[W]\left([E]_0 - [X]\right) - k_R[X]^2 = 0 \tag{77}$$

From the solution of this equation one sees that:

- If $4k_R\,[E]_0\,/k_H\,[W] \ll 1$, then $[X]_{equ} \sim [E]_0$, hydrolysis is almost total, the reverse reaction can be neglected. Polyesters often belong to this family. Polycarbonates correspond to an almost ideal case because the acid resulting from hydrolysis decomposes easily into alcohol (phenol) and volatile carbon dioxide. Thus the reverse reaction cannot occur:

$$P - O - CO - O - P \; + \; H_2O \rightarrow P - O - CO - OH \; + \; HO - P$$
$$P - O - CO - OH \rightarrow P - OH \; + \; CO_2$$

- If $4k_R\,[E]_0\,/k_H\,[W] \gg 1$, then $[X]_{equ} \sim (k_H\,[W][E]_0\,/2k_R)^{1/2}$, equilibrium occurs at a low conversion of the hydrolysis process. Polyamide 11 is a typical case of equilibrium at low hydrolysis conversion [104].

Effect of ionic species

Hydrolysis is an ionic process. It is catalyzed by acids or bases. Possible mechanisms are schematized in Fig. 13, for instance, in the case of polyester:

Experimental results of hydrolysis in hydrochloric acid solutions are available for both PET [105] and for PA 11 [106]. In both cases, it appears that diluted HCl has only a small effect on the hydrolysis rate (see for instance [107] for HCl 0.1 M

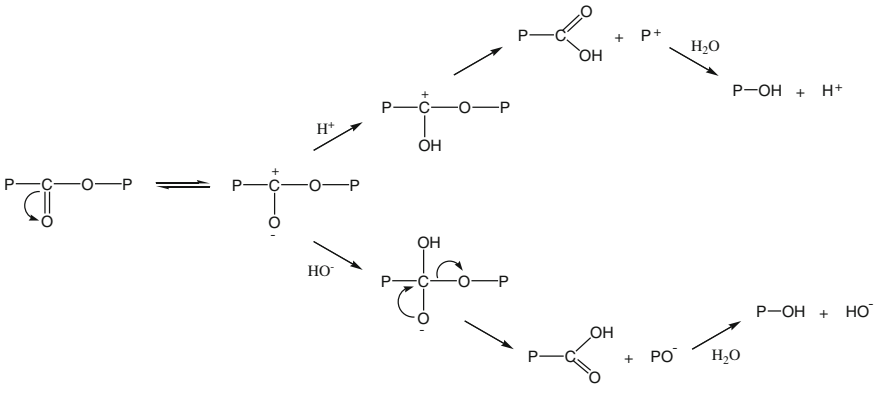

Fig. 13 Possible mechanisms of acid or base catalyzed ester hydrolysis

in PET). But, the hydrolysis rate increases almost exponentially with the acid concentration. The explanation of this behavior was first proposed by Ravens [105]. Ionic species are highly polar and thus almost insoluble in polymers of low polarity. What can penetrate in a polymer is the non-dissociated form of the acid. Then, it can dissociate into the polymer matrix, the dissociation yield being an increasing function of the matrix polarity. These considerations led Merdas et al. [108] to the following relationship for the hydrolysis rate r, using the above notations with [AH] the non-dissociated acid concentration in the polymer:

$$r = K\,[E][W]^{3/2}(1 + \gamma[AH])^{1/2} \tag{78}$$

The pre-factor K is mainly linked to the hydrolysis rate constant and to the dissociation constant of water into the polymer matrix. The parameter γ is defined by:

$$\gamma = \frac{k_A}{k_w[W]} \tag{79}$$

where k_A is the equilibrium constant of the acid AH dissociation and k_w is the equilibrium constant of water dissociation, both in the polymer matrix.

These quantities are extremely difficult to determine experimentally, but the trends predicted by this equation can be checked experimentally. They allow the following cases to be distinguished:

(a) Weak acids in low concentration. In this case, both γ and [AH] are small, $\gamma[AH] \ll 1$, the catalytic effect is negligible. This is the case of terminal acid groups in polyamide 11. If they had a catalytic effect, hydrolysis would be auto-accelerated, which is not the case [104]. Let us recall that the concentration of terminal acids is equal to the reciprocal of number average molar mass (see below).
(b) Weak acids in high concentration. This is the case of many organic acids. The proportion of dissociated acid (γ) is small but the non-dissociated acid is highly soluble in the polymer ([AH] high), so that the catalytic effect can be important.
(c) Strong (e.g. mineral) acids. Here, the fraction of non-dissociated acid in the aqueous phase becomes significant only at high acid concentration (for instance, pH $\leq$ 1). The AH concentration in the polymer can be low, but γ is high and the catalytic effect is noticeable at moderate pH values and can be strong at very low pH values.

NB: Catalytic species such as acids not only accelerate hydrolysis, but also shift equilibrium towards low conversions since they scavenge the terminal groups (e.g. alcohols in the case of polyesters, or amines in the case of polyamides) which, in their absence, would react with acid chain ends. Sometimes, for instance in the case of PA 11 hydrolysis in the presence of carbon dioxide [108], the accelerating effect is low, while the shift of equilibrium is noticeable.

Hydrolysis induced hydrophilicity changes

In certain cases, for instance polyesters, hydrolysis substitutes a moderately polar group (ester) by a pair of strongly polar groups (alcohol + acid). Since hydrolysis rate is an increasing function of the water concentration in the polymer, this increase in hydrophilicity can induce an auto-acceleration of hydrolysis [109] in the absence of auto-catalysis. Assuming that, in a first approach, hydrophilicity is an additive molar function, one can modify the kinetic equation as follows:

$$\frac{dE}{dt} = -k_H[E]\left\{[W]_0 + b\left([E]_0 - [E]\right)\right\} \tag{80}$$

where $[W]_0$ is the initial water concentration and b a parameter expressing the increase in water concentration per hydrolysis event.

4.2 Hydrolysis as a Chain Scission Process: Consequences and Experimental Approaches

In linear polymers

In the simplest case, all the hydrolysable groups are equi-reactive, so hydrolysis is a random chain scission process. In this case, if *s* is the number of moles of chain scissions per mass unit, M_n and M_w are the molar mass averages respectively in number and in weight, the following equations can be written [110, 111]:

$$\frac{1}{M_n} - \frac{1}{M_{n0}} = s \tag{81}$$

$$\frac{1}{M_w} - \frac{1}{M_{w0}} = \frac{s}{2} \tag{82}$$

It can be deduced from these equations that, if the initial polydispersity ratio ($PI_0 = M_{w0}/M_{n0}$) is higher than 2, it must decrease and tend towards 2. If $PI_0 < 2$, it must increase and tend towards 2. If $PI_0 = 2$, it must remain constant. The change of PI during hydrolysis is the best way to check the random (or non-random) character of hydrolysis.

Non-random character can result from various causes:

- Specific reactivity of certain groups, for instance at chain ends;
- Loss of small fragments extracted by liquid water or evaporated;
- Limitation of hydrolysis by crystallites (see below).

In the two former cases, the non-random character is revealed by a gravimetric study [112]. In a purely random process, each hydrolysis event induces a mass increase:

$$\frac{dm}{dt} = 18\frac{ds}{dt} \tag{83}$$

where m is the mass uptake expressed in $g.g^{-1}$ and s is the number of moles of chain scissions per gram.

For a polymer of initial $M_{n0} = 50$ $kg.mol^{-1}$ undergoing a decrease of 10 % after hydrolysis, the number of chain scissions would be about 2×10^{-3} $mol.g^{-1}$ and the mass uptake (for the dry sample) would be 36 mg per gram. Gravimetry is thus an interesting tool for investigating hydrolysis. Chemical or spectrochemical titration of terminal groups can be used in the domain of relatively low molar masses, where these methods are sensitive enough. In the same way, spectrochemical titration of hydrolysable groups, for instance NMR titration of ester groups, can be used, provided it is precise enough.

For linear polymers, molar mass measurements are however the best way to determine the number of chain scissions using the above equations. Molar mass can be determined by viscosimetry. From viscosity measurements on dilute polymer solutions one can determine the reduced viscosity η_{red} from which one can obtain, by extrapolating to zero concentration, the intrinsic viscosity $[\eta]$. This latter is linked to the average molar mass by a power law. The intrinsic viscosity can also be obtained from a single value of the reduced viscosity:

$$\eta_{red} = \frac{\eta - \eta_0}{\eta_0} \tag{84}$$

$$[\eta] = \lim_{C \to 0}\left(\frac{\eta_{red}}{C}\right) \tag{85}$$

$$[\eta] = \frac{1}{2k_H C}\left[-1 + (1 + 4k_H \eta_{red} C)^{1/2}\right] \tag{86}$$

$$[\eta] = KM^a \tag{87}$$

where η and η_0 are the viscosities of the polymer solution and the pure solvent respectively, C is the polymer concentration and k_H is the Huggins coefficient generally of the order of 0.5 ± 0.2. K depends of the nature of solvent and polymer, and temperature; a is an exponent of the order of 0.7 ± 0.2. M is an average molar mass closer to M_w than to M_n. In a first approach, one can consider that: $M = M_w$.

There is also another viscosimetric approach using the Newtonian viscosity η_N determined from rheometric experiments in the molten state. It can be linked to the weight average molar mass using a universal scaling law:

$$\eta_N = KM^{3.4} \tag{88}$$

This method is, indeed, very sensitive, but must be used with caution because the measurements are made at relatively high temperature where the polymer can be reactive (for instance, the reverse reaction of hydrolysis can occur) in the

timescale of experiments. The latter can require a prior neutralization of chain ends.

Steric exclusion chromatography (SEC or GPC for gel permeation chromatography) or mass spectrometry (MALDI TOF), but only when the polymer is polar and the molar mass is not too high (typically $\leq$25 kg.mol^{-1}), allow the molar mass distribution to be established, from which all the average values can be determined. These methods give access to the polydispersity index which allows detecting eventual non-random characteristics.

In semi-crystalline polymers

Since water is insoluble in the crystalline phase, hydrolysis concerns only the amorphous phase. Chain scissions in this latter liberate initially entangled chain segments which have then sufficient mobility (in the rubbery state) to join the crystalline phase. This process of secondary crystallization has been called chemi-crystallization. The amorphous phase is thus destroyed by two phenomena: the "chemi-crystallization" induced by chain scissions [113], which is expected to occur without significant mass change, and the eventual loss of small chain fragments by extraction or evaporation (involving mass loss).

When all the amorphous phase has been destroyed, hydrolysis stops. The kinetic curves of molar mass changes then display an asymptote at a molar mass corresponding to the lamella thickness. In PET, for instance, total hydrolysis leads to an increase in density from 1.413 to 1.453 (theoretically, the density of a 100 % crystalline PET is 1.457), and an increase in the melting point from about 265 °C to more than 270 °C. The degree of polymerization, initially about 70, decreases to an asymptotic value of about 9. The polydispersity index, initially about 2.2, decreases to about unity [114]. Hydrolytic etching (at $T_f > T > 100$ °C under pressure, T_f being the melting point) is an interesting way to determine the lamella thickness in hydrolysable semi-crystalline polymers.

Case of networks

Let us first consider an ideal network in which all the chains are elastically active, i.e. connected at both ends to the network. In this case, each chain scission destroys ζ elastically active chains (EACs). $\zeta = 3$ for a network node functionality $f = 3$ (number of chains starting from a node) and $\zeta = 1$ for $f > 3$ [115]. If s is the number of chain scissions per mass unit, one can thus express the crosslink density ν (EACs concentration) at low conversions of the degradation process by:

$$\nu = \nu_0 - \zeta s \tag{89}$$

For ideal or quasi-ideal networks, we dispose of essentially two methods: (1) rubber elasticity and glass transition temperature for thermosets; (2) rubber elasticity and equilibrium swelling in solvents for rubbers. Concerning swelling, we dispose of the Flory-Rehner theory (paragraph 1.9.1), but it must be used with caution because structural changes (increase in polarity) induced by hydrolysis can modify the polymer–solvent interaction parameter χ and lead to erroneous crosslink density values.

Rubber elasticity

In the simplest approach [116], the stress σ is linked to the draw ratio λ by:

$$\sigma = \mathrm{RT}\rho\,\nu\left(\lambda^2 - \lambda^{-1}\right) \tag{90}$$

The tangent shear modulus G or the tangent Young's modulus E are linked to the crosslink density by:

$$\mathrm{G} = \mathrm{RT}\rho\nu \tag{91}$$

$$\mathrm{E} = 3\mathrm{G} \tag{92}$$

Thus the number s of chain scissions is given by:

$$\mathrm{s} = \frac{1}{\zeta \mathrm{RT}\rho}\left(\mathrm{G}_0 - \mathrm{G}\right) \tag{93}$$

Glass transition temperature

The glass transition temperature T_g is linked to the crosslink density by the Di Marzio relationship [117]:

$$\mathrm{T_g} = \frac{\mathrm{T_{gl}}}{1 - \mathrm{KF}\nu} \tag{94}$$

where K is an universal constant, T_{gl} and F are parameters linked to the (dynamic) chain stiffness.

The derivation gives:

$$\frac{\mathrm{dT_g}}{\mathrm{d}\nu} = \frac{\mathrm{KFT_{gl}}}{\left(1 - \mathrm{KF}\nu\right)^2} \tag{95}$$

The numerator can be typically of the order of 10^4 K.g.mol^{-1} for flexible (aliphatic) chains and of 3×10^4 K.g.mol^{-1} for stiff (aromatic) chains. It appears that the glass transition temperature is sensitive to chain scissions for stiff chain (thermosets), but almost insensitive for flexible chain networks (rubbers).

There are, however, many possible causes of non-ideality. The first one comes from interactions between neighboring EACs. This is taken into account in the Mooney-Rivlin equation [118, 119] which expresses the stress σ against the draw ratio λ:

$$\sigma = \mathrm{RT}\rho\nu\left(1 + \mathrm{c}_2\lambda^{-1}\right)\left(\lambda^2 - \lambda^{-1}\right) \tag{96}$$

In the case of long EACs (rubbers in general), the parameter of non-ideality c_2 can be of the order of unity and must be taken into account. In networks swollen by solvents, c_2 decreases and tends towards zero when the swelling ratio increases. It can thus be interesting to perform mechanical measurements on swollen samples. In dense networks (generally thermosets), c_2 is small and can be often neglected.

The most important cause of non-ideality, in the context of degradation studies, is that chain scission transforms an ideal network into a non-ideal one. A non-ideal

network is constituted of EACs connected on both ends to the network, dangling chains (DC) linked by only one end to the network, and free chains (FC) not linked to the network. A chain scission in an EAC creates two DCs. A chain scission in a FC creates two smaller FCs. A very simple kinetic model can be based on the following considerations:

- The whole concentration [E] of hydrolysable groups (HG) is the sum of the concentrations $[E]_e$ of HGs present in EAC and $[E]_b$ of HGs belonging to non-elastically active chains (DCs and FCs). One EAC contains N_e HGs.
- The reverse reaction is negligible and all HGs are equi-reactive so that:

$$\frac{d[E]}{dt} = -k[W][E] \tag{97}$$

$$[E] = [E]_0 \exp(-k[W]t) \tag{98}$$

$$\frac{d[E]}{dt} = -k[W][E]_0 \exp(-k[W]t) \tag{99}$$

Moreover:

$$[E]_b = [E] - [E]_e = [E] - \nu N_e \tag{100}$$

$$\frac{d[E]_b}{dt} = \frac{d[E]}{dt} - N_e \frac{d\nu}{dt} \tag{101}$$

Let us consider the HGs belonging to non-elastically active chains: they are destroyed by hydrolysis events occurring on DCs or FCs, but each hydrolysis event on an EAC creates $(N_e - 1)$ new "non-elastically active" HGs, thus:

$$\frac{d[E]_b}{dt} = -k[W][E]_b + (N_e - 1)\frac{d\nu}{dt} \tag{102}$$

Combining Eqs 101 and 102 leads to:

$$k[W]N_e\nu + (2N_e - 1)\frac{d\nu}{dt} = 0 \tag{103}$$

With pertinent boundary conditions, this differential equation leads to:

$$\nu = \nu_0(2N_e - 1)\exp(-Kt) - 2\nu_0(N_e - 1) \tag{104}$$

where $K = \frac{k[W]N_e}{(2N_e - 1)}$.

The theories linking a given physical property to the crosslink density ν have been established for ideal networks. Do these theories remain valid for non-ideal ones? There is no clear answer to this question. It is simply assumed that, at least at low departures from ideality, they are applicable, but their limits of validity remain unknown.

In the case of styrene cured unsaturated polyesters, there are, in principle, two kinds of dangling chains: those resulting from terminations and transfer reactions during the styrene-fumarate copolymerization, and those corresponding to the acidic and alcoholic chain ends of the polyester prepolymer. The concentration of the latter is directly linked to the prepolymer molar mass. Furthermore, the corresponding acid and alcohol functions are the same as those created by hydrolysis. In other words, schematically, a polyester of molar mass M is equivalent to a polyester of infinite length having undergone M^{-1} chain scissions per mass unit. It is therefore possible to use polyester networks of known structure to calibrate crosslink density determinations from elastic modulus measurements [120].

4.3 Effect of Structure

Structure-hydrolytic stability relationships have been abundantly investigated in the case of ester-containing polymers. In the simplest case of linear polymers, the initial rate R_s of chain scission is:

$$R_s = \frac{ds}{dt} = k[W][E]_0 \tag{105}$$

Some values of R_s at 100 °C, compiled by Bellenger et al. [121], are reported in Table 9.

It appears that hydrolysis is not slower in networks than in linear polymers. VE are considerably more stable than UP, that can be attributed to the lower reactivity

Table 9 Initial rate of hydrolysis. Data compiled by Bellenger et al. [121]

Polymer	$R_s \times 10^{10}$ (mol.L^{-1}s^{-1})	Activation energy (kJ.mol^{-1})
Polycarbonate bisphenol A (PC)	67	75
Polyethylene terephthalate (PET)	600	107
Unsaturated polyesters (UP)	2,000–15,000	70 ± 10
Vinyl esters (VE)	20–100	–

Table 10 Hydrolysis characteristics of some linear polyesters modeling unsaturated polyesters according to [60]

Code	$[E]_0$ (mol.kg^{-1})	[W] (mol.kg^{-1})	K × 10^8 (kg.mol^{-1}s^{-1})
I-NPG	8.7	2.6	2.7
I-PG	9.7	6.7	2.8
I-EG	9.4	3.2	40
I-DEG	8.5	7.2	2.5
M-NPG	10.9	3.3	41
M-PG	12.4	9.5	38
M-EG	14.1	3.9	192
M-DEG	9.4	10.5	50

of methacrylates (VE) compared to fumarates or phthalates (UP). A detailed study of model compounds of UPs [60, 78] gave more information about the reactivity of the various kinds of esters which may be present in UPs (Table 10). The substrates are homopolymers resulting from the polycondensation of two diacids: isophthalic acid (I) or maleic acid (M) with four diols: neopentyl glycol (NPG), propylene glycol (PG), ethylene glycol (EG) or diethylene glycol (DEG).

These results call for the following comments: In both isophthalate and maleate series, NPG, PG and DEG have close reactivity; esters of ethylene glycol are one order of magnitude more reactive. This is presumably due to the fact that ethylene segments allow interactions between an acid group resulting from hydrolysis and the neighboring ester, which is forbidden with the other diols. One can note that, if NPG systems have the same reactivity as PG ones, they are 2–3 times less hydrophilic. Since the initial rate is proportional to water concentration, NPG systems are 2–3 times more stable than PG ones. In networks, the effect of the diol on hydrophilicity is "diluted" by the presence of 40 ± 5 w% styrene, but its influence on hydrolysis rate is still not negligible.

But, the most striking fact is the difference of reactivity between maleates and isophthalates. Indeed, in a network, maleate units are saturated by styrene, but the aliphatic esters remain relatively highly reactive and constitute, no doubt, the "weak points" of the network.

Styrene cured unsaturated polyesters are, by far, the most important composite matrices undergoing hydrolysis. Among other polymers in which problems of hydrolytic ageing have been observed, one can cite: polyamides, including aromatic ones (for instance, Kevlar) [122], anhydride cured epoxies, polyurethanes based on polyesters, vinyl esters, polyvinyl acetate used as low profile additive in polyester sheet molding compounds or bulk molding compounds, etc. There is not, to our knowledge a theoretical tool able to predict the hydrolysis rate of a given group in a given polymer.

4.4 Diffusion Controlled Hydrolysis

Let us consider the simplest case of almost irreversible hydrolysis where the rate of water consumption r_w is proportional to the water concentration [W]:

$$\frac{dW}{dt} = -k[E]_0[W] = -K[W] \tag{106}$$

where K is a pseudo first order rate constant depending only on temperature.

One can define a characteristic time t_R of this reaction:

$$t_R = K^{-1} \tag{107}$$

For a bulk sample of thickness L, one can define a characteristic time t_D for water diffusion:

$$t_D = L^2/D \tag{108}$$

where D is the coefficient of water diffusion into the material.

One can then consider the ratio of characteristic times:

$$J = t_R/t_D \tag{109}$$

- If $J \gg 1$, diffusion is faster than reaction and homogenizes the distribution of water concentration in the sample thickness. Hydrolysis is homogeneous.
- If $J \ll 1$, hydrolysis consumes all the available water in a superficial layer, the water concentration in the sample core is lower than in superficial layers. Hydrolysis is diffusion controlled and degradation is heterogeneous.

The kinetic problem of diffusion controlled hydrolysis in polyesters was first solved by Golike and Lasoski [123]. When the reverse reaction is negligible, the kinetic equation can be written:

$$\frac{\partial W}{\partial t} = D\frac{\partial^2 W}{\partial z^2} - k[E][W] \tag{110}$$

At low conversions, [E] can be considered constant and $k[E] = K =$ constant. If a steady state is rapidly reached, $\delta W/\delta t = 0$ and, if the sample is exposed on both sides:

$$D\frac{\partial^2 W}{\partial z^2} = K[W] \tag{111}$$

This equation can be solved taking, for instance, the origin of z at a surface:

$$[W] = [W]_s \frac{\cosh B\left(z - \frac{L}{2}\right)}{\cosh B\frac{L}{2}} \tag{112}$$

where $B = (K/D)^{1/2}$.

One sees that, if $L \ll B^{-1}$, hydrolysis is almost homogeneous. In contrast, if $L \gg B^{-1}$, the sample core will remain non-degraded, hydrolysis will affect only a superficial layer whose thickness is of the order of $3B^{-1}$. It is noteworthy that, in this model, the shape of the water concentration profile in superficial layers is exponential (Fig. 14) and the thickness of the degraded layer is independent of hydrolysis conversion. In a polyester composite at 20 °C, the coefficient of water diffusion is of the order of 10^{-13} $m^2.s^{-1}$, and the extrapolated first order rate constant of hydrolysis is about 10^{-11} s^{-1}. B^{-1} is therefore of the order of 0.1 m. Hydrolysis is thus expected to be almost homogeneous in samples of thicknesses of few cm.

Note that, if K and D obey an Arrhenius law with respective activation energies H_K and H_D, then B^{-1} also obeys an Arrhenius law:

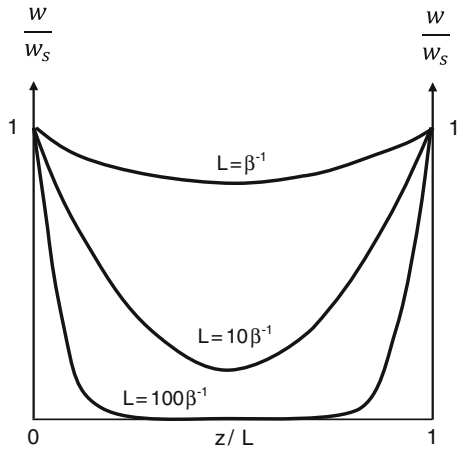

Fig. 14 Shape of the water concentration profile in reduced coordinates

$$B^{-1} = B_0^{-1} \exp\left[\frac{1}{2}(H_K - H_D)\right] \tag{113}$$

Since, generally, $H_K > H_D$, B^{-1} is expected to decrease when the temperature increases. A hydrolytic ageing can thus be homogeneous in service conditions and diffusion controlled under accelerated ageing conditions. Typically, for polyester composites, B^{-1} would be of the order of 1 cm at 100 °C.

If hydrolysis is equilibrated, as in the case of PA 11 [104], the hydrolysis rate decreases progressively and B^{-1}, which is inversely proportional to K, increases. Water invades the sample thickness and hydrolysis tends to become homogeneous.

4.5 Osmotic Cracking

In the 1970s–1980s, blistering appeared worldwide on polyester composite boat hulls and seriously affected the manufacturers. Blisters are cracks propagating parallel to the surface in the back-up layer, between the gel-coat and the first fiber reinforced layer. Blistering also appeared in other structures based on polyester matrix composites: tanks, swimming pools, etc. It was soon diagnosed as an osmotic cracking process for which the mechanism can be briefly resumed as follows [124–126]: microcavities of unknown origin are initially present, they are filled by water. Small molecules or salts, initially present in the matrix (for instance, catalyst residues) or formed during hydrolysis, are dissolved by water and accumulate into microcavities. The material layer separating a microcavity and the water bath is permeable to water, but considerably less permeable to larger molecules. It thus works as a semi-permeable membrane and an osmotic pressure

develops into the cavity. According to Van't Hoff (1882) [127] the osmotic pressure is given by:

$$p = RT \sum C_i \tag{114}$$

where C_i is the concentration of the *i*th solute in the microcavity.

Using the classical fracture mechanics concepts, one can determine the critical pressure p_c to initiate crack propagation [49]:

$$p_c = \left(\frac{3EW_s}{2h}\right)^{1/2} \tag{115}$$

where E is the Young's modulus, W_s is the surface energy and h is the cavity diameter.

Taking the following orders of magnitude: E = 3 GPa, $W_s = 1\ J.m^{-2}$ and h = 10 μm, one obtains: $p_c \sim 20$ MPa, a value not very far from the ultimate strength of the polyester matrix. Using now the Van't Hoff relationship, one obtains $\Sigma\ C_i = 8000\ mol.m^{-3}$, i.e. $8\ mol.L^{-1}$.

The osmotic cracking process can be revealed using gravimetric curves of relatively thin samples (typically ≤1 mm), where the characteristic time of diffusion is lower than the characteristic time of osmotic damage. The kinetic curves of mass variation have a typical shape (Fig. 15) [128].

Four elementary times can be distinguished:

- $0 < t < t_1$: physical water sorption. The system reaches an equilibrium linked to water solubility at t_1.
- $t_1 < t < t_2$: the system stays in pseudo-equilibrium. It undergoes hydrolysis, but the conversion ratio remains low, on this side of the sensitivity of the measuring method.
- $t > t_2$: propagation of osmotic cracks begin at t_2. The increase of mass uptake corresponds to the increase of volume created by cracking. t_2 is a quantity well

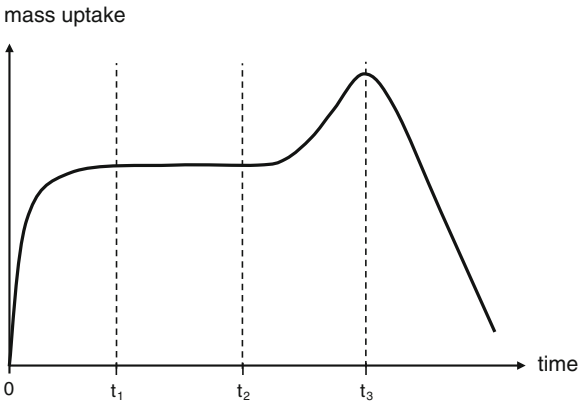

Fig. 15 Typical shape of the gravimetric curve of a thin sample undergoing osmotic cracking

representative of the material stability. It can be called the induction time of cracking.

- At t_3, the cracks coalesce. A large part of the solutes responsible for osmosis is abruptly transferred to the bath, which explains the fast mass decrease after t_3.

In the former studies of the process, the authors supposed that the small molecules were mainly catalyst residues and other additives. These products are, however, in too small concentrations to reach the value of 8 $mol.L^{-1}$ calculated above. Various studies, in the 1980s–1990s showed the importance of certain matrix structural characteristics, as well the nature and concentration of ester groups [129, 130]. Mortaigne et al. [131] confirmed the influence of the ester nature, but showed also that the induction time of osmotic cracking is almost proportional to the reciprocal of the prepolymer molar mass, i.e. almost proportional to the concentration of polyester chain ends. Osmotic crack propagation was well understood but the mechanism of crack initiation remained unexplained. The hypothesis of the presence of micro-pores is not proven. Osmotic cracking can occur in highly homogeneous polymer glasses as, for instance, polycarbonate [132], where the presence of porosities is not obvious. Gautier et al. [128] proposed the following synthetic explanation: solutes can be effectively present but the most important part results from hydrolysis events near polyester chain ends that explains the result cited above of Mortaigne et al. [131]. Indeed random hydrolysis generates new chain ends and, then, contributes also to the process. These small molecules remain dissolved in the matrix until the time when their concentration becomes higher than their solubility threshold. Then, they demix and form highly hydrophilic micro-pockets able to initiate cracking. Then, the induction time of osmotic cracking would be the time at which the concentration of small molecules reaches its solubility limit. This reasoning leads to the following equation:

$$C = C_0 + 2aKb_0t + aK^2[E]_0t^2 \tag{116}$$

where C is the solute concentration, C_0 is the concentration of initially present water soluble molecules; a is a dimensionless parameter of the order of unity corresponding to the average number of hydrolysable groups close to the chain end in a dangling chain, K is the first-order rate constant of hydrolysis, b_0 is the initial concentration of polyester chain ends, and $[E]_0$ is the initial ester concentration.

The build-up of osmotic pressure is thus decomposed into three terms which suggest three ways for stabilization: minimizing catalyst concentrations (C_0); increasing the prepolymer molar mass, i.e. reducing b_0, but there is a limit imposed by the viscosity requirements for composite processing; decreasing the hydrolysis rate constant, which depends on ester reactivity and polymer hydrophilicity. Concerning a change of ester reactivity, it is possible to optimize the choice of the saturated (aromatic) diacid. For instance, it has been demonstrated, a long time ago, that isophthalates are more stable than orthophthalates. But, this optimization must have limited effects because the weakest point of these polyesters is the

maleate unit. Replacement of maleic acid by another unsaturated diacid seems economically difficult. Minimizing hydrophilicity is possible, using bulky, non-polar diols such as neopentyl glycol.

If the end of induction period corresponds to a critical concentration C_L of small molecules, the induction time t_i can be determined by solving the above equation:

$$t_i = \frac{b_0}{K[E]_0}\left\{-1+\left[1+\frac{[E]_0(C_L-C_0)}{ab_0^2}\right]^{1/2}\right\} \tag{117}$$

Since $[E]_0$ and $(C_L - C_0) \gg b_0$, and $C_L \gg C_0$ one can reduce the above equation to:

$$t_i \approx \frac{1}{K\sqrt{a}}\left(\frac{C_L}{[E]_0}\right)^{1/2} \tag{118}$$

The diffusivity D_s of small molecules is low compared to water diffusivity but not null. One sees that, if the characteristic time of diffusion $t_D = L^2/D_s$ is shorter than t_i, small molecules cannot accumulate in the matrix, they migrate in the bath and the critical concentration C_L cannot be reached. In this case, blistering is suppressed.

4.6 Consequences of Hydrolysis on Matrix Properties

Linear polymers

The effect of random chain scissions on mechanical properties has been reviewed by Fayolle et al. [113].

The effect on elastic properties is very limited, the shear and Young's moduli remain almost constant in glassy amorphous polymers, a long time after embrittlement has occurred. In semi-crystalline polymers, a small modulus increase, linked to chemicrystallization, can be observed. Hydrolysis of PET sheets offers a good example: After 15 days in boiling water, the samples are stiffer than initially but their fracture behavior is very close to that of eggshells.

The most important effect of hydrolysis is thus a deep embrittlement linked to the destruction of the entanglement network in glassy polymers and semi-crystalline polymers having a limited crystallinity ratio such as PET or PA 11. In non-polar polymers, there is another embrittlement mechanism linked to the decrease of interlamellar spacing, but there are no hydrolysable polymers in this latter category.

Studies of the molar mass dependence of toughness have revealed the existence of a discontinuity at a molar mass M_D (Fig. 16).

This critical molar mass is clearly related to the entanglement molar mass M_e, typically $M_D \sim (2–10) \times M_e$. The high initial toughness is linked to the existence

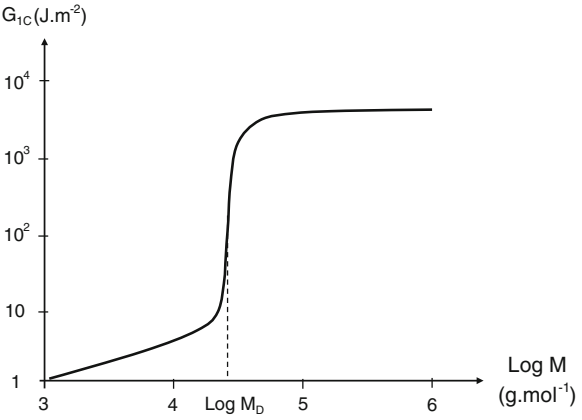

Fig. 16 General shape of the molar mass dependence of toughness (G_{1C} is the critical rate of elastic energy release in mode I)

of plastic deformation involving chain drawing. This latter is only possible if the chains participate in a network. In amorphous linear polymers, the network structure is due to chain entanglements and these exist only when the chains have a length higher than a critical value corresponding to a small multiple of M_e. Hydrolysis destroys this entanglement network. When it reaches the state where the chains disentangle easily during stretching, i.e. when M approaches M_D, the toughness decreases suddenly by 2 or 3 decades. As a result, ageing can be assimilated to a ductile–brittle transition. The characteristics of this transition constitute an ideal end-life criterion because it is almost independent of experimental parameters and corresponds to a deep change in fracture properties. Let us consider the simplest kinetic model:

$$\frac{ds}{dt} = k[W][E]_0 \tag{119}$$

Thus:

$$s = k[W][E]_0 t \tag{120}$$

The end-life criterion is:

$$s_f = \frac{1}{M_D} - \frac{1}{M_{n0}} \tag{121}$$

The lifetime t_f is thus:

$$t_f = \frac{1}{k[W][E]_0}\left(\frac{1}{M_D} - \frac{1}{M_{n0}}\right) \tag{122}$$

Note that, $s_f < M_D^{-1}$ always, and generally, $M_D \geq 10$ kg/mol. Thus, embrittlement occurs at a very low conversion of the hydrolysis reaction, that justifies the approximation made in the expression for degradation rate, except in rare cases where hydrolysis reaches its equilibrium at low conversion (case of PA 11).

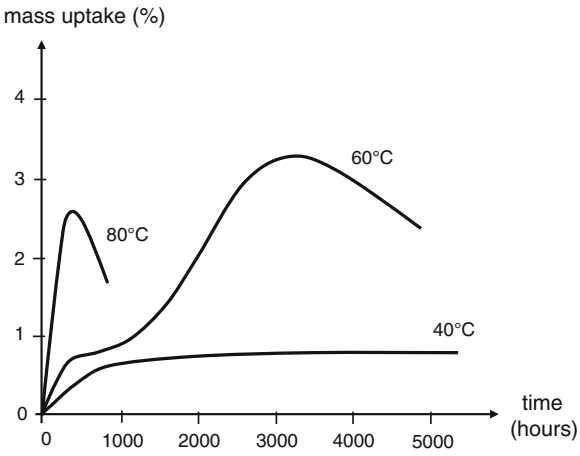

Fig. 17 Mass uptake against exposure time in distilled water for composites based on 50 w% glass E fibers and orthophthalic polyester matrix. Adapted from Jacquemet and Lagrange [77]

In polymers such as PA 11, PET or PC, the critical molar mass M_D is about 15 kg.mol^{-1} when the initial molar mass M_{n0} is generally in the 30–100 kg.mol^{-1}. In other words, just a few scissions per chain are sufficient to induce embrittlement.

Tridimensional polymers

In polyester composites, hydrolysis effects can be observed on weight uptake curves as shown, for instance, by the behavior of glass E-orthophthalic polyester composites ([77], Fig. 17).

There is a great amount of published data on humid ageing of polyester composites, but they are not easy to interpret in terms of degradation mechanisms. There are also data about the influence of crosslink density on matrix mechanical properties [115], but they are not applicable to degradation studies. As a matter of fact, these studies consider ideal networks in which all the chains are assumed to have a small polydispersity.

In the case of ideal networks, a decrease of crosslink density results from an increase of the chain length: $\nu = M_e^{-1}$. In the case of degradation, the molar mass M_{e0} of EACs remains constant, but the number of EACs decreases. In the simplest case: $\nu = \nu_0 - s$. The consequences of a crosslink density decrease on rubbery elastic modulus are the same, in both cases: $E = 3RT\ \rho\ \nu$.

In contrast, there is little practical influence on elastic modulus in the glassy state. In the case of networks having a transition β of low activity as, for instance, unsaturated polyesters or vinyl esters, there are only small modulus variations. In the case of networks having a transition β of high activity, chain scissions induce an antiplasticization effect, i.e. a decrease in the activity of the β relaxation and an increase of modulus on the glassy plateau between T_β and T_g. This phenomenon has not been observed in hydrolysis cases, but it has been shown in the case of oxidation of amine crosslinked epoxies [133].

The consequences of a crosslink density decrease on fracture properties of ideal and degraded networks are opposed: the toughness increases in the case of ideal

networks [115], but decreases in the case of degraded networks. This is the reason why ideal networks are not good models for the study of relationships between structure and fracture properties of degraded networks. Unfortunately, to our knowledge, there is no physical theory predicting fracture properties of networks with broken chains. Model networks of degraded thermosets can, however, be synthesized as, for instance, in the case of unsaturated polyesters (UP) [131].

Let us consider an UP matrix based on a polyester prepolymer of molar mass M_0. After ageing it has undergone s chain scissions per polyester mass unit. The degraded matrix cannot be distinguished from a virgin (model) polyester of molar mass M such as:

$$\frac{1}{M} = \frac{1}{M_0} + s \tag{123}$$

Networks based on polyester prepolymers of known molar mass can thus be used as model compounds for degraded networks based on initially longer prepolymers in order to appreciate degradation effects on mechanical properties and to calibrate crosslink density measurements, for instance, from rubber elastic modulus.

In initially brittle networks such as, for instance, polyester networks, fracture properties decrease progressively with the number of chain scissions. According to Vincent [134] or Seitz [135], the ultimate stress would be proportional to the number of chains crossing the fracture plane, that would give, for an initially ideal network of ultimate stress σ_{R0} and EAC molar mass M_e:

$$\sigma_R = \sigma_{R0}(1 - 2sM_e) \tag{124}$$

4.7 Stress Effects on Hydrolysis

Let us return to the hydrolysis mechanism shown in Sect. 4.1. There are two main steps: first, water addition to the hydrolysable group giving an unstable structure; second, rearrangement of this structure with a chain scission. One can suppose that, if the chain is under a tension σ, this must essentially affect the second step. If the rate controlling step is the first one, stresses are expected to have no direct influence on hydrolysis kinetics (an indirect influence can come from stress effects on water solubility and diffusivity seen previously). If, in contrast, the rate controlling step is the second one, the stress will accelerate hydrolysis. According to the simplest theory of stress assisted reactions, the hydrolysis rate r would be linked to the stress by:

$$r = r_0 \exp\left(-\frac{H - V\sigma}{RT}\right) \tag{125}$$

where H is the activation energy of hydrolysis and V an activation molar volume expressing the sensitivity of the reaction to stresses.

The problem, here, is that experimental studies of this phenomenon need to dispose of a method for precise measurement of the hydrolysis rate, that is generally easier on linear than on tridimensional polymers. The activation volume V must be high enough to have measurable effects at stress levels lower than yield stress, otherwise creep, damage or fracture would complicate the analysis in the case of isoptropic or quasi-isotropic samples. These problems do not arise in the case of highly oriented samples such as, for instance, aramid fibers which have very high yield stress values and can thus support hydrolytic ageing experiments under high tensile stress [136].

Experiments made on isotropic unreinforced polymers are very scarce. In the case of polycarbonate, for instance, measurable effects have been observed, but the stress dependence of hydrolysis rate does not obey the above law [137].

Experiments on composites in wet or aqueous media have often been reported in the literature. A classical way of presenting results consists in plotting the applied stress σ against the logarithm of time to failure t_f. The problem, here, is to interpret highly scattered results. As a example, Philips [138] made a detailed study of this data scatter and obtained a plot having the shape of Fig. 18.

At high stress values, typically more than the half of instantaneous fracture strength, the dependence is linear, the slope lower than unity. It may be noted that this dependence is compatible with Eyring's law expressing the strain rate ε' as a function of stress and temperature:

$$\varepsilon' = \varepsilon'_0 \exp\left(-\frac{H - V\sigma}{RT}\right) \tag{126}$$

Considering that $\varepsilon = \varepsilon' \times t$ and that there is an ultimate strain ε_f, one defines the time to failure t_f by:

$$t_f = \frac{\varepsilon_f}{\varepsilon'} \tag{127}$$

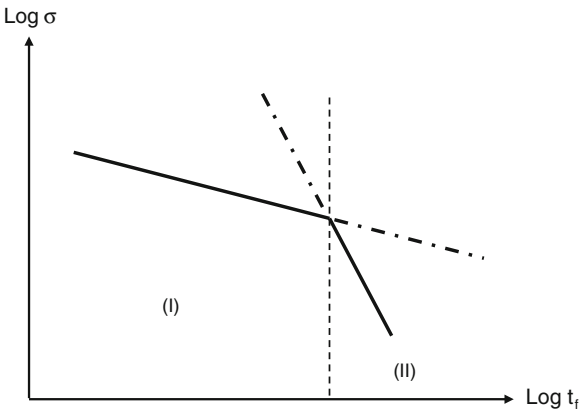

Fig. 18 Stress normed by the instantaneous failure stress against log(time to failure) for polyester laminates according to Philips [138]

$$\mathrm{Log}\, t_f = A - b\frac{\sigma}{\sigma_0} \tag{128}$$

with:

$$A = \mathrm{Log}\frac{\varepsilon_f}{\varepsilon_0'} + \frac{H}{RT} \tag{129}$$

and:

$$\frac{b}{\sigma_0} = \frac{V}{RT} \tag{130}$$

In this stress/time domain, failure would only be due to physical processes (creep) and would be independent of environment. Beyond a certain time (about 20 days at 60 °C, 40 days at 40 °C, and 500 days at 20 °C), the absolute value of the slope b increases abruptly, showing that another failure mechanism takes place. At 23 % of instantaneous ultimate stress, the lifetime is one month at 60 °C, 11 months at 40 °C, and 30 months at 20 °C. The second process can be resin plasticization, inducing a creep acceleration, and/or polyester hydrolysis. The effect of this latter presumably predominates at 60 °C and is responsible for the steep slope value.

4.8 Hydrolytic Processes in the Interfacial Region

Let us consider the results reported by Theberge [139] on humid ageing by immersion in boiling water for three thermoplastics: polycarbonate (PC), polyoxymethylene (POM), and impact modified poly(2–6 dimethyl oxyphenylene) (PPO), and their short glass fiber (30 w%) composites (Table 11).

Polycarbonate undergoes hydrolysis. In the short term, the composite degrades faster than the matrix, which can be attributed to interfacial degradation, but, at long term, both the matrix and the composite are strongly degraded, which can be, at least in part, attributed to the matrix hydrolysis. More interesting are the results obtained on both non-hydrolysable polyethers, POM and PPO. In these cases, the

Table 11 Strength retention (SR) after immersion in boiling water for 100 and 1,000 h of three thermoplastics and their glass fiber composites. After Theberge [139]

Polymer	Glass fiber (%)	SR (%) after 100 h	SR (%) after 1,000 h
PC	30	51	28
PC	0	100	28
POM	30	71	57
POM	0	100	98
PPO	30	84	65
PPO	0	100	100

matrix is stable, even at long term, while the composite undergoes a significant degradation. The only possible explanation is that the composites fail by interfacial degradation. No information was available about interface/interphase, but this result clearly shows that composites based on non-hydrolysable matrices are ideal candidates for studies on hydrolytic degradation of the interfacial zone because it is the unique possible cause of mechanical property changes.

Despite about 40 years of intensive research, it remains difficult to have a clear and exhaustive vision of the role of the interface/interphase in humid ageing. Considering, first, the case of uncoupled fibers, one sees various possible causes of a specific attack of water in the interfacial region: first, the presence of interfacial voids allowing a fast penetration of water in deep layers (for instance [140]). Glass fibers have an alkaline character, which may be able to play a catalytic role on ester hydrolysis. Mortaigne [141] studied the hydrolysis of glass microspheres/polyester composites at 100 °C and compared the apparent first-order rate constants of hydrolysis of samples containing 10, 30 or 60 w% coupled or uncoupled glass microspheres. The results are presented in Fig. 19.

Hydrolysis is accelerated in the presence of glass, which can be attributed to basic catalysis, and the coupling agent (of unknown nature) displays a limited but significant stabilizing effect, especially at high glass content. Thus, at least for the above two reasons: interfacial voids and catalytic effect of reinforcing agent (in the case of glass), coupling agents are expected to have a positive effect on the composite stability in humid ageing conditions. There is an impressive number of published works confirming this stabilizing role of coupling agents, for instance Kaelble et al. [142], Joshi [143], Woo and Piggott [144, 145], Di Benedetto and

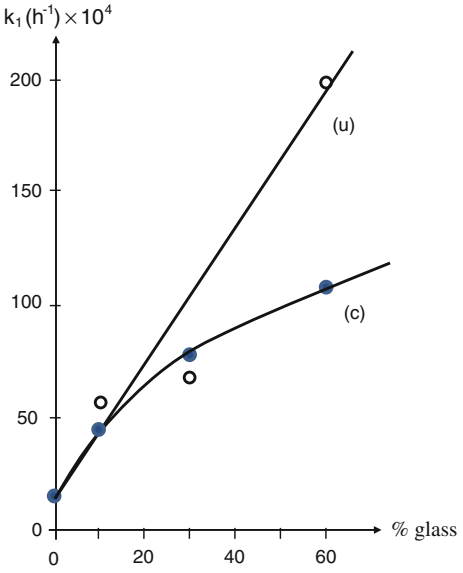

Fig. 19 Pseudo first-order rate constant of polyester hydrolysis against mass fraction of coupled (c) and uncoupled (u) glass microspheres of 50 μm diameter and 1,600 kg.m^{-3} density

Lex [146], etc. However, despite this role, the interphase can remain the weakest zone of the composite because it is susceptible to undergo hydrolysis. This is now well recognized in the case of silane coupling agents where the interphase can be schematized as follows:

The coupling agent is a trialkoxy silane (Alk-O-)$_3$Si-R where -Alk is an alkyl group, generally -CH_3 or -C_2H_5, and -R is a function able to establish a bond with the polymer through a reaction with a reactive group Y of this latter:

$$\mathrm{Si-R} \; + \; \mathrm{Y-Polym} \rightarrow \mathrm{Si-R'-Polym} \; + \; \text{products}$$

Hydrolysis of the Si-O bonds of the coupling agent generates silanol groups able to condensate with the silanol groups present at the glass surface or with themselves:

Coupl-Si-O-Alk + H_2O → Coupl-Si–OH + Alk-OH (hydrolysis of coupling agent)
Coupl-Si–OH + Glass-Si–OH → Coupl-Si–O-Si-Glass + H_2O (chemical bonding with glass fibers)
Coupl-Si–OH + Coupl-Si–OH → Coupl-Si–O-Si-Coupl + H_2O (polycondensation of coupling agent).

The interphase can be then schematically represented by the model of Fig. 20.

One can distinguish three layers separated by diffuse boundaries. The intermediary layer (II) is made of a network resulting from the polycondensation of the coupling agent. In this layer, groups –R are non-reacted. The layer (II) is linked to glass by Si-O– bonds (layer (I)) and to polymer by –R′– bonds (layer (III)). The extension of the latter depends on the diffusion conditions of the monomers used for crosslinking layer (II) [53]. Since, generally, the group –Y used to react with the coupling agent is also reactive in polymer crosslinking, one can expect a local perturbation of the polymer structure resulting from the local deficit of –Y groups [56, 147]. This interphase structure has been described by various authors, among whom Ishida [148, 149] has been a prominent contribution.

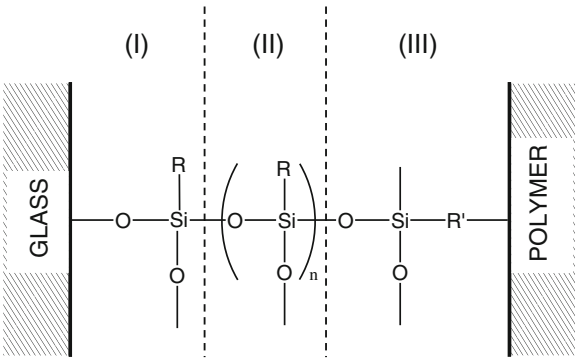

Fig. 20 Schematization of the interphase in the case of glass fiber coupled by trialkoxysilane

Table 12 Time to dissolution in water for networks resulting from the polycondensation of three distinct coupling agents. After Salmon et al. [58]

Network code	Time to complete dissolution at 100 °C (h)	Time to complete dissolution at 65 °C (h)
Am	0.08	1
Ep	35	300
Alk	8.000	–

It was soon recognized that such interphases can undergo hydrolysis [55, 150–153]. There are now sophisticated methods to reveal structural changes in the interfacial zone of a fiber composite, but in general these methods lack sensitivity for quantitative measurements in order to determine the kinetic parameters of hydrolysis. Salmon et al. [58] prepared bulk samples of networks resulting from the polycondensation of common coupling agents based on triethoxy amino (Am), epoxy (Ep) or alkyl (Alk) silanes. It has been shown in paragraph 2.8 that the water equilibrium concentration varies in the order: Am $\gg$ Ep $>$ Alk. The diffusion coefficients at 20 °C are comparable: $D \sim (2 \pm 1) \times 10^{-12}$ $m^2.s^{-1}$. From gravimetric experiments, it was possible to estimate the time for complete network hydrolysis (total solubility in water). The results are reported in Table 12.

In such networks, the functional group of the coupling agent remains unreacted. Salmon et al. also studied model compounds resulting from the condensation with polymer reactive groups. As an example, the amino silane was reacted with an epoxide group (phenyl glycidyl ether (PGE)). The resistance of these compounds to hydrolysis was considerably better than the preceding ones, showing the importance of the reactive group, especially the primary amine in Am networks, in the reactivity with water. It appears thus that hydrolytic degradation in the interfacial zone must occur preferentially in zones (I) or (II) (Fig. 20), and that the choice of the reactive group (when several options exist) can be crucial. The authors checked the validity of their approach by comparing the stability of glass/silane/glass joints immersed in distilled water at 60 °C. The joint lifetime was 1–2 days for Am, 5–7 days for Ep, and more than 90 days for Alk. The hierarchy is respected, but the difference between Am and Ep is less marked. The authors showed, however, that transposition of these results to industrial fiber composites is not obvious, other components than silanes are present in the fiber sizing and can affect the hydrolysis behavior.

It can be noticed that, in composites, the interphase is confined. Water absorption and hydrolysis are expected to induce volume changes, but the latter are hindered, so that hydrostatic pressure must grow in the interfacial zone. Does this pressure affect the mechanical behavior ? Could it shift the hydrolysis equilibrium towards lower conversions ? These questions, among many others, show that our current knowledge remains far from what would be needed for a non-empirical lifetime prediction in this domain.

5 Conclusion

Research on composite durability began almost half a century ago. It was soon recognized that there are two main matrix categories. The first category includes the polymers which react chemically with water, for instance polyesters. Here, it is supposed that failure results from the following causal chain:

$$\text{Polymer} + \text{water} \rightarrow \text{water absorption} \rightarrow \text{polymer hydrolysis} \rightarrow \text{degradation of the macromolecular backbone} \rightarrow \text{embrittlement} \rightarrow \text{failure}.$$

It appeared that, in these polymers, kinetic modeling of hydrolysis would be the most important objective of research.

The second category includes the non-reactive polymers, for instance amine cured epoxies, for which failure results from the following causal chain:

$$\text{Polymer} + \text{water} \rightarrow \text{water absorption} \rightarrow \text{polymer swelling} \rightarrow \text{stress state} \rightarrow \text{failure}.$$

In both categories, water concentration is an important quantity. Its prediction involves a series of research objectives relative to the mechanism(s) of water dissolution in the polymer, the role of thermodynamic parameters (temperature, hygrometry, stress state), and the solubility-structure relationships. Indeed, in thick samples, water does not invade instantaneously the whole volume, it is thus important to establish the kinetic laws of diffusion. This is especially important for the second category where swelling stresses are generated by water concentration gradients in the sample thickness. In this chapter, have shown that, in many aspects, water solubility and diffusivity in composite matrices remain largely open research areas.

In the case of the first category, the most critical questions are, in our opinion, those relative to embrittlement mechanisms, especially in networks: relationships between the network structure and fracture properties; role of degradation gradients; role of matrix mechanical properties in composite fracture.

In the case of the second category, the mechanical analysis of swelling effects has been the subject of sophisticated approaches profiting from the advances in mechanics of heterogeneous materials. Surprisingly, the swelling phenomenon itself has been the subject of few studies, one cannot consider that it is a fully elucidated mechanism, and it remains an open research area.

To summarize the above aspects, when the composite fails by matrix chemical degradation or by matrix swelling, there is sufficient knowledge to build reasonably non-empirical lifetime prediction models. Certain elements, for instance the prediction a priori of clustering or swelling ratio, remain out of reach, but can be replaced by empirical relationships. When the composite fails by its interfacial zone, we have now elements for a partial understanding of mechanisms, but we lack almost totally basic quantitative data to build non-empirical kinetic models able to predict failure. It seems to us that this domain requires considerable research efforts in the future.

References

1. Lubin G, Donohue P (1980) Real life ageing of composites. In: 31st ANTEC, reinforced plastics/composites section, The Society of the Plastics Industry, paper 17E
2. McCall DW, Douglass DC, Blyler LL Jr, Johnson GE, Jelinski LW, Bair HE (1984) Solubility and diffusion of water in low-density polyethylene. Macromolecules 17(9): 1644–1649
3. MKacher I (2012) Vieillissement thermique des gaines PE et PVC de câbles électriques, PhD Thesis, ARTS ET METIERS ParisTech Paris, France
4. Li SZ, Chen RS (1995) NMR studies of water in polyimide films. J Polym Sci Part B Polym Phys Ed 33(3):403–409
5. Zhou J, Lucas JP (1999) Hygrothermal effects of epoxy resin. Part I: the nature of water in epoxy. Polymer 40:5505–5512
6. Popineau S, Rondeau-Mouro C, Sulpice-Gaillet C, Shanahan MER (2005) Free/bound water absorption in an epoxy adhesive. Polymer 46:10733–10740
7. Reid JD, Lawrence WH, Buck RP (1986) Dielectric properties of an epoxy resin and its composite I. Moisture effects on dipole relaxation. J Appl Polym Sci 31(6):1771–1784
8. Grave C, McEwan I, Pethrick RA (1998) Influence of stoichi- ometric ratio on water absorption in epoxy resins. J Appl Polym Sci 69(12):2369–2376
9. Lim RS, Nowick AS, Lee KW, Viehbeck A (1993) Sorption of water and organic solutes in polyimide films and Its effects on dielectric properties. J Polym Sci Polym Phys Ed 31: 545–555
10. Illinger JL, Schneider NS (1980) Water vapor transport in an epoxy resin based on TGMDA and DICY. Polym Eng Sci 20:310–314
11. Cotugno S, Larobina D, Mensitieri G, Musto P, Ragosta G (2001) A novel spectroscopic approach to investigate transport processes in polymers: the case of water–epoxy system. Polymer 42(15):6431–6438
12. Brunauer S, Emmett PH, Teller E (1938) Adsorption of gasses in multimolecular layers. J Amer Chem Soc 60(2):309–319
13. Barrett EP, Joyner LG, Halenda PP (1951) The determination of pore volume and area distributions in porous substances. I. Computations from nitrogen isotherms. J Amer Chem Soc 73:373–380
14. Desvaux H, Gautier T, Le Goff G, Petro M, Berthault P (2000) Direct evidence of a magnetization transfer between laser-polarized xenon and protons of a cage-molecule in water. Eur Phys J D 12:289–296
15. Zimm BH, Lundberg JL (1956) Sorption of vapours by high polymers. J Phys Chem 60(4): 425–428
16. Barrer R, Barrie J, Slater J (1958) Sorption and diffusion in ethyl cellulose. Part III. Comparison between ethyl cellulose and rubber. J Polym Sci 27:177–197
17. Merdas I, Thominette F, Tcharkhtchi A, Verdu J (2002) Factors governing water absorption by composite matrices. Compos Sci Technol 62:487–492
18. Tcharkhtchi A, Bronnec Y, Verdu J (2000) Water absorption characteristics of diglycidylether of butane diol-3,5-2,4-diaminotoluene networks. Polymer 41(15):5777–5785
19. Derrien K, Gilormini P (2007) The effect of applied stresses on the equilibrium moisture content in polymers. Scr Mater 56(4):297–299
20. Weitsman YJ (1987) Stress assisted diffusion in elastic and viscoelastic materials. J Mech Phys Solids 35(1):73–93
21. Weitsman YJ (2000) Effects of fluids on polymeric composites—a review. Compre Compos Mater 2:369–401
22. Adamson MJ (1980) Thermal expansion and swelling of cured epoxy resin used in graphite/ epoxy composite materials. J Mater Sci 15:1736–1745
23. Enns JB, Gilham JK (1983) Effect of the extent of cure on the modulus, glass transition, water absorptio, and density of an amine-cured epoxy. J Appl Polym Sci 28(9):2831–2846

24. Gupta VB, Drzal LT, Rich M (1985) The physical basis of moisture transport in a cured epoxy resin system. J Appl Polym Sci 30(11):4467–4693
25. Johncock P, Tudgey GF (1986) Some effects of structure, composition and cure on the water absorption and glass transition temperature of amine-cured epoxies. Brit Polym J 18(5): 292–302
26. Barrie JA (1968) Water in polymers. In: Crank J, Park GS (eds) Diffusion in polymers, 4th edn. Academic Press, London, pp 259-313
27. Morel E, Bellenger V, Verdu J (1985) Structure-water absorption relationships for amine cured epoxy resins. Polymer 26:1719–1724
28. Van Krevelen DW, Te Nijenhuis K (2009) Properties of polymers. Their correlation with chemical structure. Their numerical estimation and prediction from additive group contributions, 4th edn. Elsevier, Amsterdam
29. Bellenger V, Verdu J, Morel E (1989) Structure properties relationships for densely crosslinked epoxy-amine system based on epoxide or amine mixtures. J Mater Sci 24:63–68
30. Bellenger V, Mortaigne B, Verdu J (1990) Water sorption in styrene crosslinked polyesters. J Appl Polym Sci 41:1225–1233
31. Bellenger V, Verdu J, Ganem M, Mortaigne B (1994) Styrene crosslinked vinylesters. II: water sorption, water diffusion and cohesive properties. Polym Polym Compos 2(1):17–25
32. Gaudichet-Maurin E, Thominette F, Verdu J (2008) Water sorption characteristics in moderately hydrophilic polymers. Part 1: effect of polar groups concentration and temperature in water sorption in aromatic polysulphones. J Appl Polym Sci 109(5):3279–3285
33. Pethrick RA, Hollins EA, McEwan L, Pollock A, Haymard D, Johncock P (1996) Effect of cure temperature on the structure and water absorption of epoxy/amine thermosets. Polym Int 39(4):228–275
34. Pimentel GC, McClellan AL (1960) Methods of detection: infrared and Raman Spectroscopy. In: Freeman WH (ed) The hydrogen bond. San Francisco, pp 67–141
35. Razumovskii LP, Zaikov GE (1985) Determination of the solubility and diffusion coefficients of water in aliphatic polyamides as a step to studying their hydrolytic stability. Polym Degrad Stab 12(1):1–12
36. Maxwell ID, Pethrick RA (1983) Dielectric studies of water in epoxy resins. J Appl Polym Sci 28:2363–2379
37. Muller-Plathe F (1998) Diffusion of water in swollen poly(vinyl alcohol) membranes studied by molecular dynamics simulation. J Membrane Sci 141(2):147–154
38. Starkweather HW (1975) Some aspects of water clusters in polymers. Macromolecules 8(4):476–479
39. Marais S, Métayer M, Nguyen QT, Labbé M, Saiter JM (2000) Difusion and permeation of water through unsaturated polyester resins-influence of of resin curing. Europ Polym J 36:453–462
40. Pitkethly MJ, Favre JP, Gaur U, Jakubowski J, Mudrich SF, Caldwell DL, Drzal LT, Nardin M, Wagner HD, Di Landro L, Hampe A, Armistead JP, Desaeger M, Verposet I (1993) A round-robin program on interfacial test methods. Compos Sci Technol 48:205–214
41. Elberaïchi A, Daro A, David C (1999) Water vapour transport in polyethylene oxide/ polymethyl methacrylate blends. Europ Polym J 35(7):1217–1228
42. Marque G, Neyertz S, Verdu J, Prunier V, Brown D (2008) Molecular dynamics simulation study of water in amorphous kapton. Macromolecules 41(9):3349–3362
43. Henderson SM (1952) A basic concept of equilibrium moisture content. Agric Eng 33(1): 29–32
44. Peleg M (1993) Assessment of a semi-empirical four parameter general model for sigmoid moisture sorption isotherms. J Food Proc Eng 16:21–37
45. Timmermann EO, Chirife J, Iglesias HA (2001) Water sorption isotherms of foods and foodstuffs: BET or GAB parameters? J Food Eng 48:19–31
46. Detallante V, Langevin D, Chappey C, Metayer M, Mercier R, Pineri M (2002) Kinetics of water vapor sorption in sulfonated polyimide membranes. Desalination 148(1):333–339

47. Dewimille B, Bunsell AD (1982) The modelling of hydrothermal aging in glass fibre reinforced epoxy composites. J Phys D Appl Phys 15(10):2079–2091
48. Wong TC, Broutman LJ (1985) Moisture diffusion in epoxy resins. Part I: non-fickian sorption processes. Polym Eng Sci 25:521–528
49. Walter E, Ashbee KHG (1982) Osmosis in composites materials. Composites 13(4): 365–368
50. McKague L (1977) The thermal spike effect on wet composites. In: Proceedings of conference on environental degradation of engineering materials, Blacksburg, USA, pp. 353-362
51. Thomason JL (1990) Investigation of composite interphase using dynamic mechanical analysis: artifacts and reality. Polym Compos 11(2):105–113
52. Chiang CH, Koenig JL (1984) Fourier transform infrared spectroscopic study of the adsorption of multiple amino silane coupling agents on glass surfaces. J Colloïd Interf Sci 83(2):361–370
53. Hoh KP, Ishida H, Koenig JL (1986) The diffusion of epoxy resin into a silane coupling agent interphase. In: Koenig JL, Ishida H (eds) Composite interfaces, Elsevier, New York
54. Ishida H, Koenig JL (1978) Fourier transform infrared spectroscopic study of the silane coupling agent/porous silica interface. J Colloïd Interf Sci 64(3):555–564
55. Ishida H, Koenig JL (1980) A fourier-transform infrared spectroscopic study of the hydrolytic stability of silane coupling agents on E-glass fibers. J Polym Sci Part B Polym Phys 18:1931–1943
56. Serier A, Pascault JP, Lam TH (1989) Modeling of interphase in composite materials: characterization of epoxy resin/aminosilane system. Makromol Chem Macromol Symp 25(1):85–90
57. Wolff V (1996) Influence de l'ensimage sur les propriétés mécaniques de tissus de verre enduits de résine phénolique ou de latex, PhD Thesis, University of Lille I, Lille, France
58. Salmon L, Thominette F, Pays M-F, Verdu J (1997) Hydrolytic aging of polysiloxane networks modelling the glass fiber epoxy-amine interphase. Compos Sci Technol 57:1119–1127
59. Flory PJ, Rehner J Jr (1943) Statistical mechanics of cross-linked polymer networks. II. swelling. J Chem Phys 11(11):521–526
60. Belan F, Bellenger V, Mortaigne B, Verdu J (1997) Relationship between the structure and hydrolysis rate of unsaturated polyester prepolymers. Polym Degrad Stab 56:301–309
61. McKague EL Jr, Reynolds JD, Halkias JE (1978) Swelling and glass transition relations for epoxy matrix material in humid environments. J Appl Polym Sci 22(6):1643–1654
62. Marque G, Verdu J, Prunier V, Brown D (2010) A molecular dynamics simulation study of three polysulfones in dry and hydrated states. J Polym Sci Part B Polym Phys 48:2312–2336
63. Hahn HT (1987) Hygrothermal damage in graphite/epoxy laminates. J Eng Mater Technol 109(1):3–11
64. Delasi R, Whiteside JB (1978) Effect of moisture on epoxy resins and composites. In: Vinson JR (ed) Advanced composite materials. Environmental effects, ASTM-STP 658, American Society for Testing and Materials, Philadelphia, pp 2–20
65. Hahn HT, Kim RY (1978) Swelling of composite laminates. In: Vinson JR (ed) Advanced composite materials. Environmental effects, ASTM-STP 658, American Society for Testing and Materials, Philadelphia, pp 98–120
66. Xiao GZ, Shanahan MER (1997) Water absortion and desorption in an epoxy resin with degradation. J Polym Sci, Part B: Polym Phys 35:2659–2670
67. Cohn D, Marom G (1978) A proposal for a coefficient of hygroelasticity. Polyym Eng Sci 18:1001–1005
68. Gazit S (1978) Dimensional changes in glass-filled epoxy resins as a result of absorption of atmospheric moisture. J Appl Polym Sci 22:3547–3558
69. Ishai O (1975) Environmental effects on deformation, strength, and degradation of unidirectional glass-fiber reinforced plastics. I. Survey. Polym Eng Sci 15(7):486–490
70. Kelley FN, Bueche F (1961) Viscosity and glass temperature relations for polymer-diluent systems. J Polym Sci 50:549–556

71. Zhou J, Lucas JP (1999) Hygrothermal effects of epoxy resin. Part II: variations of glass transition temperature. Polymer 40:5513–5522
72. Carfagna C, Apicella A, Nicolais L (1982) The effect of the prepolymer composition of amino-hardened epoxy resins on the water sorption behavior and plasticization. J Appl Polym Sci 27(1):105–112
73. Sandorff PE, Tajima YA (1979) The experimental determination of moisture distribution in carbon-epoxy laminates. Composites 1:37–62
74. Ghi P, Hill DJT, Maillet D, Whittaker AK (1997) NMR imaging of the diffusion of water into poly(tetrahydrofurfuryl methacrylate-co-hydroxyethyl methacrylate). Polymer 38:3985–3989
75. Braun J, Klein MO, Bernarding J, Leitner MB, Mika HD (2003) Non-destructive, three-dimensional monitoring of water absorption in polyurethane foams using magnetic resonance imaging. Polym Test 22(7):761–767
76. Shen CH, Springer GS (1976) Moisture absorption and desorption of composite materials. J Compos Mater 10(1):2–20
77. Jacquemet R, Lagrange A (1990) Aspects de la diffusion de l'eau de mer dans le vieillissement de matériaux composites à base de résines polyester. Composites 30(1):17–25
78. Belan F (1995) Amélioration de la résistance à l'hydrolyse de résines polyester, PhD Thesis, ENSAM Paris, France
79. Crank J (1990) The mathematics of diffusion. Clarendon Press, London
80. Derrien K, Gilormini P (2006) Interaction between stress and diffusion in polymers. In: Proceedings of DSL 2006 conference, defect and diffusion forum 258/260, Lisbon, Portugal, pp. 447-452
81. Vaddadi P, Nakamura T, Singh RP (2003) Transient hygrothermal stresses in fiber-reinforced composites: a heterogeneous characterization approach. Compos A 34:719–730
82. Vaddadi P, Nakamura T, Singh RP (2003) Inverse analysis for transient moisture diffusion through fiber-reinforced composites. Acta Mater 51:177–193
83. Valançon C, Roy A, Grandidier JC (2006) Modelling of coupling between mechanics and water diffusion in bonded assemblies. Oil Gas Sci. Technol (IFP) 61(6):759–764
84. Wu CH (2001) The role of Eshelby stress in composition-generated and stress-assisted diffusion. J Mech Phys Sol 49(8):1771–1794
85. Fahmy AA, Hurt JC (1980) Stress dependence of water diffusion in epoxy resin. Polym Compos 1:77–80
86. Neumann S, Marom G (1986) Free volume dependent moisture diffusion under stress in composite materials. J Mater Sci 21(1):26–30
87. Barrie JA, Machin D, Nunn A (1975) Transport of water in synthetic cis-1,4-polyisoprenes and natural rubber. Polymer 16:811–814
88. Hopfenberg HB, Frisch HL (1969) Transport of organic micromolecules in amorphous polymers. Polym Lett 7:405–409
89. Koros WJ, Paul DR (1978) CO_2 sorption in poly(ethylene terephthalate) above and below the glass transition. J Polym Sci Part B Polym Phys 16(11):1947–1963
90. Stern SA (1994) Polymers for the gas separation: the next decade. J Membr Sci 94:1–65
91. Yang DK, Koros WJ, Hopfenberg HB, Stannet VT (1985) Sorption and transport studies of water in Kapton polyimide. J Appl Polym Sci 30(3):1035–1047
92. Cohen HH, Turnbull D (1959) Molecular transport in liquids and glasses. J Chem Phys 31:1164–1169
93. Bellenger V, Dahoui W, Morel E, Verdu J (1988) Packing density of the amine-crosslinked stoichiometric epoxy networks. J Appl Polym Sci 35:563–571
94. Thominette F, Gaudichet-Maurin E, Verdu J (2006) Effect of structure on water diffusion in moderately hydrophilic polymers. In: Proceedings of DSL 2006 conference on defect and diffusion forum 258/260, Lisbon, Portugal, pp 442–446
95. Carter HG, Kibler KG (1978) Langmuir-type model for anomalous moisture diffusion in in composite resins. J Compos Mater 12:118–131
96. Morgan RJ, O'Neal JE (1978) The durability of epoxies. Polym Plast Technol Eng 10(1):49–116

97. Alfrey T, Gurnee EF, Lloyd WG (1966) Diffusion in glassy polymers. J Polym Sci Part C Polym Symp 12:249–261
98. Thomas NL, Windle AH (1982) A theory of case II diffusion. Polymer 23(4):529–542
99. Argon AS, Cohen RE, Patel AC (1999) A mechanistic model of case II diffusion of a diluent into a glassy polymer. Polymer 40(25):6991–7012
100. Barrer RM (1968) Diffusion and permeation in heterogeneous media. In: Crank J, Park GS (eds) Diffusion in polymers, 4th edn, Academic Press, London, pp 165–217
101. Kondo K, Taki T (1982) Moisture diffusivity of unidirectional composites. J Compos Mater 16(2):82–93
102. Roy S, Singh S (2009) Analytical modelling of orthotropic diffusivities in a fiber reinforced composite with discontinuities using homogenization. Compos Sci Technol 69(11–12): 1962–1967
103. Roy S (2012) Moisture-induced degradation. In: Pochiraju KV, Tandon GP, Schoeppner GA (eds) Long term durability of polymeric matrix composites. Springer, New York, pp 181–236
104. Jacques B, Werth M, Merdas I, Thominette F, Verdu J (2002) Hydrolytic ageing of polyamide 11. I. Hydrolysis kinetics in water. Polymer 43(24):6439–6447
105. Ravens DAS (1960) The chemical reactivity of poly(ethyelene terephthalate). Heterogeneous hydrolysis by hydrochloric acid. Polymer 1:375–383
106. Serpe G, Chaupart N, Verdu J (1997) Ageing of polyamide 11 in acid solutions. Polymer 38(8):1911–1917
107. McMahon W, Birdsall HA, Johnson GA, Camilli CJ (1959) Degradation studies of polyethylene terephthalate. J Chem Eng Data 4:57–79
108. Merdas I, Thominette F, Verdu J (2003) Hydrolytic ageing of polyamide 11. Effect of carbon dioxide on polyamide 11 hydrolysis. Polym Degrad Stab 79:419–425
109. Ballara A, Verdu J (1989) Physical aspects of the hydrolysis of polyethylene terephthalate. Polym Degrad Stab 26:361–374
110. Saito O (1958a) On the effects of high energy radiation to polymers. I. Crosslinking and degradation J Phys Soc (Japan) 13(2):198–206
111. Saito O (1958b) On the effects of high energy radiation to polymers. II. End-linking and gel fraction. J Phys Soc (Japan) 13(12):1451–1464
112. Launay A, Thominette F, Verdu J (1994) Hydrolysis of po1y(ethy1ene terephthalate): a kinetic study. Polym Degrad Stab 46(3):319–324
113. Fayolle B, Richaud E. Colin X, Verdu J (2008) Review: Degradation-induced embrittlement in semi-crystalline polymers having their amorphous phase in rubbery state. J Mater Sci 43:6999–7012
114. Miyagi A, Wunderlich B (1972) Etching of crystalline poly(ethylene terephthalate) by hydrolysis. J Polym Sci Part A2 Polym Phys 10:2073–2083
115. Pascault J-P, Sautereau H, Verdu J, Williams RJJ (2002) Thermosetting polymers. Marcel Dekker, New York
116. Flory PJ (1953) Principles of polymer chemistry. Cornell University Press, New York
117. Di Marzio EA (1964) On the second-order transition of rubber. J Res Nat Bur Stand Sect A Phys Chem 68:611–617
118. Rivlin RS (1948a) Large elastic deformations of isotropic materials. I, II and III. Phil Trans Roy Soc (London) A240:459–525
119. Rivlin RS (1948) Large elastic deformations of isotropic materials. IV. Further developments of the general theory. Phil Trans Roy Soc (London) A241:379–397
120. Bellenger V, Mortaigne B, Grenier-Loustalot MF, Verdu J (1992) Structure–property relationships for styrene crosslinked polyesters. I. Network structure and rubbery elastic modulus. J Appl Polym Sci 44(4):643–651
121. Bellenger V, Ganem M, Mortaigne B, Verdu J (1995) Lifetime prediction in the hydrolytic ageing of polyesters. Polym Degrad Stab 49(1):91–97
122. Derombise G, Schoors V, Vouyovitch L, Davies P (2010) Degradation of aramid fibers under alkaline and neutral conditions: relations between the chemical characteristics and mechanical properties. J Appl Polym Sci 116(5):2504–2514

123. Golike RC, Lasoski SW (1960) Kinetics of hydrolysis of polyethylene terephthalate films. J Phys Chem 64:895–898
124. Ashbee KHG, Franck FL, Wyatt RC (1967) Water damage in polyester resins. Proc Roy Soc A300:415–419
125. Ashbee KHG, Wyatt RC (1969) Water damage in glass fibre/resin composites. Proc Roy Soc A312:553–564
126. Steel DJ (1967) Trans J Plast Inst 35:429
127. Van't Hoff J (1888) The function of osmotic pressure in the analogy between solutions and gases. Philos Mag 26(5):81–105
128. Gautier L, Mortaigne B, Bellenger V, Verdu J (1999) Osmotic cracking nucleation in hydrothermal-aged polyester matrix. Polymer 41(7):2481–2490
129. Burrell PP, Herzog DJ, McCabe RT (1987) A study of permeation barriers to prevent blisters in marine composites and a novel technique for evaluating blister formation. In: Proceedings of 42nd annual conference of composite institute, the society of the plastics industry, paper 15E, Feb 2-6
130. Curry B (1987) The effect of gel coat composition on osmotic blister formation. In: Proceedings of 42nd annual conference of composite institute, the society of the plastics industry, paper 15A, Feb 2–6
131. Mortaigne B, Bellenger V, Verdu J (1991) Vieillissement hygrothermique de composites verre/polyester insaturés réticulés par le styrène, Rev Sci Techn Defense (Paris) 4ème trim., 76
132. Robeson LM, Crisafull ST (1983) Microcavity formation in engineering polymers exposed to hot water. J Appl Polym Sci 28:2925–2936
133. Rasoldier N, Colin X, Verdu J, Bocquet M, Olivier L, Chocinski-Arnault L, Lafarie-Frenot MC (2008) Model systems for thermo-oxidised epoxy composite matrices. Compos Part A 39:1522–1529
134. Vincent PI (1972) A correlation between critical tensile strength and polymer cross-sectional area. Polymer 13:558–560
135. Seitz JT (1993) The estimation of mechanical properties of polymers from molecular structure. J Appl Polym Sci 49:1331–1351
136. Morgan RJ, Pruneda CO, Butler N, Kong FM, Caley L, Moore RL (1984) The hydrolytic degradation of Kevlar 49 fibers. In: Proceedings of 29th national sampe symposium, Society for the Advancement of Material and Process Engineering, Reno, Nevada, , pp 891–900, April 3–5
137. Ghorbel I, Akélé N, Thominette F, Spiteri P, Verdu J (1995) Hydrolytic aging of polycarbonate 2: hydrolysis kinetics, effect of static stresses. J Appl Polym Sci 55(1): 173–179
138. Philips MG (1983) Prediction of long term stress-rupture life for glass fiber-reinforced polyester composites in air and in aqueous evironements. Composites 14(3):270–275
139. Theberge JE (1970) In: Proceedings of 25th Annual technical conference on reinforced plastics, composites division, The Society of the Plastics Industry, paper 2D, Washington DC
140. Wu WL, Orts WJ, Majkrzak CJ, Hunston DL (1995) Water-adsorption at a polyimide/silicon wafer interface. Polym Eng Sci 35(12):1000–1004
141. Mortaigne B (1989) Vieillissement hydrolytique de polyesters insaturés réticulés par le styrène, PhD Thesis, ENSAM Paris, France
142. Kaelble DH, Dynes PJ, Maus L (1976) Hygrothermal ageing of composite materials. Part 1: Interfacial aspects. J Adhes 8(2):121–144
143. Joshi OK (1983) The effect of moisture on the shear properties of carbon fibre composites. Composites 14(3):196–200
144. Woo M, Piggott M (1987) Water absorption of resins and composites, Part II: diffusion in carbon and glass reinforced epoxies. J Compos Technol Res 9:162–166
145. Woo M, Piggott M (1988) Water absorption of resins and composites: IV. Water transport in fiber rein- forced plastics. J Compos Technol Res 10:20–24
146. Di Benedetto AT, Lex PJ (1989) Evaluation of surface treatments for glass fibers in composite materials. Polym Eng Sci 29(8):543–555

147. Serier A, Pascault JP, My LT (1991) Reactions in aminosilane-epoxy prepolymer systems. I. Kinetics of epoxy-amine reactions. J Polym Sci, Part A: Polym Chem 29:209–218
148. Ishida H (1984) A review of recent progress in the studies of molecular and microstructure of coupling agents and their functions in composites, coatings and adhesive joints. Polym Compos 5(2):101–123
149. Ishida H (1985) Structural gradient in the silane coupling agent layers and its influence on the mechanical and physical properties of composites. In: Ishida H, Kumar G (eds) Molecular characterization of composite interfaces. Plenum Press, New York, pp 25–51
150. Hoh KP, Ishida H, Koenig JL (1990) Multi-nuclear NMR spectroscopic and proton NMR imaging studies on the effect of water on the silane coupling agent/matrix resin interface in glass fiber-reinforced composites. Polym Compos 11(3):192–199
151. Johanson OK, Stark FO, Vogel GE, Fleishman RM, Flaningham OL (1968) The physical chemical nature of the matrix—glass fiber interface. In: Schwatrz E (ed) Fundamental aspects of fiber reinforced plastic composites. Interscience Publisher, New York
152. Rosen MR, Goddard ED (1980) FDT: a technique for direct study of water attack at the silane-fiber interface. Polym Eng Sci 20:413–425
153. Schradder ME, Block A (1971) Tracer study of kinetics and mechanism of hydrolytically induced interfacial failure. J Polym Sci Part C Polym Lett 34:281–291
154. Husman G (1976) Characterization of wet composite laminates. In: Proceedungs of Mechanical Composite., Air Force Materials Laboratory, Non Metallic Materials Division, Dayton, Ohio
155. McKague EL Jr, Halkias JE, Reynolds JD (1975) Moisture in composites: the effect of supersonic service on diffusion. J Compos Mater 9:2–9
156. Damian C, Escoubès I, Espuche E (2001) Gas and water transport properties of epoxy-amine networks: influence of crosslink density. J Appl Polym Sci 80(11):2058–2066
157. Sacher E, Susko JR (1979) Water permeation of polymer films. I. Polyimide. J Appl Polym Sci 23:2355–2364

Water–Mechanical Property Coupling

F. Jacquemin and S. Fréour

Abstract The present contribution investigates the effects related to the plasticization of the polymer matrix occurring during the water sorption process on the internal mechanical state profiles, at the constituent and ply scales. Then, two multi-physics models are considered to account that the moisture sorption depends on the internal mechanical states: the free volume theory and a thermodynamic approach.

1 Introduction

A Fickian diffusion, governed by the maximum absorption capacity and the diffusion coefficient, is often considered to model the moisture sorption process occurring in composite materials subjected to ambient relative humidity. Moisture sorption can lead to a plasticization of the constitutive organic resin. This entails a decrease of some mechanical properties such as the Young modulus. This phenomenon, referred to as "*weak coupling*", as only the mechanical properties are moisture dependent, will be investigated first. The aim is to account for plasticization effects in the predictive models dedicated to the determination of the multi-scale internal mechanical states (at the ply scale and in the constituents of the ply) during the moisture diffusion process. If the moisture sorption presents a more complex behavior, more elaborated approaches can be used. In that context, instead of Fick's model, one can use Langmuir's model or "*strong*" stress-

F. Jacquemin (✉) · S. Fréour
Institut de Recherche en Génie Civil et Mécanique (UMR CNRS 6183), LUNAM Université—Université de Nantes—Centrale Nantes CRTT, 37 Boulevard de l'Université, BP 406, 44602 Saint-Nazaire cedex, France
e-mail: frederic.jacquemin@univ-nantes.fr

S. Fréour
e-mail: sylvain.freour@univ-nantes.fr

P. Davies and Y. D. S. Rajapakse (eds.), *Durability of Composites in a Marine Environment*, Solid Mechanics and Its Applications 208,
DOI: 10.1007/978-94-007-7417-9_4,

diffusion coupling models such as the free volume theory or thermodynamically based model. The so-called "*strong coupling*" models enable the fact that the moisture sorption is dependent on the mechanical states and vice versa, to be taken into account. In this work, two coupling models are considered: a phenomenological approach based on the free volume concept, and a more fundamental model, based on a thermodynamic approach.

2 Plasticization Effects on the Multi-Scale Internal Stresses

This work investigates the plasticization effects related to the evolution, as a function of the moisture content, of the hygro-elastic properties on the internal stress states during the transient part of a hygroscopic load. The proposed approach involves the coupling of the classical continuum mechanics formalism presented by Jacquemin and Vautrin [5] to Eshelby-Kröner self-consistent scale transition model recently extended to account for a hygroelastic load [4, 6, 7]. An inverse scale transition model provides, from the experimental macroscopic ply moduli (Table 1), the evolution of the local hygro-elastic properties experienced by the epoxy matrix as the moisture diffusion takes place. Figure 1 shows the moisture diffusion process inside a composite structure following a Fickian behavior. According to Fig. 2, the fact of considering the plasticization and thus an evolution of the hygro-elastic properties of both the composite plies and its constitutive matrix strongly affects the transverse stresses levels and their distributions in the plies and their constituents.

Figure 2 depicts the classical results expected in the case where a unidirectional composite is subjected to a transient hygroscopic load: the high macroscopic stresses arising at the beginning of moisture diffusion thereafter decrease and disappear as soon as the permanent state is reached. However, the absolute values of the corresponding transverse stresses at the constituent scale increase almost uninterruptedly during the moisture diffusion process, reaching their maximum when the saturation state is attained. It should be emphasized that, in this specific case, the transverse stress calculated for the carbon fiber varies significantly, depending on the choice of the hypothesis for the relationship between material properties and moisture content.

Table 1 Experimental macroscopic elastic moduli as a function of the moisture content [9]

Moisture content ΔC^I (%)	0	0.25	0.75
E_1^I (GPa)	130	130	130
E_2^I (GPa)	9.5	9.25	8.75
ν_{12}^I	0.3	0.3	0.3
G_{12}^I (GPa)	6.0	6.0	6.0
G_{23}^I (GPa)	3.0	3.0	3.0

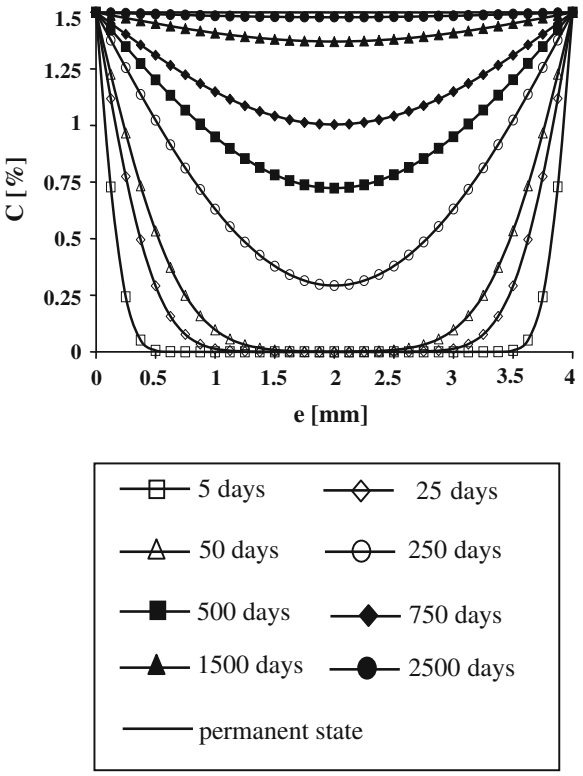

Fig. 1 Time and space dependent moisture content profiles in the composite structure

According to the foresaid, taking account of changes in the multiscale hygroelastic properties of composite plies when the matrix experiences plasticization has two main consequences, that can be considered responsible for the reduced estimated stresses compared with their reference values (calculated disregarding the effect of moisture on material properties). First, sharp distinctions occur between the effective properties of the wet materials and their counterparts in the dry composite. This effect increases with time, as the amount of water in the structure grows, and reaches its maximum when the permanent stage of the diffusion process is attained.

Since the predicted stresses are obviously intimately linked to the hygroelastic properties of the material, this effect partially explains the discrepancies between the two sets of curves displayed in Fig. 2. Second, gradients of moisture content arise in the composite during the transient stage of moisture diffusion in it, since the process is rather slow (see Fig. 1). The distribution of the hygroscopic load within the thickness of the structure directly induces a distribution of the hygroelastic properties of materials if their dependence on moisture content is taken into account in calculations. The non uniform distribution of hygromechanical properties explains the distinctions occurring at the beginning of the moisture diffusion process, between the internal stresses predicted with and without taking account of

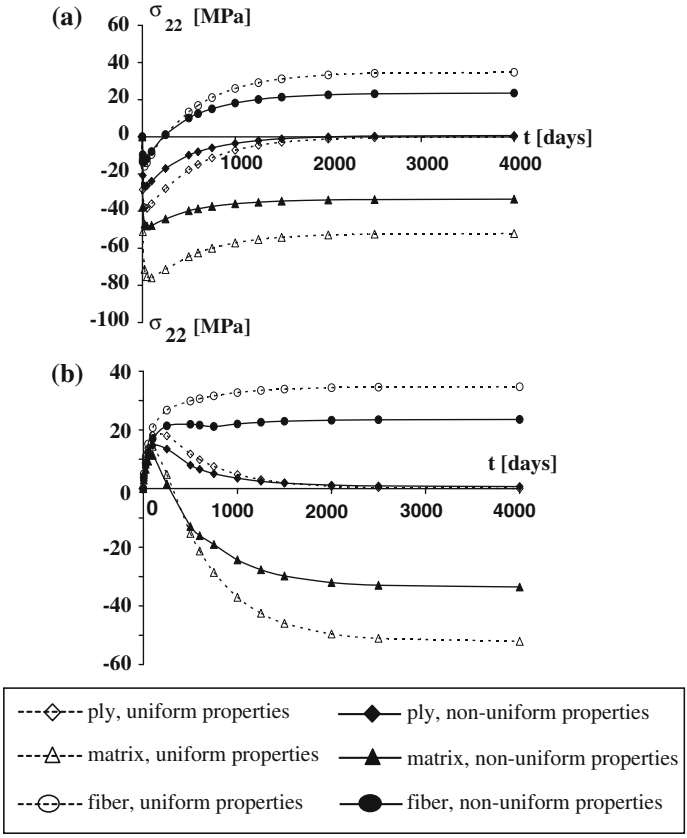

Fig. 2 Effect of the plasticization on the multi-scale stress states in (**a**) the external ply (**b**) the central ply of a uni-directional composite during the transient part of the moisture diffusion process

the effect of moisture on material properties. Thus, increased internal stresses, related to softening of the material induced by the diffusion of water, can be expected even at the beginning of hygroscopic loading of a composite structure.

3 The Free Volume Theory

Historically, a theoretical approach based on the calculation of the free-volume change in the stressed state was developed by Neumann and Marom [8]. Assuming that the Fickian diffusion coefficient was related to the free volume by the Doolittle equation, Neumann and Marom [8] proposed an expression for the ratio of the diffusion coefficients in the strained and free-of-strain states:

$$\mathrm{Ln}\left(\frac{D_{\varepsilon}^{m}}{D_{0}^{m}}\right)=\frac{a}{v^{m}}\left(\frac{1}{v_{f0}^{m}}-\frac{1}{v_{f\varepsilon}^{m}}\right) \tag{1}$$

where D_0^m and D_ε^m are the Fickian moisture diffusion coefficients for the strain-free matrix and that of the strained epoxy, respectively, where **a** is an empirical factor. v^m denotes the volume fraction of the matrix in the composite ply, v_{f0}^m and $v_{f\varepsilon}^m$ are the free volume fraction of the strain-free and strained epoxy matrix, respectively. These quantities are related by the trace of the strain tensor Tr ε^m through:

$$v_{f\varepsilon}^{m}=v_{f0}^{m}+\mathrm{Tr}\ \varepsilon^{m} \tag{2}$$

The maximum moisture absorption capacities for an unstrained matrix and a strained matrix are related through the following equation:

$$M_{\infty\varepsilon}^{m}=M_{\infty0}^{m}+\left(v_{f\varepsilon}^{m}-v_{f0}^{m}\right)\times\frac{\rho^{w}}{\rho^{m}}=M_{\infty0}^{m}+\mathrm{Tr}\ \varepsilon^{m}\times\frac{\rho^{w}}{\rho^{m}} \tag{3}$$

where ρ^w and ρ^m are respectively the densities of water and resin.

The macroscopic moisture content is assumed to be the solution of Fick's equation with a moisture diffusion coefficient dependent on the local mechanical state, as presented by Youssef et al. [14]. A scale transition approach provides relations linking the ply stresses (strains) to those of the constituents, as well as homogenization procedures enabling the evolution of the plies diffusive behaviour throughout the transient part of the diffusion process to be estimated.

According to Fig. 3, the coupled hygro-mechanical model leads to a maximum moisture absorption capacity of 1.5 % in the unidirectional structure and 1.37 % only in the case of the ±55° laminate. This is actually due to a discrepancy between the mechanical strain states experienced by the two considered structures.

Figure 4 shows the transverse stresses evolution in the internal ply of (a) the laminated (b) the unidirectional cylinders, during the transient part of the diffusion.

According to Fig. 4, whatever the considered stacking sequences, the most significant discrepancies between the transverse stresses predicted by the coupled/uncoupled models occur at the beginning of the diffusion process. However, the discrepancy rapidly fades and cancels when the permanent state is attained in this structure. On the contrary, in the laminate, an absolute deviation of 10 MPa still holds in the permanent state of the diffusion process, regarding the predicted transverse stress experienced by the organic matrix.

4 The Thermodynamical Approach

Some experimental data demonstrate that the moisture sorption that takes place in composites structures could differ from the typical Fickian uptake (Cai and Weitsman [1, 10]. As a consequence, some researchers have developed models in order to

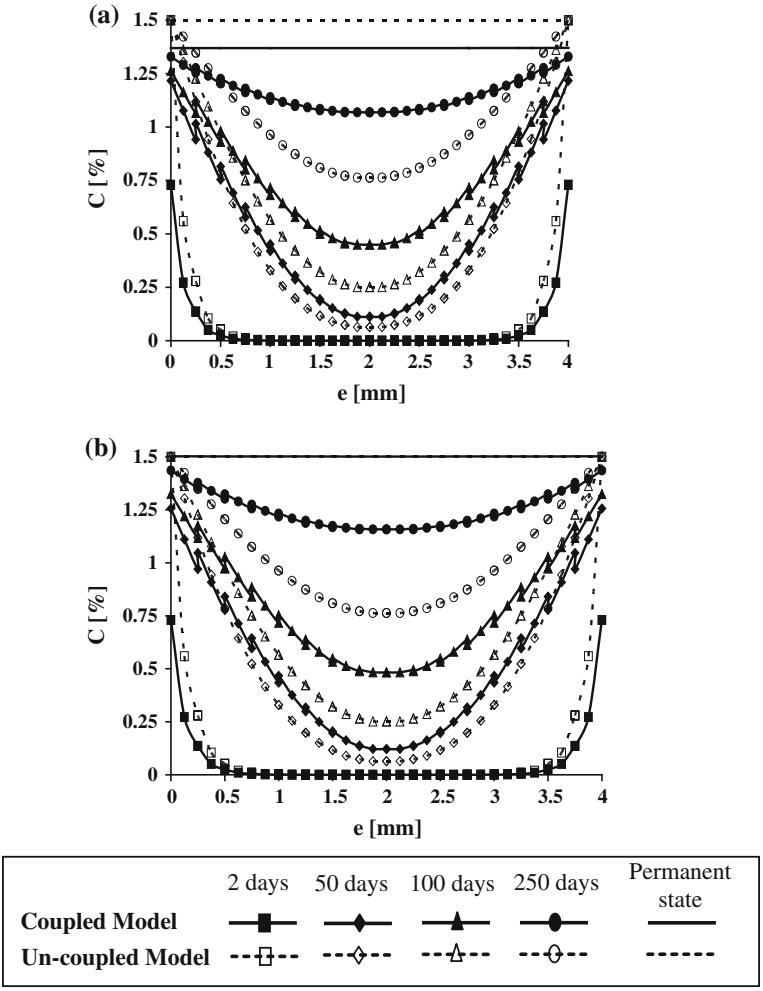

Fig. 3 Effect of a multiphysics approach on the predicted time and space dependent moisture content profiles in the (**a**) ±55° composite structure (**b**) unidirectional composite structure

reproduce the anomalous sorption curves observed in practice [2, 13]. Among the proposed methods, [11] documented a multi-physics approach to the diffusion mechanisms compatible with the thermodynamics. Recently [3, 12] published a model focused on the description of anomalous diffusion also developed upon the concept of being compatible with the thermodynamics.

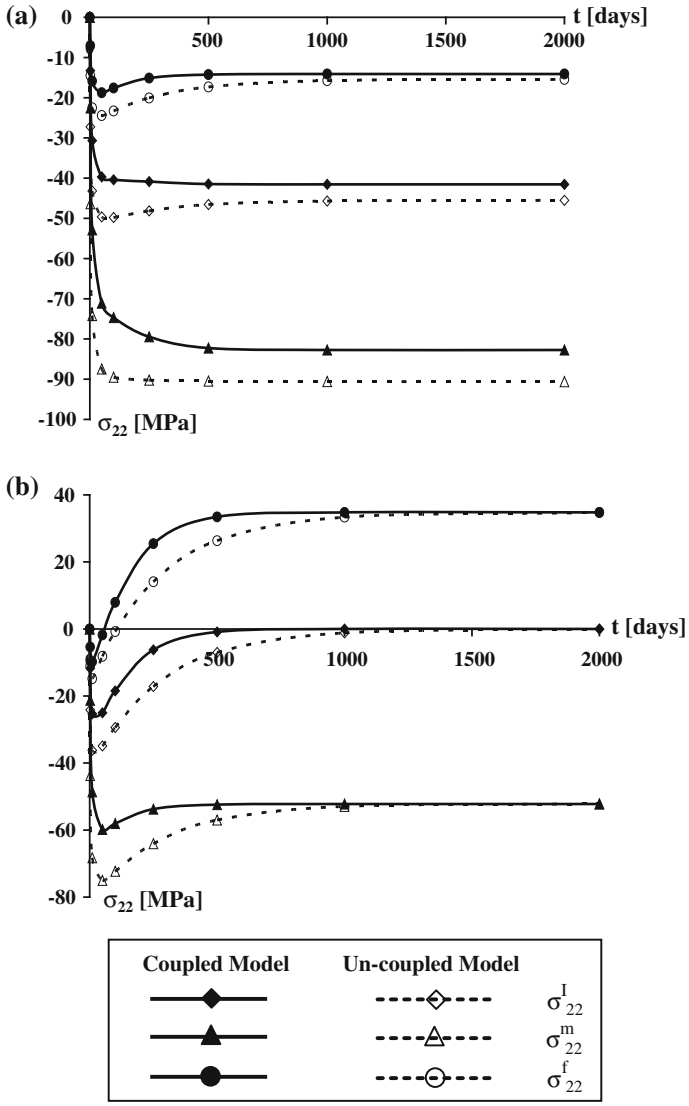

Fig. 4 Multi-scale transverse stress states in the internal ply of the **a** ±55° laminate **b** unidirectional composite structure

4.1 The Historical Model

The chemical potential $\tilde{\mu}_e$ is defined as the partial derivative of the free energy of Helmholtz F with respect to the amount of water n_w [3]:

$$\tilde{\mu}_w = \frac{\partial F}{\partial n_w} = \frac{\partial F}{\partial C}\frac{\partial C}{\partial n_w} \tag{4}$$

Starting from Eq. (4), one can express the moisture diffusion behavior law of a polymer. Let us first consider the mass density of the polymer to be constant throughout the moisture diffusion process. According to Derrien and Gilormini [3], in the case of a unidirectional diffusion in a polymer submitted to a hydrostatic load, the time dependent evolution of the moisture content respects:

$$\frac{\partial C}{\partial t} = \frac{D}{RT}\mathrm{div}\left[C\left(\overrightarrow{\mathrm{grad}}\,\tilde{\mu}_w\right)\right] = D\left[\left(1+\alpha\eta^2 C\right)\frac{\partial^2 C}{\partial x^2} + \alpha\left(\frac{\partial C}{\partial x}\right)^2\right] \tag{5}$$

$$\text{where } \alpha = \frac{2A_0 E_p}{3\left(1-\upsilon_p\right)} \text{ and } A_0 = \frac{3\omega_w}{RT\rho_0}$$

D, E_p, ν_p, $\eta$and ρ_0 respectively denote the diffusion coefficient, Young's modulus, Poisson's ratio, coefficient of moisture expansion and the strain-free mass density of the polymer. ω_w stands for the molar mass of water.

4.2 Accounting for the Average Mass Density Experienced by the Polymer

The model described above assumes that the polymer mass density is independent from the strain state. This condition is actually not fulfilled in practice. The volume V_p of a strained polymer can be expressed as a function of both its strain-free counterpart V_0 and the trace of the strain tensor ε_p. As a consequence, the mass density ρ_p of a strained polymer can be written from the principle of matter conservation, as a function of ρ_0:

$$\rho_p = \frac{m_p}{V_p} = \frac{m_0}{V_p} = \rho_0 \frac{1}{\left(\mathrm{Tr}\,\varepsilon_p + 1\right)} \tag{6}$$

In the case that the evolution of the polymer average mass density during the diffusion process is accounted for, in the context of writing the moisture diffusion equation, one obtains [12]:

$$\frac{\partial C}{\partial t} = D\left[\left(1+\alpha_1\eta^2 C + \alpha_1\eta^2 C^2\right)\frac{\partial^2 C}{\partial x^2} + \eta^2(\alpha_3 + \alpha_4 C)\left(\frac{\partial C}{\partial x}\right)^2\right] \tag{7}$$

where, $\alpha_1 = \mathrm{Tr}\left(\varepsilon_p\right)\left(2\alpha - 3A_0 k_p C\right) + \alpha$, $\alpha_2 = 3\left(A_0 k_p - \alpha\right)$, $\alpha_3 = \alpha + (2\alpha - 3A_0 k_p)\mathrm{Tr}\left(\varepsilon_p\right)$, $\alpha_4 = \eta\left[9A_0 k_p + \alpha\left(3 - \frac{2\alpha}{A_0 k_p}\right)\right]$.

Figure 5 shows the time-dependent evolution of the average moisture content, as a function of the Coefficient of Moisture Expansion.

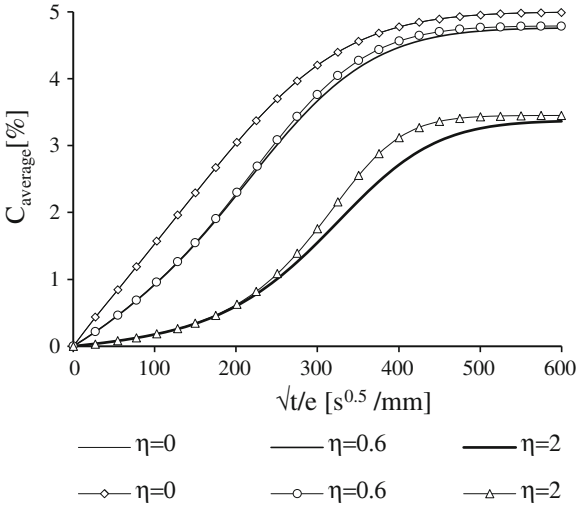

Fig. 5 Effect of CME on the average moisture content

According to Fig. 5, increasing CME reduces the maximum moisture absorption capacity of the polymer as indicated by the evolution of the average moisture content in the steady state. The continuous lines (without marks) show the results predicted by Derrien and Gilormini model, whereas the continuous lines with marks correspond to the model developed in the present work. The discrepancies between the models increase significantly with the coefficient of moisture expansion.

Figure 6 shows the effect induced by the application of an external pressure, varying from 1 to 20 MPa, on the time-dependent moisture content. The Coefficient of Moisture Expansion used in order to obtain the results depicted here is

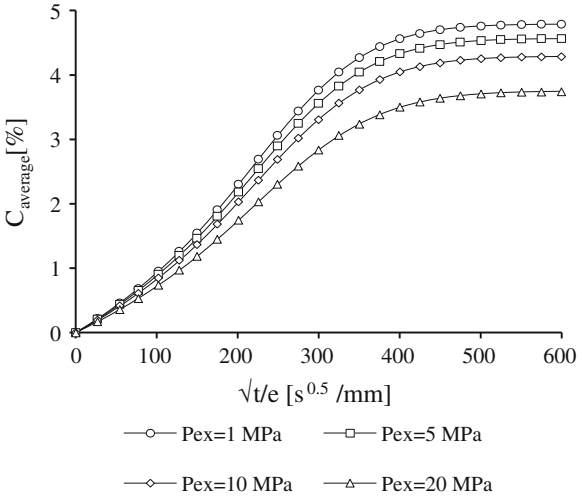

Fig. 6 Effect of applied pressure on the average moisture content

equal to 0.6. Thus, the moisture absorption capacity of the polymer varies with the magnitude of the applied external pressure.

4.3 Accounting for the Hygroscopic Swelling

Moisture absorption induces swelling strains. The mathematical formalism presented in both references [3, 12] does not enable the effects induced by the presence of an in-depth heterogeneous profile of the hygro-elastic strain on the moisture kinetics to be accounted for. Thus further developments were brought to the thermodynamic based moisture diffusion model in order to address this issue.

Swelling strains actually correspond to the existence of a hygroscopic pressure within the material. The in-depth, time-dependent hygroscopic pressure profile occurring during the transient stage of the diffusion process is determined according to three equations: (a) Hygro-elastic Hooke's law; (b) Equilibrium equations and (c) Compatibility equations.

For the case when unidirectional diffusion is assumed to occur, the internal hygroscopic pressure P_{is} induced by a possibly unsymmetrical hygroscopic load (i.e. the structure is submitted to heterogeneous boundary conditions in term of hygroscopic conditions) can be written as follows:

$$P_{is}(x,t) = \frac{\alpha}{A_0}\left[\eta\left(C(x,t) - 4\overline{C(t)}\right) + \frac{6}{L^3}\eta x\left(L^2\overline{C(t)} - 2I\right) + \frac{6}{L^2}\eta I\right] \quad (8)$$

where L stands for the thickness of the sample, $\overline{C(t)}$ is the average moisture content in the sample, and I corresponds to the following integral:

$$I = \int_0^L C(x,t)x\,dx \quad (9)$$

For the case where a symmetrical hygroscopic load is applied on the boundaries of the structure, $C(x,t) = C(L - x,\ t)$. As a result, the integration I is equal to $\frac{L^2\overline{C(t)}}{2}$.

Hence, the corresponding hygroscopic pressure is given by the simplified form: $P_{is}(x,t) = \frac{\alpha}{A_0}\eta\left(C(x,t) - \overline{C(t)}\right)$.

During the moisture diffusion process, both the average (macroscopic) change of the polymer mass density, as well as the local hygroscopic swelling are accounted for. The first condition corresponds to the modifications described in Sect. 4.2 above. The hygroscopic swelling yields an in-depth continuous evolution of the local volume of the polymer as a function of the moisture content. The following expression should then be introduced in the derivative of the free energy of Helmholtz by the moisture content featured by the fundamental relation of the model (4):

$$\frac{\partial V_\varepsilon}{\partial C} = \frac{\partial V_\varepsilon}{\partial\, \mathrm{tr}\, \varepsilon} \frac{\partial\, \mathrm{tr}\, \varepsilon}{\partial C} = V_0 \frac{\partial \mathrm{tr}\, \varepsilon}{\partial C} = \frac{n\, \omega}{\rho_0} \frac{\partial\, \mathrm{tr}\, \varepsilon}{\partial C} \tag{10}$$

The resulting time-dependent diffusive behavior for a polymer plate submitted to an unsymmetrical humid ambient load is given by:

$$\dot{C} = D \left[\begin{array}{l} \left(1 + V_1 \eta^2 C + V_2 \eta^3 C^2\right) \frac{\partial^2 C}{\partial x^2} + \eta^2 (V_3 + V_4 C) \left(\frac{\partial C}{\partial x}\right) \\ - \frac{6}{L^3} \frac{\alpha}{A_0\, k} \eta \left(L^2 \overline{C(t)} - 2I\right) (V_5 + V_6 \eta^2 C) \frac{\partial C}{\partial x} - \frac{72}{L^6} \frac{\alpha^2}{A_0\, k} \eta^3 \left(L^2 \overline{C(t)} - 2I\right)^2 C \end{array} \right] + g \tag{11}$$

where

$$\begin{aligned} V_1 &= -3\, A_0\, k\, \mathrm{tr}\, \varepsilon + 2\alpha\, \mathrm{tr}\, \varepsilon + \alpha, \quad V_2 = 9\, A_0\, k - 3\alpha, \\ V_3 &= -3\, A_0\, k\, \mathrm{tr}\, \varepsilon + 2\alpha\, \mathrm{tr}\, \varepsilon + \alpha, \quad V_4 = \eta V_2 - \frac{2\, \eta\, \alpha^2}{A_0\, k}, \\ V_5 &= 2\, \eta\, A_0\, \mathrm{tr}\, \varepsilon + A_0\, \eta, \quad V_6 = 3A_0 - 4\frac{\alpha}{k} \end{aligned}$$

Besides, the factor g could be written as follows:

$$g = D\xi \left[z_1 \frac{\partial^2 C}{\partial x^2} + z_2 \left(\frac{\partial C}{\partial x}\right)^2 + z_3 \frac{\partial C}{\partial x} + 3C \left\{ \frac{6}{L^3} \frac{\alpha}{A_0\, k} \eta \left(L^2\, \overline{C(t)} - 2I\right)^2 \right\} \right] \tag{12}$$

where

$$z_1 = -3\eta(2\, \mathrm{tr}\, \varepsilon - 3\eta\, C + 1)C + (3\, \mathrm{tr}\, \varepsilon - 6\, \eta\, C + 1)C \frac{3\, A_0\, k - \alpha}{A_0\, k} \eta \tag{13}$$

$$z_2 = -3\eta(2\, \mathrm{tr}\, \varepsilon - 6\, \eta\, C + 1) + (3\, \mathrm{tr}\, \varepsilon - 18\, \eta\, C + 1) \frac{3\, A_0\, k - \alpha}{A_0\, k} \eta + 3\, C \left(\frac{3\, A_0\, k - \alpha}{A_0\, k} \eta\right)^2 \tag{14}$$

$$z_3 = -\frac{6}{L^3} \frac{\alpha}{A_0\, k} \eta \left(L^2\, \overline{C(t)} - 2I\right) (3\, \mathrm{tr}\, \varepsilon - 18\, \eta\, C + 1) - \frac{36\, C}{L^3} \frac{\alpha}{A_0\, k} \left(L^2\, \overline{C(t)} - 2I\right) \frac{3\, A_0\, k - \alpha}{A_0\, k} \eta^2 \tag{15}$$

$$\xi = \frac{3\, A_0\, k - \alpha}{3} \eta \tag{16}$$

Figure 7 shows the time-dependent evolution of the average moisture content, as a function of the applied pressure and the coefficient of moisture expansion.

According to Fig. 7, increasing CME and pressure involve a reduction of the moisture absorption of the polymer as indicated by the evolution of the average

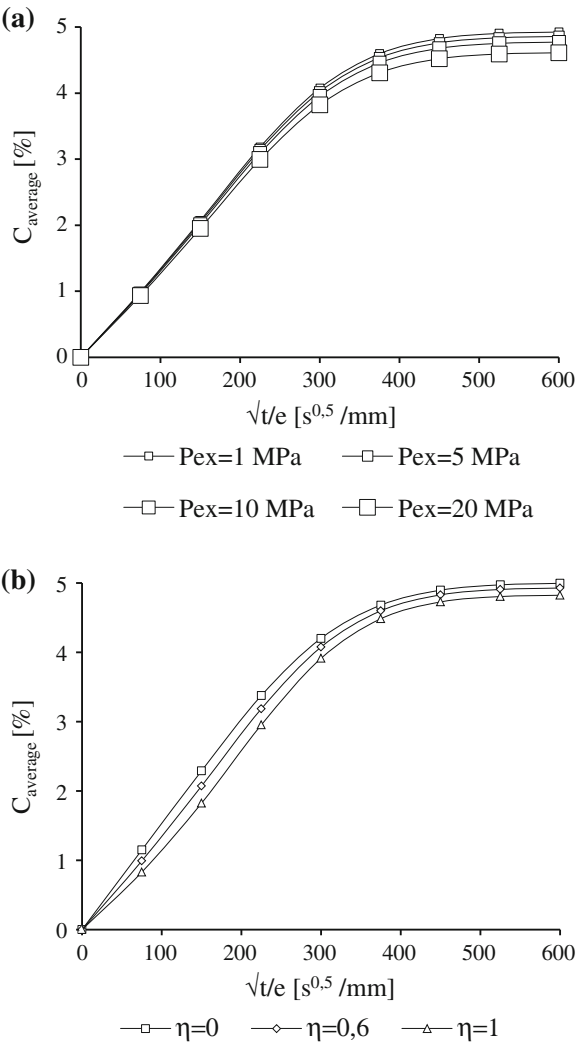

Fig. 7 **a** Effect of the applied pressure on the average moisture content ($\eta = 0{,}6$). **b** Effect of the moisture expansion coefficient on the average moisture content ($P_{ex} = 1$ MPa)

moisture content. The maximum absorption capacity decreases with increasing the pressure and the CME. We retrieve a Fickian behaviour when the CME is equal to 0. This result does not depend on the applied pressure.

Figure 8a depicts the average moisture content in the case of an unsymmetrical loading: the moisture content on the external face can take a value of 0, 2.5 and 5 % (the moisture content on the other face is fixed at 5 %).

For unsymmetrical loading, the average moisture content does not vary linearly due to the coupling phenomenon. As expected, the average moisture content increases with the boundary moisture content.

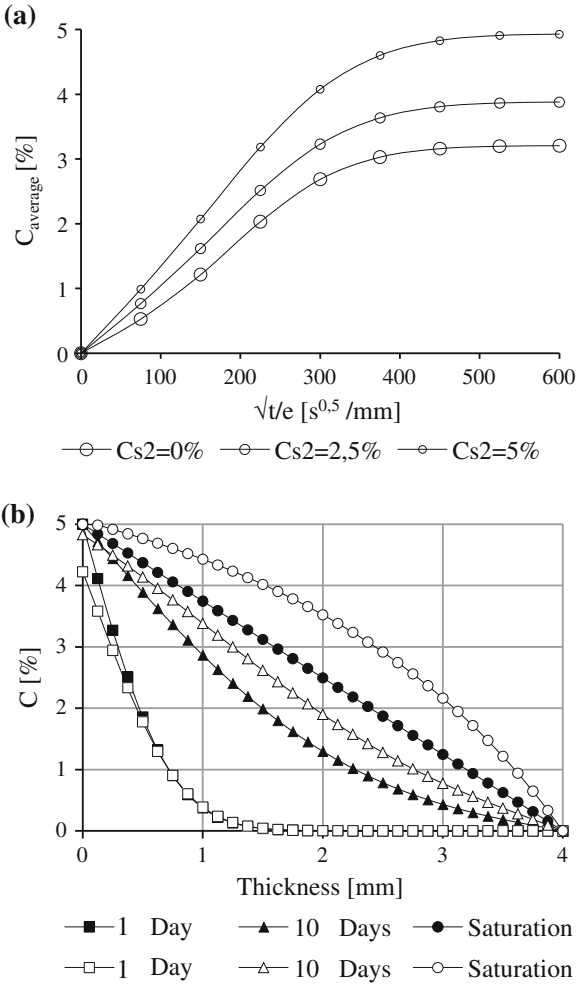

Fig. 8 Effects of an unsymmetrical hygroscopic load on (**a**) the average moisture content ($\eta = 0.6$), (**b**) the moisture content profile (*filled marks* $\eta = 0$, *marks not filled* $\eta = 0.6$)

Figure 8b shows the moisture content profile when the boundary moisture contents on the internal and external faces are equal to 5 and 0 % respectively. We consider two different values for the CME: 0.6 and 0. For a CME of 0.6, the moisture content profile at saturation is not linear. A Fickian linear variation is observed when the CME is equal to 0. An unsymmetrical loading combined with a coefficient of moisture expansion different to 0 involves more important moisture contents. Thus, the effects induced by the through-thickness differential swelling on the time-dependent diffusion are pointed out.

5 Conclusions

The aim of the present work is to propose models enabling water-mechanical property coupling due to plasticization phenomenon or coupling between moisture diffusive behavior law and internal mechanical states to be take into account, according to the free volume theory or the thermodynamic approach. For instance, the proposed development enables the effects induced by the presence of an in-depth heterogeneous profile of the hygro-elastic strain on the moisture kinetics to be accounted for. Such models can be used to represent several typical diffusive behaviors met experimentally. This field of research is under investigation by the authors: ongoing experimental studies should provide results to be compared with the numerical predictions. Finally, the thermodynamic approach presented in this work concerns only polymer samples, and will be extended to the case of polymer matrix composites.

References

1. Cai L-W, Weistman Y (1994) Non-Fickian moisture diffusion in polymeric composite. J Compos Mater 28:130–154
2. Carter HG, Kibler KG (1978) Langmuir-type model for anomalous moisture diffusion in composite resins. J Compos Mater 12:118–131
3. Derrien K, Gilormini P (2009) The effect of moisture-induced swelling on the absorption capacity of transversely isotropic elastic polymer-matrix composites. Int J Solids Struct 56:1547–1553
4. Eshelby JD (1957) The determination of the elastic field of an ellipsoidal inclusion, and related problems. Proc R Soc Lond 241:376–396
5. Jacquemin F, Vautrin A (2002) Analytical calculation of the transient thermoelastic stresses in thick walled composite pipes. J Compos Mater 38:1733–1751
6. Kröner E (1958) Berechnung der elastischen Konstanten des Vielkristalls aus des Konstanten des Einkristalls. Zeitschrift für Physik 151:504–518
7. Jacquemin F, Fréour S, Guillén R (2005) A hygroelastic self-consistent model for fiber-reinforced composites. J Reinf Plast Compos 24:485–502
8. Neumann S, Marom G (1986) Free-volume dependent moisture diffusion under stress in composite materials. J Mater Sci 21:26–30
9. Patel BP, Ganapathi M, Makhecha DP (2002) Hygrothermal effects on the structural behaviour of thick composite laminates using higher-order theory. Compos Struct 56:25–34
10. Rao RMVGK, Shylaja Kumari HV, Suresh Raju K (1995) Moisture behavior of T300-914C laminates. J Reinf Plast Compos 14:513–522
11. Roy S (1999) Modeling of anomalous diffusion in polymer composites: a finite element approach. J Compos Mater 33:1318–1343
12. Sar B-E, Freour S, Davies P, Jacquemin F (2012) Coupling moisture diffusion and internal mechanical states in polymer—a thermodynamical approach. Eur. J. Mech 36:38–43
13. Verpoest I, Springer GS (1988) Moisture absorption characteristics of aramid-epoxy composites. J Reinf Plast Compos 7:2–22
14. Youssef G, Fréour S, Jacquemin F (2009) Stress-dependent moisture diffusion in composite materials. J Compos Mater 43:1621–1637

Effect of Sea Water on Polymeric Marine Composites

Akawut Siriruk and Dayakar Penumadu

Abstract Moisture absorption in carbon fiber vinyl ester reinforced composite facings used for marine composite sandwich structures can be approximated by the Fickian diffusion model. Comparative study of water uptake for VARTM based polymer composites for exposure to tap, distilled, and sea water is presented. Evaluating moisture diffusion coefficient based on one-dimensional Fickian model usually involves errors resulting from large scatter of weight gain data at early times of exposure due to very small changes in moisture content of polymer composites. A novel measurement technique is proposed here for precisely measuring moisture absorption–desorption curves with improved precision to evaluate the diffusion coefficient. Mechanical properties of carbon fiber composite facings in terms of modulus and failure stress and associated degradation due to long-term sea water exposure are also summarized corresponding to different ply lay-up orientations. The matrix dominated lay-up orientations show considerable degradation in mechanical properties due to sea environment. Notably, tension–tension fatigue on matrix dominated composites after sea water saturation resulted in 30 % degradation of fatigue life.

1 Introduction

The investigations reported herein are motivated by an increasing interest in applying polymeric composites and sandwich materials in the construction of naval structures. In this chapter we consider a polymeric composite sandwich material consisting of a 25 mm thick closed cell PVC foam, Divinycell Diab H100 [1], having a density of 100 kg/m^3 that is placed between thin ($\sim$2 mm thick)

A. Siriruk · D. Penumadu (✉)
Civil and Environmental Engineering, University of Tennessee,
325 John D. Tickle Building, Knoxville, TN, USA
e-mail: dpenumad@utk.edu

P. Davies and Y. D. S. Rajapakse (eds.), *Durability of Composites in a Marine Environment*, Solid Mechanics and Its Applications 208,
DOI: 10.1007/978-94-007-7417-9_5,

carbon fiber reinforced vinyl ester resin based polymeric composite facings (CF/VE). These materials when used for marine applications, especially for applications involving ship structures and submersibles, are exposed to sea water for long durations, whereby both water ingress mechanisms and water induced degradations are of significant importance. The purpose of the present chapter is to summarize findings associated with water ingress and related damage of carbon fiber vinyl ester composites. The relationship between physical aging and the ingress of sea water into commonly considered polymeric composite materials are described and relatively less known effect on diffusion accounting for the type of pore-fluid considering sea water, tap water and distilled water.

The CF/VE facing material consisted of stitch-bonded fabric of carbon fiber tows embedded in vinyl ester resin. Each carbon tow consisted of 12 k Toray's Torayca T700 individual fibers and the facing was prepared from the impregnation of equi-biaxial fabric. The carbon stitch fabric used a vinyl ester compatible sizing, designated as LT650-C10-R2VE, supplied by the Devold AMT AS, Sweden. The matrix resin was Dow Chemical's Derakane 510A-40, a brominated vinyl ester, formulated for the VARTM process. The bromination imparts a fire-resistant property to the composite. Vinyl ester has a higher fracture strain than the typical polyesters, and hence produces composites with superior mechanical strength and impact resistance. The fiber volume was found to be 58 % by the areal density method and includes 2.2 % weight of polyester stitch fiber. Four plies of Devold LT650 fabric were stacked symmetrically to have 2.5 mm nominal thickness as in Fig. 1 showing that the dimensions of the CF/VE specimen prepared from the panel at different lay-up orientations, employed for mechanical testing. To obtain the mechanical properties of composite facing as a function of fiber bundle orientation, CF/VE laminated composites consisting of $[0/90]_{2S}$, $[15/75]_{2S}$, $[30/60]_{2S}$, $[\pm 45]_{2S}$, and $[90/0]_{2S}$ cross-stitched lay-ups are obtained as shown in Fig. 1. VARTM approach was implemented to make large panels of the composites and sandwich structures using facilities at the Composites Fabrication Laboratory at North Carolina A&T University using established protocols [2].

When composites are exposed to moisture or liquid water, they absorb the water molecules, typically through diffusion process and is characterized by monitoring its weight gain with time. This process is typically slow and is largely affected by the equivalent diffusion coefficient of the composite material, which strongly depends on the type of reinforcing fiber (glass vs. carbon), type of resin (epoxy vs. vinyl ester), type of sizing, lay-ups implemented, and manufacturing process. The study of moisture absorption in polymeric composites is a well-established phenomenon and leads to deleterious effects associated with debonding at fiber-matrix interface, resulting in deterioration in long-term durability properties [3–7]. Additionally moisture combined with the temperature may cause significant changes in material properties including the glass transition temperature, T_g of composites [4, 8]. However, the effect of sea water on carbon fiber reinforced composite materials have not been extensively studied, especially considering the matrix dominated layup samples. It was established in earlier work [9, 10] that matrix dominated sample of CF/VE composites exhibited mechanical degradation

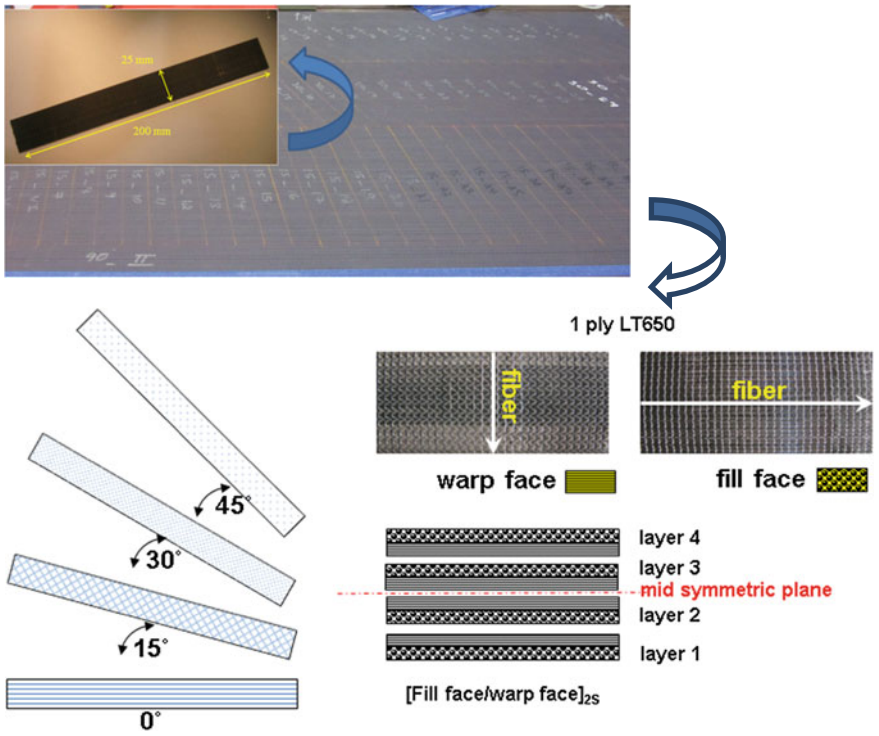

Fig. 1 A carbon fiber reinforced vinyl ester (CF/VE) composites panel prepared at different orientations with final dimension sample of 200 mm by 25 mm consisting of four cross-stich plies of Devold LT 650 (12 k Toray's Torayca T700 carbon fiber tow) and vinyl ester resin. The structure of each stitch bonded carbon fabric ply combines the fill face in 0̊ direction and warp face in 90° direction stitched with a polyester knitting thread used to form the panel of [fill face/warp face]$_{2S}$

when exposed to sea water. Ongoing research by the authors is focused on sea water effects on the mechanical response of both PVC foam and CF/VE facing individually and on the sandwich lay-up. This chapter primarily presents the effect of prolonged sea water exposure on vinyl ester based carbon fiber composites in terms of mechanical property degradation and dimensional stability by considering moisture expansion coefficients.

2 Evaluation of Fluid Effect on CF/VE

Diffusion is a process by which matter is transported from one part of a system to another as a result of random molecular motions. Diffusion is a time-dependent process, where D is the diffusion coefficient. Upon assuming, a continuous mass

distribution *m(x,t)*, the steady-state flux (*J*) is controlled by Fick's first law. More comprehensive details are given elsewhere [9].

$$J = -D\frac{\partial m}{\partial x} \tag{1}$$

Under general conditions (non-steady state), which is more applicable to polymer composites, diffusion can often be described by Fick's second law:

$$\frac{\partial m}{\partial t} = D\frac{\partial^2 m}{\partial x^2} \tag{2}$$

The property degradation due to fluids may be recoverable or irreversible and a distinction between them can be made by observing characteristic features of weight gain data. Fluid sorption in polymers and polymeric composites can be broadly identified by means of five schematic curves relating weight gain to $\sqrt{t^*}$ as presented in Fig. 2. The solid curve marked in that figure applies to the linear Fickian (LF) behavior, which is often used to describe stable polymer systems exposed to fluid ingress. Curves "A" and "B" are typical variations corresponding to both neat polymers and fiber reinforced composites having recoverable fluid-induced degradations of certain material properties. Of these, type A variation corresponds to a case where weight-gain never attains equilibrium, such as for two phase diffusion, and type B represents the circumstance of two-stage diffusion. Data represented by curves "C" and "D" are usually obtained for polymeric composites only. Of these, "C" accounts for the case of rapidly increasing fluid content, which is usually accompanied by damage growth that leads to material break down, large deformations, as well as occasional failure. Curve "D" accords with weight loss that is attributable to chemical or physical break down of the material. Materials that show a weight gain data as shown conceptually using curves "C" and "D" represent irreversible response, often associated with loss of material integrity and possible structural failure.

In this investigation, CF/VE facing samples 200 mm long and 25 mm wide and a given thickness (depending on the lay-up configurations) were initially dried in a

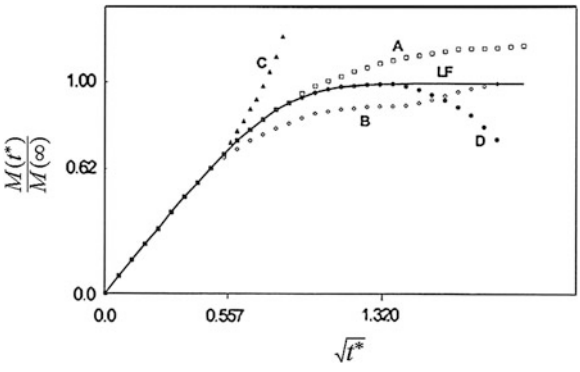

Fig. 2 Schematic curves representing a *solid line*, designated by LF, corresponds to linear Fickian diffusion and four possible categories of non-fickian weight-gain sorption data

desiccator until their weight reached a constant value. Subsequently, weight gain data were recorded periodically after immersing the material in simulated sea water baths at 40 °C for a soaking duration of at least three months which corresponds to saturation time for this polymeric composite material system. After a target duration of soaking, as suggested by ASTM D 5229 [11], these samples were removed from the water bath, padded dry to remove the surface moisture and then weighed on a Sartorius analytic balance within an accuracy of ± 0.1 mg to determine the percent weight gain ($\%M_{gain}$) or moisture content using Eq. 3 The wet condition (saturated sample) was achieved by immersing the carbon fiber reinforced vinyl ester samples in a water bath at 40 °C for at least 3 months prior to testing. The state of saturation was ascertained by monitoring the weight gain with time of soaking. The moisture content is plotted as function of the time ($\sqrt{t}$). The diffusion coefficient, D can be obtained from the initial slope of a plot using Eq. 4 if one were to assume that 1-D diffusion conditions are satisfied.

$$\%M_{gain} = \frac{M_{wet} - M_{dry}}{M_{dry}} \times 100 \tag{3}$$

$$D = \pi\left(\frac{h}{4M_{sat}}\right)^2 (\Delta\, initial\, slope)^2 \tag{4}$$

CF/VE coupon specimens went through special conditioning process to evaluate potential degradations in mechanical properties. Considering time for reaching full saturation for these composites being 3 months, the specimens were immersed in temperature controlled water baths at 40 °C for 5 months before conducting mechanical property tests and water baths having sea water, distilled water, and deionized water were also used for selective studies. In this chapter, weight gain data as observed for considered fluid, specifically distilled, tap and sea water absorption is reported. Weight gain measurements were taken after 1, 4, 9, 16 and 24 h, followed by weekly intervals. Water absorption data suggests that on relative scale, these composite facings absorbed sea water the most, followed by distilled and tap water respectively as summarized in Fig. 3. However, considering the significant scatter which is expected for this type of measurement approach, one can conclude that insignificant differences between three water types are noted for both saturated weight gain amount and temporal variation of fluid sorption behavior. Using a value of 0.5 % (Fig. 4) for saturation weight gain condition corresponding to sea water sorption, using Eq. 4 for this data, diffusion coefficient of 7.5×10^{-7}mm^2/s was obtained for this T700 carbon fiber based vinyl ester composite facing.

The most common method used in practice for the determination of the diffusion coefficient is outlined by refs [11, 12] and requires periodic monitoring of weight gain data to calculate the moisture diffusivity constant. Weight gain data in linear region corresponding to shorter time scales has considerable data and requires linear regression on noisy data to interpret slope leading to large error in the estimation of diffusion coefficient for polymeric composites [13]. Moreover,

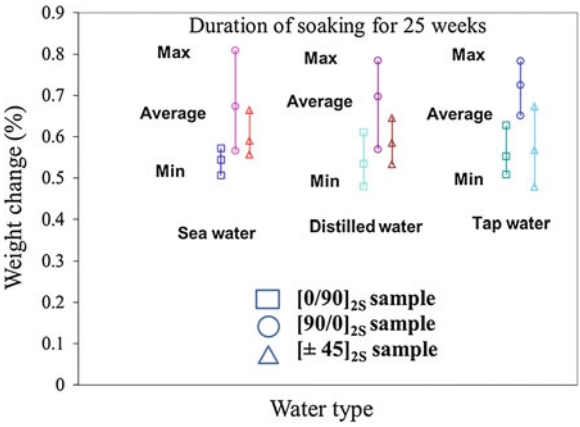

Fig. 3 Summary of weight gain data for specimens immersed in sea, distilled, and tap water

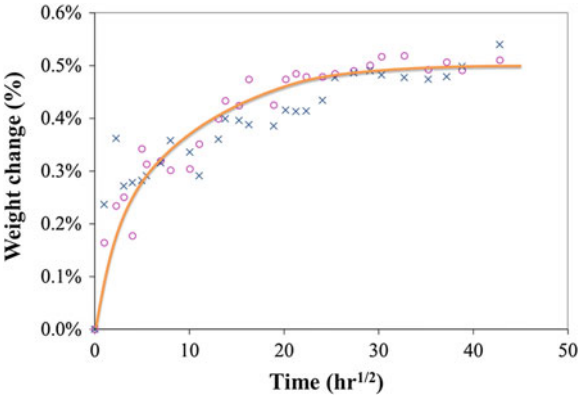

Fig. 4 Weight gain data for CF/VE immersed in sea water over 3 months

the anisotropic nature of composites introduces additional errors to diffusivities calculated by conventional methods using simple 1-D model.

One should expect considerable scatter in actual weight gain data using the method described above and an example is shown for two types of composites in Fig. 5. Availability of this type of data associated with long-term weight gain for polymer composites is rare in the literature and it is important to recognize onset of permanent damage from such simple, but time consuming measurements. Both types of composites prepared using unidirectional $[0°_6]$ AS4/3501-6 and $[0°_6]$ IM7/8551-7 graphite/epoxy coupons with dimensions of 200 mm and 25 mm (manufactured in a vacuum press following Hercules corp specification) exhibits a type "D" curve discussed earlier, indicating the onset of permanent damage in composites. If the data was not acquired for long-enough duration, once could have easily considered these materials as stable when exposed to sea water.

Authors have recently developed an experimental procedure to allow measurement of moisture uptake during adsorption/desorption kinetics with a

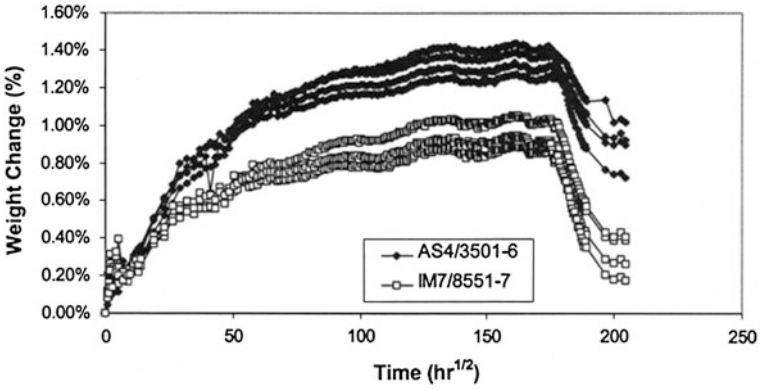

Fig. 5 Five year sorption data for [0°$_6$] AS4/3501-6 and [0°$_6$] IM7/8551-7 coupons immersed in simulated seawater at 34 °C

resolution of 0.1 μg using a highly precise gravimetric microbalance system as shown in Fig. 6. Water vapor adsorption experiments were performed by gravimetric techniques. The experimental setup consists of a high-sensitivity microbalance (Cahn Digital Recording Balance, DRB-200), customized sampling and gas handling system, and a data acquisition system. A custom-made 750 mm long and 75 mm inner diameter quartz chamber is fitted to the balance on the sampling side. The sample pan is attached using a nickel–chromium wire mesh to reduce mass transfer resistance between solid–fluid phases. The sample pan is suspended inside the quartz chamber by a Ni–Cr wire, which does not absorb moisture. The quartz chamber has an inlet gas port at the bottom and several exit ports along its length. The gas generation system consists of ultrahigh purity N_2 (99.999 % UHP N_2) as carrier gas. The carrier gas is initially passed through a gas drier/desiccator, containing anhydrous $CaSO_4$, to remove any trace gas moisture. Mass flow controllers are used to control the gas flow rates. A portion of carrier gas is allowed to purge through double-distilled water in a fritted glass bubbler creating a saturated vapor or wet stream of carrier gas. Subsequently the wet carrier gas is mixed with remaining dry carrier gas to generate controlled water vapor concentrations in the carrier gas streams. The concentration of water vapor is monitored by a relative humidity probe (Cole-Parmer Instrument, Digi-Sense) upstream of the sample pan which provides the feedback control for the flow rates of wet and dry streams to maintain a target relative humidity at the sample location. The gravimetric balance is coupled with a data acquisition system that gathers mass, time and temperature data. Figure 7 shows the typical absorption results of a CF/VE sample exposed to approximately 95 % relative humidity for 300 h. When compared with Fig. 4, percent weight gain data in Fig. 7 is accurately captured and the initial weight gain data shows proportional increase without scatter. Note that it cannot be considered as one-dimensional diffusion due to the relatively small width with respected to the thickness of CFVE sample employed for this study. Therefore, interpreting this

data using simple 1D diffusion model is simplistic at best. Since the moisture can enter the specimen through the edges, D for homogeneous material including edge effects yields [12]:

$$D = \pi\left(\frac{h}{4M_m}\right)^2\left(\frac{M_2 - M_1}{\sqrt{t_2} - \sqrt{t_1}}\right)^2\left(1 + \frac{h}{l} + \frac{h}{n}\right)^2 \tag{5}$$

where h = sample thickness (mm), n = sample width (mm), and l = length (mm).

Considering the weight gain data corresponding to 95 % relative humidity exposure shown in Fig. 7b, using sample geometry, and Eq. 5, diffusion coefficient

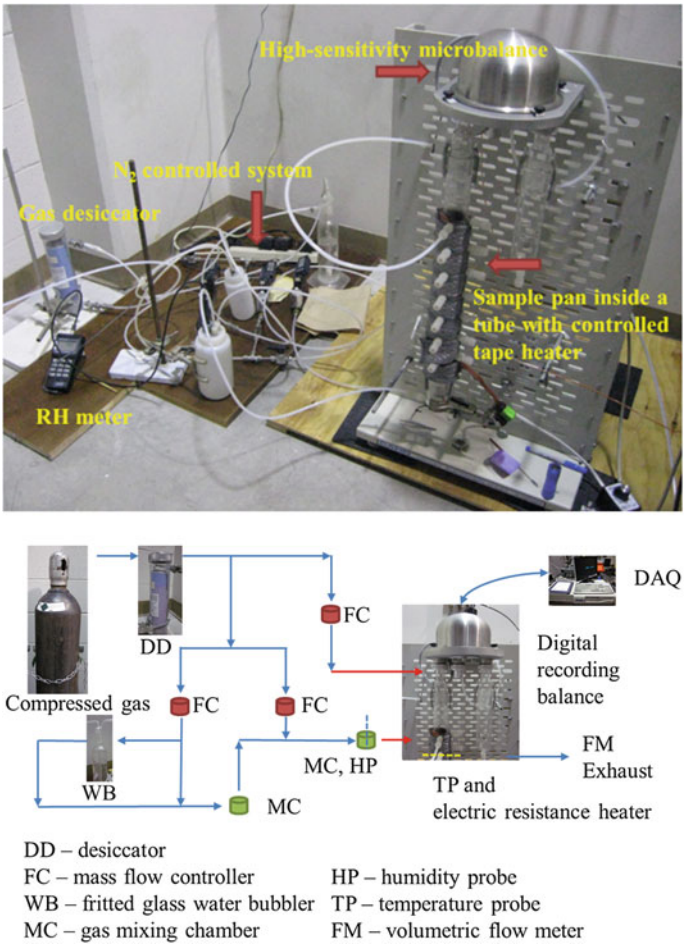

Fig. 6 A setup of gravimetric microbalance system coupled with a DAQ system

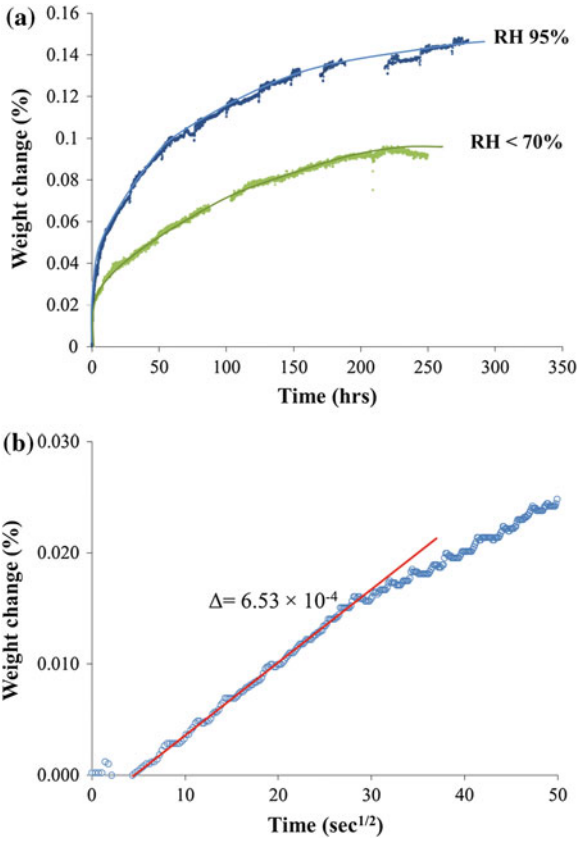

Fig. 7 **a** Moisture absorption data for CF/VE facing sample exposure to RH 95 % and 70 % and **b** initial portion of RH 95 % data set of moisture content plotted versus $\sqrt{t}(s^{1/2})$

of $5.8 \times 10^{-5} mm^2/s$ is obtained considering 0.17 % for saturation condition after 2 weeks.

The diffusion coefficient calculated by one-dimensional approach is accurate only if the correct slope of the weight gain versus $\sqrt{t}$ at $t = 0$ is obtained. If one were to calculate Fickian mass diffusion due to combined edge and anisotropic effects, the analytical solutions proposed in refs [13, 14] can be considered.

3 Mechanical Property Degradation Due to Sea Water Exposure

An MTS 610 test system using rectangular coupons having 200 mm length and 25 mm width with glued edge tabs over grip area using servo-hydraulic grips (Fig. 8) was used to carry out all the tensile tests at a fixed extension strain rate of 300 με/min. The tensile modulus was determined from the slope of the stress–strain

Fig. 8 Experimental set up of CF/VE facing and an extensometer used to capture the strain

curve well below yield point. Three cycles of load-unload data during a tensile test in Fig. 9 were monitored to infer tensile modulus. Figure 10 shows the variation of elastic modulus values at different layup orientations where 0° and 90° correspond to fill and warp direction. Multiple sample response is averaged and shows very low standard deviation for a given orientation, indicating high quality of samples from the chosen manufacturing process and repeatable testing techniques. For evaluating sea water induced degradation on elastic behavior, CF/VE facings were evaluated at room temperature in their dry state to obtain reference values for axial stress well below its failure and were subsequently subjected to tensile testing on the same samples after 16 and 20 weeks of immersion in sea water ("wet" condition). Immersion time durations were determined as described previously by our study in

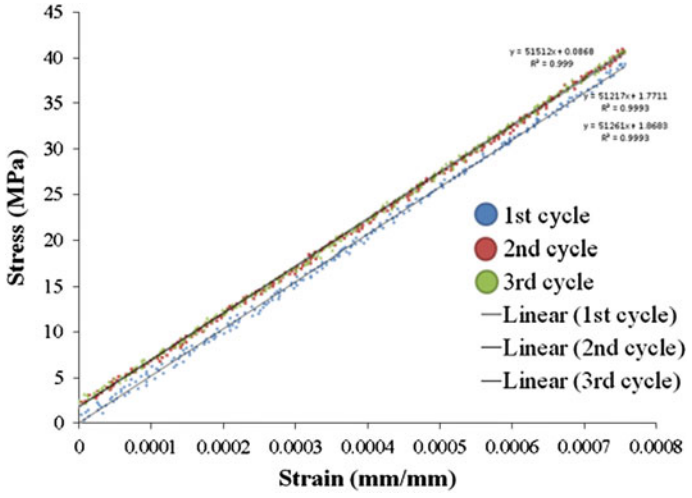

Fig. 9 Typical load-unloading data to obtain the Young's modulus of CF/VE facing

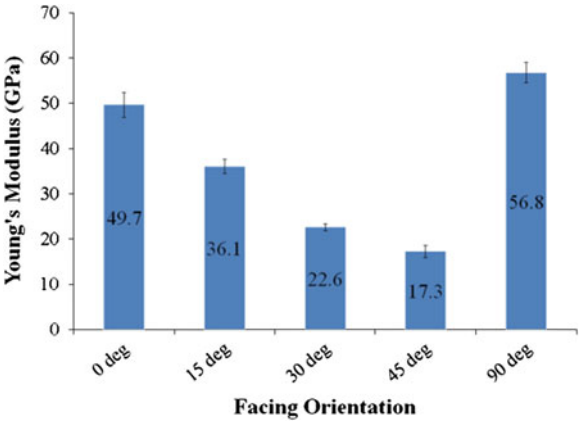

Fig. 10 Average Young's moduli of CF/VE composite facing at different fiber orientation

the past [15]. At least three replica samples on each direction were performed in this study. It was shown that sea water immersion of up to four months caused only a small global degradation of tensile moduli at different orientations. It should be noted that tensile testing response is dominated by the unaffected inner core of a sea water exposed composite sample as the degradation usually is confined to small outer core of the specimen based on authors past studies.

The small reduction in tensile modulus due to sea water as in Figs. 11 and 12 is expected because the majority of degradation occurs on the surface of the specimens where sea water is in contact. Only small amount of sea water diffuses into full thickness, thus leaving a large inner core largely unaffected by sea water soaking. Authors have observed that if similar measurements were to be made using a torsional shear test, where maximum shear stresses will be applied to the surface, then one would expect a larger degradation on the mechanical behavior as opposed to what is observed for tensile loading path here.

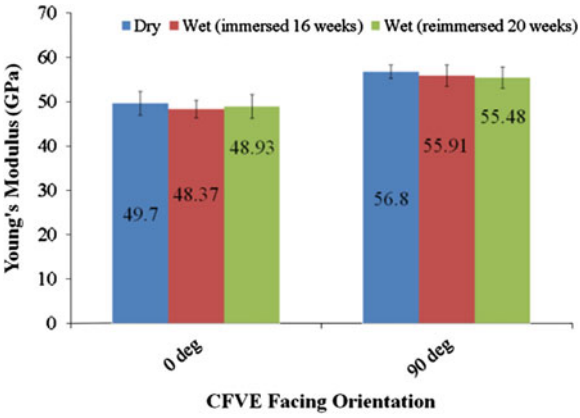

Fig. 11 Summary of elastic modulus reduction after sea water saturation at orientations of $[0/90]_{2S}$ and $[90/0]_{2S}$

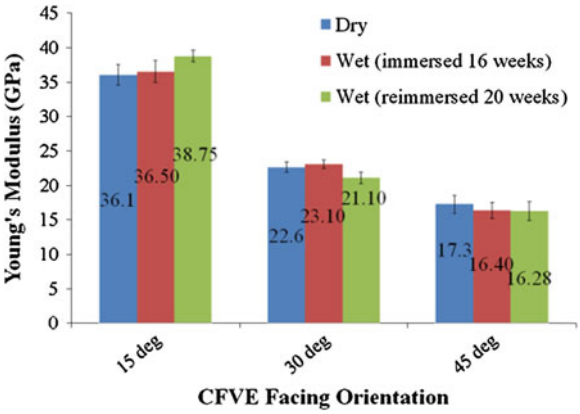

Fig. 12 Summary of elastic modulus changes after sea water saturation at orientations of $[15/75]_{2S}$, $[30/60]_{2S}$, and $[\pm 45]_{2S}$

In a similar comparative study of failure stress ($\sigma_{failure}$) on the effects of sea water, at least three dry and wet facing specimens were cut and prepared from the same region in a panel. The results in Fig. 13 shows that $\sigma_{failure}$ of $[\pm 45]_{2S}$ decreases by 6 % and $[30/60]_{2S}$ facing resulted in a 2.5 % reduction due to sea water effect. However, no difference due to sea water was found on the failure state of stress for $[15/75]_{2S}$ facing orientation, consistent with expectation that matrix dominated properties are mostly impacted by sea environment degradation.

The tension–tension fatigue test of CF/VE composites facings was obtained using procedures outlined in ASTM D3479/D3479 M standards [16]. The cyclic load was applied in a servo-hydraulic test machine at frequency of 1 Hz with an R-ratio $(\sigma_{min}/\sigma_{max})$ of 0.2 with σ_{max} = 80 MPa. The $[\pm 45]_{2S}$ specimens were subjected to in-plane tensile cyclic loading at 2/3 of ultimate strength. At least three replicate samples were tested in each of following conditions dry samples tested in air and saturated samples tested in air. More details can be found elsewhere [17, 18]. Experimental results for $[\pm 45]_{2S}$ laminates of CF/VE composites yielded failures under much fewer numbers of cycles sea water exposed samples as

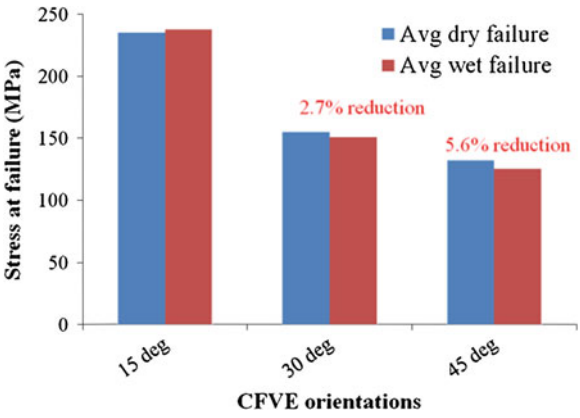

Fig. 13 Reduction in failure stress due to sea water exposure at different orientations

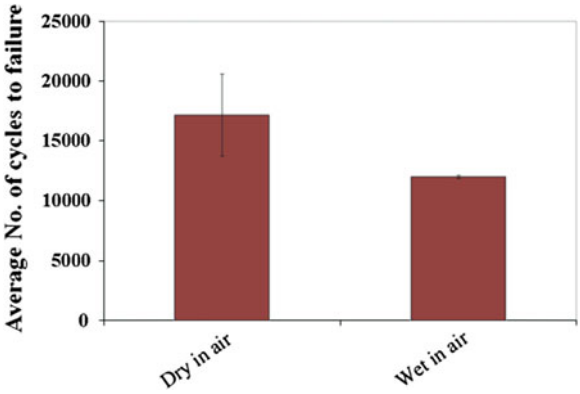

Fig. 14 Comparison of average number of cycles to failure of dry and wet sample in air under cyclic loading at 1 Hz frequency

shown in Fig. 14. These results suggest a considerable (30 %) degradation of fatigue life for samples reaching saturation state under sea water immersion conditions when compared to reference samples that have been time aged in dry conditions.

4 Concluding Remarks

The degradation associated with long-term exposure to sea water on naval composites and sandwich structures was studied by considering moisture uptake behavior under controlled conditions over long durations which are necessary to accommodate slow diffusion process of liquid (water molecules) through polymeric composites. Using test samples obtained at different orientations of lay-ups, the effects of sea water on CF/VE facing was evaluated for determining the associate damage on elastic and failure behavior under tension. A decrease of 6 % in failure strength and minimal changes in elastic moduli were obtained for VARTM based vinyl ester resin composites using T700 carbon fibers due to long-term sea water exposure. Water absorption data indicates that the considered composite facings absorbed sea water the most (0.5 % weight increase), followed by distilled and tap water. The diffusion coefficient of CF/VE composites due to exposure to simulated sea water was found to be 7.5×10^{-7}mm^2/s, and using a precise nano-balance data corresponding to 95 % relative humidity conditioning indicated a much larger diffusion coefficient of 5.8×10^{-5}mm^2/s. The type of water (sea water vs. tap vs. de-ionized) had minimum variations on the observed property degradations for $[\pm 45]_{2S}$ composite facings. The most sensitive mechanical property due to long-term sea water exposure was observed to be the fatigue response under tension–tension cyclic loading conditions. A reduction of 30 % in fatigue life in terms of number of cycles to failure was observed for samples reaching a saturation state of moisture absorption.

Acknowledgments This research was supported by ONR Contract N00014710504 under a program managed by Dr. Yapa Rajapakse and is gratefully acknowledged.

References

1. DIAB Divinycell Technical Data, Divinycell International, DeSoto, Texas (http://www.diabgroup.com/en-GB/Products-and-services/Core-Material/Divinycell-H-HP)
2. Shivakumar KN, Swaminathan G, Sharpe M (2006) Carbon/Vinyl ester composites for enhanced performance in marine applications. J Reinf Plast Compos 25(10):1101–1116
3. Kootsookos A, Mouritz AP (2004) Seawater durability of glass- and carbon-polymer composites. Compos Sci Technol 64(10–11):1503–1511
4. Yu Y, Yang X, Wang L, Liu H (2006) Hygrothermal aging on pultruded carbon fiber/vinyl ester resin composite for sucker rod application. J Reinf Plast Compos 25(2):149–160
5. Gellert EP, Turley DM (1999) Seawater immersion ageing of glass-fibre reinforced polymer laminates for marine applications. Compos A Appl Sci Manuf 30(11):1259–1265
6. Siriruk A, Jack Weitsman Y, Penumadu D (2009) Polymeric foams and sandwich composites: material properties, environmental effects, and shear-lag modeling. Compos Sci and Technol 69(6):814–820
7. Siriruk A, Penumadu D, Weitsman YJ (2009) Effect of sea environment on interfacial delamination behavior of polymeric sandwich structures. Compos Sci Technol 69(6):821–828
8. Akbar S, Zhang T (2008) Moisture diffusion in carbon/epoxy composite and the effect of cyclic hygrothermal fluctuations: characterization by dynamic mechanical analysis (DMA) and interlaminar shear strength (ILSS). J Adhes 84(7):585–600
9. Weitsman YJ (2012) Effects of fluids on mechanical properties and performance fluid effects in polymers and polymeric composites. Springer, Berlin
10. Weitsman YJ, Elahi M (2000) Effects of fluids on the deformation, strength and durability of polymeric composites—an overview. Mech Time-Depend Mater 4(2):107–126
11. ASTM Standard: D 5229 Standard test method for moisture absorption properties and equilibrium condition of polymer matrix composite materials
12. Shen C-H, Springer GS (1976) Moisture absorption and desorption of composite materials. J Compos Mater 10(1):2–20
13. Aktas L, Hamidi YK, Altan MC (2004) Combined edge and anisotropy effects on Fickian mass diffusion in polymer composites. J Eng Mater Technol 126(4):427–435
14. Grace LR, Altan MC (2012) Characterization of anisotropic moisture absorption in polymeric composites using hindered diffusion model. Compos A Appl Sci Manuf 43(8):1187–1196
15. Weitsman YJ, Siriruk A, Penumadu D (2007) Sea water effects on polymeric composites. 16th international conference on composite materials, ICCM-16, Kyoto, Japan, 8—13 July 2007
16. ASTM standard: D 3479/3479 M Standard test method for tension–tension fatigue of polymer matrix composite materials
17. Weitsman YJ, Penumadu D, Siriruk A (2009) On the immersed and dry fatigue of carbon fiber/vinyl ester composite material. 17th international conference on composite materials, ICCM-17, Edingberg, UK, 27–31 July 2009
18. Siriruk A, Penumadu D, Weitsman YJ (2010) Fatigue behavior of carbon fiber and vinyl ester sandwich facing material due to sea environment. 9th international conference on sandwich structures, ICSS-9 california institute of technology, Pasadena, California, 14–16 June 2010

Seawater Aging of Vinylester and Carbon Reinforced Vinylester

A. M. Figliolini and L. A. Carlsson

Abstract The effects of marine environmental exposure on moisture absorption and the mechanical properties of vinylester resins (VE510A and VE8084) and unidirectional carbon fiber/VE510A composites have been experimentally investigated. Two carbon fiber sizings (F and G) were examined. Neat resin specimens were exposed to humid air at 50 °C and seawater at 40 °C until saturation. The composite materials were immersed in seawater at 40 °C. The resin specimens absorbed small amounts of moisture. The composite specimens absorbed more moisture than the resins. Both the neat resins and composites displayed Fickian diffusion behavior. Mass balance analysis of moisture absorption of the composites was performed which shows that moisture up-take is dominated by the fiber/matrix interface region. The moisture absorption was found to depend on the fiber sizing. Dry and moisture saturated neat resin and composite specimens were tested in tension, compression, and shear. Moisture absorption slightly improved the ductility of the neat resin specimens. Composites with F-sized carbon fibers displayed higher strengths than those with G-sized fibers at both dry and moisture saturated conditions. Moisture absorption reduced the in-plane and interlaminar shear strengths of the composites.

A. M. Figliolini (✉) · L. A. Carlsson
Department of Mechanical Engineering, Florida Atlantic University, Boca Raton, FL 33431, USA
e-mail: alex.figliolini@ravenano.com

L. A. Carlsson
e-mail: carlsson@fau.edu

P. Davies and Y. D. S. Rajapakse (eds.), *Durability of Composites in a Marine Environment*, Solid Mechanics and Its Applications 208,
DOI: 10.1007/978-94-007-7417-9_6,

1 Introduction

Polymer matrix composite materials have received substantial attention as candidate materials for naval applications. Polymer matrix composites do not rust as metals, are lightweight, and allow more freedom to design features such as low acoustic and radar signatures. The initial attempts to develop hulls for relatively large ship structures and yachts were based on glass fibers in polyester resin [1]. More recent developments, however, have focused on vinylester resins reinforced with glass or carbon fibers [2]. A major reason for the popularity of polyester and vinylester resins in marine structures is that they cure at room temperature and absorb small amounts of moisture. Furthermore, vinylester resins have favorable flow characteristics and are able to impregnate large fiber preforms using the vacuum assisted resin transfer molding (VARTM) process [3].

Both polyester and vinylester resins undergo substantial shrinkage upon cure. Vinylester resins may shrink as much as 10 % by volume during cure [4–6] while the shrinkage of polyester resins is of the order of 5–8 % [7]. As a reference, typical epoxy resins shrink only 3–4 % [5]. The large cure shrinkage may lead to micro void formation during cure induced by phase separation from non-reactive additives mixed with unsaturated polyester and vinylester resins [7]. Drzal and his co-workers [4] found that the large cure shrinkage of vinylester may impose tensile residual stresses on the fiber/matrix interface, which tends to degrade the fiber/matrix interface adhesion. The carbon atoms in the graphite crystal are fully saturated leaving very little opportunity for chemical bonds with the surrounding matrix. Furthermore, the surface of carbon fibers is smooth, which reduces the opportunity for mechanical interlocking.

As discussed in a recent text by Weitsman [8], polymers tend to absorb moisture which changes the state of residual stress in a composite by volume change of the matrix introduced by the addition of water into the material. In addition, moisture tends to degrade the polymer by adding a liquid low-molecular phase to the polymer chain network [9]. Further, moisture present in the fiber/matrix interface region may cause hydrolysis and chemical attack, induce osmotic pressure in voids between fiber and matrix and chemically attack the reinforcing fibers, in particular glass fibers [10, 11], see Fig. 1. The above mentioned damage mechanisms may result in significant reductions in the strengths of unidirectional fiber composites especially those that are sensitive to the fiber/matrix interface quality, such as longitudinal shear strength, and transverse tensile strength [11–13].

In this chapter we will present a brief review of our recent research on durability of the vinylester resins and carbon/vinylester composites exposed to seawater. The results are obtained from a recent Master Thesis by the first author, [14], and two recent publications [15, 16]. The objectives of the review are: (1) quantify and analyze moisture up-take in 510 and 8084 vinylester resins and carbon/vinylester 510 composites, (2) examine the effects of marine environmental exposure on the mechanical response of the 510 and 8084 resins; (3) investigate

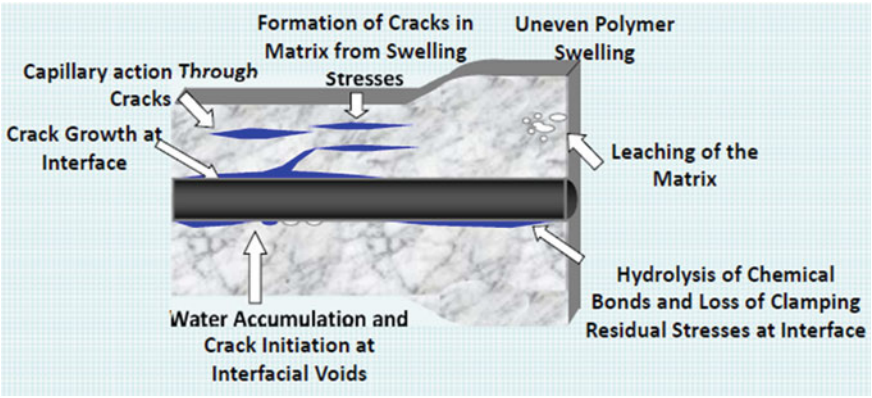

Fig. 1 Schematic of damage mechanisms of a polymer matrix composite from water absorption

the influence of carbon fiber sizing on the moisture up-take and strengths of carbon fiber/vinylester composites. The resins and composites were tested at dry and moisture saturated conditions.

2 Experimental

2.1 Materials

Derakane vinylester resins, 510A and 8084 (VE510A and VE8084), manufactured by Ashland [17] are examined. These resins are common as matrix materials in naval composites reinforced with carbon fibers. VE 510A-40 is derived from a brominated bisphenol-A resin. The VE 8084 resin is elastomer modified with favorable adhesive strength, abrasion resistance and toughness.

Unidirectional composites consisting of T700 carbon fibers from Toray, with two types of sizing, F and G, in the VE510A resin were prepared. The T700 carbon fiber is a high strain fiber commonly used as reinforcement in composite naval structures. The F sizing is developed by Toray, specifically to promote adhesion to vinylester resins, while the G sizing is a "general purpose" sizing. The sizing chemistry is unspecified by the manufacturer, and of proprietary nature.

Neat resin panels were cast in a 30.5 × 30.5 cm mold consisting of two vertical glass panels separated by sealing tape and spacers to obtain a uniform thickness of the panels in the range from 4.6 to 6.4 mm. The resin was poured into the opening between the vertical glass panels on the top of the mold. The long gel time of the resins allowed air bubbles to travel to the top of the mold, leaving the majority of the panel free from entrapped air and voids. Tensile and shear test specimens were machined from the panels. Cylindrical specimens for compression testing were molded in 12.7 mm diameter PVC pipe. For further details, see [14].

Fiber reinforced composite panels were prepared using F and G sized T700 carbon fibers with vinylester 510A resin. A comprehensive test program on the moisture absorption and mechanical performance of dry and seawater saturated vinylester and composite specimens was conducted. Specimens were tested in tension, compression and shear. The test plan was designed to examine moisture absorption and mechanical properties of the two resins and the carbon/VE510 composites with two types of fiber sizing. Specifically, for the composite specimens, the properties governed by the fiber/matrix interface were examined, such as off-axis and transverse tension, in-plane and interlaminar shear. Composite laminate lay-ups are indicated in Table 1. Impregnation of the fibers with the resin was done by vacuum assisted resin transfer molding (VATRM) [3]. Panels were fabricated utilizing a partition of a 1.2 m by 2.4 m flat glass table top as the mold surface. The panels were impregnated and cured at room temperature. Average ply thicknesses were 0.32 and 0.30 mm after cure for the C(F)/VE 510A, and C(G)/VE 510A laminates, respectively. Fiber volume fractions for the F and G sized composites were 0.63 and 0.66, respectively. Microscopic examination revealed negligible void content.

The neat resin and composite test specimens were cured at room temperature (RT) for at least 24 h, and then subjected to post cure for two hours at 120 °C for the 510A and 99 °C for the 8084 resins. Moisture absorption was conducted under controlled laboratory conditions in seawater obtained directly from the Atlantic Ocean at 40 ± 1 °C. Specimens exposed to humid air were placed in an environmental chamber controlled at 85 ± 1 % RH and 50 ± 1 °C.

3 Results and Discussion

3.1 Moisture Absorption

Figure 2 shows an example of moisture absorption curves for the neat vinylester 510 and 8084 tensile specimens immersed in seawater. It is noted that the

Table 1 Composite layups

Test specimen type	C(F)/VE 510A	C(G)/VE 510A
Tensile—Longitudinal	$[0]_3$	Not Tested
Tensile—Off-axis 45°	$[45]_{11}$	$[45]_{11}$
Tensile—Transverse	$[90]_{11}$	$[90]_{11}$
Compression—Cross-ply[a]	$[\bar{0}/90]_{9S}$	$[\bar{0}/90]_{9S}$
Compression—Off-axis 45°	$[45]_{11}$	$[45]_{11}$
Compression—Transverse	$[90]_{11}$	$[90]_{11}$
Iosipescu Shear	$[0]_{12}$	$[0]_{12}$
Short Beam Shear	$[0]_{13}$	$[0]_{11}$

[a] The over-bar for the cross ply laminates indicates the ply about which the laminate is symmetric

specimens approached saturation after about two months of exposure. Similar curves were produced for all resin and composite specimens subjected to the various environments. A simple Fickian 1D diffusion model was used to analyze the data, see [15]. The moisture transport is here characterized by an effective diffusivity, D, representing water ingress through the surfaces and the edges of the test specimens. It is noted that the 510A resin absorbs much less moisture than the 8084 resin, 0.28 versus 0.61 % at saturation. The Fickian diffusion model provides good fits to the moisture absorption data for both resins. The diffusion coefficients are similar for the two systems; $D = 3.83 \times 10^{-6}$ and $3.99 \times 10^{-6} \mathrm{mm}^2/\mathrm{s}$ for 510A and 8084, respectively.

Figure 3 shows moisture absorption curves for F sized composite $[0]_3$ tensile specimens and F and G sized composite $[45]_{11}$ tensile specimens immersed in

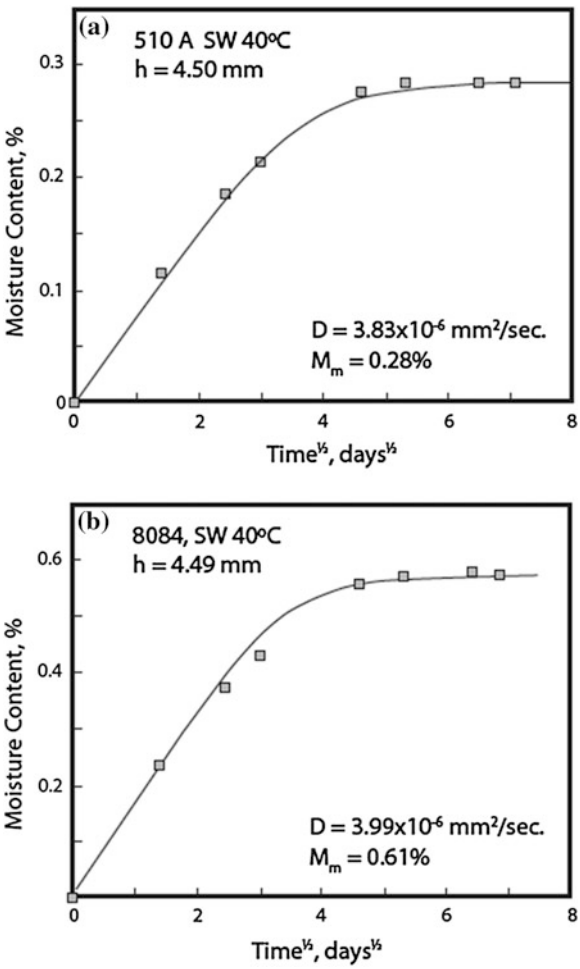

Fig. 2 Moisture absorption of neat vinylester resin tensile specimens exposed to seawater

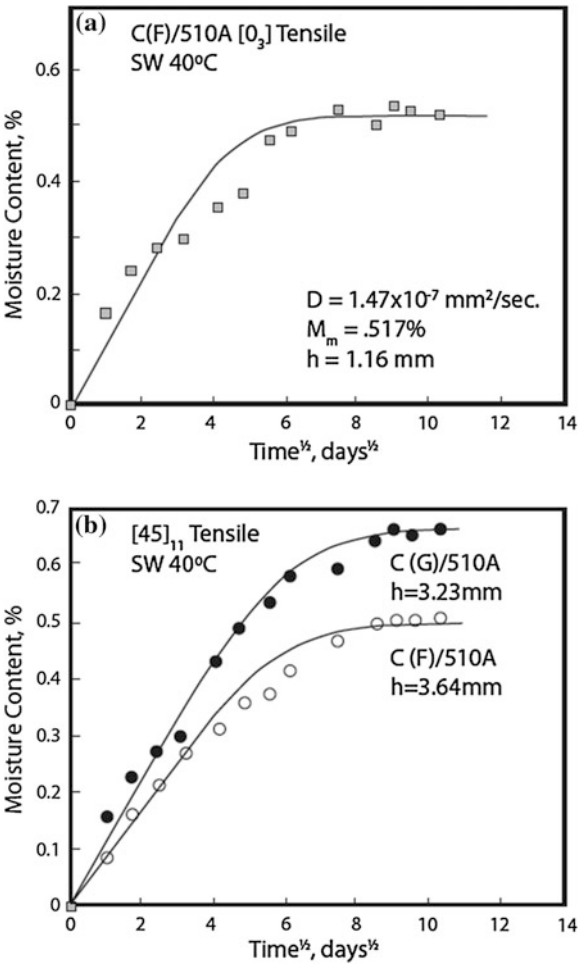

Fig. 3 Moisture absorption for C/VE 510A tension specimens immersed in seawater at 40 °C **a** longitudinal, **b** Off-axis 45°

seawater at 40 °C [16]. The moisture content increases continuously until saturation of moisture content is reached as indicated by a horizontal asymptote. The $[0]_3$ tensile specimens were saturated after about 64 days of exposure (Fig. 3a). The saturation moisture content is about 0.52 %. Figure 3b shows the moisture up-take for the $[45]_{11}$ specimens. It is apparent that the composites with the F-sizing absorb less moisture than those with G-sizing. The $[45]_{11}$ specimens are much thicker than the $[0]_3$ specimens and require longer exposure times (about 100 days) to reach saturation. The saturation moisture content for the $[45]_{11}$ C(F)/510A specimens is 0.51 %, similar to that for the $[0]_3$ specimens, Fig. 3a, as expected. Similar results were obtained for the other specimens. The solid curves in Fig. 3 represent Fickian fits to the experimental data. Good fits are observed. The diffusivity for the $[0]_3$ specimen ($D = 1.47 \times 10^{-7}$ mm^2/sec) is less than the diffusivities for the C(F) and C(G) $[45]_{11}$ specimens ($D = 8.52 \times 10^{-7}$ and

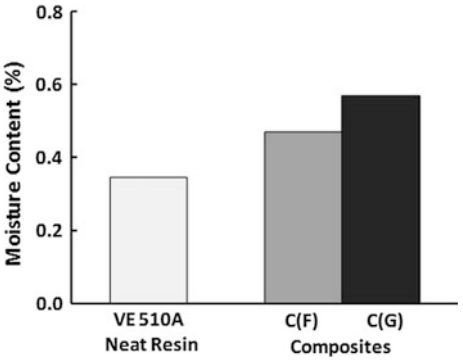

Fig. 4 Moisture contents for VE510A resin and carbon/VE510A composites with F and G sized fibers

6.29×10^{-7} mm^2/sec). This is probably the result of less exposed free fiber ends in the $[0]_3$ specimens than in the $[45]_{11}$ specimens which would result in less opportunity for moisture transport at the fiber/matrix interface, "wicking", to be discussed further below. The results in Fig. 3b show that the composite with G sized carbon fibers absorb more moisture than the composite with F sized fibers indicating a more accessible fiber/matrix interface for the G sized composite.

Average results for the saturation moisture contents in the 510A resins and carbon/VE 510 composites are displayed in Fig. 4. The results show that the composites absorb more moisture than the resin. Given that about 35 % (by volume) of the composite consists of resin and 65 % (by volume) of carbon fibers that are inert to water, the excess water must accumulate at the fiber/matrix interface, "wicking". Wicking is the phenomenon of moisture transport by capillary action along the fiber/matrix interface due to voids and un-bonded regions between the fibers and the matrix, see Fig. 1. Wicking begins by moisture transport at an exposed end of the fiber and the water molecules move inward toward the center of the specimen.

An analysis of the moisture absorption and partitioning of the moisture absorbed into the matrix and the fiber/matrix interface contributions is presented by Figliolini [14]. Knowing the saturation moisture contents for the matrix and the fiber volume fractions of the composites allows a simple mass balance analysis. The results of this analysis are shown in Fig. 5 for the composites with F and G sized fibers. It is observed that the moisture up-take is largely dominated by the fiber/matrix interface. The composite with G sized fibers shows more wicking than the one with F sized fibers, which is an indication of the importance of fiber sizing for the moisture up-take.

3.2 Mechanical Test Results

Tensile testing of the 510A and VE 8084 resins revealed that the specimens failed at relatively small strains ($\approx 3\%$) at dry conditions. After seawater immersion,

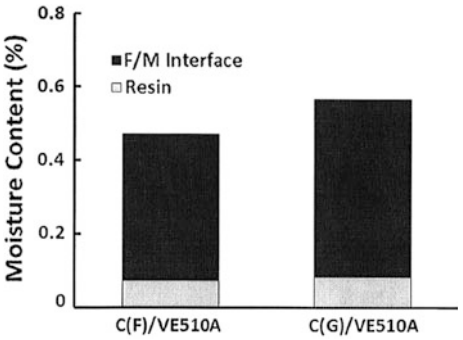

Fig. 5 Moisture partitioning into resin and fiber/matrix interface for C(F)/VE510A and C(G)/VE510A composites

however, the specimens displayed slightly more ductility, failing at larger strains ($\approx 4\%$). Although the stress–strain curves are not shown here, the test results show that the 510A resin is more brittle than the 8084 resin at dry and water saturated conditions, [15]. The ductility of VE 8084 is attributed to the elastomer modification which makes it less susceptible to defects and voids than 510A. Shear testing of resin Iosipescu specimens similarly revealed brittle behavior of both resins. Compressive testing revealed ductility for both types of resin. The VE510A resin is stronger in compression than in tension, as expected for a brittle material. For the VE8084 resin, the tensile and compressive strengths are similar. Overall, the elastic and shear moduli are not substantially influenced by moisture absorption.

As indicated in Table 1, a comprehensive test program was conducted [16] on the composite specimens with various fiber orientations and lay-ups in tension, compression and shear. Figure 6 shows an example of the influence of fiber sizing and moisture absorption on the interlaminar (S_5) and in-plane (S_6) shear strengths of the C(F)/510A and C(G)/510A composites. The results in Fig. 6 show that both shear strengths are similar. The shear strengths at dry and saturated conditions are sensitive to the type of fiber sizing; the F sizing producing higher strengths both at dry and saturated conditions. It is well-known [18] that the longitudinal shear strength is highly sensitive to the quality of the fiber/matrix interface. Absorbed moisture reduces the shear strengths, apparently as a result of a degraded fiber/matrix interface, but the F sized fiber composite undergoes less reduction in shear strength than the one with G sized fibers.

Figure 7 shows transverse and 45° off-axis tensile strength test results for the composites with two types of fiber sizing. The transverse tensile strength of the composites with F and G sized fibers are very different. The composite with F sized fibers is approximately twice as strong in transverse tension. The transverse strengths are not strongly influenced by water absorption. The higher transverse strength of the F sized composite is attributed to stronger fiber/matrix adhesion. The F sizing produces much higher 45° off-axis tensile strengths than the G sizing. Seawater exposure has small effect on the transverse and 45° off-axis tensile strengths. Corresponding results for transverse and 45° off-axis compression

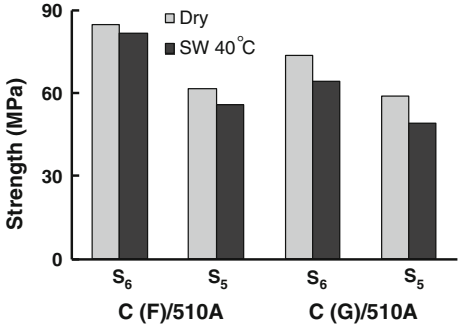

Fig. 6 In-plane (S_6) and interlaminar (S_5) shear strengths of carbon/VE510 composites with F and G-sized fibers at dry and seawater saturated conditions

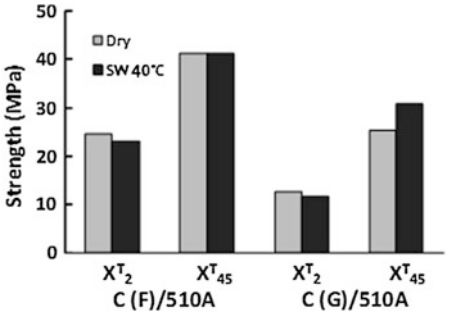

Fig. 7 Transverse and 45° off-axis tensile strengths for carbon/VE510A composites with F and G sized fibers at dry and seawater saturated conditions

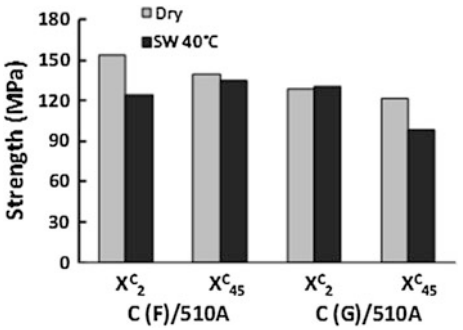

Fig. 8 Transverse and 45° off-axis compressive strengths for carbon/VE510A composites with F and G sized fibers at dry and seawater saturated conditions

strengths are shown in Fig. 8. It is observed that the transverse and 45° off-axis compressive strengths are not much affected by water absorption. Comparison of the 45° off-axis compression strengths of the composites with F and G sized fibers shows that F sizing results in slightly higher strengths, especially at seawater saturated conditions.

4 Conclusions

The results from this experimental study on vinylester resins and unidirectional carbon/vinylester composites show that both types of resin absorb small amounts of moisture, and that they remain brittle even at saturated conditions. The carbon/VE 510 composites absorbed more moisture than the resin. The fiber sizing influenced the absorption of moisture. The excess moisture absorption is attributed to wicking. Absorbed moisture reduced the longitudinal shear strengths of the composite. The composite with F sized fibers was generally stronger in shear and less influenced by moisture absorption than the one with G sized fibers.

Moisture absorption had small effect on longitudinal, transverse and 45° off-axis tensile and compressive strengths of the composites with the two types of fiber sizing. The composite strengths were overall more influenced by fiber sizing than exposure to seawater. A suitable sized fiber/matrix interface could greatly improve both the dry and wet strengths and the durability of the composite.

Acknowledgments This research project was supported by an ONR grant N00014-05-1-0341. Thanks are due to the ONR program officer, Dr. Yapa Rajapakse. Thanks go to Mark S Hoerber Jr for his help in compiling this chapter.

References

1. Hellbratt S-E, Gullberg O (1989) The development of the GRP-sandwich technique for large marine structures. In: Proceedings of the 1st international conference on sandwich constructions, 19–21 June, Stockholm, Sweden, EMAS, West Midlands, pp 425–458
2. Lonno A (1998) Experiences from using carbon fiber composites/sandwich construction in the swedish navy. In: Proceedings of the 4th international conference on Sandwich Construction, 9–11 June, Stockholm, Sweden, EMAS, West Midlands, pp 31–43
3. Advani SG (1994) Flow and rheology in polymer composites manufacturing. In: Pipes RB (ed) Composite materials. Elsevier, Amsterdam, pp 465–511
4. Drzal LT (2010) Engineering the carbon fiber-Vinylester matrix interface for naval structural systems. Presented at an ONR solid mechanics program review, Published in ONR progress report, pp 23–32
5. Xu L, Mase T, Drzal LT (2003) Cure volume shrinkage of Vinylester resins and their influence on adhesion between carbon fibers and Vinylester matrix resins. Presented by 2003 SPE automotive composites conference, Michigan State University Management Education Center, Troy, MI, 9–10 Sept 2003
6. Ramirez FA, Carlsson LA, Acha BA (2009) A method to measure fracture toughness of the fiber/matrix interface using the single-fiber fragmentation test. Compos: Part A 40:679–686
7. Li W, Lee LJ (1998) Shrinkage control of low-profile unsaturated polyester resins cured at low temperature. Polymer 39:5677–5687
8. Weitsman YJ (2012) Fluid effects in polymers and polymeric composites. Springer, New York
9. Mensitieri G, Iannone M (2008) In Ageing of composites, R. Martin ed., Woodhead Publishing Ltd, Cambridge (England), ISBN 978-1-84569-352-7CRC Press, Boca Raton FL, pp 224–281

10. Otto WH (1996) The effects of moisture on the strength of glass fibers—a literature review, US Naval Research Lab, Contract # 4522 (00). Narmco Division, The Whittaker Corp
11. Ramirez FA, Carlsson LA, Acha BA (2008) Evaluation of water degradation of Vinylester and epoxy matrix composites by single-fiber and composite tests. J Mater Sci 43:5230–5242
12. Davies P, Pomies F, Carlsson LA (1996) Influence of water absorption on transverse tensile properties and shear fracture toughness of glass/polypropylene. J Compos Mater 30: 1004–1019
13. Juska T (1993) Effect of water immersion on fiber/matrix adhesion, US Navy, Carderock Div.-SME-92/38, Ship materials engineering department research and development report, Naval Surface Warfare Center, Bethesda, Jan 1993
14. Figliolini AM (2011) Degradation of mechanical properties of Vinylester and carbon fiber/ Vinylester composites due to environmental exposure, Master Thesis, Florida Atlantic University
15. Figliolini AM, Carlsson LA (2013a) Mechanical properties of Vinylester resins exposed to marine environments, To appear in Polymer Engineering and Science
16. Figliolini AM, Carlsson LA (2013b) Mechanical properties of carbon fiber/Vinylester composites exposed to marine environments, Submitted to Polymer Composites (2013)
17. Ashland Inc., Derakane (2004) 510A-40 and 8084 epoxy Vinylester Resins
18. Drzal LT, Herrera-Franco PJ, Ho H (2000) Fiber-matrix interface tests In: Comprehensive composite materials, Kelly A, Zweben C (eds) vol 5, Elsevier Science, Oxford, pp 71–111

Effect of Water Absorption on Time–Temperature Dependent Strength of Unidirectional CFRP

Masayuki Nakada and Yasushi Miyano

Abstract Static strengths for four typical directions of unidirectional CFRP were measured under various temperatures at a single loading rate for dry and wet specimens. The four directions were longitudinal tension and bending, transverse bending, and compression. Water absorption effects on temperature dependence of these static strengths of unidirectional CFRP were assessed. Results show that the static strengths in these four directions of unidirectional CFRP as well as the viscoelastic coefficient of matrix resin decrease concomitantly with increasing temperature and water absorption. Each of four static strengths of CFRP laminates is determined uniquely by the viscoelastic coefficient of matrix resin. Therefore, the master curves of four static strengths against the reduced time at a reference temperature can be constructed and formulated using the time–temperature shift factor for the viscoelastic coefficient of matrix resin based on the time–temperature superposition principle. These master curves of four static strengths clarify that the long-term lives for four directions decrease with water absorption.

1 Introduction

Carbon fiber reinforced plastics (CFRP) are being used in primary structures of airplanes, ships, and other applications where high reliability must be maintained during long-term operations. Therefore, it is expected that an accelerated testing methodology must be established for long-term life prediction of CFRP structures exposed to actual environments of temperature, water, and other stresses.

M. Nakada (✉) · Y. Miyano
Materials System Research Laboratory, Kanazawa Institute of Technology, 3-1 Yatsukaho, Hakusan, Ishikawa 9240838, Japan
e-mail: nakada@neptune.kanazawa-it.ac.jp

P. Davies and Y. D. S. Rajapakse (eds.), *Durability of Composites in a Marine Environment*, Solid Mechanics and Its Applications 208,
DOI: 10.1007/978-94-007-7417-9_7,

We have proposed a method for formulating long-term static strength of unidirectional CFRP based on the time–temperature superposition principle (TTSP), which is used for the viscoelastic behavior of matrix resin [1].

In this chapter, the tensile and compressive static strengths in the longitudinal and transverse directions of unidirectional CFRP under Dry and Wet conditions are evaluated using the formulation method. Effects of water absorption on the time-dependence and temperature–dependence of these static strengths are examined in this study.

2 Formulation

The long-term static strength exposed to actual loading where the temperature and load change with time can be shown as the following Eq. [1].

$$\log \sigma_{\mathrm{f}}(P_{\mathrm{f}}, t', T_0) = \log \sigma_{\mathrm{f},0}\left(t_0', T_0\right) + \frac{1}{\alpha}\log[-\ln(1-P_{\mathrm{f}})] - n_{\mathrm{r}} \log\left[\frac{D^*(t', T_0)}{D_{\mathrm{c}}\left(t_0', T_0\right)}\right] \tag{1}$$

The first term of right part shows the reference strength (scale parameter for the static strength) at reduced reference time $t_0^{'}$ under reference temperature T_0.

The second term shows the scatter of static strength as the function of failure probability P_{f}. α is the shape parameter for the strength.

The third term shows variation by the viscoelastic compliance of matrix resin, which depends on temperature and load histories. n_{r} is the material parameter. The viscoelastic compliance D^* in (1) can be shown as the following equation.

$$D^*(t', T_0) = \frac{\varepsilon(t', T_0)}{\sigma(t', T_0)} = \frac{\int_0^{t'} D_{\mathrm{c}}(t'-\tau', T_0)\frac{d\sigma(\tau')}{d\tau'}d\tau'}{\sigma(t', T_0)}, t' = \int_0^t \frac{d\tau}{a_{T_0}(T(\tau))} \tag{2}$$

Therein, D_{c} shows the creep compliance of matrix resin and $\sigma(\tau^{'})$ shows the stress history. $t^{'}$ represents the reduced time at T_0, a_{T0} shows the time–temperature shift factor of matrix resin, and $T(\tau)$ shows the temperature history.

The viscoelastic compliance D^* in (2) can be shown approximately by the following equation assuming the stress history under constant deformation rate loading as step loading presented in Fig. 1.

$$D^*(t', T_0) = D_{\mathrm{c}}(t'/2, T_0) \tag{3}$$

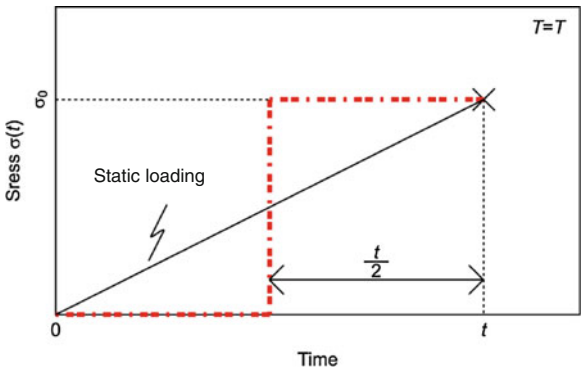

Fig. 1 Stress history under constant deformation rate loading (static loading) for determination of the viscoelastic compliance D^*

3 Experimental Procedures

Unidirectional CFRP laminates consisting of carbon fiber T300 and epoxy resin 2,500 were molded using an autoclave technique. The CFRP laminates were cured at 135 °C for 2 h and then post-cured at 160 °C for 2 h. The aging treatment for the post-cured specimen was conducted at 110 °C for 50 h. Wet specimens were obtained by soaking the aged specimen (Dry specimen) in hot water of 95 °C for 121 h for a 1-mm-thick specimen in the longitudinal direction, of 95 °C for 144 h for a 2-mm-thick specimen in longitudinal direction, and of 95 °C for 121 h for a 2-mm-thick specimen in the transverse direction. The water weight content of all wet specimens was 1.9 %.

Dynamic viscoelastic tests for the transverse direction of unidirectional CFRP were conducted at various frequencies and temperatures to construct a master curve of creep compliance for matrix resin. The static tests for four typical directions of unidirectional CFRP were conducted at various temperatures to produce the master curves of static strength for unidirectional CFRP. Longitudinal tension tests were conducted according with SACMA 4R-94. Longitudinal bending tests were conducted according with ISO 14125 to obtain the longitudinal compressive static strengths. Transverse bending tests were conducted according to ISO 14125 to obtain transverse tensile static strengths. Transverse compression tests were conducted according to SACMA 1R-94.

4 Results and Discussion

4.1 Viscoelastic Behaviors of Matrix Resin

The left side of Fig. 2a shows the loss tangent (tan δ) for the transverse direction of unidirectional CFRP (Dry specimen) versus time t, where time t is the inverse of frequency. The right side shows the master curve of tan δ, which is constructed by

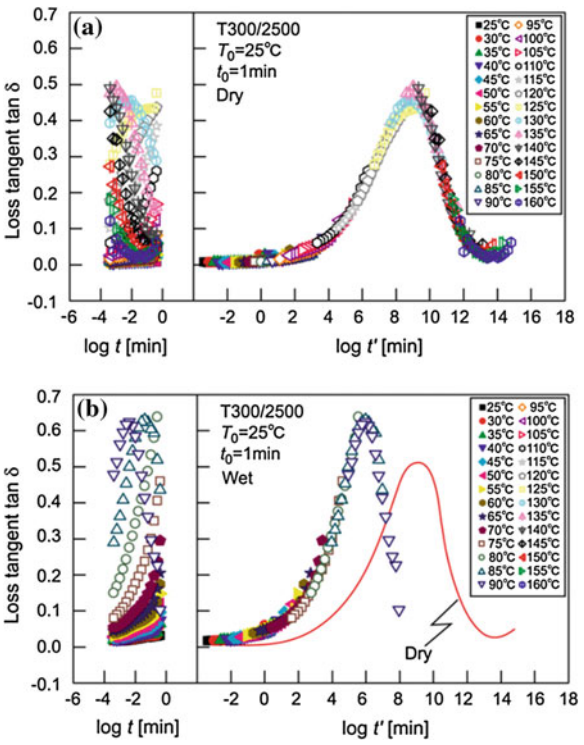

Fig. 2 Master curves of the loss tangent for transverse direction of unidirectional CFRP. **a** Dry. **b** Wet

shifting tan δ at various constant temperatures along the logarithmic scale of t until they mutually overlap, for the reduced time t' at the reference temperature $T_0 = 25$ °C. Because tan δ at various constant temperatures can be superimposed so that a smooth curve is constructed, the TTSP is applicable for tan δ for the transverse direction of unidirectional CFRP. The master curve of tan δ for Wet specimens can also be constructed as presented in Fig. 2b. The TTSP is also applicable for tan δ under wet conditions. The master curve of tan δ is shifted to the left side by water absorption as presented in Fig. 2b.

The left side of Fig. 3a shows storage modulus $E^{'}$ for the transverse direction of unidirectional CFRP (dry specimen) versus time t. The right side shows the master curve of E', which is constructed by shifting E' at various constant temperatures along the logarithmic scale of t using the same shift amount for tan δ and logarithmic scale of $E^{'}$ until they mutually overlap, for the reduced time t' at the reference temperature $T_0 = 25$ °C. Because $E^{'}$ at various constant temperatures can be superimposed to construct a smooth curve, the TTSP is applicable for $E^{'}$ for the transverse direction of unidirectional CFRP. The master curve of $E^{'}$ for wet specimens can also be constructed as depicted in Fig. 3b. The TTSP is also applicable for $E^{'}$ under wet conditions.

The time–temperature shift factor $a_{T0}(T)$, which is the horizontal shift amount portrayed in Fig. 4a can be formulated as the following equation:

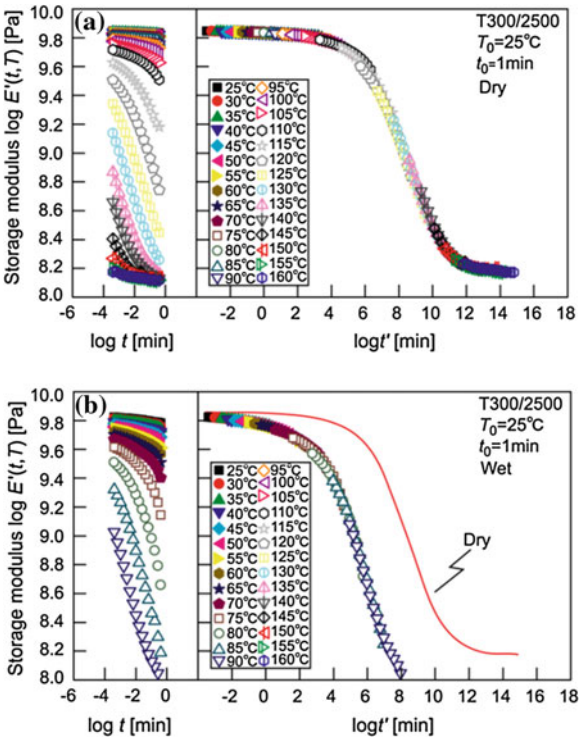

Fig. 3 Master curves of the storage modulus for the transverse direction of unidirectional CFRP. **a** Dry. **b** Wet

$$\log a_{T_0}(T) = \frac{\Delta H_1}{2.303G}\left(\frac{1}{T}-\frac{1}{T_0}\right)\mathrm{H}(T_g - T) + \left[\frac{\Delta H_1}{2.303G}\left(\frac{1}{T_\mathrm{g}}-\frac{1}{T_0}\right)+\frac{\Delta H_2}{2.303G}\left(\frac{1}{T}-\frac{1}{T_\mathrm{g}}\right)\right]\left(1-\mathrm{H}(T_\mathrm{g}-T)\right) \tag{4}$$

Therein, G is the gas constant, 8.314×10^{-3} [kJ/(K mol)], ΔH_1 and ΔH_2 respectively stand for the activation energies below and above the glass transition temperature T_g. Furthermore, H is the Heaviside step function.

Temperature shift factor $b_{T_0}(T)$, which is the amount of vertical shift portrayed in Fig. 4b can be fit with the following equation.

$$\log b_{T_0}(T) = \left[\sum_{i=0}^{4} b_i (T - T_0)^{\mathrm{i}}\right]\mathrm{H}(T_g - T) + \left[\sum_{i=0}^{4} b_i (T_\mathrm{g} - T_0)^{\mathrm{i}} + \log\frac{T_\mathrm{g}}{T}\right]\left(1-\mathrm{H}(T_\mathrm{g}-T)\right). \tag{5}$$

In the equation, b_0, b_1, b_2, b_3, and b_4 are the fitting parameters.

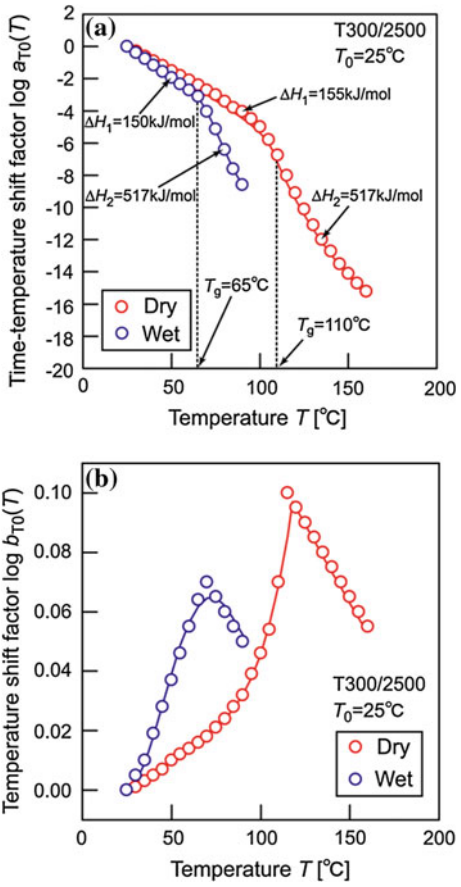

Fig. 4 Shift factors of storage modulus for transverse direction of unidirectional CFRP. **a** Time–temperature shift factor. **b** Temperature shift factor

The creep compliance D_c of matrix resin was back-calculated from the storage modulus $E^{'}$ for the transverse direction of unidirectional CFRP using [2]

$$D_c(t) \sim 1/E(t), E(t) \cong E'(\omega)|_{\omega \to 2/\pi t}, \tag{6}$$

and the approximate averaging method described by Uemura [3].

The master curve of back-calculated D_c of matrix resin is presented in Fig. 5. The master curve of D_c can be formulated as

$$\log D_c = \log D_{c,0}(t_0', T_0) + \log\left[\left(\frac{t'}{t_0'}\right)^{m_g} + \left(\frac{t'}{t_g'}\right)^{m_r}\right], \tag{7}$$

where $D_{c,\,0}$ is the creep compliance at reduced reference time $t_0^{'}$ and reference temperature T_0, and where $t_g^{'}$ is the glassy reduced time on T_0, and m_g and m_r are the respective gradients in glassy and rubbery regions of the D_c master curve.

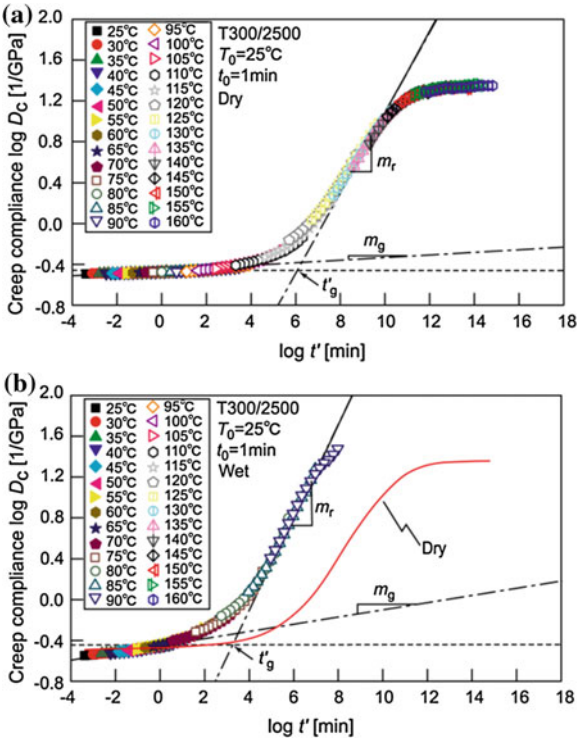

Fig. 5 Master curves of creep compliance for matrix resin calculated from the storage modulus for the transverse direction of unidirectional CFRP. **a** Dry. **b** Wet

Parameters obtained from the formulations for $a_{T0}(T)$, $b_{T0}(T)$, and D_c are presented in Table 1.

4.2 Relation Between Static Strength of CFRP and Viscoelastic Compliance of Matrix Resin

Figure 6 exhibits the relation between each of four static strengths of unidirectional CFRP and the viscoelastic compliance of matrix resin for the same conditions of time, temperature, and water absorption, respectively. The slopes of four relations are constant. Each slope depends on the loading direction; it changes slightly with water absorption. These facts demonstrate the validity of the formulation by Eq. (1) for the static strength of the employed unidirectional CFRP under wet conditions and dry conditions.

Table 1 Parameters for master curve and shift factors of creep compliance for matrix resin

	Dry	Wet		Dry	Wet
T_0 (°C)	25	25	H_1 [kJ/mol]	155	150
T_g (°C)	110	65	H_2 [kJ/mol]	517	547
$D_{c,0}$ (1/GPa)	0.337	0.351	b_0	1.65E−02	0.150
t_0' (min)	1	1	b_1	3.81E−09	1.73E−08
t_g' (min)	1.54E06	2.34E03	b_2	−8.29E−07	−4.71E−06
m_g	0.0101	0.0348	b_3	6.64E−05	4.26E−04
m_r	0.405	0.466	b_4	−1.86E−03	−1.39E−02

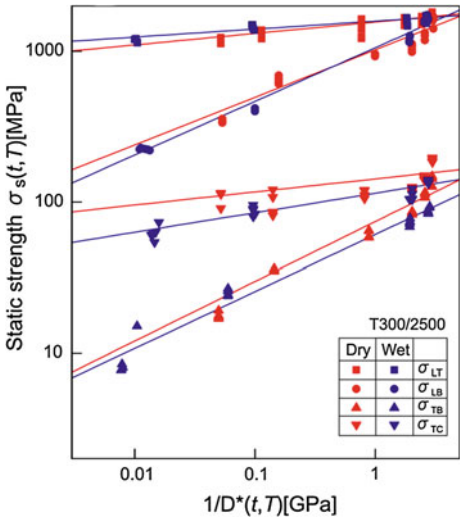

Fig. 6 Static strength of unidirectional CFRP versus viscoelastic compliance D^* of matrix resin

4.3 Master Curves of Static Strengths for Unidirectional CFRP

Figure 7 depicts the master curves of four static strengths for dry and wet specimens of unidirectional CFRP obtained from strength data at various temperatures using the time–temperature shift factors a_{T_0} portrayed in Fig. 4a. The solid and dotted curves in these figures show the fitting curves by Eq. (1) using master curves of creep compliance of the matrix resin in Fig. 5.

Three parameters of scale parameter $\sigma_{f,0}$, slope n_r and shape parameter α for the static strengths of four directions of unidirectional CFRP are presented in Table 2. These parameters depend clearly on the loading direction, although they depend only slightly on water absorption.

From the master curves of four static strengths, it is clear that all four kinds of static strengths strongly show time-, temperature- and water-absorption-dependent behavior and that the long-term lives of four directions decrease with water absorption.

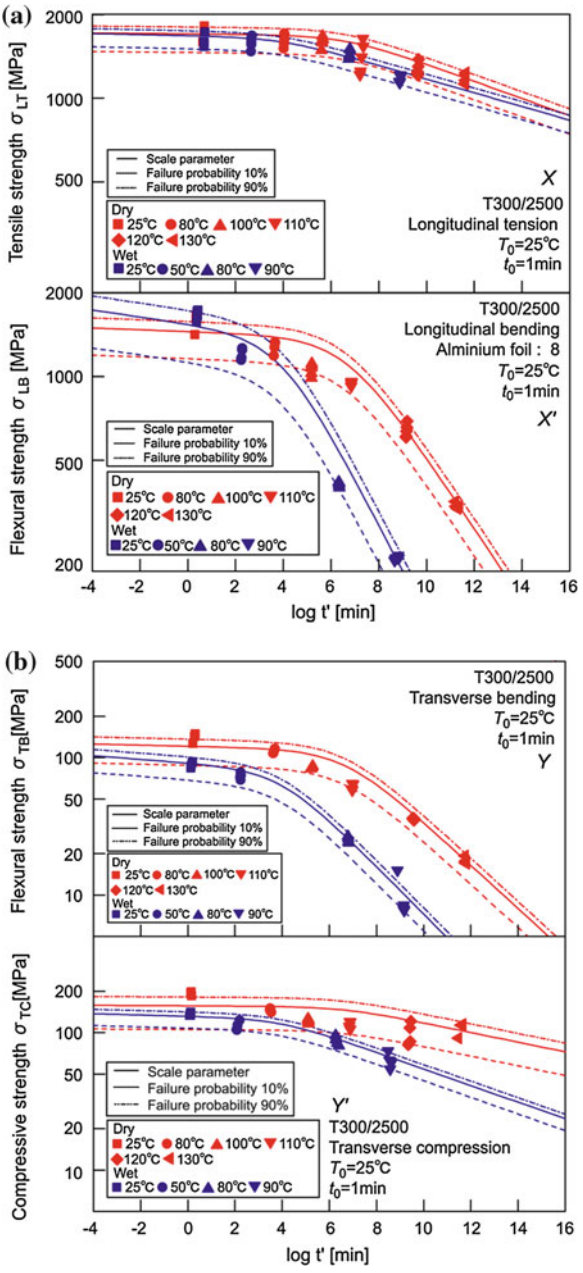

Fig. 7 Master curve of static strength for unidirectional CFRP. **a** Longitudinal direction. **b** Transverse direction

Table 2 Parameters for master curve of static strength of unidirectional CFRP

	X		*X'*		*Y*		*Y'*	
	Dry	Wet	Dry	Wet	Dry	Wet	Dry	Wet
$\sigma_{f,\,0}$ (MPa)	1,700	1,675	1,446	1,535	121	90.6	156	131
n_r	0.0762	0.0528	0.316	0.356	0.387	0.371	0.0868	0.130
α	14.7	20.7	10.0	7.18	7.04	7.97	5.68	11.4

5 Conclusion

The tensile and compressive static strengths in the longitudinal and transverse directions of unidirectional CFRP under dry and wet conditions were evaluated using our formulation method developed based on the time–temperature superposition principle, which holds for the viscoelastic behavior of matrix resin.

All four kinds of static strength strongly show time, temperature, and water absorption dependent behavior caused by the viscoelastic behavior of matrix resin.

Static strengths of these four kinds were formulated using our proposed method. These master curves of four static strengths clarify that the long-term lives for four directions decrease with water absorption.

Acknowledgments The authors thank the Office of Naval Research for supporting this work through an ONR award with Dr. Yapa Rajapakse as the ONR Program Officer. Our award, numbered as N000140611139 is for "Verification of Accelerated Testing Methodology for Long-Term Durability of CFRP Laminates for Marine Use". The authors thank Professor Richard Christensen, Stanford University as a consultant for this project.

References

1. Nakada M, Miyano Y (2012) Formulation of time- and temperature-dependent strength of unidirectional carbon fiber reinforced plastics. J Compos Mater. doi:10.1177/0021998312452025
2. Christensen RM (1982) Theory of viscoelasticity. Dover Publications Inc, NY
3. Uemura M, Yamada N (1975) Elastic constants of carbon fiber reinforced plastic materials. J Soc Mater Sci Jpn 24:156–163

Accelerated Aging Tests for Marine Energy Applications

Peter Davies

Abstract Polymer matrix fibre reinforced composites have been employed in marine applications for over 50 years, and there is considerable experience of their long term behaviour. However, the recent development of systems designed to recover ocean energy, such as tidal turbines and wave energy generators, imposes much more severe constraints on materials than traditional structures. The requirements in terms of sea water aging and fatigue resistance require specific test programmes; this presentation will describe some of these applications and the tests needed to guarantee long term behavior of composites for these structures. Some results from studies performed in this area at Ifremer over the last 5 years will be discussed.

1 Introduction

There is a growing interest in renewable energy, and the oceans could provide a significant part of energy requirements as fossil fuels become rarer and more expensive. Ocean Energy is at an early development stage, and is unlikely to contribute significantly to the European Directive requiring European Member States to generate 20 % of their energy from renewable energy sources by 2020. However, it has been suggested that by 2050 Europe could source up to 50 % of its energy needs from Marine Renewable Energy [1]. There are various ways to harvest this energy, including underwater tidal turbines, wave energy generators and offshore wind turbines [2]. Today the engineering development for all these systems is at the prototype stage, with a wide range of concepts proposed, and several now undergoing sea trials [3]. Considering tidal turbines for example, there

P. Davies (✉)
Materials and Structures group, IFREMER Centre de Bretagne, Plouzané 29280, France
e-mail: peter.davies@ifremer.fr

P. Davies and Y. D. S. Rajapakse (eds.), *Durability of Composites in a Marine Environment*, Solid Mechanics and Its Applications 208,
DOI: 10.1007/978-94-007-7417-9_8,

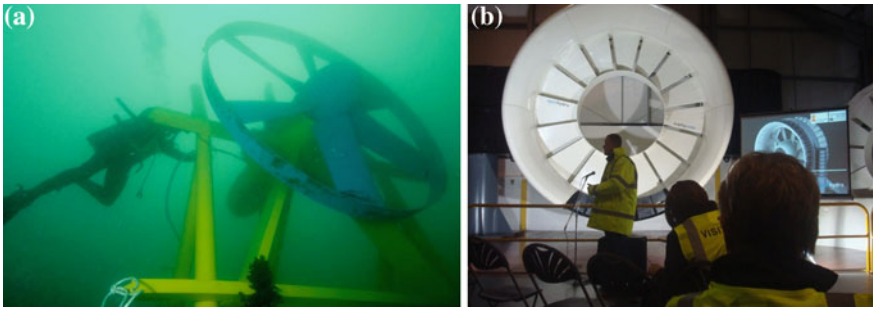

Fig. 1 Examples of tidal turbine prototypes. **a** Sabella (photo Gladu-Balao). **b** OpenHydro

Table. 1 Examples of tidal turbine project prototypes, either installed, or under construction (*)

Project	Company	Largest prototype rating (MW), turbine diameter	Blades: number, reinforcement
MCT SeaGen	Siemens	1.2 MW, 16 m	2 × 2, carbon,
DeepGen	Alstom-TGL	1 MW, 18 m	3 carbon
OpenHydro Paimpol	DCNS	2 MW, 16 m	12 glass
Atlantis AR-1000	Atlantis Resources	1 MW	3 carbon
HS1000	Andritz Hammerfest	1 MW	3 carbon
*Voith Hydro**	Voith	1 MW 13–16 m	3 composite or steel
*Sabella D10**	Sabella	1 MW 10 m	6 carbon
*CoRMaT**	Nautricity	1 MW	7 glass or carbon

are three main concepts; floating, surface-piercing, and sub-surface. The majority today are sub-surface, placed on the sea floor in shallow water (tens of meters depth). Figure 1 shows two of the designs which are closest to commercial exploitation in France. Table 1 shows a non-exhaustive list of some of the tidal turbines being developed which use composite blades.

The SeaGen tidal turbine, a surface-piercing design is installed at Strangford Lough in Northern Ireland. It is a two-blade turbine, whereas many of the competing systems have three or more blades. This choice was justified by its developer as providing significantly higher resistance to root bending, and a 20–25 % lower cost than three-blade turbines, albeit with a slightly lower efficiency [4].

TGL, a small company bought first by Rolls Royce and then in 2012 by Alstom, have a three-blade turbine design similar to a wind turbine, though the high density of sea water results in shorter blade requirements than for wind turbines to produce the same energy.

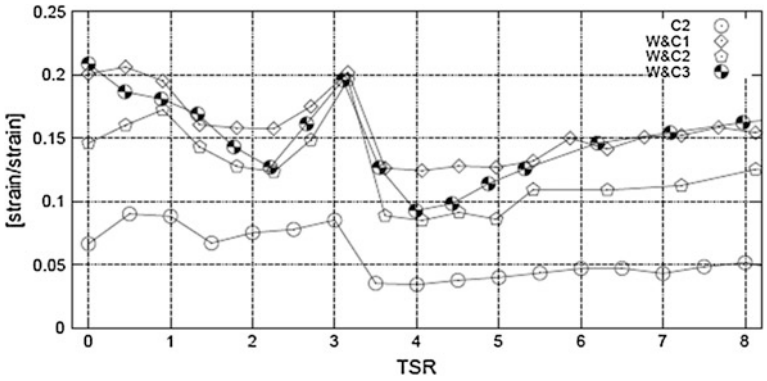

Fig. 2 Example of flume tank tidal turbine blade strain measurements [17]. *Plot* shows standard deviation divided by mean strain versus tip speed ratio, for current alone (C2) and different wave + current conditions

OpenHydro, an Irish company recently bought by DCNS, use a different design of turbine with a central hole. This enables shorter blades to be used which are supported at both ends, in contrast to most of the other designs which have blades clamped at one end.

As Table 1 indicates there are many different designs at the prototype stage, but common to all these designs is the use of composites for the turbine blades, which are up to 10 m long and made from glass and/or carbon fibre reinforced thermoset resins. Increasing the rotor size increases the extractable energy but torque and thrust on the blades increase more quickly than power extraction so blade size is limited. Composites offer significant advantages over metallic blades, in terms of reduced weight, improved corrosion resistance and formability, but design with composites is more complex and there have been some problems with blades on certain prototypes, e.g. [5]. These problems have resulted from various causes, including an under-estimation of the loading, fatigue cracks, and poor manufacturing quality. As a result durability of composites is attracting much attention, with some current projects retaining an option on steel blades.

2 Marine Experience of Composites

There is considerable experience of composites in a marine environment. Various textbooks provide overviews of materials and applications, e.g. [6–8]. Most of the materials employed are based on low cost glass reinforced polyester, which has proved an excellent choice for boat hulls and superstructures. These are usually quite thick (from several millimeters up to 100 mm in some areas of mine-hunter vessels [6]) and coated with gel-coats, so that wet aging effects are often secondary. The influence of water on composites has been widely studied and again

various documents provide an overview of current knowledge (e.g. [9–13]). The particular case of stress corrosion of glass reinforced composites under a combination of tensile loads and wet environments was identified by early work of Charles [14], and subsequently studied by various authors [15, 16].

3 Specific Loads on Ocean Energy Devices

The main difference between the loads on marine energy devices and those on other marine structures, such as pleasure boats or naval vessels is the importance of fatigue loading. Traditional marine structures are rarely designed to resist fatigue, whereas a tidal turbine blade rotates continually except when the tide direction changes. The loads are determined by three main factors:

- Tidal currents, which induce the rotation which generates energy,
- Rotation, with a pressure variation due to depth changes of up to 20 m,
- Waves, which affect underwater structures in shallow depths.

The latter is the most difficult to quantify, as interactions between waves and currents are difficult to evaluate and extreme values of one or other may not correspond to extreme loading of the structure. Some flume tank results clearly show how waves and currents can interact to produce large strain variations compared to currents alone, Fig. 2, [17]. These strain variations must be considered in design.

Nevertheless, for applications where loads are well-known fatigue of composites has been widely studied, in particular for wind turbine blades, and life prediction methods exist (e.g. [18–20]). The wind turbine industry has also developed standard load spectra, which can be applied during design to evaluate new turbine blade concepts. The presence of cyclic loads on marine energy structures, albeit significantly larger than those on wind blades due to the higher density of water than air, is not sufficient alone to justify the development of specific test programmes. There are however, two aspects which have not been studied in detail, and which do require further study:

1. the influence of wet aging in seawater on fatigue performance, and
2. the effect of coupling between mechanical loads and seawater.

There have been a small number of previous studies in which cyclic loading was performed on wet specimens. For example, Selvarathinam and Weitsman showed lower fatigue lives for water saturated carbon/epoxy specimens than for the same materials in air [21], and proposed a shear lag model to explain the differences [22]. Vauthier et al. [23] used three point bending fatigue to examine interactions between fatigue behavior and water in unidirectional glass/epoxy in a study for automotive applications. They noted that interactions between the environment and the crack tip resulted in significant increases in crack propagation rate, more marked as temperature was increased (up to 70 °C). They attributed this

to local plasticization of the epoxy matrix and weakening of bare portions of exposed glass fibres. They noted a significant difference between the effects of moisture vapour and immersion, due to enhanced hydrolysis and leaching during the latter.

Pauchard et al. [24] extended this work and presented results from static fatigue aging tests. They proposed a stress corrosion model to explain the delayed failure mechanism based on subcritical propagation from flaws on the surface of glass fibres in water.

Kotsikos et al. [25] studied 10 mm thick woven glass reinforced isophthalic polyester pecimens with dimensions conditioned in artificial seawater at 35 °C for periods up to 6 months. They noted large stiffness drops during cycling of exposed samples and used acoustic emission to follow continuous damage accumulation. More recently Poodts et al. [26] studied the flexural behavior of 4 mm thick infused glass reinforced polyester and vinylester during immersion in artificial seawater for up to 22 weeks at 15 °C. In contrast to results from other studies they noted only a small drop in quasi-static properties (<10 %) and no loss in fatigue properties.

There has been considerable recent interest in composites for civil engineering applications, and MacBagonluri et al. studied the influence of both wet aging cycles and wet testing on static and fatigue performance of a glass/vinylester pultruded composite [27]. They found a correlation between static strength and fatigue performance which was similar to that proposed earlier by Mandell [28]. This suggests that the slope of S–N plots can be normalized by ultimate tensile strength (UTS) and is around 10%UTS/decade.

Coupling between mechanical loading and water is a complex subject, which is discussed in detail in another chapter of this book by Jacquemin and Freour. The interaction between static loads and water has been studied by several authors since early work by Neumann and Marom [29], and Weitsman gives a good overview [12], but few studies have examined full coupling between cyclic loads and water. An exception is the work by Perreux and colleagues, and in particular the PhD work of Suri [30], Perreux and Suri [31], who looked at both the influence of damage on diffusion coefficients and the influence of water on damage development.

In conclusion, globally there are few data available in the published literature describing fatigue tests in seawater and very few studies in which the coupled effects of sea water diffusion and cyclic loading have been considered. For this reason a test programme was initiated at IFREMER in 2007.

4 Test Procedures

In order to ensure that the materials chosen for ocean energy applications are suitable for the loads and environments which they will encounter in service it is necessary to develop appropriate test procedures.

First, given that the lifetime required is at least 20 years these procedures will by necessity involve some element of acceleration and extrapolation. In order to validate accelerated tests it is crucial to understand the failure mechanisms, to avoid introducing parasite mechanisms. There are at least three ways of accelerating tests; increasing test temperature is the most common, but raising stress levels or reducing sample thickness can also enable a particular damaged state to be reached more quickly.

Second, the material aspects must also be examined in a framework which takes account of the structure in which they are used. This is particularly important with composites, whose micro-structure and mechanical properties depend on the manufacturing route. One approach is to include the aging procedure in a test pyramid similar to those employed for composite aeronautical structures, Fig. 3. At each level both tests and modelling are performed.

5 Examples of Test Results

Although seawater aging has been a research theme at IFREMER for over 20 years [32, 33], the first tests performed specifically to examine the effects of combined cyclic loading and seawater diffusion on composites were performed from 2007–2010, in a collaboration with glass fibre and resin suppliers. This required the development of test facilities specifically designed to provide both aging in sea water under controlled temperature conditions, Fig. 4a, and cyclic loading and a controlled sea water environment, Figs. 4b and 4c.

Figure 5 shows an example of results from cyclic four point flexure tests performed both in air and in sea water and the difference between the two is quite small, though lifetimes at lower stresses are a little lower for tests in seawater. This is perhaps not surprising, as the time the samples are in the water is quite short, a few days at most, and the diffusion of water into these materials at room temperature is quite slow.

However, when specimens which have been immersed in water for longer periods and at higher temperatures are cycled significant effects are noted, and this is clearly important for applications such as long term immersion of a tidal turbine. A detailed presentation of results for the glass reinforced composites can be found

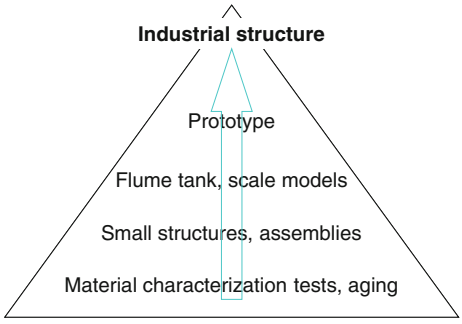

Fig. 3 Test pyramid for tidal turbine blade material qualification

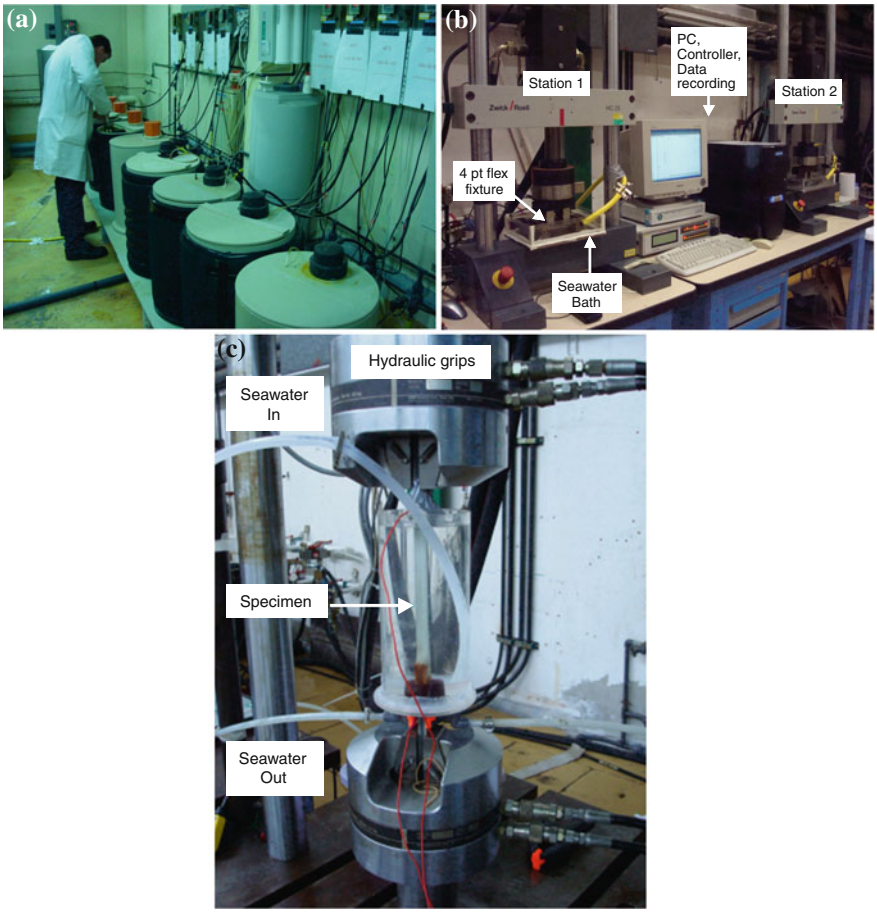

Fig. 4 Test facilities. **a** Sea water aging tanks. **b** Flexural test in seawater. **c** Tensile test in seawater

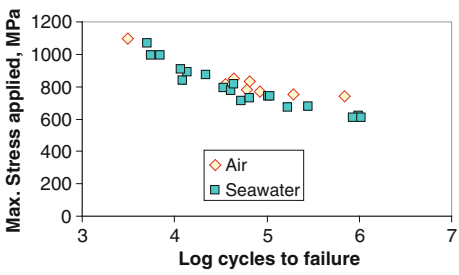

Fig. 5 Results from testing glass reinforced epoxy composites in air and in sea water

elsewhere [34–37], but two examples are shown in Fig. 6. Figure 6a shows, for an infused quasi-unidirectional glass reinforced epoxy composite which is currently used extensively for wind turbine blades, that in the wet state (fully saturated) it cannot be assumed that fatigue properties are insensitive to water. Indeed, in the higher applied stress range the aged material has significantly lower fatigue life. However, by modifying the matrix resin this effect of aging can be almost completely removed [36].

Figure 6b shows that the choice of fibre sizing also affects the fatigue behavior. Samples of the same glass fibre reinforced epoxy resin composite manufactured using the same infusion process but with different fibre treatments were tested. The optimal fibre treatment for infusion resulted in the longest fatigue lifetimes. Alternative fibre treatments, intended for other fabrication processes, gave lower fatigue lives when infusion manufacturing was employed. These results clearly show the importance of both resin selection and fibre sizing in order to ensure long term durability.

Following this study further internal research work extended the scope of the project to include carbon fibre reinforced composites. Figure 7 shows two examples of results, which again indicate that commonly available prepreg materials are not insensitive to seawater aging. Figure 7a shows an example in which unidirectional samples were cycled in four point flexure in seawater both before and after aging for 9 months at 60 °C. The support span length/thickness (L/h) ratio was around 16, which results in a mixed stress state (in-plane tension

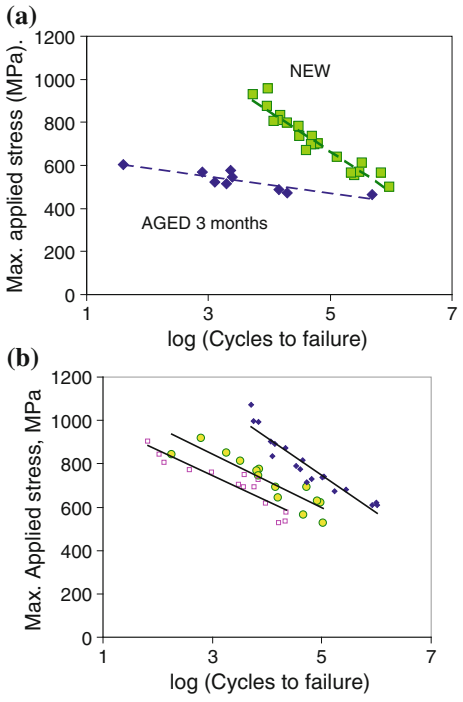

Fig. 6 Influence of **a** resin aging, and **b** fibre sizing on fatigue performance of glass/epoxy composites in seawater

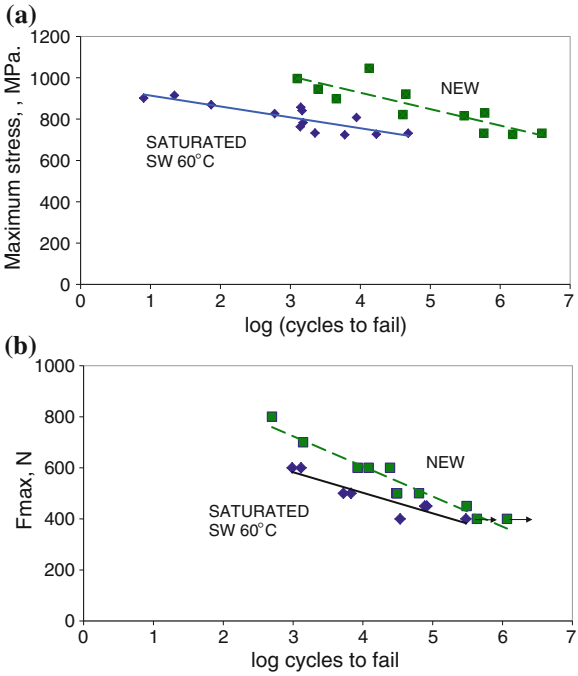

Fig. 7 Influence of sea water aging on carbon/epoxy composites subjected to four point flexure loading. **a** Unidirectional. **b** Quasi-isotropic

and compression and out-of plane shear). There is an effect of aging on results, and aged samples all failed in interlaminar shear, not due to in-plane loads. It should be noted however, that the effect of aging is significantly lower than that seen for the glass/epoxy systems. The second example is for a quasi-isotropic lay-up tested with an L/d ratio of around 24, Fig. 7b.

Once again there is an effect of aging with a shift of about a decade at higher loads. A study currently underway is looking in detail at the particular case of seawater interaction with delaminations under cyclic loads.

These results clearly emphasize the importance of a detailed understanding of the durability of composites in order to both select and design with composites in ocean energy structures. Given the prototype nature of many of the current applications there are few guidelines available to the designer. However, this is evolving, there are offshore guidelines for composites [38] and some documents specifically devoted to ocean energy are appearing which should help to establish the safety factors and certification requirements for these structures e.g. [39].

6 Accelerated Testing of Adhesives

While there is much current interest in the long term properties of fibre reinforced composites, structures such as tidal turbines are not produced in a single shot process. The most popular manufacturing method, at least for the prototypes being

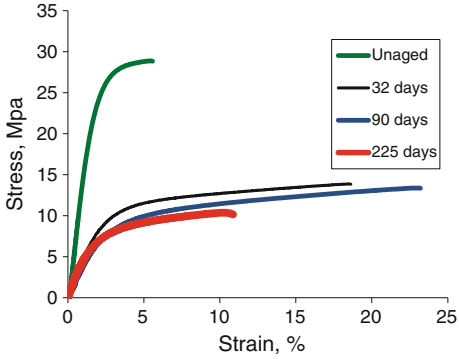

Fig. 8 Example of the change in tensile properties of a marine adhesive after immersion

tested today, involves vacuum compaction and oven curing of several constituent parts followed by an assembly operation involving adhesive bonding. The weak link in such a structure may then be the adhesive, whose long term behavior in a marine environment must be investigated. Adhesives may also be involved in the link between the blades and the rotating axis.

Various authors have examined common epoxy marine adhesives after wet aging e.g. [40, 41] and it has been shown that the properties of many of these formulations degrade after prolonged immersion. Figure 8 shows one example, for a commercial epoxy-based epoxy adhesive. After short periods of immersion at 20 °C a drop in strength and an increase in ductility are noted, corresponding to reversible plasticization. After longer periods the ductility also starts to decrease.

In that study [40] the influence of weak coupling was examined. Weak coupling takes account of the influence on mechanical properties of the diffusion of water into the polymer. This is in contrast to the more complex case of strong coupling, for which not only the influence of water on mechanical properties is considered but also the reverse effect of mechanical loads on diffusion behavior.

7 Other Ocean Energy Applications of Polymers and Composites

This brief overview has concentrated on tidal turbine blades, as these are a critical element where composite behaviour is the key to long term device reliability. However, composites are being considered for many other components of ocean energy structures, from shrouds and cowlings of turbines to buoys and floating devices. In many of these structures repeated wave impact is a major concern, and some work has been performed to examine this [42]. Impact response depends on both material behaviour and structural geometry so it is difficult to predict without extensive testing.

Fibre reinforced composites are the main subject here, but it is important to note that they are not the only polymeric materials used in these devices. Other

materials include elastomers, for certain designs of wave energy converters [43], and polymer fibres for mooring lines [44]. In both cases characterization under cyclic loads and during seawater aging are essential to ensure long term durability. Studies are currently underway at IFREMER on these and other materials.

8 Conclusions

Composite materials will be an integral part of many ocean energy devices, particularly tidal turbine blades. This is a new application for fibre reinforced composites. It clearly has some similarities to more established applications such as marine structures and wind turbines, but it also brings particular challenges such as the need to understand coupling between cyclic loads and sea water. The fatigue and environmental resistance of these materials must be thoroughly understood in order to design these devices to be sufficiently robust to guarantee their long term integrity under extreme conditions. The installation of tidal turbines in regions with very limited access means that low maintenance requirements will be critical to ensure economic success. A second key issue is the need for processes allowing faster blade production. As tidal turbine farms develop hundreds of blades will be required for each project, and this is not possible with oven-cured prepreg manufacturing. Alternative methods such as RTM (resin transfer moulding) in closed metallic moulds will be required, and the influence of these processes on the composite microstructure and properties will also need to be thoroughly studied and understood.

References

1. European Science Foundation (2010) Marine Board, Vision Document, Oct 2010
2. Bahaj AS (2011) Generating electricity from the oceans. Ren Sust Energy Reviews 15:3399–3416
3. Renewables UK (2013) Wave and tidal energy in the UK, Feb
4. Fraenkel P (2010).In: Proceedings—Fluid Machinery Group—Ocean Power Fluid Machinery Seminar, Institution of Mechanical Engineers—19th Oct 2010, London
5. Renewable Energy Focus (2010) OpenHydro tidal turbine recovered—blades missing, Dec 2010http://www.renewableenergyfocus.com
6. Smith CS (1990) Design of marine structures in composite materials. Elsevier Science, Publishers, London
7. Davies P, Lemoine L, (1992) Nautical applications of composite materials. Proceedings 3rd IFREMER Conference, Paris, France
8. Shenoi RA, Wellicome JF (eds) (2008) Composites in maritime structures. Cambridge University Press, Cambridge
9. Springer GS (ed) (1981) Environmental effects on composite materials, Technomic
10. Martin R (ed) (2008) Aging of Composites. Woodhead Publishing, Cambridge
11. Weitsman YJ (1991) Moisture in composites. In: Reifsnider KL (ed) Fatigue of composites. Elsevier, Netherland, pp 385–429

12. Weitsman YJ (2012) Fluid effects in polymers and polymeric composites. Springer, New York
13. Davies P, Mazeas F, Casari P et al (2001) Sea water aging of glass reinforced composites: shear behaviour and damage modelling. J Compos Mater 35(15):1343–1372
14. Charles RJ (1958) Static fatigue of glass I. J Appl Physics 29(11):1549–1560
15. Price JN, Hull D (1983) Propagation of stress corrosion cracks in aligned glass fibre composite materials. J Mat Sci 18:2798–2810
16. Pritchard G, Speake SD (1988) Effects of temperature on stress-rupture times in glass/polyester laminates. Composites 19(1):29–35
17. Gaurier B, Davies P, Deuff A, Germain G (2013) Flume tank characterization of marine current turbine blade behaviour under wave and current loading. Renew Energy 59:1–12
18. Harris B (ed) (2003) Fatigue in composites. Woodhead Publishers, Cambridge
19. Echtermeyer AT, Kensche C, Bach P, Poppen M, Lilholt H, Andersen SI et al (1996) Method to predict fatigue lifetimes of GRP wind turbine blades and comparison with experiments. In: Proceedings of European union wind energy conference. Göteborg, Sweden, 20–24 May 1996
20. Nijssen RPL, vanWingerde AM, vanDelft DRV (2007) Wind turbine rotor blade materials: estimating service lives. SAMPE J 43(2):7–15
21. Selvarathinam AS, Weitsman YJ (1998) Transverse cracking and delamination in cross-ply Gr/Ep composites under dry, saturated and immersed fatigue. Int J Fract 91(2):103–116
22. Selvarathinam AS, Weitsman YJ (1999) A shear-lag analysis of transverse cracking and delamination in cross-ply carbon-fibre/epoxy composites under dry, saturated and immersed fatigue conditions. Comp Sci and Technol 59(14):2115–2123
23. Vauthier E, Abry JC, Bailliez T, Chateauminois A (1998) Interactions between hygrothermal ageing and fatigue damage in unidirectional glass/epoxy composites. Compos Sci Technol 58:687–692
24. Pauchard V, Chateauminois A, Grosjean F, Odru P (2002) In situ analysis of delayed fibre failure within water-aged GFRP under static fatigue conditions. Int J Fatigue 24:447–454
25. Kotsikos G, Evans J, Gibson A, Hale J (2000) Environmentally enhanced fatigue damage in glass fibre reinforced composites characterised by acoustic emission. Comp. Part A 31(9):969–977
26. Poodts E, Minak G, Zucchelli A (2013) Impact of seawater on the quasi static and fatigue flexural properties of GFRP. Compos Struct 97:222–230
27. McBagonluri F, Garcia K, Hayes M, Verghese KNE, Lesko JJ (2000) Characterization of fatigue and combined environment on durability performance of glass/vinyl ester composite for infrastructure applications. Int J Fatigue 22:53–64
28. Mandell JF (1978) Fatigue behavior of fiber-resin composites. In: Pritchard G (ed) Developments in reinforced plastics 2. Applied Sciences Publisher, London
29. Neumann S, Marom G (1987) Prediction of moisture diffusion parameters in composite materials under stress. J Comp Mats 21(1):68–80
30. Suri C (1995) Study of the coupling of absorption and damage phenomena in a glass-epoxy composite, PhD thesis (in French). University of Franche Comté
31. Perreux D, Suri C (1997) A study of the coupling between the phenomena of water absorption and damage in glass/epoxy composite pipes. Comp Sci Tech 57(9–10):1403–1413
32. Davies P, Choqueuse D (2008) Ageing of composites in marine vessels, chapter 12 in Ref. [10]
33. Choqueuse D, Davies P (2008) Ageing of composites in underwater applications, chapter 18 in Ref. [10]
34. Boisseau A (2011) Long term durability of composites for ocean energy conversion systems, PhD thesis. Available at: http://archimer.ifremer.fr/doc/00031/14247/
35. Boisseau A, Davies P, Thiebaud F (2012) Sea water ageing of composites for ocean energy conversion systems: influence of glass fibre type on static behaviour. Appl Compos Mater 19:459–473

36. Boisseau A, Davies P, Thiebaud F et al (2013) Fatigue behavior, of glass fibre reinforced composites for ocean energy conversion systems. Appl Compos Mater 20(2):145–155
37. Davies P, Germain G, Gaurier B, Boisseau A, Perreux D (2013) Evaluation of the durability of composite tidal turbine blades. Roy Soc Philos Trans A 371
38. DNV, Offshore standard on composite components, DNV-OS-C501, Oct 2010
39. Lloyd G (2012) Guideline for the certification of ocean energy converters, part 1. Ocean Current turbines
40. Bordes M, Davies P, Cognard J-Y, Sohier L, Sauvant-Moynot V, Galy J (2009) Prediction of long term strength of adhesively bonded steel/epoxy joints in sea water. Int J Adhes Adhes 29(6):595–608
41. Leger R, Roy A, Grandidier JC (2013) A study of the impact of humid aging on the strength of industrial adhesive joints. Int J Adhes and Adhes 44:66–77
42. Blommaert C, van Paepegem et al. (2010) Large scale slamming tests on composite buoys for wave energy applications. In: Proceedings of 17th international conference on composite materials, (ICCM17). Edinburgh, 2010
43. Jean P, Wattez A, Ardoise G, Melis C, van Kessel R, Fourmon A, Barrabino E, Heemskerk J, Queau JP (2012) Standing wave tube electro active polymer wave energy converter. In: Proceedings of SPIE smart structures and materials conference, San Diego, Mar 2012
44. Weller S, Davies P, Thies P, Johanning L (2012) Durability of synthetic mooring lines for ocean energy devices. In: Proceedings of 4th international conference on ocean energy (ICOE), Dublin, Oct 2012

Integrating Durability in Marine Composite Certification

Andreas T. Echtermeyer

Abstract A brief overview is given on how design standards are written. Static strength, fatigue, stress rupture, damage tolerance and the effect of the environment are addressed. Examples are given to show how durability is or can be addressed in design standards. Extensive testing is required today to certify long-term properties. Suggestions for research topics to reduce the test effort are discussed.

1 Introduction

Certification shall demonstrate that a component is safe and functional. This needs to be ensured up to the end of the components design life, typically 25–40 years. Long-term performance is closely related to durability. Predicting long-term properties is a challenge for any material. Much work has been done for composites on this subject, but only a few marine composite standards address long-term properties directly.

Certification is done against a standard or sometimes a purchase specification. Integrating durability issues into certification is therefore directly related to addressing long-term properties and accidental conditions in the standards. The following sections will show how integration of durability can be done.

A. T. Echtermeyer (✉)
Norwegian University of Science and Technology (NTNU),
Richard Birkelands vei 2B, 7491 Trondheim, Norway
e-mail: Andreas.Echtermeyer@ntnu.no

A. T. Echtermeyer
Det Norske Veritas, Høvik, Norway

P. Davies and Y. D. S. Rajapakse (eds.), *Durability of Composites in a Marine Environment*, Solid Mechanics and Its Applications 208,
DOI: 10.1007/978-94-007-7417-9_9,

2 Design Standards

The early design standards were prescriptive. For example, a pressure vessel for 100 bar shall be made of a steel of a certain grade with a given wall thickness. These standards were very simple to use, but did not give any room for changes and innovation. They were often based on experience and the scientific reason for the requirements was unclear.

Modern standards are "performance based". They set certain requirements that need to be met, without giving specific prescribed solutions. Many of the latest standards are also based on structural reliability, where an overall annual probability of failure shall be achieved [1, 2]. Once this probability is established, safety factors can be calculated for all design/failure criteria. An acceptable level of failure obtained from similar applications can be used to obtain the annual probabilities of failure.

The performance based standards set rules that need to be followed. Any design fulfilling these rules is acceptable. Finding out what needs to be regulated and setting these rules properly, requires much knowledge about structural engineering and materials. DNV has developed the concept of "qualification of new technology" for cases where no standards exist [3]. This can be seen as a systematic approach to develop a certification procedure for a specific application that is equivalent to a design standard. It is basically a framework to write a design standard. Figure 1 shows in a simple way, how this can be done.

The "Qualification Basis" defines what the component should do and what it is exposed to. This would include the level of safety, functional requirements, loads and design phases (installation, operation, retrieval). From a durability point of view the qualification basis needs to include at least lifetime, long-term loads, environmental exposures and accidental loads.

Fig. 1 Principle of qualification of technology

In most cases, it is relatively easy to define the functional maximum loads, e.g. loads from a 100-year wave or maximum pressure. However, obtaining good descriptions of long-term load sequences, environments and accidental loads is difficult. What kind of waves does a ship experience during its lifetime? What kind of oil composition runs through a pipe of a so far unknown well? The uncertainties in the design input remain part of any further evaluation. A sophisticated lifetime analysis is not of much use if the load sequence is based on unknown assumptions.

Uncertainties in the loads are even more of a challenge for composites than for metals, because anisotropic composite components can be strongly affected by minor loads transverse to the main fiber direction or through thickness loadings. These secondary loads are typically ignored for metal designs. An engineer responsible for the global load calculations, who is used to designing metal structures, does not calculate these secondary loads, even less of their long-term distributions, because if the isotropic metal structure can tolerate the major loads, it can tolerate the minor ones.

Very conservative assumptions are often made for long-term loads and environments due to the lack of more detailed knowledge. It is often assumed that a component operates at maximum temperature during its entire lifetime. This assumption is usually conservative and works well for metal designs when the possible use temperature of the metal far exceeds the operational temperature. For a typical epoxy based marine composite material it can make a big difference whether it is exposed to 150 °C for a just a few hours or many years. The first condition may be acceptable, while the laminate would severely degrade if exposed to the high temperature and water all the time.

Failure modes and mechanisms need to be identified. The principle failure mechanisms for composites are:

- fiber failure,
- matrix cracking,
- delamination.

Other failure mechanisms, such as buckling, wear, fiber matrix debonding, and impact damage also need to be considered, but they are failures combining the principle failure mechanisms stated above.

A design for any component would have to identify which failure mechanisms are critical for its use. The DNV offshore standard DNV-OS-C501 “Composite Components” [4] gives a checklist for the failure modes and mechanisms that shall be considered. Fiber failure is always a critical failure mechanism, because the component breaks apart when the fibers are broken. A pressure vessel with an internal metal or thermoplastic liner can tolerate matrix cracks without any problems, because the pressure vessel remains tight as long as the inner liner stays intact. A pipe without an inner liner will start to leak (seep) once a sufficient number of matrix cracks has formed, allowing the fluid to penetrate the laminate. In this case, matrix cracks are critical.

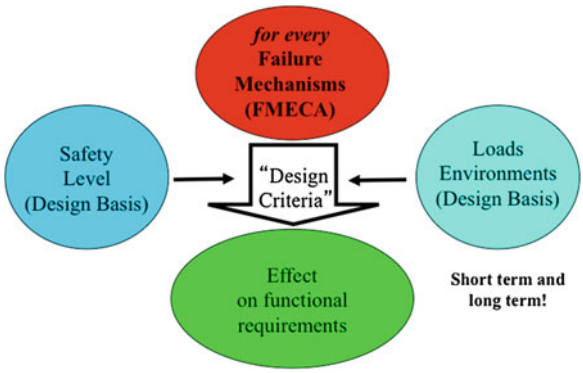

Fig. 2 Analytical approach to qualification

Once the critical failure mechanisms are identified, the component is often redesigned to improve the concept before a full qualification is done. This tendency to change the design during the project complicates a certification process, but it will not be addressed here.

In a next step, it has to be shown that none of the critical failure mechanisms will happen during the design life. This is the selection of the qualification process. The process can be done by analysis or testing. Analysis is the preferred method, because it is faster and cheaper than testing. The approach is shown schematically in Fig. 2. The analysis needs to be reliable. If the uncertainties in the analysis are too high, testing is required. A reliable analysis requires that the design criteria are well established, the stress analysis can be considered accurate (no high stress concentrations etc.) and the material properties are well known. The material properties need to be known for the first day of using the design up to the last day, i.e. after degradation during the entire lifetime.

If testing is required, it is important that tests are chosen that give insight into the basic question whether a certain failure mechanism will happen during the design life. A very important aspect is the phrase "during the design life"; it includes explicitly durability. It is essential from a certification point of view that the long-term aspects are included in the testing, because it is the only way to show that the component is still fit for purpose on the last day of the design life. Finding the best approach for answering the long-term question is usually the biggest challenge in the certification process and it will be discussed for some examples in the following sections.

Once the qualification process is defined, analysis and testing can start. Obtaining an answer for long-term performance requires frequently long term testing, up to 10,000 h, more than one year. Such tests are costly and time consuming.

The final step of the qualification process is the evaluation of the analysis and test results. If the results show that the component is strong enough with a sufficient margin of safety for all critical failure mechanisms it can be considered as fit for service.

3 Static Strength

Static strength is the condition that is typically checked first in a qualification. Fiber failure of composites is a brittle failure mechanism; there is no reserve capacity. For this reason safety factors against fiber failure are usually higher than for metals against yield. The safety factors for composite risers can be seen as an example [5]. Table 1 shows one possible set of safety factors for safety class high. The partial material resistance factor is 10 % higher for a brittle failure mode than for ductile failure. The resistance factor needs to be combined with load effect factors. The load effect factors are dependent on the uncertainty in the loads. Environmental loads, such as forces from wind and waves are typically less well defined than functional loads from pressure or self-weight. Note that other factors e.g. system factors and model factors should be applied in a design. The material resistance factors are also dependent on the coefficient of variation COV (the standard deviation of test results divided by the mean value) of the material. Only the case for COV <10 % is given here. More details can be found in the standards [4, 5].

The factors shall be applied to the characteristic strength defined as the 2.5 % quantile in distribution of arbitrary strength with 95 % confidence [4, 6]. For high safety class the DNV standards require that the strength needs to be measured on materials made by the same production process as the real application. The tensile strength of a composite ply in fiber direction depends on the strength of the fibers and the fiber volume fraction. The manufacturing process can influence both. This makes it difficult to use standard strength values provided by the manufactures of the fibers. Compressive strength is even more affected by the production process, because it depends on fiber strength, fiber alignment and matrix properties. Testing actual materials ensures that realistic strengths are used for the component in the design calculations.

The strength of a laminate can be calculated from the ply properties using laminate theory (e.g. [7–9]). A generic design criterion for static strength in the LRFD Format (Load and Resistance Factor Design) is shown in Fig. 3. Detailed failure criteria for each failure mechanisms are given in DNV-OS-C501 [4]. It is important that safety factors and ways to combine different loads are incorporated into the failure criteria in a way that the overall target reliability can be properly calculated.

The available material data are typically reported for room temperature in air. Properties will change with different temperatures and environments. What is the strength of a pipe with hot oil in the inside and cold water on the outside? Some

Table 1 Partial safety factors for safety class high for materials with a coefficient of variation less than 10 %

	Functional load	Environmental load	Resistance factor
Brittle failure	1.1	1.3	1.47
Ductile failure	1.1	1.3	1.34

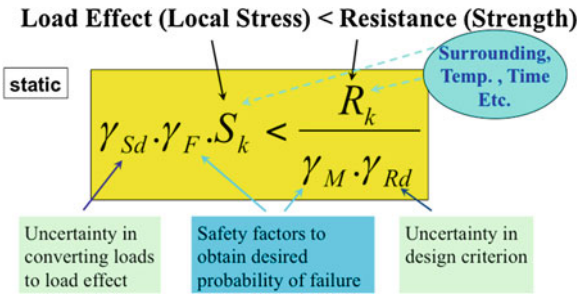

Fig. 3 Design criterion for static strength incorporating safety factors, load and material values

design standards give very conservative strength values and "knock down factor" for service in water and high or low temperature etc. Standard values and general knock down factors are problematic, because they do not give credit for materials with good properties. However, some of these standards, such as BS4994 [10] have been used very successfully over many years. The alternative today is more testing under the actual operating conditions. Theoretical work giving a quantitative link between dry room temperature data and actual service conditions could reduce the testing effort considerably. Reduced testing would require a fundamental and quantitative understanding of the changes in the material with temperature and exposure to water and chemicals.

Much attention is usually paid to the fiber-dominated strength of a composite; this is the most dramatic failure. However, matrix cracking and delamination may be just as important. A pressure vessel or pipe without internal liner will leak (or seep) if extensive matrix cracking and delamination is present. A ships hull may soften and eventually leak, although some matrix cracking would not be critical. In a superstructure, matrix cracks would just be a cosmetic issue.

An example are couplers based on the trap lock principle. They are used for tubes exposed to high axial loads, such as risers [11]. The axial fibers of the tube are put over a "bump" in the metal connector. The fibers are held in place by hoop fibers behind the bump. In addition everything is held in place by the epoxy matrix. Figure 4 shows an experimental small scale coupler tested in tension. It was made to study the behavior of the joint in simple arrangement compared to a larger riser joint. The observed failure mechanism was delamination.

If matrix cracks and delamination are critical, properties related to them are typically not easily available. Onset of matrix cracking depends on the matrix properties, fibers and their sizing as well as the production process. Neither the fiber producer nor the resin producer can provide these data, because they are not responsible for each other's products. Matrix cracking and delamination are also influenced by production and design related aspects, e.g. the stacking sequence of the laminate and the quality of the edges. Even more important, matrix properties are affected by temperature and environment. Testing is needed to obtain the proper material properties for the actual production conditions and the environment during operation. Currently, credit for a good choice of matrix and fibers and making good laminates can only be given by testing of the actual product.

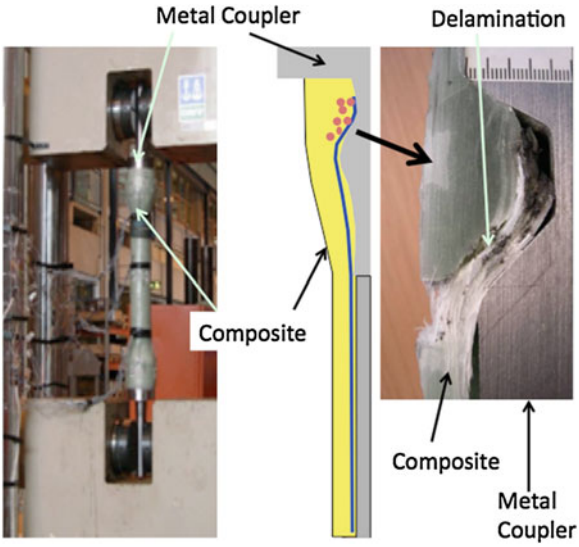

Fig. 4 Axial testing of an experimental composite tube with a simple metal coupler based on the trap lock principle. The *left* phote shows the test setup. The *middle* phote is a schematic of half the tube, showing the trap lock design. The *right* phote shows the failure mechanism delamination

4 Cyclic Fatigue

Resistance to cyclic fatigue is critical for all dynamically loaded structures. The DNV offshore standard for composite components DNV-OS-C501 [4] requires a full fatigue analysis using SN curves at different R-ratios and a Miner sum analysis. Similar to the static data, long term data shall also be measured for the actual product. An example of predicted fatigue life for typical materials used on wind turbine blades and measured life is shown in Fig. 5 [12]. Good agreement between predictions and measurements can be seen.

The challenge for many projects has been the lack of good fatigue data. Just like for static data, the DNV standards require that characteristic values are obtained for long term data with 2.5 % tolerance and 95 % confidence. Figure 6 shows how the characteristic fatigue SN curves are obtained for design. The mean SN curve is calculated as a curve fit from the measured data.

$$log(N_{mean}) = log(N_0) - \alpha log(\sigma)$$

where N_{mean} are the number of cyclces to failure, σ is the stress amplitude and N_0 and α are fit parameters. The characteristic design curve is shifted towards a lower number of cycles by the equation:

$$log(N_{char}) = log(N_0) - \alpha log(\sigma) - \chi\rho$$

The shift is given by the factor χ as shown in Table 2. χ is related to the number of measurements and the standard deviation ρ of the measured data. Depending on whether results are used within the measurement range or if they need to be extrapolated, different shift factors need to be used. This is approach is a simplified

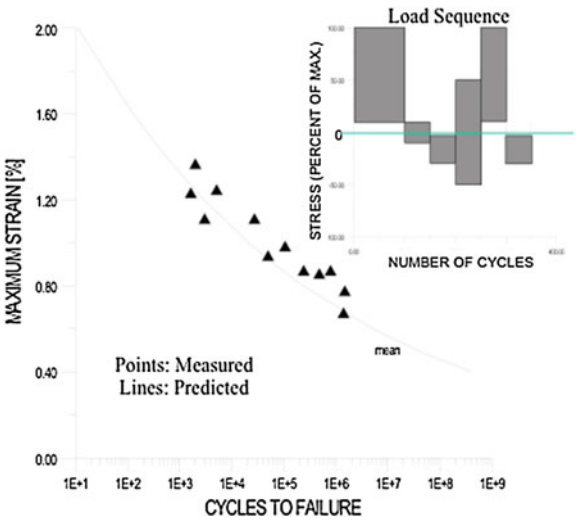

Fig. 5 Number of cycles to failure of a 0/90 glass vinylester laminate exposed to a load sequence with variable amplitudes. Experimental and prediced data are shown. Testing was done in load control. The maximum strain is the initial strain at the beginning of the test, from [12]

way to account for the increasing uncertainty of the slope of the SN curve with extrapolation of the data [13]. For this reason range of the extrapolation is also limited by the standard. It can be seen that testing many samples reduces the uncertainty resulting in a characteristic curve closer to the mean data curve. More testing tends to give a more optimal characterization of long-term performance.

For E-glass fibers and well-known carbon fibers, well-characterized SN curves can be found. In that case only a few tests are required to confirm that the actual material has the same properties as the reference material. DNV-OS-C501 states that nine fatigue tests have to be done if it is expected that the actually used material is represented by a known set of data [4]. The criteria for similarity are defined in the standard. Simplified, data points should show the same slope and standard deviation as the reference data. If the testing shows that the above

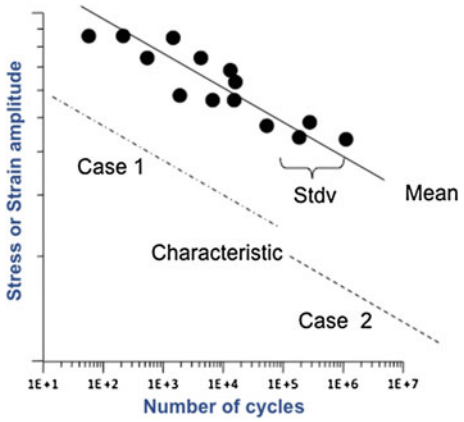

Fig. 6 Obtaining characteristic SN curves for design according to DNV-OS-C501 [4]. The mean curve is a best fit of the experimental data. The characteristic curve is shifted according to Table 2

Table 2 Shift factors χ for obtaining characteristic SN curves

	χ	
Number of tests	Case 1	Case 2
10	3.9	4.7
15	3.4	4.0
20	3.1	3.7
50	2.6	3.0
100	2.4	2.6
Infinite	2.0	2.0

requirements are fulfilled, the data are considered similar to the representative material and the characteristic curve of the reference material can be used for design. If the data are not similar an independent test series needs to be carried out.

The long-term data need to be known for all service conditions. This means fatigue performance needs to be characterized for wet and dry conditions, low and high temperature, possibly also exposure to chemicals. The change of the SN curve with temperature, under exposure to seawater and chemicals etc. is usually not known. Many SN curves need to be measured for marine or offshore applications to ensure durability under all these conditions.

In addition to obtaining the material data some large scale testing needs to be carried out to confirm that calculated fatigue properties are representative for the real components. Overall, an extensive test program is needed to establish SN curves and to demonstrate long-term performance [11, 14].

Few data exist for the development of matrix cracks or delamination during fatigue. On the certification side growth of matrix cracks or delamination due to cyclic loads is not explicitly addressed in many standards. Pipe standards consider mainly static loading and limit fatigue cycles to about one per day, resulting in 7,300 cycles in a lifetime of twenty years [15]. Within this small number of cycles not much crack growth is expected, so the standards are satisfactory. However, if the pipes are used differently, fatigue should be considered. Pressure vessel standards require some limited full scale fatigue testing [16–19]. Ship design is typically based on extreme loads only [20].

If matrix dominated properties are important, e.g. for the joint shown in Fig. 4, fatigue data for this failure mechanism need to be obtained. Fatigue data for matrix dominated interlaminar shear strength of a glass epoxy laminate in oil at 120 °C is not easy to find. Some measurements were done for composites with epoxy [21] and vinylester [22] matrices in air and in water. Even if data can be found, can they be applied to a slightly different material system, produced slightly differently? Figure 7 shows another example where a carbon fiber rod is tested in fatigue in seawater at high temperature. Such carbon fiber rods are used in tethers and umbilicals [14]. The main focus of this test was not measuring the fatigue performance of the carbon rod, but the focus was the fatigue performance of the potting resin connecting the rod to the metal end coupler. The blue plastic piping attached to the test was installed to allow water circulation.

Fig. 7 Fatigue testing of a carbon fiber rod and its termination in hot seawater. The carbon fiber rod is the small *black line* between the big metal end terminations. The *blue* piping circulates the hot seawater

In order to bring research data into design standards, the data need to be quantifiable and they need to be relevant for many material systems. Showing that the fatigue curve of glass epoxy "A" is shifted down by 10 % in sea water at 80 °C compared to dry room temperature data shows that this effect needs to be considered in a certification process. But what does it mean for glass epoxy B at 90 °C? Is it the same shift? Does the slope of the SN curve change? Is epoxy "B" suitable for seawater at all? If these questions cannot be answered, the research results cannot be put into design standards as general trends and extensive test programs will also be required in the future.

5 Stress Rupture

Stress rupture is important for all equipment permanently loaded. In marine applications the permanent loading is mostly pressurizing. Most pressure vessel design standards do not consider stress rupture explicitly, but just add it to the static safety factor. This approach implies that a certain lifetime is implicitly assumed. Stress rupture data are, like most long-term performance data, difficult to find.

The standard stress rupture curve given in DNV-OS-C501 [4] for E-glass works well to predict fiber failure for the common glass laminates. The stress rupture curve is given as:

$$log(\sigma_{mean}) = log(\sigma_0) - 0.0423log(t)$$

$$log(\sigma_{test}) = log(0.944\sigma_0) - 0.0423log(t)$$

$$log(\sigma_{char}) = log(0.888\sigma_0) - 0.0423log(t)$$

where σ_0 is the static strength and time t is given in minutes. When comparing a material against this reference curve, some testing on the materials level should be done to show that the reference data are representative for the actual material. Figure 8 shows the stress rupture and possible material data that would confirm that the reference curve is relevant. This is based on the same statistical considerations as were described for cyclic fatigue. The characteristic curve should then be used for design purposes. It is advantageous to be able to use the standard characteristic curve, because this curve is based on many measurements and experience. If the standard curve cannot be used, the characteristic curve needs to be calculated from the measurement data directly and the characteristic curve will be shifted away from the mean curve by more standard deviations due to the smaller number of test samples, as described for cyclic fatigue. In order to check whether the full-scale component behaves as predicted survival tests for 1,000 h should be carried out. The stress level is given by the test curve and the test point is also shown in Fig. 8.

Firewater or ballast tank pipes are made without an inner liner. A resin rich layer in the inside is sometimes called a liner, but it is not a separate thermoplastic liner or steel liner as used in high-pressure equipment. These pipes start to leak when extensive matrix cracking and delamination develops. This means these pipes cannot just be characterized by stress rupture of the fibers, but stress rupture of this leaking failure mechanisms needs to be characterized as well.

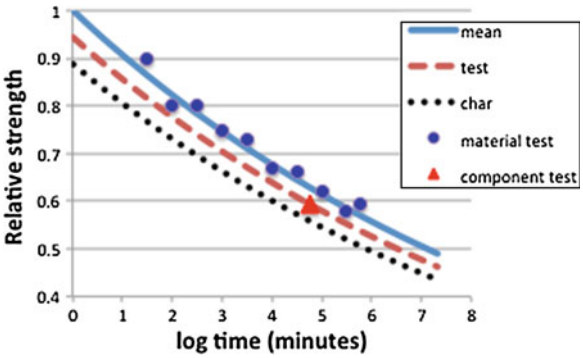

Fig. 8 Standard stress rupture curve for E-glass composites at room temperature according to DNV-OS-C501. Material testing shall be done to confirm the relevance of the curve for a particular material choice. The characteristic curve can be used for design, if test data show relevance. Component testing needs to be done for the final check of compliance

There is no good existing method to predict onset of matrix cracking and delamination under permanent static loads today, even less to find the level of matrix cracking that causes leaking. Therefore testing is required. The standards require testing up to 10,000 h to establish a regression curve allowing definition of the design pressure at 25 years [4, 15]. This approach is well described in terms of statistical analysis of the data, but the physical understanding of the processes involved is limited. Testing also needs to be done at the extreme temperatures and environments.

6 Damage Tolerance

In some cases composites can tolerate some matrix cracks or some delaminations, as long as their size is limited. Pressure vessels or pipes with an inner liner as fluid barrier are an example of composite structures where matrix cracking is not critical. It is also possible to make composites that can tolerate more damage than others, for example by rubber toughening the matrix. These materials would have better durability.

Resistance to impact damage is another important aspect. Tools can fall on composite components, the components can fall down themselves during handling, or they can get hit or collide with their surrounding. The consequence of possible impact damage on the performance of the component needs to be evaluated.

Full-scale tests on pressure resistance of pressure vessels [16–19] and risers [5], after being impacted, are required and are an indirect measurement of damage tolerance and durability. This is the typical evaluation approach in most standards, requiring exposure of the full-scale component to a predefined impact event and to determine the remaining strength afterwards. The remaining strength should not drop under a specified value. Very often the required impact resistance can only be achieved by adding extra material or protective layers that can be destroyed during the impact event.

This approach is practical, but it is also unsatisfactory. Testing on full-scale components requires large resources. Like any full scale testing it can only evaluate a few selected events and not the much wider spectrum of expected scenarios.

A calculation approach would be easier and would give more insight into the failure mechanisms involved. Much testing and modeling of impact has been done (e.g. [23–26]). Figure 9 shows an example of a plate with impact damage and a finite element simulation of this impact event [27]. The simulation was based on basic ply properties as they are measured for most materials. It required a complicated, large 3-D model and progressive failure analysis, but as computational power increases all the time, such modeling methods may become more readily available in the future. The modeling may also help to identify layups and designs that are inherently more impact resistant.

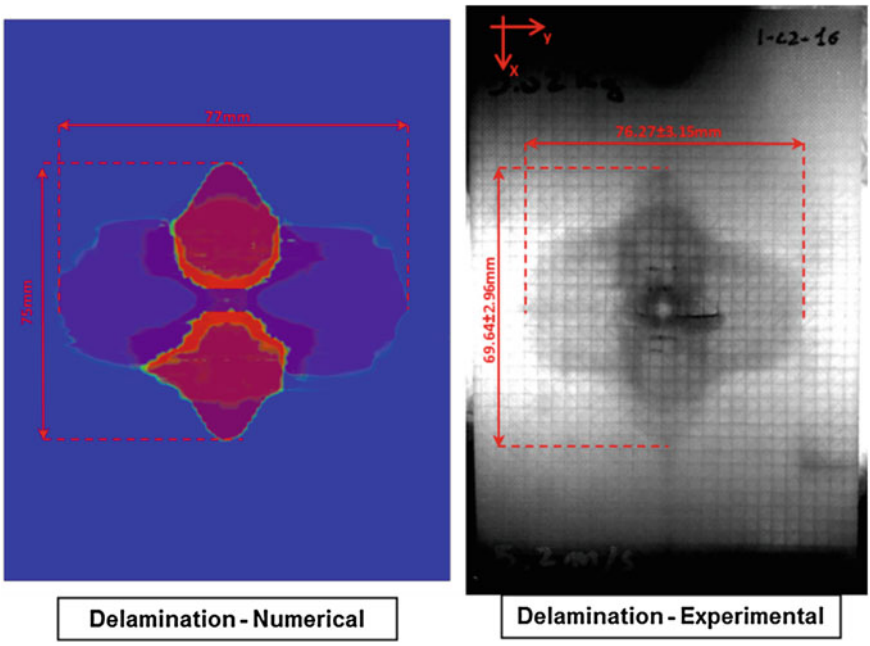

Fig. 9 Comparison of measured and calculated damage in a plate exposed to impact. **a** Delamination-numerical, **b** Delamination-experimental

Due to the complexity of modeling impact it may take a while until testing can be replaced by calculations in design standards. It will be important that calculations can be based on readily available and easy to test material data. In plane properties are usually fairly easy to test and readily available. But through thickness properties needed to model delamination (e.g. input for cohesive elements) are not so easy to obtain, especially for materials like filament wound pipes [28–30].

Indirectly, damage tolerant materials should have better fatigue performance, giving them better SN curves. The aerospace approach of using compressive strength after impact addresses damage tolerance to some extent. Also here the damage tolerant design would require fracture mechanics or progressive failure calculations. Some standards regarding adhesive joints use already fracture energy approaches [31, 32].

7 Effect of the Environment

A major reason for the large testing effort for documentation of long-term properties is the lack of quantitative understanding of how degradation happens in composite laminates. For example, stressed glass fibers exposed directly to water

suffer badly from stress corrosion. Stressed glass fibers in dry air show only a slight reduction of strength with time. A stressed glass fiber epoxy laminate exposed to water shows a strength reduction between the two extremes, because the matrix protects the fibers. The protection works, because less water gets to the fibers and the reaction products from the glass degradation process cannot move easily away from the glass fibers. The water may, however, travel more rapidly along the fiber matrix interface than through the bulk matrix [33]. It is difficult to describe all these effects as quantitative predictive models.

All long-term testing described before shall be done in the relevant environments for the application. This ensures that the effect of the environment is considered during the test. Testing is typically done at high stresses or strains and data are extrapolated to longer times for lower stresses/strains. Increasing temperature may also allow extrapolation to longer times at lower temperatures, if an Arrhenius type relationship can be found. All extrapolations with time require that the material does not go through a phase change. Such an evaluation should be made. It should mainly be evaluated whether some chemical reactions may happen during the lifetime and whether some additives such as antioxydants are being depleted. Chemical degradation is described to some extend for liner materials used in flexible risers [34]. Chemical degradation of polyamide liners is well described [35]. For most other materials chemical degradation needs to be evaluated without the direct guidance of standards.

Molecular dynamics (e.g. [36–38]) may be a method allowing the prediction of degradation of polymers on a molecular level and converting the local degradation to global engineering constants. Figure 10 shows a picture of polymer chains under stress [39]. Due to simplifications in the models the simulations give good qualitative results today, but with ever increasing computer power, they may one day also give the right quantitative answers. This would allow prediction of degradation from first principles on the molecular level. Eventually this approach could also work for composites.

If such models could be developed for fiber degradation and all the other failure mechanisms, as well as environmental conditions, durability could be more easily treated in the certification process.

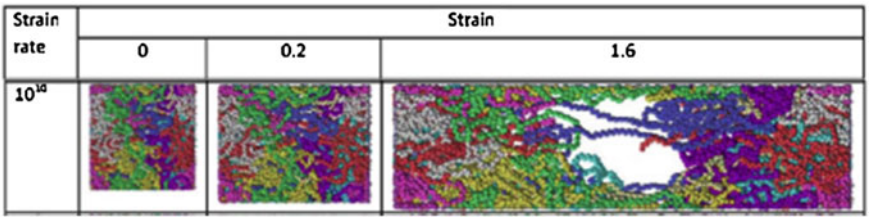

Fig. 10 Molecular dynamic simulation of a stressed polyethylene polymer

8 Conclusions

Durability of marine composites is only indirectly adressed in most design standards today. Some standards for pipes, pressure vessels and the DNV offshore standard for composite components address long term properties of composites directly. The long term performance and credit for good durability are established through fairly extensive test programs. A better quantitative understanding of the effects of temperature and chemicals on the degradation processes could help to reduce the testing efforts and improve the design standards.

References

1. Mørk KJ, Sødahl N, Bjørnsen T (2000) Optimised design procedures for deep water risers. Deep water pipeline and riser technology conference, Houston, 7–9 March 2000
2. Mørk KJ, Sødahl N, Souza L (2000) Present and future fatigue analysis procedures for dynamic risers. In: Proceedings of OMAE' 2001, 20th international conference on offshore mechanics and arctic engineering, Rio de Janeiro, Brazil, 3–8 June 2001
3. DNV Recommended Practice DNV-RP-A203 Qualification of new technology 2011
4. DNV Offshore Standard DNV-OS-C501 Composite components 2010
5. DNV Recommended Practice DNV-RP-F202 Composite risers 2010
6. DIN 55303-2, Statistische Auswertung von Daten; Testverfahren und Vertrauensbereiche für Erwartungswerte und Varianzen 1984
7. Halpin JC (1984) Primer on composite materials: analysis. Technomic Publishing Co., Lancaster, Pennsylvania
8. Agarwal BD, Broutman LW, Chandrashekhara K (2006) Analysis and performance of fiber composites, 3rd edn. Jhon Wiley & Sons, July 2006
9. Daniel IM, Ishai O (2005) Engineering mechanics of composite materials, 2nd edn. Oxford University Press, USA, July 2005
10. British Standard BS 4994—(1987) Design and construction of vessels and tanks in reinforced plastics
11. Salama MM, Stjern G, Storhaug T, Spencer B, Echtermeyer A (2002) The first offshore field installation for a composite riser joint, OTC 14018. Offshore technology conference, Houston, Texas, 6–9 May 2002
12. Echtermeyer T, Kensche C, Bach P, Poppen M, Lilholt L, Andersen SI, Brønsted P (1996) Method to predict fatigue lifetimes of GRP wind turbine blades and comparison with experiments. In: Proceedings of the 1996 European Union wind energy conference and exhibition, 20–24 May, Göteborg, Sweden, H.P. Stephens&Associates, Bedford, UK, pp 907–913 (1996)
13. Ronold KO, Echtermeyer AT (1996) Estimation of fatigue curves for design of composite laminates. Compos A 27A:485–491
14. Storhaug T, Echtermeyer AT, Sund OE, Salama MM, Bjørn P (2002) Composite tethers—qualified for ultra deep waters. Deepwater Offshore Technology (DOT), New Orleans
15. ISO 14692 Petroleum and natural gas industries—glass-reinforced plastics (GRP) piping, parts, 1–4 2002
16. FRP-3-Guideline for filament wound composite cylinders with non load sharing liners, 2nd edn. CGA C-19-2002, Compressed Gas Association, Inc., Chantilly, 2002
17. ANSI/CSA NGV2-2000, American National Standard for "Basic requirements for compressed gas vehicle (NGV) fuel containers", 3rd edn. CSA International, Cleveland, Ohio, USA, March 2000

18. ISO/DIS 11119-3.2 Gas cylinders of composite construction—specification and test methods—part 3: fully wrapped fiber reinforced composite gas cylinders and tubes up to 450L with non-load-sharing metallic or non-metallic liners
19. ISO/DIS 11515.2 Gas cylinders—refillable composite reinforced tubes of water capacity between 450L and 3,000L—design, construction and testing
20. DNV Rules for high speed, light craft and naval surface craft, part 3 Chapter 4, "Hull structural design, fibre composite and sandwich constructions" 2011
21. Pipes RB (1974) Interlaminar fatigue characteristics of fibre reinforced composite materials. Composite materials: testing and design (3rd conference), ASTM STP 546, American Society for Testing Materials, Philadelphia Pa., 1974, pp 419–432
22. Echtermeyer AT, Ekeberg TS, Sund OE (2004) Long-term testing of composite through-thickness properties. Research report 131, Health and Safety Executive, HSE, United Kingdom
23. Sutherland LS, Guedes Soares C (2005) Impact behaviour of typical marine composite laminates. Compos B Eng 37(2–3):89–100
24. Abrate S (1998) Impact on composite structures. Cambridge University Press, Cambridge, p 289
25. Aymerich F, Dore F, Priolo P (2009) Simulation of multiple delaminations in impacted cross-ply laminates using a finite element model based on cohesive interface elements. Compos Sci Technol 69(11–12):1699–1709
26. Pinho STD, Dávila CG, Camanho PP, Iannucci L, Robinson P (2005) Failure models and criteria for FRP under in-plane or three-dimensional stress states including shear non-linearity. NASA technical reports, NASA/TM-2005-213530, L-19089
27. Perillo G, Vedvik NP, Echtermeyer AT Low velocity impact on GRP plates. NTNU, to be published
28. Ozdil F, Carlsson LA (2000) Characterization of mixed mode delamination growth in glass/epoxy composite cylinders. J Compos Mater 34:420–441
29. de Morais AB, Silva JF, Marques AT, de Castro PT (2002) Mode II interlaminar fracture of filament wound angle-ply specimens. Appl Compos Mater 9(2):117–129
30. Davies P, Rannou F (1994) The effect of defects in tubes: part 1. Mode I delamination resistance. Appl Compos Mater 1(5):333–349
31. ISO TS 24817 Composite repairs for pipework—qualification and design, installation, testing and inspection 2008
32. DNV Recommended Practice DNV-RP-C301 Design, fabrication, operation and qualification of bonded repair of steel structures 2012
33. Ramirez FA, Carlsson LA, Acha BA (2008) Evaluation of water degradation of vinylester and epoxy matrix composites by single fiber and composite tests. J Mater Sci 43(15): 5230–5242
34. API 17J "Specification for unbonded flexible pipe", 3rd edition, 1 January 2009, ISO 13628-2:2006 (Identical), Petroleum and natural gas industries—design and operation of subsea production systems—part 2: unbonded flexible pipe systems for subsea and marine application, 2006
35. API (2003) The ageing of PA-11 in flexible pipes. API technical report 17TR2. API Publishing Services, Washington DC
36. Brown D, Clarke JHR (1991) Molecular dynamics simulation of an amorphous polymer under tension. 1. phenomenology. Macromolecules 24(8): 2075–2082. 7
37. Lavine MS, Waheed N et al (2003) Molecular dynamics simulation of orientation and crystallization of polyethylene during uniaxial extension. Polymer 44(5):1771–1779
38. Hossain D, Tschopp MA et al (2010) Molecular dynamics simulations of deformation mechanisms of amorphous polyethylene. Polymer 51(25):6071–6083
39. Sahputra IH, Echtermeyer AT Effect of temperature and strain rate on the deformation of amorphous polyethylene: comparison between molecular dynamics simulations and experimental results. NTNU, to be published

Durability of Composite Materials for Underwater Applications

D. Choqueuse and P. Davies

Abstract Deep sea applications of composite materials are increasing rapidly (Choqueuse D and Davies P in Ageing of Composites Woodhead, 2008). Light weight is critical for submarines structures, in order to facilitate their underwater deployment and increase pay-load, and various specific properties (buoyancy, thermal insulation, remarkable behavior with respect to contact with water,…) strongly favor the use of composite materials. Currently the three main sectors concerned are: the offshore oil and gas industry, the navy, and oceanographic equipment. Important developments are ongoing in the oil and gas offshore sector in particular for riser application (Airbone, 2012). In the oceanographic field, a composite pressure capsule was recently developed for a manned submarine to reach the deepest point of the oceans (Black S, High performance composites, 2010). For submarine housings the first point to be solved is the capability to withstand the hydrostatic pressure, which is the main design factor. Safety factors applied are generally high in order to take into account the difficulty in designing composite structures subjected to compression loads. Generally the parameters affecting durability (creep, fatigue, water absorption) can be neglected and are integrated in the static safety factor. Nevertheless, considering that long life times are expected (nominally 25 years) the durability of underwater composite structures has to be considered, and the main question marks, specific for underwater applications, still globally unsolved are the following: (1) Fatigue in sea water, for riser applications; (2) Creep-fatigue interactions and high compressive strains; (3) Effect of pressure on water uptake kinetics and resulting degradation.

D. Choqueuse · P. Davies (✉)
IFREMER, Centre de Bretagne, Plouzané, France
e-mail: peter.davies@ifremer.fr

D. Choqueuse
e-mail: dominique.choqueuse@sfr.fr

P. Davies and Y. D. S. Rajapakse (eds.), *Durability of Composites in a Marine Environment*, Solid Mechanics and Its Applications 208,
DOI: 10.1007/978-94-007-7417-9_10,

1 Context

Over the last decade, demand for the use of composites materials in deepsea applications has been increasing significantly [1–3]. Currently the main application sector is the offshore oil industry, where water depths >2,000 m are now routinely reached with exploitation perspectives down to 4,000 m expected in the next decade (Fig. 1).

The main criteria for material use for this type of exploitation are light weight and durability. The main requirements for lightness of underwater structures are to ease the installation process, to make the in-service structure buoyant in the environment in order to limit induced stresses, and to limit the size of the buoyancy support (e.g. FPSO). Large developments for composite risers are currently on-going [2] and this represents a very challenging use of composite materials, with a large potential market in terms of composite tonnage.

Another point where the use of composite materials can be very attractive is long term durability. Deep sea installations are requested with a life time of about 20–25years, with limited maintenance operations. Considering the cost of maintenance offshore, composite materials, which are quasi inert in the marine environment, may present an attractive alternative to solve the corrosion problem.

In addition to these points other specific properties of composite materials are now widely used for special applications (electrical insulation, thermal properties ….). A special mention should be made of syntactic foams (polymers filled with hollow glass microspheres) [4], as these materials, a typical underwater material widely used to provide buoyancy, are now being employed for passive thermal insulation of flow-lines. These materials are discussed in sect. 6.

Oceanography is also a demanding sector for composite materials. Here again the lightness and long term behavior are the main points of interest. For ultra deep sea exploration (down to 6,000 m depth) [5] composite materials appear to be very attractive in terms of high specific properties, and they can also be a cheap solution compared to other solutions such as titanium alloys. A recent development for

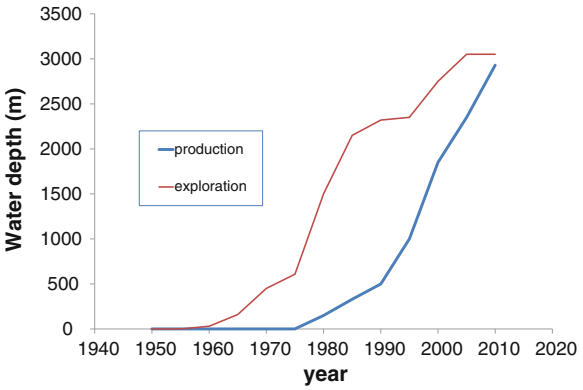

Fig. 1 Offshore water deep exploration and production

lagrangian drift buoys [6] has shown that composite materials provide a very attractive solution for deep sea containers when compared with the current solution which uses aluminum alloy tubes.

2 Deep Sea Marine Environment

The purpose of this section is not to describe the marine environment in detail, but simply to highlight the parameters acting on the durability of materials which differ between surface and deep sea applications.

The first point concerns the pressure. A simple equation gives an approximate relation between depth and hydrostatic pressure with an increase of pressure of 1 MPa every 100 m. A more accurate relation is provided by AFNOR [7] with:

$$P = 0.0101\ z + 0.05 \times 10^{-6} z^2$$

where P corresponds to pressure (in MPa) and z to depth (in meters). The exact correspondence between pressure and depth can be found in [8].

The second parameter which can act on the long term behavior of composite materials in deep sea is the temperature of the water. It is usually considered that in a deep environment the water temperature is about 4 °C. In situ data are now easily available on the Coriolis website [9] where in situ data for operational oceanography are provided.

An example of the kind of data accessible, is shown on Fig. 2

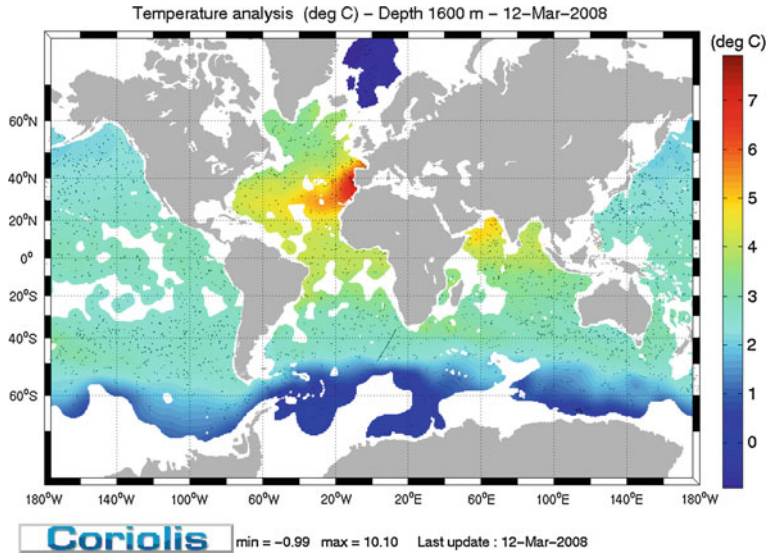

Fig. 2 Deep sea (1,000 m) temperature from Coriolis database

Table 1 Deep sea (1,000 m) physico-chemical parameters parameters

	Guinea	Gulf of Mexico	Brazil	Norway	Australia
Temperature (°C)	2	4	3	−1	2
Salinity (g/kg)	35	35	35	35	35
Dissolved oxygen (mg/litre)	6	5	6	7	4

Temperature and pressure are the main parameters which affect the behavior of materials or structures in deep sea. For some materials such as elastomers the salinity and dissolved oxygen may also have an influence.

In Table 1 the mean parameters observed at 1,000 m in different parts of the world are reported.

3 Influence of Pressure and Temperature on Composite Properties

In order to evaluate the effect of environmental parameters on the long term behavior a large number of samples of different composite materials were followed during 2 years of immersion at different temperatures and pressures [10]. The compositions of the materials were as follows (Table 2).

This study has revealed an influence of both temperature and pressure on the diffusion kinetics for all the materials, Fig. 3 shows an example.

In general the diffusion appears to be Fickian with no effect of the pressure on the saturation level and a small effect on the apparent diffusion coefficient as shown in Table 3.

Analysis of mechanical test results (flexure and shear) on samples aged at different pressures did not reveal any significant effect of pressure on degradation processes.

Considering:

- the thickness of the specimens which for this and most other studies is very small (about 3 mm) in comparison with the material used for underwater structural applications (often tens of millimeters thick), and

Table 2 Materials references and composition

Reference	PE	VE	EP1	EP2	PEEK
Fibre	E glass	E glass	E glass	E glass	Carbon XAS
Resin	Polyester isophthalic	Vinylester	Epoxy	Epoxy	PEEK
Fibre weight content (%)	59	61	52	60	60
Thickness (mm)	2.9	2.8	3.3	2.3	3.3
Fabrication technique	Contact moulding	Contact moulding	Contact moulding	Prepreg vacuum	Prepreg autoclave

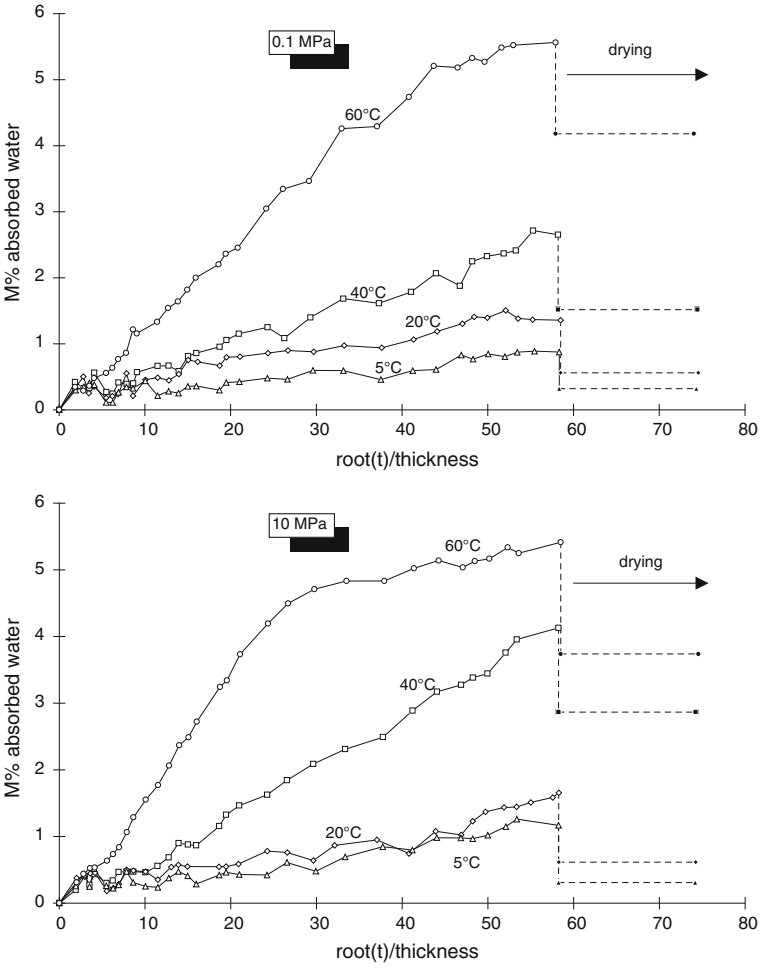

Fig. 3 Water absorption curve for material EP2: effect of pressure and temperature

Table 3 Diffusion coefficients of the different materials (10^{-2} mm $h^{-1/2}$)

	PE		VE		EP1		EP2		PEEK	
	0.1 MPa	10 MPa	0.1 MPa	10 MPa	0.1 MPa	10 MPa	0.1 MPa	10 MPa	0.1 MPa	10 MPa
5 °C	1.51	3.24	0.69	0.92	15	18.7	13.4	16.4	0.62	0.64
20 °C	4.58	4.47	1.16	1.01	27.5	26.9	20.9	23.8	0.67	1.12
40 °C	12.75	14.32	3.43	2.29	68.1	80	40.3	74.6	1	1.5
60 °C	16.56	17.68	4.6	3.49	109	152.5	120.9	185.1	2.1	1.5

- the low temperatures (about 4 °C) observed in deep sea,

it can be argued that with this type of material, the effect of contact with water in deep sea will be very small, and be of second order when considering the mechanical performance of the structure.

4 Deep Sea Electronic Containers

An extensive test programme has been performed in order to evaluate the behavior of deep-sea containers made of composite [11] subjected to hydrostatic compression (Fig. 4).

In this program numerous structures have been tested under external pressure and correlation between tests and predictive models has shown the difficulty to predict the collapse of this type of structure accurately. The collapse of the structure can be governed by buckling for small thickness/diameter ratios or by a compression material failure for thick structures (Fig. 5).

Various parameters can affect the quality of the prediction:

- difficulty to obtain the real mechanical properties of the material
- imperfect geometry of the structure
- numerical model simplifying assumptions

Fig. 4 Deep sea cylinders before and after hydrostatic compression testing

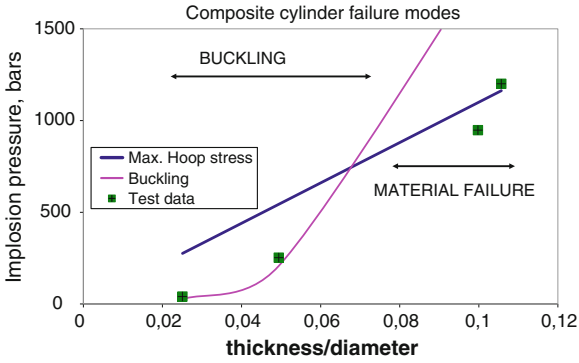

Fig. 5 Hydrostatic compression failure modes for cylinders

- residual stresses due to manufacturing process
- sensitivity to internal defects.

Results from a number of studies of the wet aging of composite tubes have suggested that when the matrix has been correctly chosen and provided the manufacturing procedure is correct the effect of aging on the properties of thick composite cylinders is a secondary effect [12, 13].

5 Long Term Behaviour of Deep Sea Structure for Oceanographic Exploration

Ultra deep sea exploration is an exciting field of application for composite structures. In terms of durability the life cycles of different kinds of equipment can be quite different: deep sea static benthic stations will have to support static loading for long periods (sometimes up to 25 years) while ROV, AUV or other dynamic systems will be subjected to cyclic loads and potential oligocyclic (low fatigue cycle) fatigue behavior.

In order to verify the long term integrity of composite cylinders a number of creep and cyclic loading tests have been performed in recent projects (Fig. 6).

The first tests were performed in pressure vessels but later cylinders were instrumented with data loggers and placed at sea, at depths down to 2,500 m for up to one year, Fig. 7. The data recovered, such as that shown in Fig. 7, enable shorter term qualification tests in pressure vessels to be validated, and the potential risk of creep buckling collapse can be estimated by considering maximum strain criteria.

A second aspect of long term behavior is the response of the structure to cyclic loads. Very few data are available on this topic. In the framework of an European project [14] fatigue behavior of composite cylinders has been examined. Some data, limited to 500 pressure cycles, are reported on Fig. 8, and reveal the low sensitivity of such structures to fatigue degradation in this loading range (Fig. 8). Only cylinders tested at 80 % of the nominal static implosion pressure failed during cycling.

Fig. 6 Half scale AUV composite hull before hydrostatic compression test

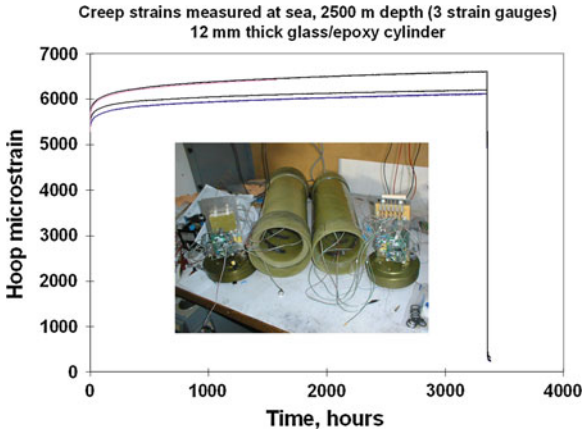

Fig. 7 Creep hoop strains recorded on inner cylinder surface by data loggers on ±55° glass/epoxy cylinders immersed at sea at 2,500 m depth

In order to normalize test procedures an AFNOR French standard [7] has been established, aiming to define test requirements for certifying immerged oceanographic equipment. A special chapter in this document is dedicated to deep sea composite material containers, and the two aspects of long term behavior are considered (fatigue and creep).

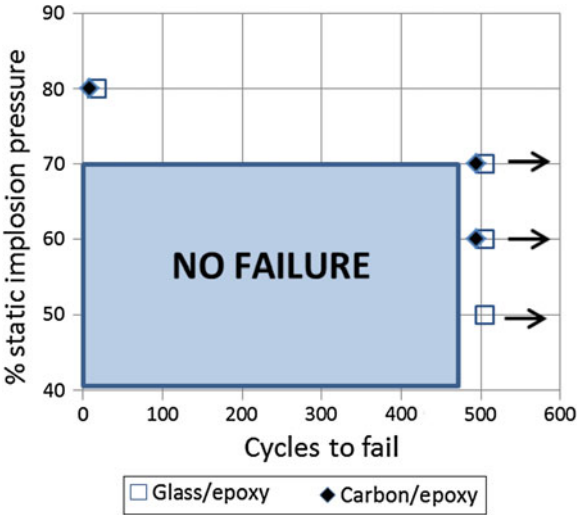

Fig. 8 Fatigue behavior of composite cylinders under external hydrostatic pressure

Three classes of material robustness are defined and fatigue tests at the service pressure and a 96 h creep test at 1.2 or 1.1 times the service pressure are included. Strain gauge indications are used to establish the service life time of the structure.

6 Syntactic Foams

Syntactic foams are another type of composite material, specially developed for underwater applications, which have recently been the object of important evaluation programs in the Oil and Gas sector [15–18]. These materials are composed of hollow glass microspheres embedded in polymeric matrix.

In a single grade of microspheres the diameter varies from 100 to 10 μm and the thickness of the glass bubbles is about 1–1.5 μm.

On account of their excellent buoyancy and thermal properties (Table 4) large volumes of these materials have been used in deep sea (riser tower, buoyancy modules, thermally insulated flow-lines …), (Fig. 9).

Under service conditions these materials can be subjected to hot wet conditions at temperature >120 °C. Taking into account the more and more stringent requirements (increase of depth and higher oil temperatures), the long term

Table 4 Nominal physical properties of syntactic foams

Material	ρ (Kg/dm^3)	λ (W/m K)	Max depth (m)
Glass syntactic polyurethane	0.72	0.17	2,000
Glass syntactic epoxy	0.6	0.14	3,000
Glass syntactic polypropylene	0.66	0.17	3,000

Fig. 9 Syntactic foam materials for deep sea oil and gas applications (pipe, buoyancy module, riser tower)

Fig. 10 Syntactic foam materials samples and aging test equipment enabling simultaneous application of pressure, temperature and sea water immersion

behavior coupling the effect of pressure and temperature of different material has been studied and evaluation programs have been defined where samples were tested in simulated deep sea environmental conditions. Tests were performed in natural sea water, at temperature (up to 160 °C) under hydrostatic pressure (Fig. 10).

Under such extreme conditions degradation of the material can occur. High water uptake (>70 % by weight) has been observed for temperatures >100 °C.

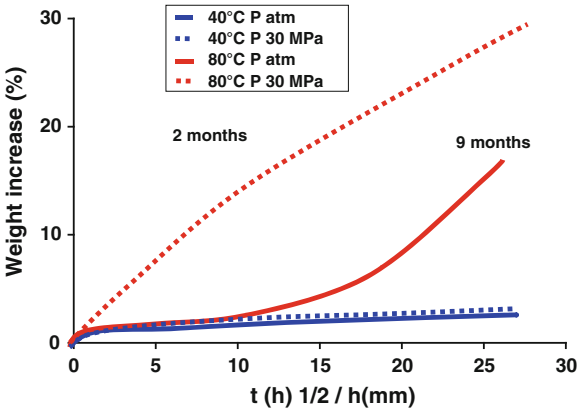

Fig. 11 Water uptake kinetics for glass syntactic polyurethane. Temperature–pressure coupled phenomena

This water uptake leads to detrimental loss of buoyancy properties and a significant reduction in thermal properties. Coupled phenomena have been observed on some materials where a significant influence of the hydrostatic pressure has been noted (Fig. 11).

The significant water uptake phenomenon corresponds to the filling of the glass microspheres by diffused water and may be induced by glass hydrolysis considering the small thickness (about 1 μm) of the glass microspheres. The glass

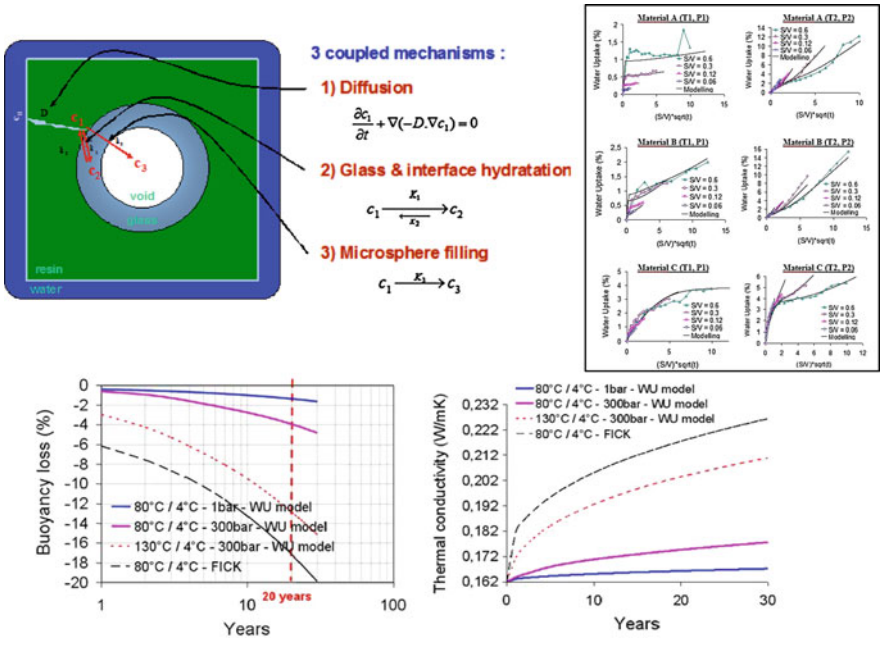

Fig. 12 Predictive model of water uptake in syntactic foam material

hydrolysis phenomenon under hot, wet conditions has been reported previously and widely studied [19]. The coupled mechanism including diffusion in the matrix, glass hydrolysis and microsphere filling has been modeled [20] in order to provide a predictive tool to estimate long term behavior of such structures (Fig. 12).

7 Conclusions

The potential for use of composite materials in a deep sea environment is very attractive. For classical structural application, considering the low environmental temperature and thick wall structures, durability problems can generally be taken to be of second order in design.

For specific applications however, in particular when syntactic foams are to be used under hot wet conditions ($T > 100$ °C) coupled phenomena (temperature–pressure) have been identified and must be correctly included in design calculations.

References

1. Choqueuse D, Davies P (2008) Ageing of composite in underwater applications. In: Martin R (ed) Ageing of composites, Woodhead, ISBN 978-1-84569-352-7
2. Airbone (2012) Thermoplastic composite riser, White paper. http://www.airborne.nl/attachments/118_White_Paper_Thermoplastic_Composite_Riser.pdf
3. Black S (2010) Deep sea submersible incorporates composite pressure capsule. High performance composites
4. Bibin John (2010) CPRN Update on syntactic foams 2010: iSmithers
5. Smith CS (1990) Design of marine structures in composite materials. Elsevier Science, London
6. Le Reste S et al (2012) Deep-Arvor: a CTD & DO profiling float for Argo, available at. http://archimer.ifremer.fr/doc/00115/22627/20352.pdf
7. AFNOR (2012) Materiel immergé. Standard XP X 10–812
8. Copin-Montegut G (2002) Propriétés physiques de l'eau de mer. In: Techniques de l'Ingénieur (ed)
9. *Coriolis*: In situ data for operational oceanography. www.coriolis.eu.org/
10. Choqueuse D et al (1997) Aging of composite in water. ASTM STP1302. pp 73–96
11. Choqueuse D et al (2010) Composite cylinders for dee sea applications. ASME 2010. Pressure vessels and piping division, PVP 2010
12. Davies P, Le Flour D (2001) Long term behavior of fiber reinforced structures for deep sea applications, Paper 21. In: Proceeding of oilfield engineering with polymers, London, pp 255–268
13. Davies P, Choqueuse D (2003) Fatigue and durability of marine composites. In: Harris B (ed) Fatigue in composites, Woodhead Press, ISSBN 1 85573 608 X
14. Euclid RTP3.8 project (2000) Composite structures guidelines. Part 4 Submersibles
15. Choqueuse D, Chomard A, Chauchot P (2004) How to provide relevant data for the prediction of long term behavior of insulation materials under hot/wet conditions? OTC 16503, Houston

16. Choqueuse D et al (2005) Recent progress in analysis and testing of insulation and buoyancy materials. In: Fourth international conference on composite materials for offshore operations, Houston, TX 4–6 Oct 2005
17. Grosjean F et al (2009) Comprehensive analyses of syntactic foam behaviour in deepwater environment. J Mater Sci 44(6):1462–1468
18. Choqueuse D (2012) Experimental study and analysis of the mechanical behaviour of syntactic foams used in deep sea. PhD thesis, University of Franche Comté. Available on IFREMER "Archimer" website: http://archimer.ifremer.fr/
19. Sauvant V, Gimenez N, Sauterau H (2006) Hydrolytic ageing of syntactic foams for thermal insulation in deep water.Degradation mechanisms and water uptake model. J Mater Sci, 4047–4054
20. Lefèbfre X, Sauvant-Moynot V, Choqueuse D, Chauchot P (2008) Durability of syntactic foams during ageing in severe conditions In: Modeling of water uptake and ingress in order to predict buoyancy and thermal conductivity evolutions. J Oil Gas, 08049

Design of Racing Yachts for Durability

H. Devaux, A. Miller, R. Balze, S. Guého and J. Maguet

Abstract This chapter describes the design of racing yachts with composite materials at HDS, an SME specialized in marine design and calculation. Three case studies are presented to illustrate the company expertise. First, a study of keel flutter is described. The development of an analytical tool is discussed and validation by comparison with numerical modeling is presented. Then wave impact is discussed, a regular source of damage in fast craft, and the development of a specific test to evaluate material systems is described. Finally, adhesive bonding is discussed and a specific application to mast tracks is detailed. These three studies underline the importance of a detailed understanding of composite mechanics in developing durable marine structures.

1 Introduction

Ships and sailing vessels have always been challenging applications, and an active field for technology improvements. Recent decades have seen the development of faster and lighter boats, with the help of composite materials, to achieve higher speeds and lower fuel consumption. For example, the time required to complete the famous sailing race "The Transat", between England and the USA, decreased from 40 days in 1960 (Sir Francis Chichester) to 8 days and 8 h in 2004 (Michel Desjoyeaux). This performance shift has been possible with the development of the knowledge of sailing and its engineering, but has also led to new issues in terms of durability. Sailing vessels and motor boats are particularly good laboratories for durability testing, due to the variety of the loads (wind and wave), their amplitude and frequency (wave impacts), but also because of their exposure to salt

H. Devaux · A. Miller · R. Balze · S. Guého (✉) · J. Maguet
HDS, 45 rue de l'Elorn, Batiment le Fromveur 29200 Brest, France
e-mail: sebastien@hds-design.com

P. Davies and Y. D. S. Rajapakse (eds.), *Durability of Composites in a Marine Environment*, Solid Mechanics and Its Applications 208,
DOI: 10.1007/978-94-007-7417-9_11,

water and UV. When combined with the quest for ultimate performance and competition, it is easy to understand how the racing boat field can be a major driver for materials and mechanics understanding and improvements.

HDS has grown in this competitive and demanding environment, working to improve the performance in sailing boat racing for more than 15 years. Looking back at the past decade, this chapter will give an overview of three challenges HDS has spent significant energy on, in order to understand, model and optimize its design:

- Keel flutter, a phenomenon of fluid–structure instability similar to the one well-known in aircraft design; however, the case of this coupling interaction in water for the keel was not extensively documented until it was witnessed recently;
- Water impact on sandwich materials: this topic addresses the need to understand the behavior of sandwich panels subject to water, i.e. "soft" repeated impact loading;
- Bonded assembly of mixed materials to replace bolted assemblies, on parts subject to tensile and peeling loads. This section will describe the work done on sail track assembly to the mast, and its reliability.

These case studies will illustrate some of the developments and improvements proposed by the world of yacht racing. This field has a constant and growing appetite for new technology, with particular attention to reliability, which can without doubt find applications in more classical industries, like aeronautics or ground transportation.

Since 1994, HDS has been a major player in the structural design of complex composite parts, especially for racing yachts. Masts, monohull and multihull structure design is the core activity, but HDS is also involved in cutting-edge marine, automotive and aerospace industries.

The company was founded in 1994 by Hervé Devaux who, before creating the company had worked for eleven years in academia, managed the data center structures of the CRAIN, in La Rochelle, and had been responsible for the sailing construction department in the ACX shipyard in Brest.

Based on experience gained in the field of competitive sailing, HDS performs design and calculations to offer a range of solutions that includes:

- structural analysis with analytical and numerical methods of various degrees, including finite elements analysis (FEA) and fluid structure interactions,
- composite expertise and materials properties calculation,
- production of manufacturing drawings (DAO)
- project management and structural consultancy on materials,

HDS also devotes significant energy and time to R&D around composites and mechanics. In addition to human skills, HDS makes intensive use of computer simulation tools:

- powerful simulation software, addressing static to complex fluid–structure interaction (FSI) analysis: FEMAP/NX NASTRAN, ADINA, SOLIDWORKS

- drafting and CAO softwares AUTOCAD, SOLIDWORKS and RHINOCEROS
- a variety of in-house dedicated design and FEA softwares, including AUTOSPAR/SIMSPAR, dedicated to optimized mast/rigging design.

Among other achievements, showing the possible synergies between the technologies developed in racing projects and industrial topics are:

- America's Cup projects, since 1992 until today:
  - Victory in the 33rd edition with design of the American team winged trimaran,
  - Class America boat and mast structure design since 1992.
- Masts and platforms for racing yachts
  - Around the world maxi-multihulls : Banque Populaire V, IDEC, Groupama III, Orange II, …
  - Hydroptère
  - IMOCA 60' : Foncia structure and mast (Vendée Globe winner 2008),
  - Volvo Ocean 70 : Groupama IV mast (winner 2012), ABN Amro boat (winner 2006).
- Motor Multihulls, King-cat, Iris, and Ocean Alchemist.
- Industry.
  - Helicopter parts and simulators
  - 6 m wide reflectors for military and civil antennas
  - Parts for submarines and subsea systems (Fig 1).

Fig. 1 Three examples of recent HDS achievements BMW Oracle racing, America's Cup 2010 winner, Groupama IV, Volvo Ocean Race 2012 winner, and FONCIA IMOCA 60', Vendée Globe 2008 winner

2 Case Study 1: Keel Flutter

In September 2004 the racing yacht 'Cheminees Poujoulat—Armor Lux' lost her composite keel in mid-Atlantic. Her skipper Bernard Stamm recalls: 'I was going down below at the end of a surf at 27 knots when I felt the keel making horrendous thrashing vibrations, almost immediately the keel broke and the boat capsized.' Earlier that year Roland Jourdain on the yacht 'Sill et Veolia' had disturbing vibration problems in the composite keel when sailing at around 20 knots in calm sea. His experience raised concern for Jean Le Cam aboard 'Bonduelle'—an identical sistership to 'Sill et Veolia'—although she had never had such problems. Because of safety precautions, both pulled out of The Transat race before it started. An increase of the torsional rigidity of the foil, by adding to the laminate permitted thereafter, on these two boats, to overcome the problem. But the composite keel flutter phenomenon remained an open question for yacht designers.

Following these problems, HDS tried to identify the sailing conditions and the parameters of a keel design that could cause flutter. The main questions asked were 'Why are composite keels susceptible to flutter', and 'Is it possible to predict and prevent this behaviour ?' and, 'Can a fair indication of the flutter critical speed be given at low cost and in the first design loops of a keel ?'.

In this section, the semi analytical model implemented to predict keel flutter at an early stage of a keel design will be described first. Then, results obtained from a 3 dimensional multi-physics simulation of a keel flutter case will be shown and compared with the results obtained using the semi analytical model. The multi-physics simulation allows some of the model assumptions to be confirmed, and it provides an indication of some terms that are important in semi analytical model to predict the flutter phenomenon, especially with respect to fluid damping at zero flow velocity.

2.1 Nomenclature

X_b, Y_b, Z_b	Boat axis system
X_k, Y_k, Z_k	Keel axis system
x, y, z, t	Space and time variables
u_x, u_y, u_z	Translation degree of freedom
θ_x, θ_y, θ_z	Rotation degree of freedom
C_t	Torsional center (neutral line position)
F	Lift center
Λ	Keel sweep angle
K	Stiffness matrix
M	Mass matrix
V	Fluid velocity
i	Incidence angle

A	Slice area
c	Linear lift coefficient
ρ_w	Water density
j	Complex number $j^2 = -1$
ξ_i	Damping terms
η_i	Damping rates $\eta_i = 2.\ \xi_i$
ω_i	Eigen frequencies in rad/s
F_i	Eigen frequencies in Hz
F_{iw}	Eigen frequencies in water in Hz
ε_i,	Ω_i Real (imaginary) part of the system roots
α_i	Global "damping" rates including flow
M_a	Added mass due to bending
I_a	Added inertia due to torsion
ε	Symbol used for a value close to zero
δ_{ii}	Phase
a_{ii}	Amplitude

2.2 Keel Description

IMOCA 60' keels are vertical weighted wings, on the bottom of the hull. This wing is properly called keel fin and the weight on the bottom of it is called 'bulb' because of it shape.

Anti-drift and stability functions are usually dissociated. Thus the keel fin is more a bulb support than an anti-drift profile (Daggerboards are actually the anti-drift profiles of the yacht). This allows the maximum righting moment to be increased, using canting keels Fig. 2, which means that we can change the keel's angle to the vertical axis.

The main features of an IMOCA 60' keel are the following: keel length is about four meters (m), keel fin mass about five hundred kilograms (kg), bulb mass about three tons (T) and bulb inertia about one thousand two hundred kilograms square meters (kg m^2).

2.3 Model Principle

The model developed at HDS to calculate flutter critical speeds is based on the equations introduced by Mazet [1], applied to aircraft wing vibrations. In our case, hydrodynamic efforts are simplified and represented as distributed along the keel fin over two-dimensional slices. The systems' dynamics are represented just by the first two eigenmodes. In fact, the first eigenmode will mainly represent bending behavior,

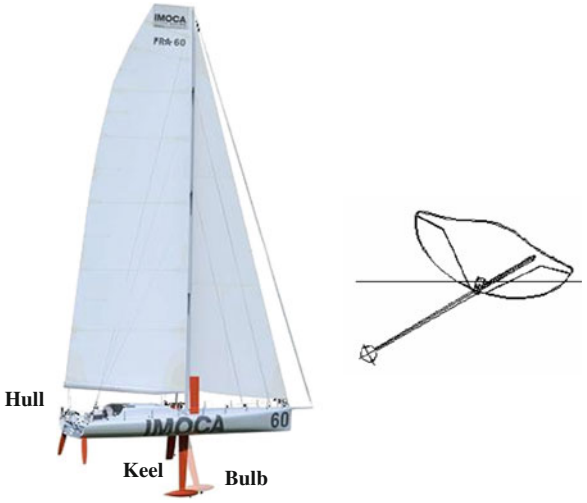

Fig. 2 IMOCA 60' Keel description (*left*) and canting keel (*right*)

and the second will represent torsional behavior. Mazet assumes that these two modes represent pure bending and pure torsion respectively. However, when dealing with IMOCA 60' keels, the presence of a solid bulb and the possible gap between its center of gravity and the main axis of the keel fin, leads to important coupling between bending and torsion. The model developed takes this coupling into account for the calculation of bending and torsional displacements before projecting the equations on the truncated modal basis. Hydro-elastic vibration equations provide the "damping" rates for each speed. The flutter phenomenon appears when one of these rates becomes zero (self maintained vibrations).

2.4 Definitions

We will now only focus on the part of the keel under the hull, using the axis system presented on Fig. 3.

The keel axis system is defined by a rotation of an angle $\pi + \Lambda$ around Y_b axis. Λ is the sweep angle and is generally between 0° and 15°. In the following sections, we only present the case $\Lambda = 0$.

2.5 Eigenmodes Calculations

The calculation of Eigenmodes is performed using the discretized finite elements method, using six degrees of freedom beam elements (one translation and two rotations by node, representing bending and torsion). The beam element model used is the bending-torsion beam model presented by Bezine [2].

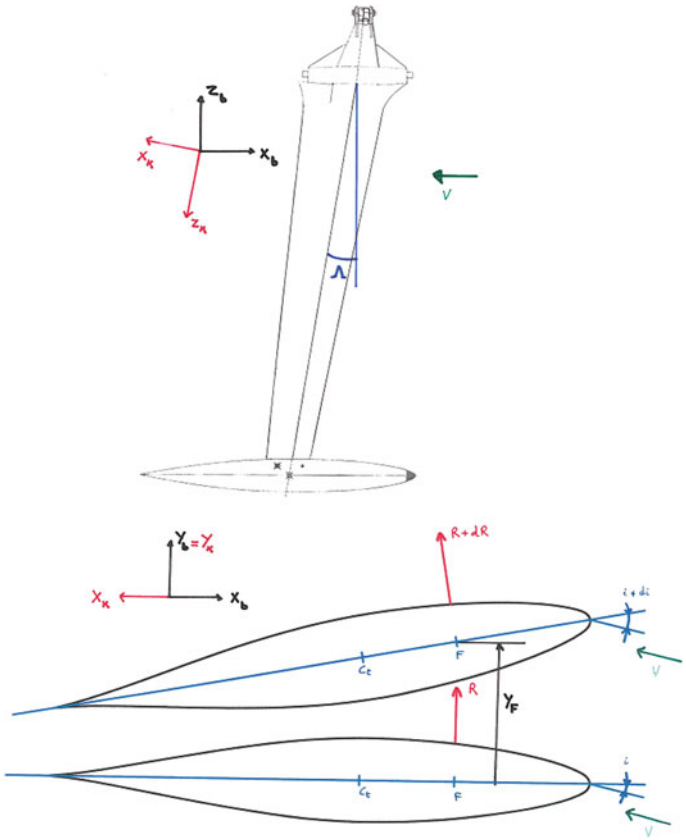

Fig. 3 Axis system used in the model (Profile view on the *top*, upper view on the *bottom*)

Two types of keel will be considered:

- Cantilever keel
- Canting keel: the keel is pinned at the upper edge and at the hull bearing, and unable to twist at the hull bearing.

On Fig. 4, the point N represents the intersection between the main fiber of the fin neutral fiber and the bulb axis. The point G represents the bulb's center of gravity. We assume that the segment NG is infinitely stiff and that the bulb's weight and inertia are transported to the point N using Huygens theorem. (Segment NG is not represented in the beam FEA model)

We have to solve the following classical system:

$$M\ddot{X} + KX = 0 \text{ or } (K - \omega^2 M)X = 0 \tag{1}$$

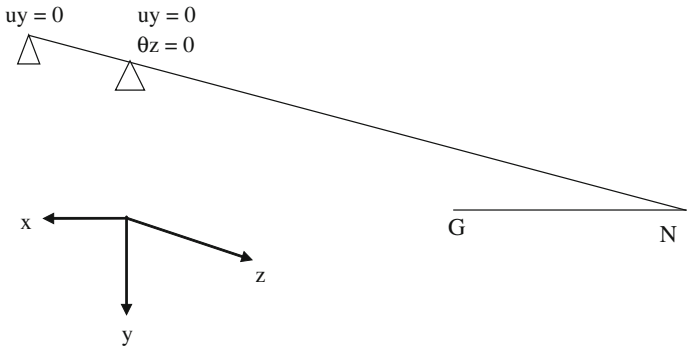

Fig. 4 The canting keel beam finite element model

This method of eigenmode calculation gives good results for keels, compared to eigenmodes experimentally obtained or calculated with a complete 3D composite finite element model, provided the composite material properties of the finite element beam model are properly defined.

2.6 Lift Force

To calculate the hydrodynamic lift force, the slice method is used. It's not possible to give a strictly accurate linearized expression of the resultant of water pressures on the slice except if the slice is motionless, animated with a uniform translation or with a sinusoidal vibration. However, an approximate expression of a lift force can be given, considering that we are in quasi-static regime.

Thus, for a flow velocity V, this lift force is applied on the Lift Center F and can be decomposed into two forces:

- The first is related to the incidence angle i between the slice and the flow direction:

$$-\frac{1}{2}c \times \rho_w \times A \times V^2 \times i \tag{2}$$

- The second is linked to the translation speed of the lift center F, orthogonally to flow direction:

$$-\frac{1}{2}c \times \rho_w \times A \times V^2 \times \frac{\dot{y}_F}{V} \tag{3}$$

The global lift force is the sum of the two previous expressions. The coefficient c is the linear lift coefficient, equal to 2π for a flat plane in linear theory without viscous effects [3]. For a 3D wing profile with viscous effects, this coefficient, averaged on the height of the keel, is lower and depends on the wing aspect ratio.

2.7 Results

Applying the theorem of virtual work to the two eigenmodes at each flow velocity, we obtain a system of two homogeneous second order equations whose determinant must be zero. This determinant has four roots, two conjugated complexes:

$$-\varepsilon_1 \pm j\Omega_1 \text{ and } -\varepsilon_2 \pm j\Omega_2 \tag{4}$$

The following ratios represent the "damping" rates for a particular flow velocity V:

$$\alpha_1 = \frac{\varepsilon_1}{\Omega_1} \text{ and } \alpha_2 = \frac{\varepsilon_2}{\Omega_2} \tag{5}$$

The flutter phenomenon appears when one of these "damping" rates becomes zero. In fact, to find the critical speed, we will iterate on the speed until one of these "damping" rates becomes zero. On Fig. 5, α_1 becomes zero at a flow velocity of 18 knots.

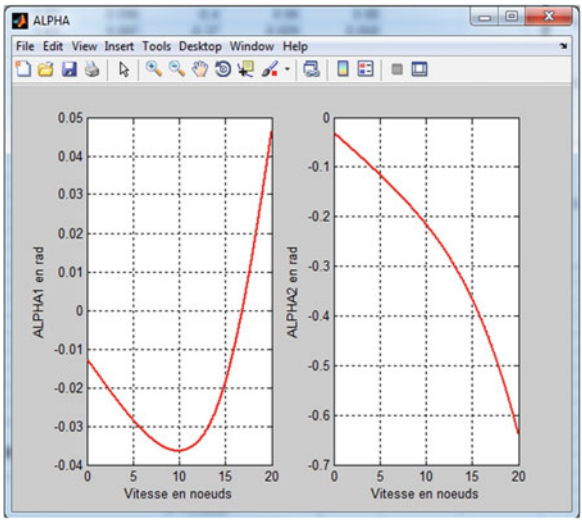

Fig. 5 *Curves* showing the damping rate α_i versus flow velocity (knots)

2.8 Multiphysics Simulation Model

To verify the quality of the semi analytical model and to have an estimation of some of its terms, various multi-physics simulations were set up using ADINA™ software. One of these simulations is shown below.

2.8.1 Solid Model

A cantilever keel has been modeled as follows:

- Keel fin with constant profile
- Upper section embedded
- Solid bulb concentrated at a single node (inertia matrix).

The profile used is a typical keel fin profile and the keel height is 4 m. The bulb mass is 3.1T and its inertia is 900 kg m^2 as for an IMOCA 60' keel bulb.

The 3D keel model is presented on Fig 6. Most of the elements are hexahedral (8 nodes per elements, 3 degrees of freedom per node). The material model chosen is an orthotropic composite.

The bulb was placed at two different positions depending on the simulation:

- on the torsional center C_t of the bottom section of the keel
- behind this torsional center (in the boat axis system).

A Newmark time integration scheme was used for the structure with the classical values $\beta = 0.25$ and $\gamma = 0.5$, which allow energy to be conserved, thus avoiding numerical damping on the structure.

2.8.2 Fluid Model

Fluid model dimensions are the following: L = 7 m, W = 2 m, H = 4 m. The 3D CFD mesh used and its details around the profile are shown on Fig. 7.

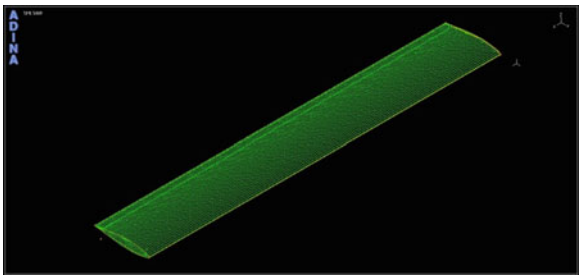

Fig. 6 Keel model

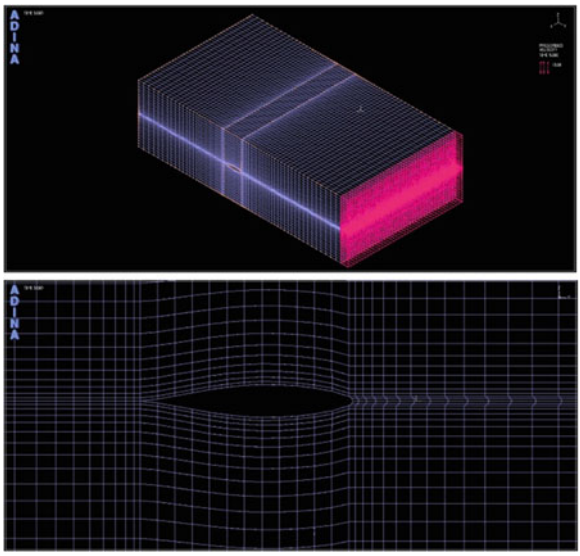

Fig. 7 3D CFD Mesh

The fluid is modeled as a laminar incompressible Navier–Stokes fluid and is discretized using the ADINA FCBI-C [4] fluid elements. The time integration method is an Euler α-method in which the parameter α is varied in order to evaluate the numerical damping. A priori the choice $\alpha = 0.5$ allows numerical damping to be avoided, but this causes convergence problems unless the velocity is extremely small.

The fluid inlet velocity is varied from 8 to 12 m/s (except for the fluid damping analysis, for which the inlet velocity is 0 m/s). The outlet is set to be traction free and the rest of the fluid boundaries are modeled with sliding wall boundary conditions.

To generate a time response of the keel (damped for the stable regime or amplified for the unstable regime), a small transverse perturbation load is applied to the bottom of the keel at the first time step.

2.9 Added Mass Estimation

To have an estimation of the added mass generated by the bending and torsion of the fin, the eigenmodes were calculated in both cases with and without water around the keel. The following tables compare the frequencies obtained without and with the water for a bulb placed on the torsional center of the bottom section of the keel (bending and torsion being decoupled):

- Without water:

F1 (Hz)	F2 (Hz)
1.056	2.119

- With water:

$F1_w$ (Hz)	$F2_w$ (Hz)
1.013	2.112

F1 corresponds to the first eigen frequency (only bending) and F2 corresponds to the second eigen frequency (only torsion). The index w denotes a frequency in water.

By comparing the frequencies obtained in presence and in absence of water, the added mass terms generated by bending and torsion motion of the fin can be estimated:

M_a (bending) (kg)	I_a (torsion) (kg m^2)
252	5.8

We can note that Ma is about the same order of magnitude as the fin's own weight (240 kg in this simulation) and significantly less than the bulb's weight. Moreover, compared to bulb's inertia, Ia is negligible.

For a bulb placed 0.160 m behind C_t (bending and torsion coupled):

- Without water:

F1 (Hz)	F2 (Hz)
1.041	2.148

- With water:

$F1_w$ (Hz)	$F2_w$ (Hz)
1.000	2.136

2.10 Damping Estimation

For any vibrating structure subjected to damping, the time response signals to a load impulse can be decomposed into sums of exponentials taking damping into consideration. If we focus on the two first eigenmodes of the structure, signal analysis allows the damping rates of each mode to be known.

2.10.1 Fluid Damping

We analyze the time response of the keel after an impulse. There are two kinds of impulse, a transverse effort for a bending response of the keel and a torque for a torsion response, both applied on the bulb node. In order to run the analysis more easily, the eigenmodes are decoupled by placing the bulb at the torsional center. Therefore we can estimate separately the bending damping term η_1 (Fig. 8) and the torsion damping term η_2 (Fig. 9), with the fluid model.

Using these time response curves, we can deduce the damping rates η_i (%) for each eigenmode:

$$\eta_1 = 10.6\,\% \text{ and } \eta_2 = 13.4\,\% \tag{6}$$

These damping rates are not negligible but contain both fluid and numerical damping here, linked to the time step choice, the Euler integration scheme parameter α choice, and the mesh. The influence of time step (Fig. 10) and Euler

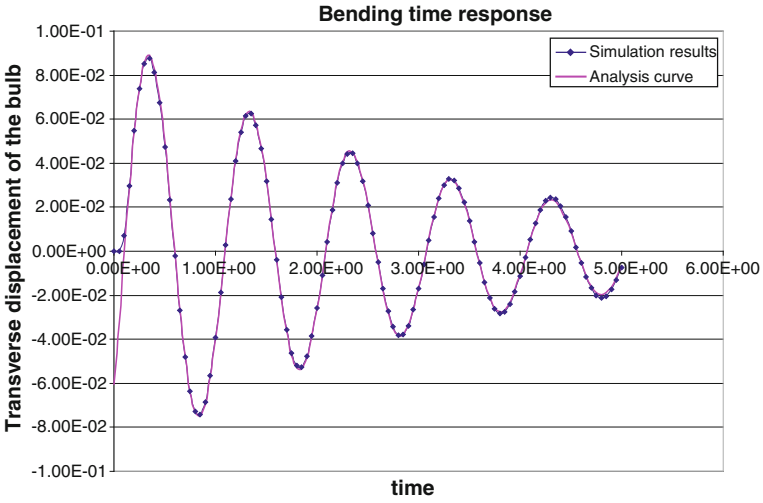

Fig. 8 Bending time response of the keel in water for Euler integration scheme parameter $\alpha = 1$ and time step = 0.01. The points are from simulation results, the *continuous curve* is the analysis curve to estimate the bending damping rate

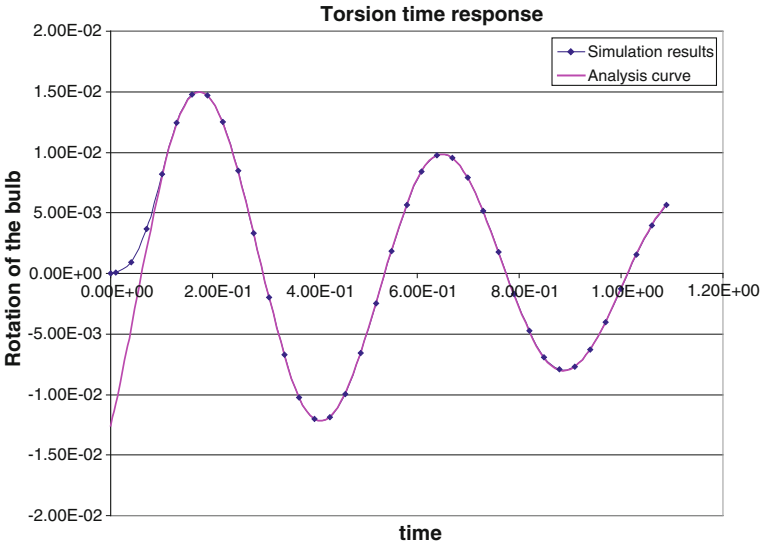

Fig. 9 Torsion time response of the keel in water for Euler integration scheme parameter $\alpha = 1$ and time step $= 0.01$. The points are from simulation results, the *continuous curve* is the analysis curve to estimate the torsion damping rate

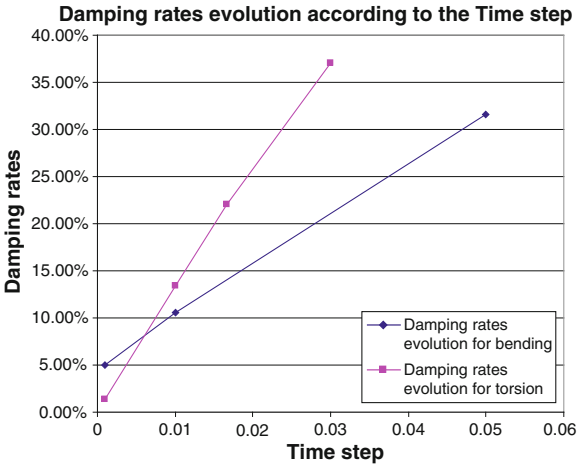

Fig. 10 Damping rates evolution according to the time step with an Euler integration scheme parameter $\alpha = 1$

integration scheme parameter α choice (Fig. 11) on these damping rates was evaluated.

The evolution of damping rates according to time step and to Euler integration scheme parameter α shows that fluid damping rates at zero flow velocity tend to the values:

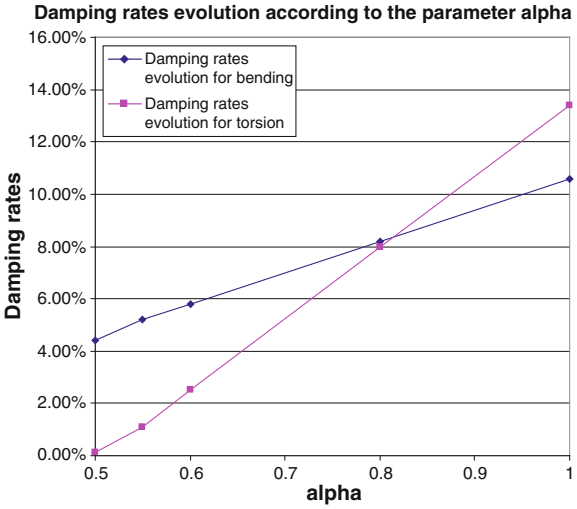

Fig. 11 Damping rates evolution according to the Euler integration scheme parameter α with time step = 0.01

$$\eta_1 = 4.4\,\% \text{ and } \eta_2 \approx 0.2\,\% \tag{7}$$

These damping rates have to be taken into account in the semi analytical model to compare the estimated flutter critical speed given by both simulation model and semi analytical model. However, to avoid convergence problems in the multi-physics simulation model, we have to choose a parameter $\alpha > 0.5$ which implies the unavoidable presence of a small numerical damping. We choose the smallest parameter α for convergence and low numerical damping and take into account this damping in the analytical model, to allow proper comparison of results.

2.10.2 Solid Damping

This damping term is not taken into account in the multi-physics simulation model. However, thanks to keel eigen frequencies measurement, recently imposed by the IMOCA 60' rules, a structural damping term can be estimated using the time response curves of the behavior of the keel after an impulse excitation. We note that these terms vary strongly between the different keels; they depend particularly on the materials chosen and the construction method.

2.11 Critical Speed Comparison

In the following two paragraphs, the bulb is placed at 0.160 m from the torsional center C_t.

2.11.1 Multiphysics Simulation

Figures 12 and 13 show the bulb time response for a flow velocity of 9 m/s and 10 m/s respectively. The blue curves represent the transverse displacement of the bulb, while pink ones represent the bulb rotation.

We note that for a flow velocity of 9 m/s, the bulb oscillations are decreasing, while for a flow velocity of 10 m/s the oscillation amplitude grows with time; there is flutter instability. Therefore, with this choice of time step and Euler parameter α, **critical flutter speed is between 9 and 10 m/s**.

It is also interesting to note that the frequencies of transverse displacement and rotation of the bulb are very similar, that is a characteristic of the flutter phenomenon, and that the phase between the two signals is about $\pi/2$.

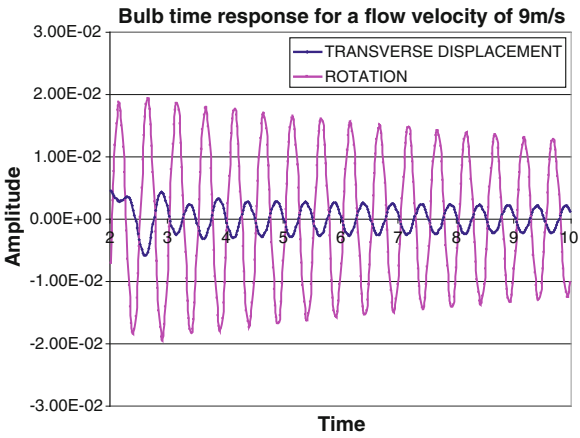

Fig. 12 Bulb time response for a flow velocity of 9 m/s ($\alpha = 0.6$ and time step $= 0.01$)

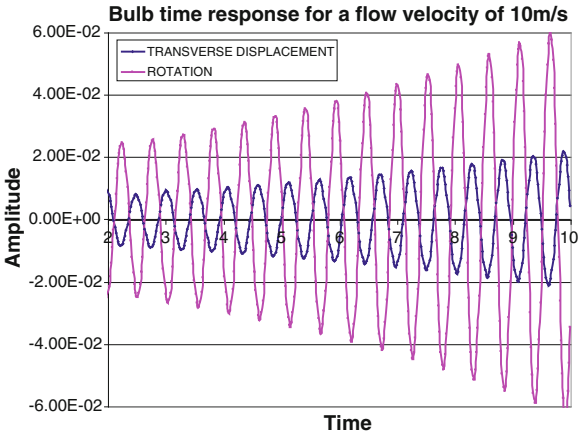

Fig. 13 Bulb time response for a flow velocity of 10 m/s ($\alpha = 0.6$ and time step $= 0.01$)

2.11.2 Semi Analytical Model

The eigen frequencies calculated with the semi-analytical model are the following:

F1 (Hz)	F2 (Hz)
1.041	2.147

With a linear lift coefficient of 2π the model predicts a critical speed of 15.0 knots, corresponding to 7.7 m/s. This result takes into consideration damping rates previously predicted by the multiphysics simulation model, but it considers added mass as negligible. If we consider the bending added mass (resp. torsional added inertia) previously computed into the mass (resp. inertia) of the bulb, we obtain the following eigen frequencies:

F1 (Hz)	F2 (Hz)
1.002	2.140

Therefore the critical speed becomes 15.3 knots, corresponding to 7.9 m/s.

In fact, if we consider the 3D effects (especially aspect ratio), the average linear lift coefficient will be smaller. For such a keel, the average lift coefficient is approximately 5.2. With this lift coefficient and taking into account the added mass, we find a critical speed of 16.9 knots, corresponding to 8.7 m/s.

2.12 Conclusion

In this section, a rather simple semi analytical model was presented which provides a good estimation of the critical flutter speed of a bulb keel at low cost. This model, based on some strong assumptions, especially concerning structure dynamic and calculation of hydrodynamic pressure loading, is compared to results from a complete 3 dimensional multi-physics simulation and the comparison shows good agreement. With this semi analytical model, it is possible to calculate a good estimation of the flutter critical speed of a keel in about half a day compared to the full multiphysics approach which takes several days.

The damping terms—fluid damping at zero flow velocity and solid damping—are important parameters that must be well estimated for a good prediction of flutter. An estimation of fluid damping rates to use in the prediction of flutter critical speed for an IMOCA 60' keel is given here. The effect of added mass effects due to the fin deformation appears to be negligible in the prediction of keel flutter.

3 Case Study 2: Wave Impact

3.1 Introduction

Today one of the most important causes of failure for cruising boats, racing boats and high speed vessels, is damage due to wave impacts, Fig. 14. Composite hulls with sandwich materials have many qualities, and they are widely used for passenger boats and leisure boats. However, during the Route du Rhum in 2002 only 18 % of the ORMA fleet managed to finish. The impact response is difficult to predict and there is a need to find efficient tools to identify the proper core material for durable boats.

The response of polymer matrix sandwich composite is driven by various parameters: local versus global behavior, ratio of fibers to matrix, in plane and through-thickness properties etc. A lot of studies have focused on this topic but few of them have been specifically dedicated to marine applications. The following section reports on work performed with IFREMER (French Research Institute for Exploration of the Sea) to develop a predictive tool for impact damage and use it for our racing boats [5].

3.2 Global overview of previous work on impact testing

Much of the studies made on impact for marine composites and sandwich materials deal with local and rigid impacts. Work on foam cored sandwich materials has really started in the 1980s and 1990s, particularly in Scandinavia, when PVC foam core sandwich materials were adopted there for both military and high speed passenger vessels, first with glass composite skins then with carbon reinforced skins [6–8].

Fig. 14 **a** Areas exposed to wave impacts. **b** Example of damage area due to wave impacts

Other industries have worked on impact on sandwich panels, and the first studies on honeycomb sandwiches were intended for aircraft and the aerospace industry [9, 10]. There has also been some work on energy absorption for offshore topside applications [11] and some large scale testing has been performed. Such tests are useful to demonstrate or validate new concepts but they are expensive and difficult to perform for an 18 m long racing yacht.

3.3 Wave Impact Testing

The studies mentioned above do not represent the repeated interaction between waves and racing boat structures. The damage observed is then very different and in order to reproduce it a new testing protocol was required. The particular load that HDS is interested in is wave impact on sandwich materials: a small scale, and repeatable test was needed and to suit this particular need IFREMER developed the so-called "medicine ball" test.

The original idea for the test developed here was suggested by the late Hubert Desjoyeaux of the CDK boatyard in Brittany, during discussions with the architects Finot-Conq. The stiffened panels to be tested were initially placed with the stiffeners directly on the floor, Fig. 15a. Later sand-filled boxes were placed below the panel to reduce stiffener damage, and then a rigid square steel frame system was used, Fig. 15b.

The current IFREMER test set-up is shown in Fig. 16, more experimental details can be found in [12].

This set-up allows a rapid evaluation of different core types and hence to select the grades required in different areas. Various test campaigns have been performed over the last fifteen years and there is now a useful database for typical marine industry core types. There are three cores frequently used in racing yachts, and they have all been tested:

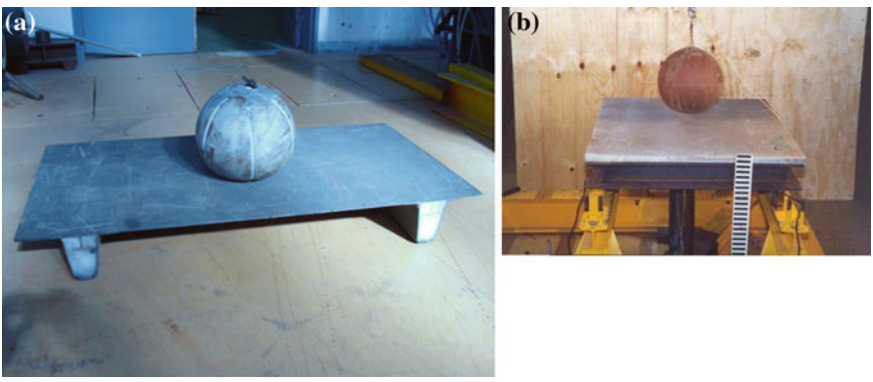

Fig. 15 **a** Initial test set-up. **b** Panel simply supported on steel frame

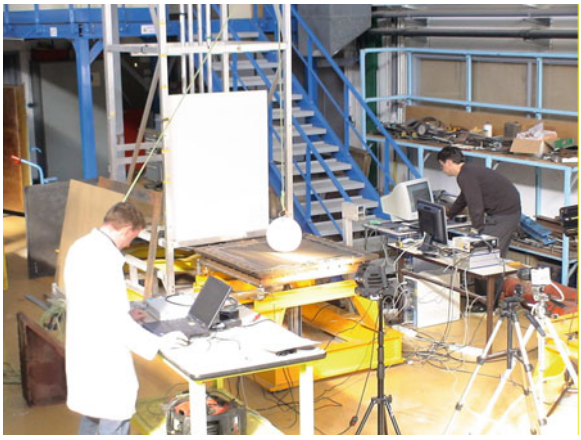

Fig. 16 Current instrumented medicine ball test set-up, with high speed camera

- Nomex honeycomb (see Fig. 17a: *Nomex honeycomb*
- Aluminium alloy honeycomb (see Fig. 17b)
- Polymer Foam (see Fig. 17c).

In these figures some of the forms of soft impact damage commonly observed can be seen. For the nomex honeycomb core crushing occurs, while for the aluminium core and polymer foam core shear is more common.

Relevant parameters for yacht design used routinely by HDS are:

- Energy at first damage: linked to the resistance to wave impacts, and
- Energy allowed for repeated impact: representative of fatigue strength and damage propagation.

In the next 2 paragraphs the application of these 2 parameters will be illustrated.

3.4 Energy at First Damage

The energy at first damage, Fig. 18, is a direct indication of the resistance of a sandwich structure to wave impacts. Using these values, we are able to select the proper core material depending on the yacht use and the area concerned.

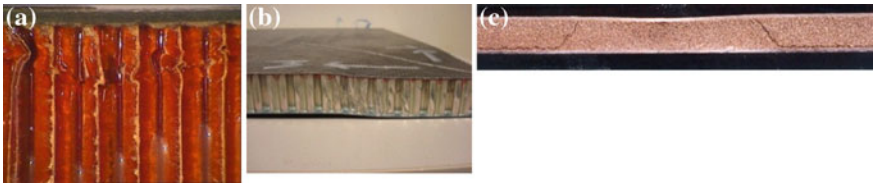

Fig. 17 **a** Nomex honeycomb. **b** Aluminium alloy honeycomb. **c** Polymer foam

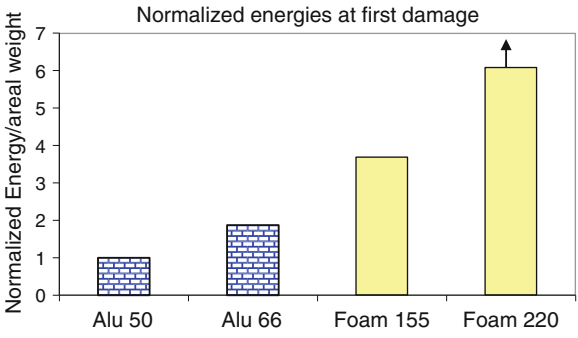

Fig. 18 Example of energies to first damage for two aluminium honeycomb and two polymer foam core densities. Values are normalized with respect to the 50 kg/m^3 aluminium honeycomb value

These data show that the energy required to damage foam cored sandwich panel is considerably higher than for alloy honeycomb sandwich panels (though the weight of the latter is also higher). For HDS applications the result is that we will put polymer foam in areas exposed to strong wave impacts.

3.5 Repeated Impact

The repeated impact test allows us to identify the durability of a core material under slamming loads. Slamming loads are a repeated wave impact that all racing yachts encounter. Following tests to determine the energy to first damage an energy just below this value is chosen. Multiple impacts are then performed in order to determine the sensitivity of the material to repeated impacts at this level. Two examples are shown in Fig. 19, where strain gauges bonded to the lower facing were used to follow properties. Even at these low numbers of impact repeats a clear increase in panel strain is visible for the foam core sandwich, while the honeycomb response remains stable.

There is a need for more data of this type, in order to establish criteria for damage development and failure under slamming loads which are more accurate than the experience-based limits applied today.

3.6 Conclusions

Over the past fifteen years we have performed a large number of tests with our clients and IFREMER, in order to improve the durability and the performance of racing boats. The wave impact testing procedure which has been developed allows us to choose the correct core material for each area of the boat. The data from these tests have also been used to validate numerical models, an example is given in [5]. These data are not the only ones used at HDS to select core materials, but they

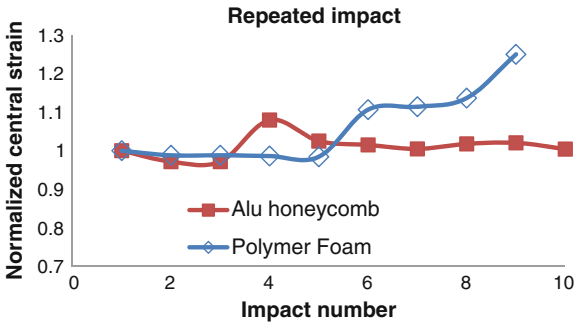

Fig. 19 Strains recorded during repeated impact, normalized with respect to the strain at first impact, for aluminium honeycomb (60 kg/m^3) and polymer foam (220 kg/m^3) cores

represent an efficient and rapid tool to assist selection. They also enable other parameters such as manufacturing quality to be assessed on samples of a reasonable size.

4 Case Study 3: Adhesively Bonded Mast Track

4.1 Introduction

In order to fix the mainsail to a yacht mast, the common solution is to use a bolted metallic track, on which moves a slider with the sail, Fig. 20. This system allows the mainsail to be hoisted on the mast and rotate around it in order to have the best direction according to the wind. To ensure a proper connection, the distance between bolts is short, its value is typically between 50 and 100 mm. On an oceanic racing yacht, the weight introduced by bolts, washers and reinforcement plates is significant and badly placed. Moreover drilled holes tend to weaken the mast.

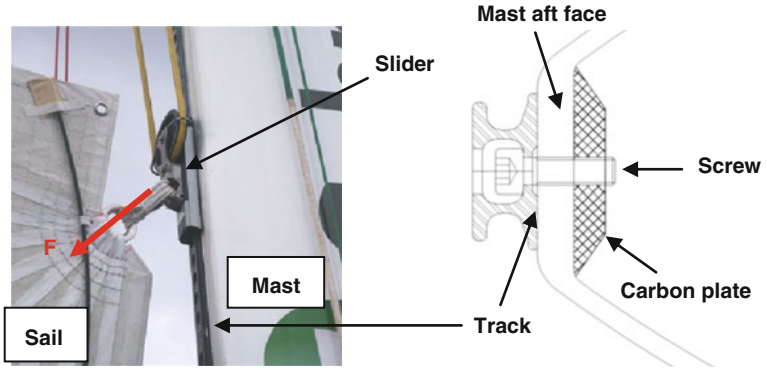

Fig. 20 Overview of traditional mast track assembly

Between 2004 and 2007, HDS associated with CDK (boatyard), IFREMER (marine research institute), ENSIETA (engineering school, now ENSTA-Bretagne), and UBO, (university), and with the aid of Bretagne Region of France performed a research program in order to evaluate bonding efficiency and the replacement of the traditional assembly process by adhesive bonding. Mast/track assembly is one practical application of this study.

4.2 Comparison of Assembly Processes

Mechanical assemblies (bolting, screwing) offer significant advantages:

- The process is well-known and can be properly managed by shipyards and designers
- Removal is possible after assembly

But these processes suffer several drawbacks, mainly:

- Drilling tends to weaken composite parts by cutting fibres and by concentrating stresses around the hole.
- Increased weight, which is a key aspect on competitive yachts.

The advantages and disadvantages of adhesive bonding assembly are the opposite of those for mechanical assembly. On the one hand, light weight and no loss of strength, because stresses are smoothed; but on the other hand the assembly cannot be dismantled and above all, the quality of the process must be well managed by boatyards and designers.

4.3 Experimental Tests

4.3.1 Mechanical Behaviour

The first input needed by the designer is the mechanical behavior of the adhesive, and data provided by manufacturer's datasheets are usually insufficient. In order to characterize the full behavior of assemblies, a butterly-shaped Arcan type fixture, Fig. 21a, b has been developed at ENSTA [13]. This type of fixture allows the adhesive to be loaded with tensile or compressive loads combined with shear, so that the full failure envelope can be determined, (Fig. 21 b).

The fracture envelope obtained for a structural adhesive shows the large influence of the loading conditions on the limits of the adhesive. In the past only one value was generally available, a lap shear strength, whereas now we are able to design the assembly taking the real loads into account, in order to stay in the elastic domain.

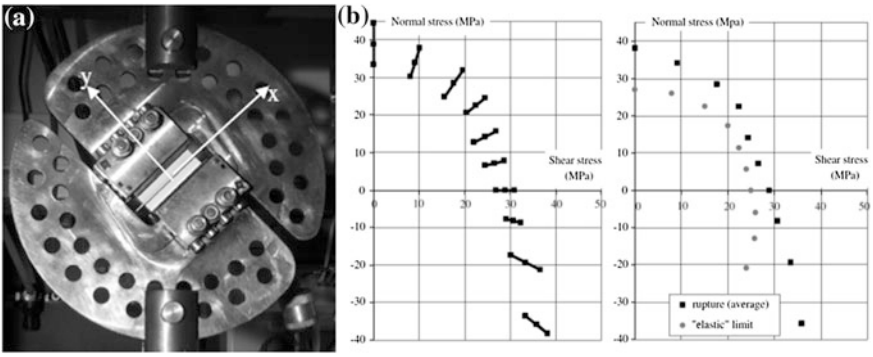

Fig. 21 **a** Modified Arcan type fixture. **b** Fracture and elastic domains [13]

4.3.2 Important Factors in the Marine Industry

In a boatyard environment, several factors may decrease the mechanical characteristics of the assembly determined in the laboratory on small samples under ideal conditions. The following parameters have a significant influence, and will affect the repeatability of the process:

- Thickness of the adhesive joint: Maintaining a constant bonding joint thickness along a 30 m mast is difficult. Tests on samples of different bonded joint thickness showed that shear strength may be reduced by 25 % [13].
- Roughness of surfaces: these are commonly prepared by manual abrasion. The result depends on the operator, the geometry…
- Temperature and humidity: these are difficult to maintain constant in a large volume boatyard.
- Storage of the adhesive.

These factors are considered in the design process, by employing conservative values of adhesive strength.

4.3.3 Mini-Structure Test

In order to have results which are as close as possible to the real structure, a length of 60' IMOCA mast was recovered and its aft face settled on a fixture, Fig. 22a, b. A special test fixture was designed which enables the bonded track to be loaded at different angles, representative of the real conditions. Results showed that it was the mast laminate which broke first, by delamination of the first ply, Fig. 22b. This point has to be considered at an early stage of mast design with an adhesive bond, as when bolts are used they can prevent delamination propagation.

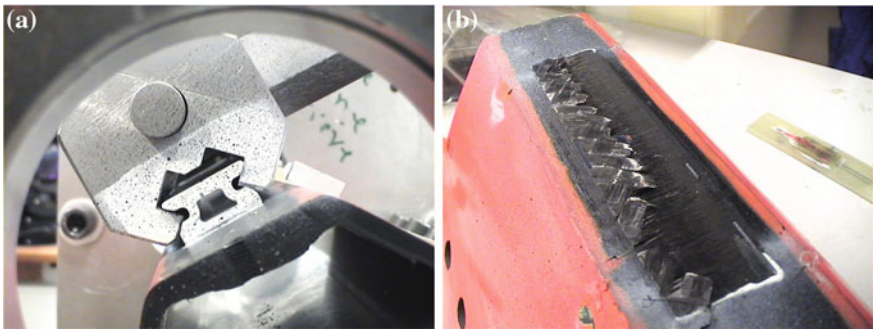

Fig. 22 **a** Mini-structure fixture. **b** Delamination of aft face

4.4 Finite Element Analysis

4.4.1 1st Model: Bonding Behaviour

Description

A first model was set up to evaluate strains and stresses in the adhesive film, Fig. 23. A 200 mm length portion of mast with identical geometry to that of the mini-structure-test was meshed. The track and a 0.3 mm thick adhesive film were also modeled. Boundary conditions were applied to represent the mini-structure test. Loads applied correspond to the maximum load at the head of a 60' IMOCA mainsail.

Results

Strain:

The displacement of the adhesive is about 1.5 % of the initial thickness, so this does not cause debonding.

Stress:

With few elements in the thickness of the adhesive, the measurement of stress is not easy. However, results, confirmed by analytical calculations, show that values of stresses in the adhesive film are low enough to validate the bonding assembly process for track on mast.

Mini-structure tests showed that the weak point of the bonded track is delamination of mast's aft face, not the adhesive. This first FE model is insufficient to analyze the damage process in the composite because the load is applied normal to shell elements.

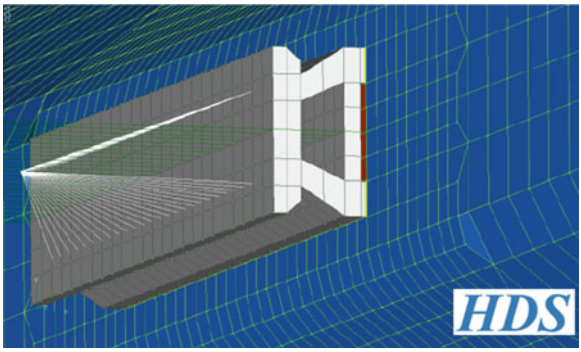

Fig. 23 1st FE model: meshing of aft face and track

4.4.2 2nd Model: Mast Laminate Behaviour.

Description

A new type of model was then considered, where the laminate is modelled by 3D orthotropic elements for the plies with an interface simulated by isotropic 3D elements between each one, Fig. 24. Loads applied were similar to those for the previous model and corresponded to the mainsail loads.

Results

By applying a Von Mises criterion to the interfaces, the influence of two essential parameters for mast design was evaluated:

- the radius of the aft face of the mast
- the stacking sequence of the mast laminate (plies orientation through the thickness).

Radius Influence

R	Von Mises criterion (MPa)
R∞	17.4
R150	10.8
R90	10.64
R60	10.85

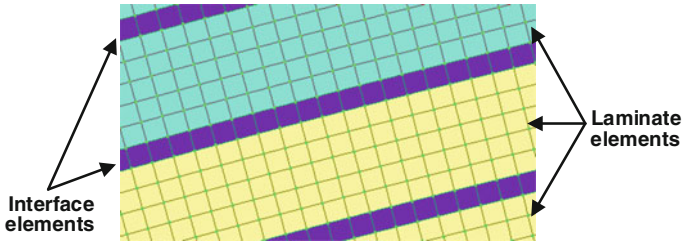

Fig. 24 2nd FE Model: Refined model of composite plies

Conclusions from these results are:

- Between 60 and 150 mm, the value of aft face radius has no influence on delamination,
- Using a flat mast aft face (infinite radius) raises the risk of delamination by about 60 %.

Influence of Stacking Sequence

By changing the position of plies at 0°, 90°, +45° and −45° through the thickness the properties of the global laminate may differ. Eleven different arrangements of plies were tested, for confidentiality reasons these will be referred to as sequences 1–11.

Stacking sequence	Von Mises criterion (MPa)
1	10.85
2	12.25
3	13.88
4	20.49
5	33.68
6	19.53
7	12.21
8	12.73
9	12.05
10	13.59
11	14.3

These results show the large influence of the lamination scheme; a ratio of 3 is measured between the Von Mises criteria for the highest (Stacking sequence 5) and the lowest (Stacking sequence 1). So the best stacking sequence with regards to the delamination risk is the first one. This is a common stacking sequence in masts designed by HDS.

4.5 Conclusion

Improved understanding of bonding behavior enabled us to have sufficient confidence in the process to use it for mast/track assembly in recent HDS projects. In this new generation of mast, the length of track where bolting is applied has been reduced by a factor of ten, and remains important only in reinforced areas. The Recent Volvo Ocean Race winner Groupama 4 had this type of bonded track, and completed the around the world race without any reliability issues.

5 General Conclusion

This chapter describes how HDS has developed expertise in composite durability and solved complex issues for design. Strong links with laboratories and research institutes have allowed us to stay at the cutting edge of the composite technology. Roughly every five years a new phenomenon appears, due to the fact that racing yachts are faster and faster, lighter and lighter.

Significant energy has been spent on research and experimentation to:

- improve the reliability of keels, through detailed flutter analysis. We have now developed and validated an efficient and quick tool to design keels for racing boat. Today our semi-analytical method is often applied for the safety validation of IMOCA keels.
- understand the behavior of current core materials under wave impacts. The use of high tech core materials in racing boats is now well mastered and this knowledge could be extended to the classical marine industry, to reduce the motor boat weight and therefore fuel consumption.
- optimize the mast track assembly. Today ocean racing boats are mostly designed with composite technology but some areas remain traditional such as mast track assemblies. Based on these recent developments we have improved our confidence in fully composite assemblies, and we can expect to extend them to other industrial fields in the near future.

HDS has faced many issues to improve the reliability and the durability of his designs and others will appear. Composite materials are increasing their position in other industries, such as aeronautics and ground transportation, and the challenge is always the same: to develop, test and validate new composite technologies in high technology fields and to extend them to larger areas of industry.

References

1. Mazet R (1966) Mécanique vibratoire. Dunod
2. Bezine G (1998) La méthode des Eléments Finis en Calcul des Structures, Notes De Cours. Ecole Nationale Supérieure de Mécanique et d'Aérotechnique

3. Abhott IH, Von Doenhoff AE (1958) Theory of wing sections. Dover, NY
4. Bathe KJ et al (2011) ADINA on-line manuels
5. Davies P, Bigourdan B, Choqueuse D, Lacotte N, Forest B, Development of a test to simulate wave impact on composite sandwich marine structures, In: Abrate S, Castanié B, Rajapakse Y (eds) Dynamic failure of composite and sandwich structures. Springer, Berlin
6. Gullberg O, Olsson K-A (1990) Design and construction of GRP sandwich ship hulls. Mar Struct 3(2):93–109
7. Remen W (1992) The use of FRP sandwich. In: Davies P, Lemoine L (eds) Proceedings of nautical construction with composite materials. Ifremer editions, Paris, pp 432–439
8. Bull PH, Edgren F (2004) Compressive strength after impact of CFRP-foam core sandwich panels in marine applications. Compos B, 35(6–8) 535–541
9. Herup EJ, Palazotto AN (1997) Low velocity impact damage initiation in graphite/epoxy/nomex honeycomb sandwich plates. Comp Sci Tech 57:1581–1598
10. Meo M, Vignjevic R, Marengo G (2005) The response of honeycomb sandwich panels under low velocity impact loading. Int J Mech Sci 47:1301–1325
11. Choqueuse D, Baizeau R, Davies P (1999) Experimental studies of impact on marine composites, Proceedings of ICCM12, Paris
12. Baral N, Cartié DDR, Partridge IK, Baley C, Davies P (2010) Improved impact performance of marine sandwich panels using through-thickness reinforcement: experimental results. Compos B 41(2) 117–123
13. Cognard JY, Davies P, Sohier L, Creac'hcadec R (2006) A study of the non-linear behaviour of adhesively-bonded composite assemblies. Compos Struct 76:34–46
14. Créac'hcadec R (2008) PhD thesis, ENSTA Bretagne

Service Experience and Life Time Prediction of Naval Composites

J. Dalzel-Job, G. Kotsikos and J. Mawella

Abstract Water diffusing into the bulk of glass reinforced plastics (GRP) can, over time, degrade the mechanical properties of the polymer matrix and the fibre/matrix interface. Residual strength and modulus measurements on samples taken from aged minehunter hulls in 1995 enabled the life of the Hunt Class vessels to be extended. Because no methodology existed for accurately predicting mechanical property degradation through the whole of life, a programme was carried out by QinetiQ in collaboration with DCN CESMAN which applied accelerated ageing at 40 and 60 °C to glass/polyester laminates and correlated the results with real-time data generated for the Hunt Class mid-life update. This chapter presents results and through-life predictive models plus Nuclear Magnetic Resonance (NMR) images of water uptake from that study, and describes the effects of water immersion on fatigue life, fatigue limit and damage development, from another study.

J. Dalzel-Job (✉)
QinetiQ, Farnborough, Hampshire, UK
e-mail: jsdjob@qinetiq.com

G. Kotsikos
University of Newcastle upon Tyne, Newcastle, UK
e-mail: george.kotsikos@newcastle.ac.uk

J. Mawella
UK MOD, DES NAG-MT, London, UK
e-mail: DESNAG-MT@mod.uk

P. Davies and Y. D. S. Rajapakse (eds.), *Durability of Composites in a Marine Environment*, Solid Mechanics and Its Applications 208,
DOI: 10.1007/978-94-007-7417-9_12, © Springer Science+Business Media Dordrecht 2014

1 Introduction

Aqueous environments diffusing into the bulk of glass reinforced plastics (GRPs) can, over time, degrade the mechanical properties of the polymer matrix and the fibre/matrix interface. Through a programme funded by the UK Ministry of Defence in 1995, residual strength and modulus measurements on samples taken from aged minehunter hulls enabled the life of the Hunt Class vessels to be extended. Because no methodology existed for accurately predicting mechanical property degradation through the whole of life a programme was carried out by QinetiQ in collaboration with the French government and DCN CESMAN which applied accelerated ageing at 40 and 60 °C to glass/polyester laminates and correlated the results with real-time data generated for the Hunt Class mid-life update. Gravimetric measurements demonstrated Fickean (diffusion-only) water uptake for the 40 °C aged samples, whereas a second-stage, Langmuir, behaviour was exhibited in addition by the 60 °C aged samples. Predictive equations were developed for tensile, compression, flexural and interlaminar shear strengths and their agreement with accelerated laboratory and real-time data assessed. Apart from additional cross-linking, there were no changes to the resin structure in material conditioned at 40 °C therefore 40 °C was recommended as a suitable temperature for accelerated ageing. The nuclear magnetic resonance technique has also been used in an attempt to image the diffused water and determine its position within the composite. This has revealed that the water concentrates on the fibre/matrix interface and the concentration there is twice that of the bulk of the matrix. The diffusion process appears to be aided by 'wicking' along the fibre/matrix interface.

The effect of a seawater environment on the fatigue performance of naval composites under flexural load has also been studied. By measuring modulus reduction and inspecting the microscopic damage of sectioned specimens during the fatigue test conclusions have been reached about the evolution of fatigue damage and recommendations made for using this knowledge for in-service decisions.

2 Service Experience and Lifetime Prediction

In 1972, the Royal Navy launched the world's first Glass Reinforced Plastic (GRP) ship, the minesweeper HMS WILTON. At that time, very little data existed to define its long-term physical and mechanical properties in a seawater environment. The ship's hull was protected by paint and exposed to water on one side only and the data on which the design was based was limited by the short duration of immersion tests compared to the life of the ship [1].

The condition of the Hunt Class mine countermeasures vessels was reviewed in a mid-life update during 1994 and 1995. Material was extracted from several

vessels and residual mechanical properties were plotted against age using a logarithmic time scale. The regression line for the plotted data was extrapolated to obtain an estimate of the property at the end of a 40-year life. These degraded properties were then applied to a whole-ship finite element model to determine the adequacy of the material. This approach, though adequate, was simplistic since it did not consider factors including the continued cure of the GRP and the differing dynamic load histories of the vessels studied.

Subsequently, as confidence with GRP ships increased, the structural design of minehunters was refined and parts of the structure of later vessels were made from improved materials and manufacturing techniques. Since 1995, the Ministry of Defence (MOD) has funded work using accelerated ageing techniques to characterise the long-term degradation of marine composites. These programmes have studied the effect of seawater immersion at elevated temperature on the strength and fatigue life of the applicable composite materials.

Data on the residual (or degraded) mechanical properties obtained from the 1994/1995 mid-life update was probably insufficient to inform decisions for vessels in-service, such as for routine revalidation through a ship's life (for example, when considering the weight of additional equipment) or, if required, emergency assessment of structural strength following an incident.

Following these programmes, the next step was to assess in detail the applicability of accelerated laboratory techniques for predicting the long-term behaviour of marine GRP. In particular, it was important to ensure that the elevated temperature selected to accelerate ageing, whilst as high as possible to allow the shortest time scale, did not introduce degradation mechanisms additional to those found during long-term ageing of the ships. The programme reported here, correlated accelerated ageing data with observed, real-time measurements, and by studying the changes in physical, chemical and mechanical performance of minehunter laminates, assessed whether they replicated the actual degradation which takes place during the service life of a vessel. This enabled the development of predictive models to determine the through-life mechanical properties of minehunter material. The programme was conducted in collaboration with the French government and DCN.

2.1 The Test Programme

Panels of glass reinforced plastic (GRP) laminate, similar to the material used to fabricate UK minehunter hulls, were conditioned in baths of artificial seawater (using test standard ASTM D1141-98) at 40 and 60 °C. Properties were measured for the as-received material and thereafter for panels removed at intervals up to 24,000 h of conditioning time. Tensile, compressive, flexural and interlaminar shear properties were investigated. Glass transition temperature was measured to detect changes in the resin. Infrared spectrometry was employed to record any changes in the resin polymer bonds.

The laminates studied in the accelerated laboratory tests consisted of YO530 (780 g/m^2) 0°/90° woven glass reinforcement made by Fothergill in a Crystic 489PA isophthalic polyester resin matrix manufactured by Scott Bader. All test laminates were manufactured by the hand lay-up process using 9 plies of glass. There was no post-cure. The laminate had a fibre content of approximately 55 % (wt) and a manufactured thickness of approximately 7 mm.

2.2 Results

Accelerated ageing: Results for two resin-dominated properties are included below. Figures 1 and 2 show the effect of exposure in seawater at 40 and 60 °C on the laminate's compressive and interlaminar shear strength respectively. Both elevated temperatures, by providing some post-cure, cause an initial increase in strength. This is soon overtaken by the property reduction expected from water uptake by the resin and interfacial effects.

Hunt Class data after real-time ageing: The condition of the Hunt Class mine countermeasures vessels (MCMV) was reviewed in a mid-life update during 1994 and 1995. Material was cut out of Minehunter vessels (aged 14.5 and 23 years) and the 2/3 scale MCMV model which had been in water for 22 years. Additionally, some material recovered from the bilge keel of another Minehunter (aged 8 years) became available. Baseline data of properties at build were obtained from several sources. The compression and interlaminar shear strength results from this programme are included in Sect. 2.3 and compared with predicted values. Real-time and predicted values are presented together in Figs. 4 and 5.

Physical and chemical characterisation of core plug material extracted from Minehunters in 1995 yielded information on moisture uptake, glass transition temperature and chemical changes in hull material that had been in contact with water for up to 23 years. Microscopy was used to investigate any small-scale damage. It was found that there had been no chemical changes to the laminate resin in either vessel. The moisture content in the samples varied between 0.3 and

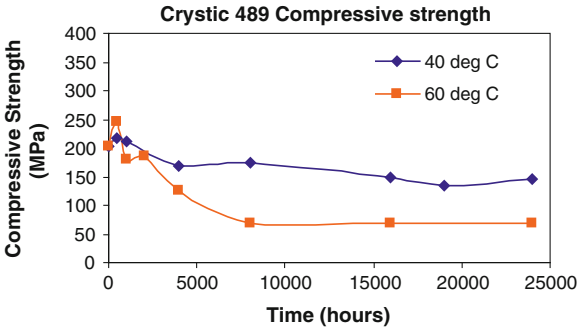

Fig. 1 Compressive strength

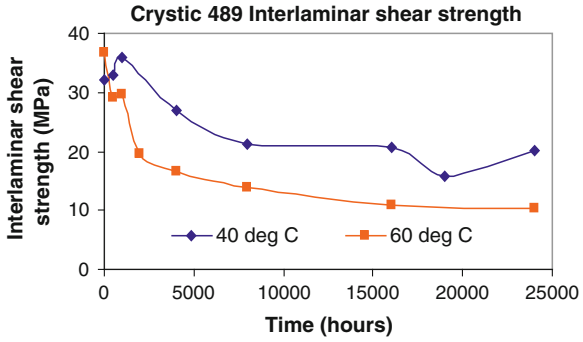

Fig. 2 Interlaminar shear strength

0.4 % (wt). The glass transition temperature, Tg, ranged between 84 and 90 °C. Microscopy was unable to detect any micro damage such as cracking or fibre-matrix debonding in the samples investigated. The study concluded that the hulls of these Minehunters had suffered very little degradation during their lives of 20 years and more.

2.3 Predictive Models

The results of the gravimetric analysis are shown in Fig. 3.

The results from the mechanical tests have shown that property changes are directly dependent on the amount of absorbed water in the laminates, with water content defined by immersion time and temperature. Therefore, two steps are necessary to predict long term material properties:

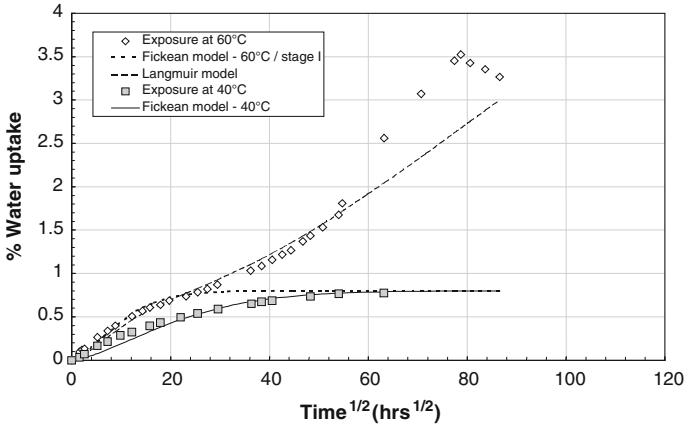

Fig. 3 Water uptake curves for glass-reinforced Crystic 489 laminate

- The prediction of water absorption kinetics.
- The establishment of empirical relationships between water content and properties.

The first step was carried out using the gravimetric data for the two conditioning temperatures [2, 3]. For the second step, a curve-fitting programme was used to fit the experimental mechanical property data in Figs. 1 and 2. The best fits were obtained by an equation of the form:

$$p = p_0\left(1 - e^{-b\exp(-cM_t)}\right) + d \tag{1}$$

where p is the residual property, p_0 is the property of the dry material, M_t is the moisture content at time t and b, c and d are empirical constants. An equation of this form seems to predict the strength degradation of the Crystic 489 composite laminate reasonably well, for both 40 and 60 °C. The equation cannot, however, predict the strength changes associated with post-curing of the resin during the early stages of immersion. These early changes are more pronounced for the specimens exposed at 40 °C.

Using diffusion coefficients derived for 40 and 60 °C, an Arrhenius plot extrapolation was made between these two temperatures. This allowed diffusion coefficients to be estimated for realistic ageing temperatures of 5, 10 and 15 °C.

Predictive equations, based on these coefficients, were developed and used to obtain plots of mechanical property degradation at ambient temperature over time. These curves are presented in Figs. 4 and 5. Hunt Class data (mean values) is also presented in these figures and values for weft and warp fibre directions of the Hunt Class samples are given by the 'x' and 'o' points respectively. The curves over-predict property loss, however the laboratory samples were totally immersed whereas the ship laminates from which the samples were cut were in contact with water on one face only and this face was painted.

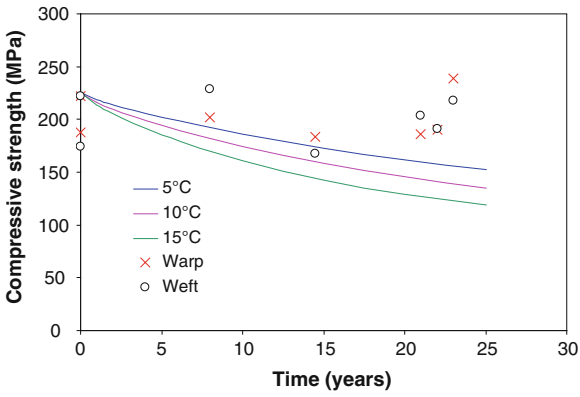

Fig. 4 Predicted curves and real-time data for glass/polyester laminate compressive strength

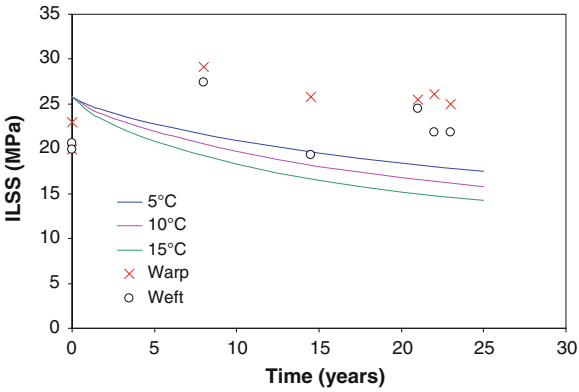

Fig. 5 Predicted curves and real-time data for glass/polyester laminate interlaminar shear strength

2.4 Nuclear Magnetic Resonance

The NMR technique has been used successfully to image the diffused water in Naval composite laminate. NMR can detect and distinguish between the two forms of water present:

- Molecular (diffused) water.
- Liquid (physical) water.

This is possible since the interaction with the magnetic field of the nuclei of hydrogen atoms differs for the two forms of water. The NMR images of the specimens, although they appear as photographic representations, actually show the density of molecular (or liquid) water: the brighter the image, the higher the concentration of water.

The NMR image in Fig. 6 demonstrates that the diffused water concentrates at the matrix/reinforcement interface of the woven glass fabric. The concentration of the diffused water at the interface is about three times higher than in the bulk of the resin.

The bonding layer (thin film) between the resin and fibre is extremely reactive because of its large surface area per unit volume and so is a preferential site for water molecules to accumulate. Therefore the degradation of the interfacial bond mechanical properties is more rapid than for the other two phases (matrix and fibre). Furthermore, the diffusion of water along the fibre-matrix interface is much faster due to a 'wicking' effect.

A scan for 'liquid water' on the sample aged at 40 °C showed no evidence of liquid water present.

The NMR image in Fig. 7 is a scan for liquid water on a sample aged at 60 °C. This reveals that physical water is present which in turn indicates microcracking of the resin and absorption of water through capillary action caused by prolonged exposure of the sample in water at 60 °C.

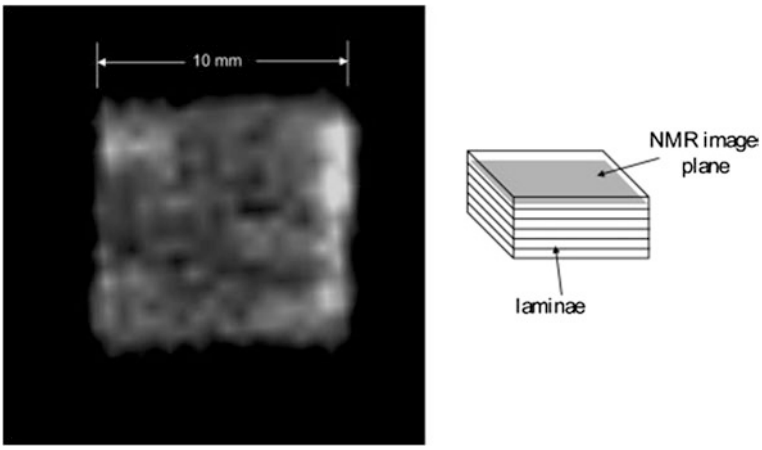

Fig. 6 In plane NMR image, 0.7 mm below surface, of sample exposed in seawater at 40 °C for 6,000 h

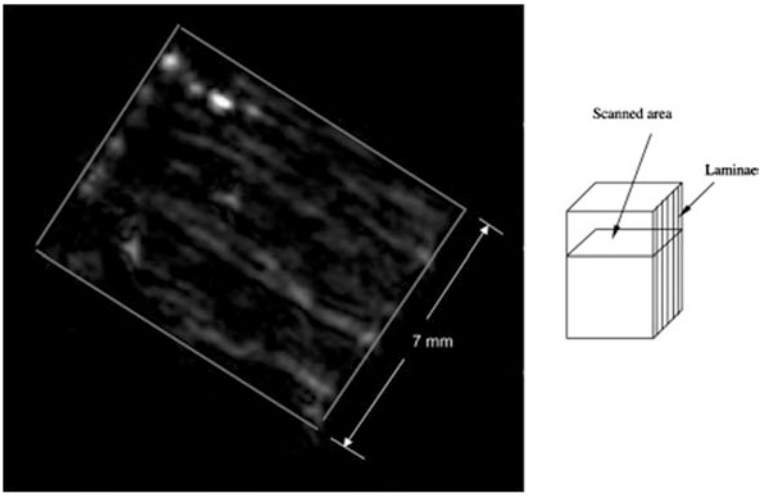

Fig. 7 Through thickness NMR image of 'liquid' water in glass reinforced polyester laminate exposed at 60 °C for 7,000 h

3 Evolution of Damage and Property Loss Under Cyclic Load

The previous sections have considered the effect of water uptake on residual (quasi-static) mechanical properties and translated this knowledge into a method for predicting long term property loss for ship hull material in a realistic sea-going

environment. It does not take account of additional degradation mechanisms that arise from cyclic loading. The following sections describe a mechanical test programme conducted by the Defence Evaluation and Research Agency (DERA) comparing the effects of cyclic flexural load on:

1. Dry, unconditioned laminate.
2. Laminate that was previously conditioned in water and then tested in air.
3. Previously conditioned material that was tested while immersed in water.

The pre-conditioning in (2) and (3) consisted of laminate immersion in artificial seawater at 35 °C for six months. The purpose of this study was to investigate the combined effect of absorbed water and cyclic loading on the damage mechanisms which lead to mechanical property reduction:

- Micro-cracking of the resin.
- Fibre debonding.
- Delamination.

Whilst fibre breakage also contributes to property reduction, the presence of water will have no, or minimal, effect on this mechanism.

3.1 Environmental Fatigue

The test materials are listed in Table 1.

Test details: Maximum cyclic loads of 85, 60, 45 and 30 % of ultimate flexural strength (UFS) were applied under displacement control with an amplitude ratio of 0.1 ($R = a_{min}/a_{max}$). The cycling frequency was 2 Hz (considered low enough to avoid hysteresis heating effects) with a maximum test duration of 10^7 cycles.

Results of modulus degradation: Fig. 8 shows modulus degradation curves for the hand lay-up polyester using pre-conditioned specimens tested while immersed. Each curve exhibits a transition point at which there is a change in slope.

The key features of degradation of the flexural modulus for all materials were:

- A modest drop in modulus (of up to 10 % of the initial value) until a transition point is reached.
- A different rate of damage development beyond the transition point.

S–N Curves: Figs. 9, 10 and 11 show the fatigue lives of specimens of polyester and vinylester composite material for a range of initial load levels (%UFS).

Table 1 Materials tested in the environmental fatigue programme

Material 1	E-glass WR (50 % [wt])	Isophthalic polyester 'new' hand lay up (HLU)
Material 2	E-glass WR (70 % [wt])	Vinyl ester resin infused new laminate
Material 3	E-glass WR (50 % [wt])	Isophthalic polyester HLU, 23-year old laminate

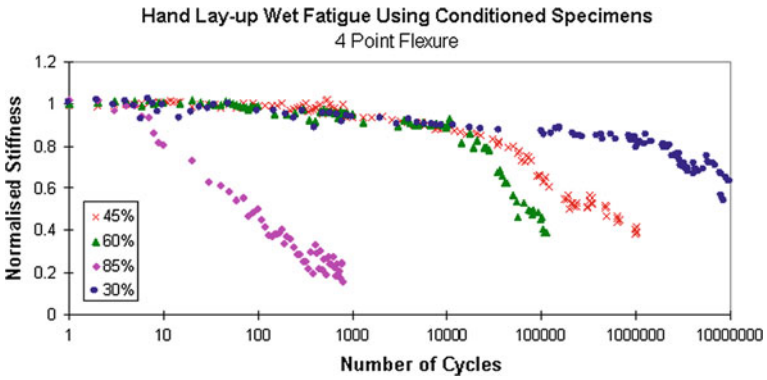

Fig. 8 Typical degradation curves for environmental flexural fatigue

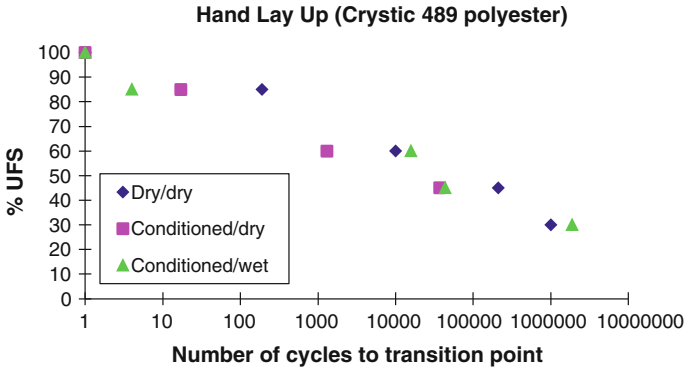

Fig. 9 S–N curves for HLU polyester laminate

Fig. 10 S–N curves for 23 year-old. HLU polyester laminate (taken from the 2/3 scale MCMV model)

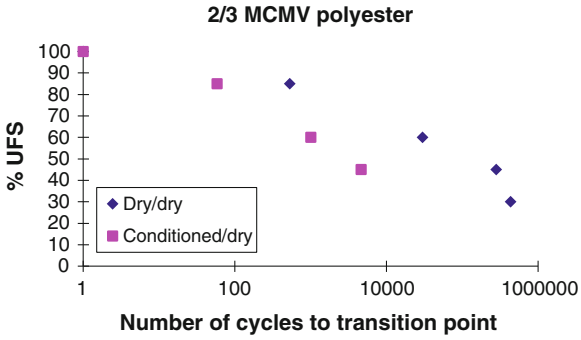

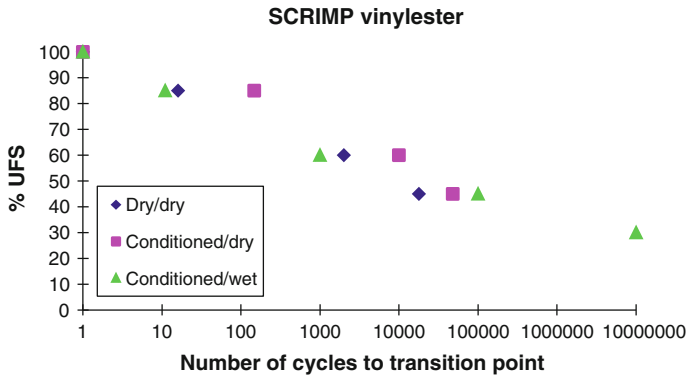

Fig. 11 S–N curves for SCRIMP vinylester laminate

Unlike metals, fibre reinforced composites fail as a result of an accumulation and coalescence of small areas of damage. It is therefore necessary to define 'failure' of the composite and in this instance it is taken as the transition point (change in slope) on the modulus degradation curves, as exemplified in Fig. 8. The transition point indicates a change in damage mechanism from matrix microcracking and fibre debonding to (predominantly) delamination. Once delaminations take hold, stiffness reduces more rapidly, and reduces linearly with log(number of cycles) as shown in Fig. 8.

Each point on these three S–N graphs marks the transition point on the corresponding modulus degradation curve, as exemplified in Fig. 8. For the different conditioning and immersion regimes the following observations can be made:

- Compared to the dry material tested in air, there was an earlier transition point for polyester laminate specimens preconditioned in seawater and tested in air; water uptake and test environment both hasten 'failure'.
- This effect was more marked for the preconditioned 2/3 scale MCMV model HLU polyester laminate.
- Compared to the dry material tested in air, there was a delayed transition point for vinylester RIFT laminates preconditioned and tested in air. This implies that the presence of diffused water may enhance the fatigue life of this material.
- Testing the polyester and vinylester laminates while they were immersed tended to shorten their fatigue lives.

Fatigue limit: The results of this DERA programme on environmental fatigue and related researches in the literature led to the following conclusions:

- Talreja [4] identifies a fatigue limit for unidirectional FRP laminate under tensile loading which is determined by the strain limit of the resin. Similar reasoning can be applied to angle-ply laminate, and by extension, to laminates with woven reinforcement.

- Research at Newcastle University [5] for Marinetech (for which both DERA and MoD were Industrial Sponsors) has related fatigue performance to strain. They tested woven glass/Crystic 489 polyester laminate in fully reversed flexure for 6×10^5 cycles and found a strain limit of about 0.65 % strain for dry (unconditioned) material. They believe that there is no fatigue limit for pre-conditioned specimens (immersion in seawater at 35 °C for 6 months) because the immersion causes its own damage. Micrographs of the DERA composite specimens which were similarly conditioned but not fatigue tested show significant microcracking, in agreement with this theory.
- For the DERA dry Hand Lay-Up Crystic 489 polyester laminate under environmental fatigue there appeared to be no reduction in modulus (i.e. no accumulation of damage) at a stress range of 0–30 % of UFS. The maximum strain in the specimens at this stress was 0.55 %.The next stress range tested was 0–45 % of UFS (maximum strain 0.82 %), which resulted in a (gradual) 10 % loss of modulus over the test duration but no sudden increase in damage accumulation leading to an increased rate of modulus loss (as for example in tests with stresses up to 60 and 85 % of UFS). It is therefore possible that a 'dry' fatigue limit lies somewhere between these two values of maximum strain. This agrees with the Newcastle results.
- WR/Crystic 489 specimens pre-conditioned (through immersion in seawater at 35 °C for 12 months) and then tested at 0–30 % of UFS while immersed in seawater exhibited a 50 % loss in modulus following 10^7 cycles. This supports the Newcastle findings that water uptake affects fatigue limit.
- No dry SCRIMP vinylester specimens were tested at a stress range 0–30 % of UFS. However, preconditioned specimens were tested at 0–30 % of UFS while immersed, which resulted in a (gradual) 15 % loss in modulus over 10^7 cycles. Preconditioning appears to have a beneficial effect on the fatigue performance of SCRIMP.
- To conclude, there is a fatigue limit for 'dry' polyester laminate lying somewhere between 0.55 and 0.8 % maximum strain. There appears to be no fatigue limit for a laminate which contains diffused water, although in both the Newcastle and DERA programmes the specimens were fully immersed and had cut edges with exposed fibre ends, which is much more severe than the situation for full-hull laminate exposed to water on only one side.

4 Conclusions

A life-prediction methodology has been presented here based on residual static mechanical property reduction caused by immersion of composite laminates in water.

Because the laminates, like the minehunter ships, were not post-cured, the application of a temperature of 40 °C caused further cure and consequently an

initial increase in mechanical properties and glass transition temperature (Tg). When 60 °C conditioning was applied, this initial increase was masked by more rapid property loss caused by water uptake. For all specimens the mechanical properties generally decreased with prolonged conditioning time and eventually levelled off. No chemical changes were found in the resins of specimens conditioned at 40 °C.

A model was developed to predict long-term mechanical properties, based on Fickean and Langmuir diffusion kinetics. The model for each mechanical property was then compared with real-time ageing data and achieved reasonably good agreement, especially when taking into account the fact that the test samples were fully immersed in water while the material extracted from the vessels was exposed to the environment on one side only. 40 °C is a safe temperature for accelerating the ageing of glass/polyester laminates. More extensive gravimetric data is required for laminate conditioned at 60 °C in order to obtain an accurate value of diffusion coefficient and reliable property prediction. The method of correlation and life prediction is based on physical principles of diffusion and corresponding property degradation.

The NMR technique is a useful tool for the study of water absorption in composite laminates because it highlights the significance of water accumulation at the fibre-resin interface. In turn, this effect is highly dependent on the type of fibre sizing (or coating) applied by the fibre manufacturers, which is often proprietary information.

The environmental fatigue programme indicates that there are several possible approaches that can be taken when designing marine composite structures for cyclic loading through life:

- Ensure that the strain limit of the 'dry' laminate is not exceeded, although there may be microcracking caused by the effects of immersion alone.
- Design for a fatigue life that is less than the number of cycles at the transition point.
- Select an allowable modulus reduction, for example 20 %, that lies beyond the transition point and therefore gives a longer life under cyclic load but the damage is understood. This can be backed with appropriate NDE.

It should be noted that this fatigue programme is more severe than in-service conditions experienced by ship structure because it has not accounted for a realistic cyclic load spectrum.

Acknowledgements The support of the UK Ministry of Defence in funding several programmes investigating durability and degradation of marine GRP is gratefully acknowledged.

References

1. Dixon RH, Ramsey BW, Usher PJ (1972) Design and build of HMS WILTON. RINA symposium on GRP ship construction
2. Pritchard G, Speake SD (1987) The use of water absorption kinetic data to predict laminate property changes. Composites 18(3):227–232
3. Springer GS (ed) (1981) Environmental effects on composite materials, vol 2. Technomic Publishing, Westport
4. Talreja R (1981) Fatigue of composite materials: damage mechanisms and fatigue-life diagrams. Proc R Soc Lond A 378:461–475
5. Speake SD, Evans JT, Hale J, Gibson AG (1999) Fatigue of offshore composites in liquid environments. Advanced research partnership (formerly Marinetech) project CP411. Centre for Composite Materials Engineering, University of Newcastle upon Tyne

Conclusion

Future Research Requirements

Peter Davies, Yapa D. S. Rajapakse

At the end of the workshop a session was devoted to the subject of future research needs for the improvement of long term reliability of marine composite structures. The following topics were discussed:

- Modelling of water diffusion
- Water induced damage
- Accelerated testing
- Modelling of fatigue behaviour
- Durability considerations in design
- In-service experience.

Modelling of Water Diffusion

Water diffusion is usually discussed in terms of Fickian absorption and desorption. Fickian models are used in the majority of published studies. However, when the data is carefully examined, Fickian behavior is found primarily in pure resins, but non-Fickian behaviour is often observed in composite materials. Other models are available, and in some studies a Langmuir and Carter-Kibler two-mechanism diffusion approach is effectively utilized. The general consensus is that suitable mathematical models exist that capture the diffusion behaviour reasonably well, and that there is no need for the development of new diffusion models. However, coupling of these models with mechanical loading, and the consequences of this coupling for failure and durability assessments, are areas that need attention. In addition, reliable experimental data is needed for the validation of the coupled models.

P. Davies and Y. D. S. Rajapakse (eds.), *Durability of Composites in a Marine Environment*, Solid Mechanics and Its Applications 208,
DOI: 10.1007/978-94-007-7417-9,

Water Induced Damage

Damage induced by water absorption includes matrix hydrolysis, interface damage due to swelling, loss of adhesion, and in some cases fibre damage (stress corrosion of glass). In many studies these are qualitatively noted, but few authors provide quantitative descriptions. This is an area where research is still needed, in particular to clarify the effects of exposure to water of the fibre/matrix interface. Part of the difficulty in the study of interface effects is that fibre surface treatments remain proprietary. Thus while fibre suppliers can modify fibre coatings to optimize their products for different manufacturing processes and applications, this parameter remains outside the scope of most research projects. Closer collaboration between the fibre manufacturers and the research community could result in the development of scientifically based, improved composite materials for the marine environment. Validated coupled modelling tools are needed to account for the influence of damage on diffusion, and the effects of water on damage development. Improved tools for the detailed investigation of water induced damage at all scales, including for example high resolution microtomograhy, would be beneficial.

Accelerated Testing

Accelerated testing is essential in order to assess the long term in-service behaviour of materials to be used in the marine environment. Accelerated testing is also a valuable tool for rapid screening of several candidate materials. As a 20-year lifetime requirement is commonly specified in the offshore and renewable marine energy industries, the accelerated test protocol must aim to reproduce the effects of 20 year exposure in a few months.

The key issues are: (1) Reliable methodology for accelerating testing, (2) Validation of elevated temperature testing as a means of predicting long term effects, and (3) Definition of standards. The ONR sponsored research at Kanazawa Institute of Technology, which focusses on the viscoelastic behaviour of the resin matrix, has helped to develop a framework for accelerated testing based on the time-temperature superposition principle. This could provide a valuable framework, and now it is important to verify the validity of this approach for all realistic loading conditions, and to identify its limitations, so that it may be adopted as a standard test procedure and be more widely implemented.

Modelling of Fatigue Behaviour

Regarding fatigue behavior there are also a number of issues to be addressed: (1) Life prediction under cyclic or spectrum loading, (2) Modeling for continuous or intermittent immersion in sea water. The wind energy industry has produced an

extensive test database which has been generated in Europe and the USA, together with many years of in-service experience. The design, however, is based on specific fibre and resin materials. For renewable marine energy applications there is no such database. Recent exploration of the use of composite blades on prototype tidal turbines in very severe environments has revealed numerous problems. In this situation, and in other situations where the submerged composite structure is subjected to highly dynamic loading in water, the importance of including (in the analysis) fluid-structure interaction and hydroelastic effects, should be emphasized. These coupling effects are being studied in current ONR programs.

Durability Considerations in Design

In the design of marine composite structures, it is important to consider and design for durability. It is also important to account for realistic loading and environmental conditions in this process. In situations where the structures are subjected to dynamic loads, or to temperature extremes, the analysis and design of marine structures should account for fluid-structure interaction, hydroelasticity, and thermo-mechanical effects, and their interactions (where applicable). In addition it is important to understand the role of certification bodies. The chapter by Professor Echtermeyer addresses this issue directly. He concludes that durability is only indirectly addressed by most design standards today, and that the emphasis is on extensive testing. A better understanding of the degradation processes would allow reduced testing and improve the standards.

In-service Experience

Finally, there was a discussion on what we have learnt from in-service experience, particularly of military ship structures in service with the French and British Navies. Extensive studies on the state of minesweeper vessels after 20 years in service showed that residual properties appear generally satisfactory. However, whether this is the result of over-design, low service loads, or age-resistant materials, it is not easy to decipher without further information. An additional but very important topic is the long term durability of hybrid structures. Composite structures are frequently attached to existing metallic structures and this connection may become the weak link. There has been considerable research on composite bonding, but the key technology developments required here may be non-destructive testing and evaluation tools rather than adhesive improvements.

Composite Durability Research Initiatives

There have been various national and European projects on marine composites over the last 20 years. In Europe today it is much easier to propose projects for renewable energy than for Naval applications, but many of the durability questions can be applied to both.

The Office of Naval Research Solid Mechanics Program is already addressing some of these questions. Three chapters in this volume provide overviews of ONR supported research at the University of Tennessee, Kanazawa Institute of Technology, and Florida Atlantic University. Areas of research at these (and other) institutions include:

- assessment of damage induced by sea water absorption in composites, foam core, and composite sandwich structures
- fatigue of composites in air, and in sea water (fully immersed, one-side exposed)
- effect of sea water absorption on failure modes of composite sandwich structures, and fracture of foam core
- influence of fiber-matrix interface on absorption, and the role of wicking
- degradation of strength of fiber-matrix interface due to sea water
- tailoring of interface/interphase to mitigate degradation and enhance strength and durability
- multi-scale models for coupled effects of sea water absorption, temperature variations, and stress fields
- investigations of effects of sea water absorption, temperature, on fatigue life
- establishment of accelerated testing methods
- effect of coupled effects of sea water absorption and ultra violet radiation exposure
- damage assessment using high resolution micro-tomography
- failure criteria under combined sea water absorption and multi-axial loading
- effects of sea water absorption on impact damage at different temperatures
- implications of fluid-structure interaction on dynamic failure criteria, and consequences for design of submerged composite structures subjected to dynamic loads.

SELECTED REFERENCES TO ONR RESEARCH

"Major Accomplishments in Composite Materials and Sandwich Structures"
Editors: I. M. Daniel, E. E. Gdoutos, and Y.D.S. Rajapakse Springer, 2010

"Dynamic Failure of Materials and Structures"
Editors: Arun Shukla, Guruswami Ravichandran, and Yapa D. S. Rajapakse, Springer, 2010

"Dynamic Failure Composite and Sandwich Structures"
Editors: Serge Abrate, Bruno Castanie, and Yapa D. S. Rajapakse, Springer 2013

Special Issue of International Journal of Multiphysics on
"Marine Application of Composite Structures and Materials"
Editors: Young Kwon, and Yapa D.S. Rajapakse, 2012

Special Issue of Journal of Experimental Mechanics on
"Sandwich Structures"
Editors: G. Ravichandran, and Yapa D. S. Rajapakse, 2012

==========

THESE ARE NOT PUBLISHED
THEY WILL APPEAR AS DTIC REPORTS SHORTLY:

"Proc. 2012 ONR Solid Mechanics Review, November 2012"
Editor:. Yapa D. S. Rajapakse

"Proc. 2013 ONR Solid Mechanics Review, October 2013, "
Editor:. Yapa D. S. Rajapakse

Index

A
Accelerated testing, 156, 165, 173, 242, 254
Activation energy of diffusion, 73
Adhesive, 173, 230
Arcan fixture, 231
Arrhenius equation, 54, 55, 73
AUV hull, 202

B
Biocomposite, 6
Blistering, 3, 95

C
Case II diffusion, 82
Cavitation, 5
Certification, 179
Chain scission, 87
Chemical potential, 18, 121
Composite diffusion, 82
Compression failure, 201, 242
Coupling, 115, 170
Coupling agent, 5
Clustering, 59, 75
Creep, 157, 202

D
Damage mechanisms, 145, 247
Damage tolerance, 190
Damping, 221
Deep sea environment, 197
Density, 122
Design standards, 180, 209, 255
Diffusion models, 70, 253
Dual sorption, 20

E
Eigenmodes, 214
Environmental fatigue, 141, 171, 188, 247
Environmental resistance, 1
Epoxy, 36, 171, 199
Epoxy diffusion coefficients, 77, 198
Equation of state approach, 17
Erosion, 5
Eshelby-Kröner model, 116

F
Fatigue, 140, 168, 185, 203, 254
Fibre orientation, 140
Fibre sizing, 148, 172
Fickian diffusion, 71, 76, 132
Flory-Huggins, 51
Fluid model, 218
Flume tank, 167
Fouling, 4
Free volume theory, 74, 118
FTIR spectroscopy, 27

G
Galvanic corrosion, 6
Glass microsphere, 205
Glass transition temperature, 24, 90
Glassy polymer, 20
Gravimetric analysis, 28
Gravimetric microbalance, 136

H
Henry's law, 54, 55
Henry's solubility coefficient, 62
Hydrogen bonding, 17, 58

P. Davies and Y. D. S. Rajapakse (eds.), *Durability of Composites in a Marine Environment*, Solid Mechanics and Its Applications 208,
DOI: 10.1007/978-94-007-7417-9, © Springer Science+Business Media Dordrecht 2014

Hydrolysis, 83
Hydrolysis rate, 92
Hydrophilic groups, 56
Hygroscopic swelling, 124
Hydrostatic pressure, 197

I
Impact damage, 228
Interfacial water absorption, 64
Interface degradation, 103
Internal state variables, 21
Internal stress, 116
Interphase, 105

K
Keel flutter, 212

L
Langmuir diffusion, 53, 63, 78
Lattice fluid theory, 17
Life Cycle Assessment, 8
Long term behavior, 156

M
Marine energy, 165
Master curve, 157, 161
Mast laminate, 234
Minesweeper, 240
Molecular dynamics, 192

N
Naval composites, 239
NMR, 245

O
Ocean energy, 165
Oceanographic application, 201
Offshore, 181, 204
Osmosis, 3, 95

P
PEEK, 34, 198
Plasticization, 24, 69, 75, 116
Polyamide, 58
Polycaprolactone, 40
Polyester, 198, 248
Polyimide, 28
Polysulfone, 57
Pressure effect, 126, 198
PVC foam, 129

Q
Qualification, 180

R
Randomicity, 25
Rubbery polymer, 17, 40, 90

S
Safety factors, 183
Sandwich material, 129
SCRIMP, 249
Seawater aging, 129, 143, 171, 247
Semi-crystalline polymer, 26, 89
Service experience, 239, 255
Sizing effects, 150
Slamming loads, 229
Sorption mechanisms, 16
Stress corrosion, 4
Stress effect, 55, 101
Stress rupture, 188
Swelling, 66, 124
Syntactic foam, 203

T
Temperature, 2, 53
Temperature shift factor, 159
Thermodynamics, 15, 119
Tidal turbine, 166
Transverse strength, 151

U
Underwater applications, 195

V
VARTM, 130
Vinyl ester composite, 130, 145, 198, 249
Viscoelastic behavior, 157

W
Water activity, 50
Water concentration measurement, 49
Water concentration profile, 95, 117, 127
Water diffusion, 70

Wave impact, 70
Wicking, 149

Z
Zimm-Lundberg, 51, 60